First Passage Times of Diffusion Processes and Their Applications to Finance

A thesis presented for the degree of
Doctor of Philosophy

Luting Li

Department of Statistics
The London School of Economics and Political Science
United Kingdom

April 2019

Declaration

I certify that the thesis I have presented for examination for the Ph.D. degree of the London School of Economics and Political Science is solely my own work other than where I have clearly indicated that it is the work of others (in which case the extent of any work carried out jointly by me and any other person is clearly identified in it).

Statement of conjoint work

- A version of parts of Chapters 3-6 has been submitted for publication in two articles jointly authored with A. Dassios.
- A version of Chapter 7 has been submitted for publication jointly authored with H. Xing.

Acknowledgements

Just before writing down the words appearing on this page, I sit at my desk on the 7^{th} floor of the Columbia House, recalling those countless yet enjoyable days and nights that I have spent on pursuing knowledge and exploring the world. To me, the marvellous beauty of this journey is once in a lifetime.

I would like to, first and foremost, express my sincere gratitude to my supervisors Angelos Dassios and Hao Xing, for providing me the opportunity of carrying out my research under their supervisions, for their constant support and the freedom they granted me to conduct my work according to my preferences. Whenever I was struggling on the research, it was Angelos who always pointed me towards the right direction, guided me out of puzzles, and taught me that persistence is the key to success. I am grateful to him for not only offering invaluable academic advice, but also spending time with me having coffees, talking travels, and sharing experiences, which broadened my horizons outside the academic world. I am indebted to Hao as my secondary supervisor for inviting me to the FRTB project which enriched this thesis in the dimension of quantitative risk management. He was more like a friend than a teacher to inspire and encourage me to excel in my work.

Nevertheless, without the enormous help and precious comments from many experts, this thesis would not be presented in its current complete format. I am honoured for Goran Peskir and Luciano Campi being my examiners to give me invaluable suggestions and help in finalising this thesis. In addition, I would like to thank José A. Scheinkman and Michael Schatz for providing insightful advice on the financial bubble topic. I am grateful to Paul Embrechts, Demetris Lappas, Dirk Tasche, and Ruodu Wang, for their comments on the capital allocation project. I would also like to express my gratitude to the referees and editors from the *Applied Probability Journals*, the *International Journal of Theoretical and Applied Finance*, and the *Risk Magazine*, for their helpful comments and advice on three papers in this thesis.

Great thanks go to Citigroup for providing the funding which allowed me to undertake my research. Particularly, I would like to express my sincere gratitude to Demetris Lappas, Wei Zhu, and Kevin Jian, for providing me with the opportunity of joining the Citi-LSE programme and gaining industrial experience alongside my research. My special thanks go to Damien Quinn for sharing his knowledge and introducing me a real financial world. I would also like to extend my thanks to Pierre-Yves Casteill, and George Dimitropoulos, for beautiful birthday gifts, offering me all those unforgettable and relaxing times of having drinks, dinners, and going for hiking, etc.

Moreover, I express my sincere gratitude to all the staff and colleagues from the Department of Statistics at LSE for providing such a pleasurable environment. Particularly, I would like to thank my neighbour José M. Pedraza for his constant support in both academic and non-academic aspects. I gratefully acknowledge the helpful discussions from Yan Qu and Junyi Zhang about the research. And I would like to thank Ian Marshall and Penny Montague for their administrative support.

I would like to express my deep friendship to Longjie Jia, Phoenix H. Feng, Cong Liu, Yusong Li, and Yupeng Jiang to share with me all those joy and sadness moments in the past four years in London. I wish to express my gratitude to Shuren Tan, for providing me timely help in Edinburgh. Also, I would like to give my special thanks to my car, for always driving me to office and journey, no matter sunny, raining, or snowing, and never abandoning me on its halfway.

Naturally, I should not forget my teachers who gave me knowledge prior to my doctoral training and those friends who accompanied me though not in this country. I would like to thank my junior high school teacher Haiying Zhou who inspired me to realise the beauty of mathematics; my senior high school teacher Chengsheng Ma who encouraged me to always follow my heart; and my teacher Goran Peskir at the University of Manchester who introduced the stochastic calculus world to me. I would like to express my gratitude to Honghua Qiao, Chao Zhang, and Xuheng Lu, for their encouragement throughout these years.

Given it is the last paragraph, I would like to express my deepest and the most heartfelt gratitude to my parents Chenghong Li and Peilan Ding, for their endless love and ultimate support which surround me all the time. My sincere thanks also go to all my family members, my dear friends, and to whom that have walked with me in this once in a lifetime journey.

Abstract

This thesis consists of three submitted papers and one working paper. It begins with the study of asymptotic solutions for the first passage time densities of various diffusion processes, and the thesis ends up with an application of such findings in the area of systematic trading. In between, financial bubbles and the regulatory risk management for the banking industry are studied additionally. The purpose of this thesis is to, by combining probability theory with financial practice, provide quantitative tools for investment decision and risk management.

Chapters 3-5 are reorganised from the first passage time paper [31]. Our research method is mainly based on the potential theory and the perturbation theory. In Chapter 3, a unified recursive framework for finding first passage time asymptotic densities has been proposed. Besides, we prove the convergence of our framework and provide an error estimation formula. Examples related to the Ornstein-Uhlenbeck and the Bessel processes are demonstrated in Chapters 4 and 5, respectively.

The second paper [30] is documented in Chapter 6. It introduces a new diffusion process which is relevant to financial bubbles. During the study of the first passage time, we occasionally found that the sample path of the new process coincides with log-price features of bubble assets. In Chapter 6, we show that the new model is a power-exponential transform of the Shiryaev process [116, 117]; and we prove that the model itself, indeed, satisfies various technical requirements for defining a financial bubble [107]. Furthermore, by using our previous framework, we solve the closed-form asymptotic for the model's first passage time; and according to which, we have made predictions to the burst time of BitCoin.

Chapter 7 is a modified version of the third paper [75]. We consider the risk capital allocation issue under the forthcoming regulatory framework, namely the *Fundamental Review of Trading Book*. Apart from studying coherent properties of the new risk measure, we propose two alternative capital allocation schemes within the range of *Internal Modelling Approach*. Our analysis shows that, different choices in allocation methods can lead significantly dif-

ferent allocated capitals, therefore, impacting on bank's performance measure and capital optimisation.

Our current working paper about systematic trading is demonstrated in Chapter 8. We propose two mathematical frameworks for, respectively, defining executable trading strategies and identifying the strategy-associated trading signals. Based on our definitions, we show how the first passage time can be employed in systematic trading. As a summary of applications to previous chapters, we use simulation analysis to illustrate the trading idea and the implementation of risk capital allocation. In the end, real data backtest on China stock market indicates that the first passage time could be an effective tool in recognising trading opportunities.

Contents

List of Figures

List of Tables

Chapter 1

Introduction

The majority of this thesis is technical discussions about the first passage time. Apart from its theoretical results which are based on time-homogeneous diffusion processes, this thesis also considers applications in economic bubble forecasting and trading signal identification. Simultaneously, a separate topic about the regulatory risk capital allocation is presented. From the financial practice aspect, this thesis could be regarded a self-contained material relevant to investment decision and risk management.

This chapter provides an overview of the thesis, where general motivations of the research and an outline of following chapters are explained. On its whole, this thesis contains 4 different topics. Later for each topic, the background introduction, motivation, and literature review are documented separately.

Our research about the first passage time was originally motivated by the pricing and hedging problems in credit derivatives. According to R.C. Merton's earlier work [88], and followed by the extensions from F. Black and C. Cox [15], and many others (cf. [108] for a brief summary), the stochastic barrier crossing problem has attracted much attention in the area of the *structural modelling approach*. On the other hand, point processes are usually used in the *intensity-based modelling approach* for credit risk (cf. A. Dassios and H. Zhao [37]). And those processes would require the information about first passage time distributions. Therefore, calculations involved in but not limited to credit risk/derivative pricing, would be benefited from by knowing the closed-form densities of first passage times.

Unfortunately, apart from the Brownian motion, there is a very limited number of diffusion processes which posses closed-form first passage time densities. One of the standard

methods of studying the first passage time distribution is to employ the killed version potential theory (cf. G. Peskir [101]). By solving ODEs with Dirichlet-type boundaries, such a theory generates Laplace transforms of first passage times. But the problem comes from the fact that most those transforms are given by ratios of special functions, and which are rarely known of having closed-form inverses. In order to simplify the problem, we further adopt the perturbation theory. The perturbation technique was initially applied in the area of quantum physics [110], while our inspiration for using it is from the works about the stochastic volatility modelling [45] and the *Parisian* option pricing [35].

In the first topic of this thesis, we present a recursive framework for solving the first passage time asymptotics of time-homogeneous diffusion processes. The research began with the perturbation analysis on the Ornstein-Uhlenbeck and Bessel models. After gaining successes from these two processes, plus our observations of commonalities in their perturbed ODEs, we realised that the perturbation mechanism might be effective to a more general class of diffusion processes. This motivates us to deduce a unified framework for solving the constant barrier crossing problem in an asymptotic manner. However, the perturbation technique in general would not provide error estimation results. Though under certain circumstances our numerical exercises have shown that perturbed densities are accurate, we want to further understand the error terms remained in the perturbed ODEs. In the end, by referring again to the potential theory, we were able to derive an error estimation formula. And as a by-product of this formula, we have proved that under the L^1-boundedness condition, the perturbed density is $o(\epsilon^N)$-accurate, where N is the truncation order in the recursion system and ϵ is the perturbation parameter.

The second topic introduces a new financial bubble model. It can be seen as a continuation of the previous topic. During the study of the Ornstein-Uhlenbeck process, we found that the recursion structure under perturbation produced a series of mathematically neat functions. Considering that our recursion mainly involves operations of integration and differentiation and that the drift of the Ornstein-Uhlenbeck process is a polynomial (which is closed under integration/differentiation), therefore, we inferred that a stochastic process with an exponential drift may also yield neat density functions. In view of this, we studied the new SDE with an exponential drift and proved that such a SDE constitutes a *submartingale*. Besides, the sample path of the new process shows a similarity in comparison with log-prices of bubble assets. Motivated by these observations, we decided to investigate the connection

between the new model and the financial bubbles. Later by extending the original SDE with a negative drift parameter, we have demonstrated that our model is a well-defined bubble process[1] [107]. From the investor behaviour point of view, the new model explains the *positive feedback mechanism (pro-cyclicality)* as well. At the end of this research, we applied our previous perturbation framework and made predictions to the BitCoin price collapse time.

The third topic is independent[2] to previous discussions about the first passage time. It focuses on financial regulation and provides two risk capital allocation schemes under the *Fundamental Review of Trading Book*. In January 2016, the Basel Committee on Banking Supervision overhauled the quantitative methodologies for bank's minimum capital requirements [12]; according to which, banks need to reevaluate their capital efficiency and optimise their capital structures. Within this context, the industry is awaiting a tailored allocation scheme to the new regulation. And this research responds to such a need. Although there is no sophisticated mathematics in this topic, two main challenges arise from the conceptual and computational aspects. In this study, we established a mathematical framework translated from the original regulation document. Based on this framework, we analysed the coherent properties of the new regulatory risk metric and deduced two allocation schemes by using the Euler approach and the constrained *Aumann-Shapley* approach. Numerical exercise shows that our new methods could effectively reflect bank's capital structure, meanwhile, computationally they are no more complex than the current VaR-based allocation methods. In the end, evidence from our work indicates that the allocation results could be used in the future capital optimisation problem.

The last topic of this thesis summarises some of our thinkings about systematic trading. The motivation for conducting this research comes from two dimensions. On the one hand, inspired by the Ornstein-Uhlenbeck process and its first passage time in pairs trading [47], we want to generalise this trading idea to various diffusion processes with clear economic meanings. On the other hand, considering that our third and first two topics are distinct in theory, in order to maintain the integrity of this thesis, we include Chapter 8 to illustrate how the theoretical parts of this thesis can be applied in a whole investment life cycle: from decision making to risk evaluation. In this topic, we discuss the *trading signal identification* problem. The 'identification' here refers to an extra step prior to the portfolio weight allocation (cf.

[1] And mathematically, it is closely related to the Shiryaev process [116, 117].

[2] This research problem was initially proposed by Udit Mahajan and Diane Pham at Deloitte, and Hao Xing at LSE. And the research combines my part-time working experience at Citigroup.

the *modern portfolio theory* [83, 84]). During this step, quantitative criteria associated with *executable strategies* should be specified; and such criteria constitute the decision metric for portfolio investment. Following this thinking, we demonstrate how the probability of the first passage time can be adopted as a trading signal identification metric. And we use simulated portfolios to show that the investment performance could be evidently enhanced under the new strategy[3]. In addition, as an illustration of the risk capital allocation topic, we report the risk capital and its allocated numbers in our simulated investments.

We now conclude this chapter by outlining the structure of the thesis. Topic 1 is distributed in Chapters 3-5. And Topics 2-4 are documented separately through Chapters 6-8. In general, each topic has its own abstract, introduction, and conclusion. And in each chapter, apart from its main body, we may also include separate appendices to record supporting materials or less-relevant but interesting findings. Based on these principles, the rest of this thesis is organised as follows.

In Chapter 2, we introduce notations, concepts, and major theorems, which are used throughout this thesis. Chapter 3 presents the unified recursive framework, together with its convergence results, for solving the first passage times of time-homogeneous diffusion processes. Chapter 4 demonstrates the application of our framework on the Ornstein-Uhlenbeck process. In this chapter, we provide the N-th order results of perturbed densities, their tail asymptotics, and the proof for the first order convergence. Chapter 5 is the same in structure as Chapter 4, but discussions are based on the first order results of the Bessel process. Note that, an abstract and an introduction of Topic 1 are given at the beginning of Chapter 3, and the conclusion is provided at the end of Chapter 5. In Chapter 6, we summarise our findings in the financial bubble model. This chapter can be read in two parts. The first part conducts stochastic analysis about the model itself; and the second part calculates its first passage time. Chapter 7 reports our third topic about the risk capital allocation. And Chapter 8 illustrates our thoughts about systematic trading, which, meantime, can be regarded as an application summary of the technical parts of this thesis. In the end, Chapter 9 concludes this thesis and highlights further works.

[3] 11 years real data backtest on China stock market is provided in the appendix this chapter.

Chapter 2

Preliminary Definitions and Results

This chapter reviews major theoretical results that are relevant to the work of this thesis. In order to accommodate notations and settings in this thesis, theorems in this chapter could be modified versions from classical conclusions. In general, apart from where it is mentioned, there is no new material in this chapter.

This chapter is organised into three parts. Sections 2.1, 2.2, and 2.3 form the first part. In this part, we review classical theorems in stochastic analysis and numerical methods for the inverse Laplace transform. These results will be referred to later by Chapters 3, 4, 5, and 6. In the second part, Section 2.4, we introduce relevant concepts in portfolio selection, risk management, and capital allocation. The second part can be seen as a partial literature review of Chapters 7 and 8. The last section (Section 2.5) of this chapter summarises notations that will be used throughout this thesis, and it forms the last part of this chapter.

2.1 Stochastic Differential Equation

Consider a filtered probability space $\left(\Omega, \mathcal{F}, \{\mathcal{F}_t\}_{t\geq 0}, \mathbb{P}\right)$ which satisfies the usual conditions (completeness and right-continuity) and is generated by a (standard) Brownian motion $\{W_t\}_{t\geq 0}$. Let D be an open interval on the real line $\mathbb{R}$, and on which we define two continuous measurable functions $\mu(\cdot)$ and $\sigma(\cdot)$. Given the settings above, the stochastic process $\{X_t\}_{t\geq 0}$ with the following SDE

$$dX_t = \mu(X_t)dt + \sigma(X_t)dW_t,\ X_0 = x \in D, \tag{2.1}$$

is Markovian and has a continuous path. Let C^2 be the short for the $C^2(D)$-space[1]. For $f \in C^2$, denote the *infinitesimal generator* of $\{X_t\}_{t\geq 0}$ by

$$\mathcal{A}f(x) := \lim_{t\downarrow 0} \frac{\mathbb{E}_x f(X_t) - f(x)}{t},\ x \in D, \tag{2.2}$$

where $\mathbb{E}_x \cdot := \mathbb{E}[\cdot|\mathcal{F}_0] = \mathbb{E}[\cdot|X_0 = x]$ by the Markov property. If the limit on the right-hand side of (2.2) exists, we say $\{X_t\}_{t\geq 0}$ is a 1-dimensional *time-homogeneous diffusion process*. Correspondingly, the infinitesimal generator of $\{X_t\}_{t\geq 0}$ is explicitly given by

$$\mathcal{A}f(x) = \mu(x)\partial_x f(x) + \frac{1}{2}\sigma^2(x)\partial_{xx} f(x). \tag{2.3}$$

Example 2.1.1 (Brownian Motion)**.** Let $\{W_t\}_{t\geq 0}$ defined on $\mathbb{R}$ be a Brownian motion, then its infinitesimal generator is given by

$$\mathcal{G}f(x) = \frac{1}{2}\partial_{xx} f(x). \tag{2.4}$$

The first concept related to our work is the *existence* and *uniqueness* of solutions to SDEs. Intuitively, the existence of a unique solution guarantees that we can depict the sample path of $\{X_t\}_{t\geq 0}$ by using its specified SDE and a realisation of a Brownian motion path. In Chapter 6 of this thesis, a new stochastic process has been introduced. And the first thing we should be clear is that whether the process possesses a unique strong solution. The answer is given by the following theorem.

Theorem 2.1.2 (Existence, Uniqueness, and Square-Integrability)**.** *Let $K > 0$ be a constant, and assume that $\mu(\cdot)$, $\sigma(\cdot)$ satisfy the conditions*

$$|\mu(z) - \mu(y)| + |\sigma(z) - \sigma(y)| \leq K|z - y|, \tag{2.5}$$

$$\mu(y)^2 + \sigma(y)^2 \leq K^2(1 + y^2), \tag{2.6}$$

where $y, z \in D$. If $\mathbb{E}|X_0| < +\infty$, then there exists a unique, continuous and adapted process $\{X_t\}_{t\geq 0}$ which is a strong solution of SDE (2.1)*. Moreover, $\{X_t\}_{t\geq 0}$ is square-integrable,*

[1] A set of continuous functions defined on D that have continuous derivatives at least for the first 2 orders.

i.e., $\forall T > 0$ *and* $0 \leq t \leq T$*, there exists a constant* $C := C(K, T)$*, such that*

$$\mathbb{E}|X_t|^2 \leq C(1 + X_0^2)e^{Ct}.$$

Proof. Please refer to [68, Theorems 2.5 & 2.9, Section 5.2]. □

On the other hand, as a part of the study of the Markov process, very often we are interested in the *transition density* of $\{X_t\}_{t\geq 0}$. Our main research tool is using the *Kolmogorov Forward equation* (*Fokker-Planck equation*). Define the *adjoint operator* of $\mathcal{A}$ (in Equation (2.3)) as

$$\mathcal{A}^* g(u) := -\partial_u(\mu(u)g(u)) + \frac{1}{2}\partial_{uu}(\sigma^2(u)g(u)),\ g \in C^2 \text{ and } u \in D. \tag{2.7}$$

According to classical probability theory, the *fixed time* transition density, denoted by

$$p_x(u,t) := \frac{\mathbb{P}_x(X_t \in du)}{du},\ t > 0,\ \text{where } \mathbb{P}_x(\cdot) := \mathbb{P}(\cdot|X_0 = x), \tag{2.8}$$

solves the following Fokker-Planck equation:

$$\mathcal{A}^* p_x(u,t) = \partial_t p_x(u,t). \tag{2.9}$$

The initial condition is specified by $p_x(u,0) = \delta_x(u)$, where $\delta_x(u)$ is the *Dirac delta function*. In addition, by finding the *infinite time* distribution, we can further check whether a given process is *stationary*. Denote the *stationary distribution* by (note that such a distribution should be independent of the initial state x):

$$p(u) := \lim_{t\uparrow+\infty} p_x(u,t).$$

Then substitute $\partial_t p(u) = 0$ into (2.9), $p(u)$ solves

$$\mathcal{A}^* p(u) = 0, \tag{2.10}$$

given the full-integration condition $\int_D p(u)du = 1$ holds.

Later in Chapter 3 of this thesis, we provide a unified framework for finding the *first passage times (FPTs)* of diffusion processes. There are two basic requirements in applying our method. First, the process should be strong Markov; and secondly, the FPT of such a

process should be finite *a.s.* For a given diffusion process, the following two theorems can be used to check if these two technical conditions are satisfied.

Theorem 2.1.3 (Strong Markov Property)**.** *If conditions* (2.5) *and* (2.6) *are satisfied, then the solution* $\{X_t\}_{t\geq 0}$ *to SDE* (2.1) *is strong Markov.*

Proof. Since $\mu(\cdot)$ and $\sigma(\cdot)$ are continuous on D, therefore they are bounded on compact subsets of $D \subseteq \mathbb{R}$. Combine the Lipschitz continuity and linear growth conditions, $\{X_t\}_{t\geq 0}$ then has a unique strong solution. According to [68, Theorem 4.20, Section 5.4], we conclude that $\{X_t\}_{t\geq 0}$ is strong Markov. □

The finiteness of FPT can be justified by that $\{X_t\}_{t\geq 0}$ is a *recurrent process*. More precisely, a recurrent Markov process means, with probability 1 that the process will hit any predefined crossing level in its domain. Before stating the second theorem, we introduce the following notations related to the *scale function*. Define the left and right boundaries of D by l and r, respectively, i.e.

$$\partial D = \{l, r\}, \text{ with } -\infty \leq l < r \leq +\infty. \tag{2.11}$$

For the functions $\mu(\cdot)$ and $\sigma(\cdot)$, we introduce the *non-degeneracy* and *local-integrability* conditions by:

$$\sigma^2(y) > 0, \ \forall y \in D; \tag{2.12}$$

$$\int_{y-\delta}^{y+\delta} \frac{1+|\mu(z)|}{\sigma^2(z)} dz < +\infty, \ \forall y, \ y+\delta, \ y-\delta \in D \text{ with some } \delta > 0. \tag{2.13}$$

Consider a fixed number $c \in D$, define

$$s(y) := \int_c^y \exp\left\{-2\int_c^\xi \frac{\mu(\zeta)d\zeta}{\sigma^2(\zeta)}\right\} d\xi, \ y \in D \tag{2.14}$$

to be the scale function of $\{X_t\}_{t\geq 0}$. Then,

Theorem 2.1.4 (Recurrent Process)**.** *Under assumptions* (2.12) *and* (2.13)*, if*

$$\lim_{y\downarrow l} s(y) = -\infty, \ \textit{and} \ \lim_{y\uparrow r} s(y) = +\infty,$$

then $\{X_t\}_{t\geq 0}$ *is recurrent.*

Proof. Please refer to [68, Proposition 5.22, Section 5.5]. □

Example 2.1.5 (Ornstein-Uhlenbeck Process)**.** Let $\{X_t\}_{t\geq 0}$ defined on $\mathbb{R}$ be the *Ornstein-Uhlenbeck (OU)* process with

$$\mu(X_t) = \epsilon(\theta - X_t),\ \sigma(X_t) = \sigma, \tag{2.15}$$

where $\epsilon > 0$ is the mean-reversion rate, $\theta \in \mathbb{R}$ is the equilibrium level, and $\sigma > 0$ is the instantaneous volatility. The OU process is a strong Markov process which possesses a unique strong solution. Moreover, $\{X_t\}_{t\geq 0}$ is recurrent and the stationary distribution is Gaussian, with mean θ and variance $\frac{\sigma^2}{2\epsilon}$.

Now we introduce the last theorem of this section, known as the *time-change* technique for martingales. In practice, for the purpose of simplifying calculations, we usually want to reduce either $\mu(\cdot)$ or $\sigma(\cdot)$ to known forms. For example, one can use the *Girsanov theorem* to remove the drift term; or, as an alternative, the *stochastic clock* introduced in below enables us to simplify the diffusion term.

Theorem 2.1.6 (Dambis, Dubins & Schwarz Theorem)**.** *Let $\{M_t\}_{t\geq 0}$ be a continuous local-martingale generated by a completed Brownian filtration $\mathcal{F}^W$. If $\lim_{t\uparrow+\infty}\langle M\rangle_t = +\infty$ a.s., then there exists a Brownian motion $\{B_t\}_{t\geq 0}$ which is adapted to $\mathcal{F}^B$, and such that*

$$M_t = B_{\langle M\rangle_t}\ a.s.,\ 0 \leq t < +\infty.$$

Proof. Please refer to [68, Theorem 4.6, Section 3.4]. □

In the theorem above, it should be noticed that $\{B_t\}_{t\geq 0}$ and $\{M_t\}_{t\geq 0}$ are from two different but interconnected filtrations. In fact, for $0 \leq s < +\infty$, define the stopping time

$$T(s) = \inf\{t \geq 0 : \langle M\rangle_t > s\},$$

then $\mathcal{F}^B$ is given by the original filtration but which is indexed on the stochastic clock $T(s)$:

$$\mathcal{F}^B_s := \mathcal{F}^W_{T(s)},\ 0 \leq s < +\infty.$$

Example 2.1.7 (Cox-Ingersoll-Ross Process)**.** Let $\{X_t\}_{t\geq 0}$ defined on $\mathbb{R}^+ \cup \{0\}$ be the *Cox-Ingersoll-Ross (CIR)* process with[2]

$$\mu(X_t) = \epsilon(\theta - X_t),\ \sigma(X_t) = \sigma\sqrt{X_t}. \tag{2.16}$$

According to [50], $\{X_t\}_{t\geq 0}$ can be expressed via a *squared Bessel process* $\{Y_t\}_{t\geq 0}$. More precisely,

$$X_t = e^{-\epsilon t} Y_{\frac{\sigma^2}{4\epsilon}(e^{\epsilon t}-1)}, \tag{2.17}$$

where

$$dY_t = \frac{4\epsilon\theta}{\sigma^2}dt + 2\sqrt{Y_t}dW_t. \tag{2.18}$$

If we further consider the transform $Z_t = \sqrt{Y_t}$, then by definition and the Itô's lemma, $\{Z_t\}_{t\geq 0}$ is the *n-dimensional Bessel process (BES(n))* with SDE

$$dZ_t = \frac{n-1}{2Z_t}dt + dW_t, \tag{2.19}$$

where $n = \frac{4\epsilon\theta}{\sigma^2}$.

2.2 First Passage Time

The FPT, known also as the *first hitting time*, describes the randomness of time for which a stochastic process would spend to enter or exit a specific state. Let $\{X_t\}_{t\geq 0}$ defined on D solve SDE (2.1), and assume that $\{X_t\}_{t\geq 0}$ satisfies various conditions (especially with continuous path) that we have discussed in Section 2.1. Denote the *complement set* of D in $\mathbb{R}$ by $D^c := \mathbb{R} \setminus D$. Then,

$$\tau := \inf\{t \geq 0 : X_t \in D^c\} \tag{2.20}$$

defines a *stopping time*. We follow the convention that $\inf \emptyset = +\infty$.

In particular, for some constant $a \in \mathbb{R}$ and $D = (a, +\infty)$, Equation (2.20) defines the *single-side downward* FPT of $\{X_t\}_{t\geq 0}$. Similarly, by letting $D = (-\infty, a)$, we say τ is the *single-side upward* FPT of $\{X_t\}_{t\geq 0}$.

The FPT itself is a random variable. In order to find its probabilistic description, we

[2]Note that the volatility for the CIR process is only Hölder continuous, hence the existence result in Theorem 2.1.2 does not apply; nonetheless there exists a unique strong solution to the CIR SDE.

start with solving the corresponding *Laplace Transform (LT)* of the *FPT density (FPTD)*. Roughly speaking, there are two major ways of finding the LT of τ, namely the *martingale approach* and the *Markov approach*. Although derivations are different in these two methods, in the end, they both link the LT to the Dirichlet-type *Boundary Value Problem (BVP)*. In this section, we follow [101] and focus on theoretical settings under the Markov approach. The second step, finding the FPTD by inverting the LT, will be discussed in Section 2.3 and in other chapters of this thesis.

According to our assumptions, $\{X_t\}_{t\geq 0}$ is adapted to a *Brownian filtration* and has a continuous path. Therefore, the FPTs to either an open interval or its closure are equal *a.s.* (i.e. the boundary of D is *regular*). *W.l.o.g.*, we define

$$\mathbb{P}(\tau = 0 | X_0 \in D^c) = 1. \tag{2.21}$$

And as a result of (2.21), we can also show that

$$\mathbb{P}(\tau > 0 | X_0 \in D) = 1.$$

For a single-side level crossing problem, if we consider the *extended real set*, then the complement set of D will include $\{-\infty, +\infty\}$. In this case, since $\{X_t\}_{t\geq 0}$ is well-defined and should not explode, so we can further require

$$\mathbb{P}(\tau = +\infty | X_0 \in \{-\infty, +\infty\}) = 1. \tag{2.22}$$

On the other hand, we have also assumed that $\{X_t\}_{t\geq 0}$ is a recurrent process. Therefore, by definition, for the process starting in D, we have

$$\mathbb{P}(\tau < +\infty | X_0 \in D) = 1.$$

Consider that $\{X_t\}_{t\geq 0}$ is strong Markov. Based on our notations and assumptions above, we have the following result.

Theorem 2.2.1 (Killed Version Dirichlet-Type BVP)**.** *For $\beta \in \mathbb{C}$ with Real$(\beta) > 0$ (i.e.*

$\beta \in \mathbb{C}^+$), let $f(x) \in C^2$ be the unique solution to the killed version Dirichlet problem:

$$\mathcal{A}f(x) = \beta f(x),\ x \in D, \tag{2.23}$$

with boundary conditions

$$f(\partial D) = \underline{V},\ x \in \partial D, \tag{2.24}$$

where ∂D is defined on the extended real set and $\underline{V}$ is determined by conditions (2.21) *and* (2.22)*. Then*

$$f(x) = \mathbb{E}_x \left[e^{-\beta\tau} \right]. \tag{2.25}$$

Proof. Please refer to [101, Section 7.1]. □

There are a few points should be noticed on Theorem 2.2.1. First, even though we write $f(x)$ as a function of $x \in D \cup \partial D$, in fact, it also depends on the complex parameter β. Therefore, in this thesis, we will use either $f(x)$, or

$$f(x, \beta), \tag{2.26}$$

to refer to the LT of τ (Equation (2.25)). And correspondingly, the C^2 set in the theorem above should be understood as the set of functions defined on $(D \cup \partial D) \times \mathbb{C}^+$, and which are twice differentiable on the first argument and first order differentiable on the second argument, i.e.

$$C^2 := C^{2,1}\left((D \cup \partial D) \times \mathbb{C}^+\right). \tag{2.27}$$

Secondly, in the theorem above, we do not require the domain D to be bounded (actually for a single-barrier problem it is not); however, the function $f(x)$ is indeed bounded. To see this, consider the boundary condition (2.22), it implies $f(x) = 0$ for $x = \pm\infty$ and $\beta \in \mathbb{C}^+$.

The conclusion from Theorem 2.2.1 is very similar to that from the *Feynman-Kac theorem*; while for the second theorem, when we apply it on the stopping time, extra boundedness conditions on τ should be taken into account. Therefore, using the Feynman-Kac theorem would introduce further technical discussions in our work. In fact, by digging into the proof details[3] in [101, Section 7.1], one can find that the connection between ODE (2.23) and

[3]We refer to [68, Section 4.2] as a simpler example for understanding the link between the harmonic functions and the Dirichlet problem.

the probabilistic representation (2.25) is derived from the *mean-value property* of *harmonic functions*. And the idea behind the mean-value property is very akin to the concept of 'fair game' under the martingale settings. As a quick remark, we emphasise that the reason we choose the Markov version is due to its simplicity in technical treatments.

Example 2.2.2 (Single-Side FPT of Brownian Motion)**.** Let

$$X_t = x + W_t,\ t \geq 0,$$

be a Brownian motion starting from $x \in \mathbb{R}$. Then the LT for the FPT of $\{X_t\}_{t\geq 0}$ hitting a, is given by [18, Equation 2.0.1, Page 198]:

$$f_0(x, \beta) = e^{-\sqrt{2\beta}|x-a|}. \tag{2.28}$$

Moreover, the inverse transform (i.e. the FPTD) is given by

$$p_\tau^{(0)}(t) = \frac{|x-a|}{\sqrt{2\pi t^3}} e^{-\frac{(x-a)^2}{2t}}. \tag{2.29}$$

As an extension to (2.25) and Theorem 2.2.1, in the last part of this section, we introduce the Dirichlet problem with an extra Lagrange functional.

Theorem 2.2.3 (Killed Version Dirichlet-Type BVP with Lagrange Functional)**.** *Let $l(x)$ defined on D be continuous, and let $f(x) \in C^2$ be the unique solution to the killed version Dirichlet problem with Lagrange functional $l(x)$:*

$$\mathcal{A}f(x) - \beta f(x) = -l(x),\ x \in D, \tag{2.30}$$

with boundary conditions

$$f(\partial D) = \underline{0},\ x \in \partial D. \tag{2.31}$$

Then

$$f(x) = \mathbb{E}_x \left[\int_0^\tau e^{-\beta s} l(X_s) ds \right].$$

2.3 Inverse Laplace Transform Algorithm

In this section, we introduce three algorithms for computing the *inverse Laplace transform (ILT)*. These algorithms later will perform the benchmarking purpose.

Consider a real function $p(t)$ with $t \geq 0$ and a complex function $f(\beta)$ defined on $\mathbb{C}^+$. We say $f(\beta)$ is the LT of $p(t)$, if the integral exists:

$$f(\beta) = \mathcal{L}\{p(t)\}(\beta) := \int_0^\infty e^{-\beta t} p(t) dt. \tag{2.32}$$

In (2.32), by definition $\mathcal{L}$ is a *linear operator* on functions $p(t)$. Conversely, if $\mathcal{L}$ has an inverse, denoted by $\mathcal{L}^{-1}$, then we have

$$p(t) = \mathcal{L}^{-1}\{f(\beta)\}(t). \tag{2.33}$$

According to classical theory of linear operators, $\mathcal{L}^{-1}$ is also *linear*. And by the *Mellin inversion formula*, $\mathcal{L}^{-1}$ can be explicitly given by

$$\mathcal{L}^{-1}\{f(\beta)\}(t) := \frac{1}{2\pi i} \int_{a-i\cdot\infty}^{a+i\cdot\infty} e^{t\beta} f(\beta) d\beta. \tag{2.34}$$

The real number a in above should be chosen such that the real parts of all singularities in $f(\beta)$ are smaller than a. And since $e^{t\beta}$ is *analytic* on the positive half-plane, so the singularities of $f(\beta)$ are equivalent to those of $e^{t\beta} f(\beta)$.

One way of solving the inverse transform is to use *Jordan's lemma* and *Cauchy's residue theorem*. Denote the set of all singularities of $f(\beta)$ by

$$\mathcal{P} := \{\beta : |f(\beta)| = +\infty\}. \tag{2.35}$$

Then (2.34) can be further written as:

$$\mathcal{L}^{-1}\{f(\beta)\}(t) = \sum_{\hat{\beta} \in \mathcal{P}} Res\left(f(\hat{\beta}) e^{t\hat{\beta}}\right). \tag{2.36}$$

Nowadays, for most of the LT functions, we can find their inverse transforms from [9, Chapter V]. For example, using [9, Equation (1), Section 5.6], one can show that the inverse of (2.28) is indeed given by (2.29). However, there are still many LTs which may not have

closed-form inverses, or, they have not been found yet. Especially, for most of the FPTD LTs in this thesis, they are given in terms of ratios of special functions. Those LTs are very difficult (or even impossible) to be inverted explicitly. Therefore, we may need the help from numerical schemes.

Before demonstrating the main results in this section, we first recall the *initial-* and *final-value theorems* of LT. These two theorems are important to the algorithms which we will introduce soon; also, they will be constantly used in many proofs of this thesis.

Fact 2.3.1 (Initial- and Final-Value Theorems of LT)**.** *If $p(t)$ is bounded on $(0, +\infty)$, and its limits on $t \downarrow 0$ and $t \uparrow +\infty$ exist, then*

$$\lim_{t \downarrow 0} p(t) = \lim_{\beta \to +\infty} \beta f(\beta); \tag{2.37}$$

$$\lim_{t \uparrow +\infty} p(t) = \lim_{\beta \to 0^+} \beta f(\beta). \tag{2.38}$$

We now introduce three numerical schemes for the ILT. The contents below mainly follow from [1], and the basic idea is to express the inverse transform as a truncated series:

$$p(t) \approx \frac{1}{t} \sum_{k=0}^{n} \omega_k f\left(\frac{\alpha_k}{t}\right).$$

Theorem 2.3.2 (The Gaver-Stehfest (GS) Algorithm)**.** *Let M be a positive integer. For $1 \leq k \leq 2M$, let*

$$\zeta_k = (-1)^{M+k} \sum_{j=\lfloor (k+1)/2 \rfloor}^{k \wedge M} \frac{j^{M+1}}{M!} \binom{M}{j} \binom{2j}{j} \binom{j}{k-j},$$

where $\lfloor \cdot \rfloor$ and $\binom{\cdot}{\cdot}$ are the floor function and the binomial coefficients, respectively. Then the GS inverse, denoted by $p_{GS}(t)$, is given by

$$p_{GS}(t) = \frac{\ln(2)}{t} \sum_{k=1}^{2M} \zeta_k f\left(\frac{k \ln(2)}{t}\right).$$

Theorem 2.3.3 (The Euler Algorithm)**.** *Let M be a positive integer. For $0 \leq k \leq 2M$, let*

$$\alpha_k = \frac{M \ln(10)}{3} + i\pi k,$$

$$\psi_k = (-1)^k \xi_k,$$

where $\{\xi_k : 0 \le k \le 2M\}$ *is recursively determined by*

$$\xi_0 = \frac{1}{2};\ \xi_k = 1,\ \textit{for}\ 1 \le k \le M;\ \xi_{2M} = \frac{1}{2^M};$$

and

$$\xi_{2M-k} = \xi_{2M-k+1} + 2^{-M}\binom{M}{k},\ \textit{for}\ 0 < k < M.$$

Then

$$p_{Euler}(t) = \frac{10^{M/3}}{t}\sum_{k=0}^{2M}\psi_k Real\left(f\left(\frac{\alpha_k}{t}\right)\right).$$

Theorem 2.3.4 (The Talbot Algorithm)**.** *Let* M *be a positive integer. For* $0 \le k \le M-1$*, let*

$$\{\delta_k : 0 \le k \le M-1\},\ \{\gamma_k : 0 \le k \le M-1\}$$

be determined recursively by

$$\delta_0 = \frac{2M}{5};\ \delta_k = \frac{2k\pi}{5}\left(\cot\left(\frac{k\pi}{M}\right) + i\right),\ 0 < k < M;$$

and

$$\gamma_0 = \frac{1}{2}e^{\delta_0};\ \gamma_k = \left[1 + \frac{ik\pi}{M}\left(1 + \cot^2\left(\frac{k\pi}{M}\right)\right) - i\cot\left(\frac{k\pi}{M}\right)\right]e^{\delta_k},\ 0 < K < M.$$

Then

$$p_{Talbot}(t) = \frac{2}{5t}\sum_{k=0}^{M-1} Real\left(\gamma_k f\left(\frac{\delta_k}{t}\right)\right).$$

Proof. For proofs of Theorems 2.3.2, 2.3.3, and 2.3.4, please refer to Sections 4, 5, and 6 of [1], respectively. □

Among those three numerical schemes, only the GS algorithm dose not involve computing complex numbers. The numerical accuracy of GS algorithm, evaluated in terms of relative errors, is given by

$$\left|\frac{p(t) - p_{GS}(t)}{p(t)}\right| \approx 10^{-0.9M}.$$

The original paper also provides a metric to measure efficiencies of different algorithms.

Consider the ratio between *significant digits produced* and *precision required*, the GS algorithm has an efficiency of 0.4, Euler algorithm provides 0.6, and the Talbot algorithm is 0.6 as well. In later numerical sections of this thesis, for most of the time we will choose Talbot algorithm with $M = 6$.

2.4 Portfolio Selection, Risk Management and Capital Allocation

The investment activity of human beings could be traced back to 1700 BC. As it is known by people, in the *Code of Hammurabi*, for the first time the investment in land was protected by law. When history came to the 20th century and the modern financial market was built, the mass media gave those security investors a new name, speculators. Although from time to time, it is difficult to differentiate speculation and investment, however, a wise investor should always know where his or her investment risk lies on. From this point of view, the investment and the risk management should always be linked together. In this section, we review major concepts and classical theorems in portfolio selection and risk management. The contents below will be referred to later in Chapters 7 and 8 of this thesis.

Roughly speaking, we can split the investment activity into two groups, namely the direct investment and the portfolio investment. For the first terminology, we refer to the investment activities that would impact the day-to-day operation of a targeted company. The return of such an investment will come from the growth in values of the company. Examples of the direct investment would be venture investment on start-ups, M&A investment, etc. The focus of this thesis, however, is in the second group, the portfolio investment.

The portfolio investment can be seen as a kind of passive investment. By selecting a pool of securities and determining the amount of buying or selling on these assets, the investor earns the return on these securities according to their market price changes. We refer to this selected pool as a *portfolio*. In order to specify the *profit* and *loss* (PnL) of the portfolio, we introduce the following notations.

Consider $n \in \mathbb{N}_0$, where $\mathbb{N}_0 = \mathbb{N} \cup \{0\}$, and consider an integer set

$$I = \{i : 0 \leq i \leq n\}, \tag{2.39}$$

which represents the index of underlying assets. At time $t \geq 0$, we denote the *market price* (price or log-price) of each asset by

$$P_t^{(i)},\ i \in I. \tag{2.40}$$

Note that, for each $i \in I$, $\left\{P_t^{(i)}\right\}_{t\geq 0}$ can be seen as a stochastic process. Their observations at integer-indexed time, denoted by

$$\hat{P}_{t_j}^{(i)},\ i \in I,\ j \in \mathbb{N}_0, \tag{2.41}$$

then form a time-series.

Now we fix an index $i \in I$ and a time $t > 0$. Let $\Delta t \geq 0$ also be fixed and which refers to a *time step*. The PnL of asset i, at time t, then is defined as the difference between the market prices at t and $t - \Delta t$. However, there are two ways of calculating the difference, namely the *absolute return* and the *log-return*. The former one is very often used in computing the returns of interest rates, while the log-return is usually used in equity market. In this thesis, we assume that the market value of $P_t^{(i)}$ is already *normalised*, by which we mean $P_t^{(i)}$ is the actual market price, if the absolute return is needed; while on the other hand, if we need to compute the log-return, then $P_t^{(i)}$ refers to the log-transform of the market price. According to our normalisation, the PnL of i at t, is given by

$$X_t^{(i)} := P_t^{(i)} - P_{t-\Delta t}^{(i)}.$$

The observed PnL is correspondingly given by

$$\hat{X}_t^{(i)} := \hat{P}_t^{(i)} - \hat{P}_{t-\Delta t}^{(i)}.$$

From now onward, and unless specified, for abbreviation we do not differentiate the theoretical and observed notations, i.e. we will use $P_t^{(i)}$ and $X_t^{(i)}$ as the (observed) market price and the (observed) PnL.

Consider now we fix the index $i \in I$ only, and let $T > 0$ be a fixed time, then the set $\left\{X_t^{(i)} : 0 \leq t \leq T\right\}$ forms a *distribution of PnL* for asset i within the time range $(0, T]$. We

denote this PnL distribution by

$$X_i(T) := Dist\left(\left\{X_t^{(i)} : 0 < t \leq T\right\}\right), \tag{2.42}$$

and for short, by ignoring the argument T, $X_i := X_i(T)$.

Based on our notations above, the portfolio's PnL at time t is denoted by

$$\Psi_t := \sum_{i \in I} X_t^{(i)},$$

and the portfolio's PnL distribution in time range $(0, T]$ is correspondingly

$$\Psi := \Psi(T) = \sum_{i \in I} X_i. \tag{2.43}$$

Another relevant concept to the portfolio's PnL is the investment *strategy*. For a fixed $i \in I$, consider an $\mathcal{F}_{t^-}$ (or $\mathcal{F}_{t-\Delta t}$) measurable process $w_t^{(i)}$ to be the holding amount (positive or negative) of asset i. Note that $w_t^{(i)}$ is determined at time t^- (or $t - \Delta t$). We call the collection

$$w(T) := \left\{w_t^{(i)} : i \in I,\ 0 < t \leq T\right\}$$

an investment strategy of the portfolio.

In the notations of (2.42) and (2.43), we do not include the strategy symbol explicitly. In fact, there are two ways of understanding the symbol X_i. On the one hand, as defined in many literatures of portfolio theory, X_i is the PnL distribution of 1 unit investable asset (e.g. one share of stock or one bond contract). However, on the other hand, consider $Y_t^{(i)}$ and $w_t^{(i)}$ to be the return of 1 unit investable asset and the strategy of such an asset, respectively, then

$$X_t^{(i)} = w_t^{(i)} Y_t^{(i)}$$

defines the PnL of asset i at time t, under the strategy $w(T)$. Therefore, X_i is the PnL distribution of asset i by taking the strategy into account. In this thesis, given not causing confusion, we will use the notation X_i for both of those two scenarios. But if necessary, we will specify X_i with one clear meaning.

Now we come back to the portfolio investment problem. More precisely, we are dealing

with the question of how to select the portfolio I and determine the strategy $w(T)$. In the work [83, 84] of H. Markowitz, he referred to this problem as portfolio selection. Different to most of the studies in his time, H. Markowitz did not only consider the return, but also introduced the risk into his framework. The concept of the *efficient portfolio (mean-variance portfolio theory)* was built since then. Until today, there are still many literatures that discuss the variations of the efficient portfolio under different scenarios, see e.g. [79, 82, 85].

In Chapter 8 of this thesis, we study the possibility of identifying the trading portfolio I based on our first hitting time works; the mean-variance portfolio theory is regarded as our investment benchmark. Therefore, we only review the most basic settings of the efficient portfolio framework in below.

Consider a determined set I and the associated PnL distribution $\{Y_i : i \in I\}$. Let $\underline{w}$ be a trading strategy at time T^+. Further, let

$$\underline{r} := [r_1, ..., r_n]^T ,$$

where $r_i := \mathbb{E}[Y_i]$ is the *expected return* of 1 unit asset i; and denote the *risk-matrix* by

$$\Sigma := Cov\left(\{Y_i : i \in I\}\right).$$

The efficient portfolio (without constraint on short-selling) is then the solution to the maximisation problem

$$\underline{w}^* = \arg\max_{\underline{w}} \left\{ \underline{w}^T \underline{r} - \frac{\lambda}{2} \underline{w}^T \Sigma \underline{w} \right\}, \tag{2.44}$$

subject to

$$\underline{w}^T \mathbb{I} = 1,$$

where λ is the risk preference parameter. By setting $\lambda = 1$ and solving the *Lagrange multiplier* of the maximisation problem, we have

$$\begin{cases} \underline{w}^* = \Sigma^{-1} \left(\underline{r} - \frac{\mathbb{I}^T \Sigma^{-1} \underline{r} - 1}{\mathbb{I}^T \Sigma^{-1} \mathbb{I}} \mathbb{I} \right), \\ \mathbb{E}\left[\Psi^*\right] = \underline{r}^T \Sigma^{-1} \underline{r} - \underline{r}^T \Sigma^{-1} \frac{\mathbb{I}^T \Sigma^{-1} \underline{r} - 1}{\mathbb{I}^T \Sigma^{-1} \mathbb{I}} \mathbb{I}, \end{cases}$$

where $\mathbb{I}$ is the vector with all entries to be one and Ψ^* is the portfolio distribution under the strategy $\underline{w}^*$.

In the settings above, we treat the covariance matrix as a *risk measure* to the portfolio. However, in the area of modern quantitative risk management, more meaningful risk measures have been proposed. In below we recall relevant concepts in quantitative risk management and capital allocation. Those results will be referred to in Chapter 7 later.

Definition 2.4.1 (Risk Measure)**.** Let X be defined on the set of all essentially bounded random variables $L^\infty(\Omega, \mathcal{F}, \mathbb{P})$, then a risk measure ρ is a real map from $L^\infty(\Omega, \mathcal{F}, \mathbb{P})$ to $\mathbb{R}$:

$$\begin{aligned} &\rho \ : \ L^\infty(\Omega, \mathcal{F}, \mathbb{P}) \to \mathbb{R} \ ; \\ &X \in L^\infty(\Omega, \mathcal{F}, \mathbb{P}) \to \rho(X). \end{aligned}$$

The risk measure ρ evaluates the risk from a PnL distribution. A famous example is the *Value-at-Risk (VaR)*, which was first formally introduced by J.P. Morgan [91] in the 1990s; and afterwords the Basel Committee on Banking Supervison (BCBS) demanded the main financial institutions to meet the VaR-based minimum capital requirements [97]. However, in application, people find that the VaR metric is counterintuitive: the VaR of a diversified portfolio may not be smaller than the sum of standalone VaRs on each component of the portfolio. In order to make sure a risk measure is intuitively reasonable, people further introduced the concept of *coherent risk measure*.

Definition 2.4.2 (Coherent Risk Measure)**.** For shorthand, denote $L^\infty(\Omega, \mathcal{F}, \mathbb{P})$ by L^∞. A risk measure ρ is coherent if it satisfies the following properties:

1. **Subadditivity**, for all $X, \ Y \in L^\infty$, $\rho(X + Y) \leq \rho(X) + \rho(Y)$;
2. **Monotonicity**, for all $X, \ Y \in L^\infty$ with $X \leq Y \ a.s.$, $\rho(X) \geq \rho(Y)$;
3. **Positive homogeneity**, for all $\lambda \geq 0$ and $X \in L^\infty$, $\rho(\lambda X) = \lambda \rho(X)$;
4. **Translation invariance**, for all $c \in \mathbb{R}$ and $X \in L^\infty$, $\rho(X + c) = \rho(X) - c$.

Example 2.4.3 (Expected Shortfall)**.** Let $\Psi \in L^\infty$ be a portfolio's PnL distribution, the *expected shortfall (ES)* of Ψ at the confidence level α is defined as

$$ES_\alpha(\Psi) = \frac{1}{1-\alpha} \int_\alpha^1 VaR_u(\Psi) du,$$

where

$$VaR_u(\Psi) = q_u(-\Psi)$$

is the VaR of Ψ at level u, and $q_u(\cdot)$ is the *quantile-function* of the distribution. The ES is a coherent risk measure. Moreover, under proper conditions [122], the ES is equivalently defined as

$$ES_\alpha(\Psi) = -\mathbb{E}\left[\Psi | \Psi \leq -VaR_\alpha(\Psi)\right]. \tag{2.45}$$

In practice, a business needs to know its total risk. But on the other hand, it is even more important for the business to understand the composition of such a total risk. This raises the issue of *(risk) capital allocation*. In this thesis, we define a valid capital allocation scheme as follows.

Definition 2.4.4 (Capital Allocation)**.** Let ρ be a risk measure from Definition 2.4.1, $\Psi \in L^\infty$ be a portfolio's PnL distribution defined by (2.43), and $\{X_i : i \in I\}$ be the PnL distributions of each component in the portfolio, then a well-defined capital allocation on position i, denoted by

$$\rho\left(X_i | \Psi\right),$$

should satisfy the following conditions:

1. **Full-allocation**, $\rho(\Psi) = \sum_{i \in I} \rho\left(X_i | \Psi\right)$;
2. **Associativity**, for a subset $J \subset I$, $\rho\left(\sum_{j \in J} X_j | \Psi\right) = \sum_{j \in J} \rho\left(X_j | \Psi\right)$.

In 1999, D. Tasche [122] looked into the allocation problem from a capital-efficiency perspective. Define the *return on risk adjusted capital (RORAC)* of asset i by

$$RORAC(X_i|\Psi) := \frac{r_i}{\rho\left(X_i|\Psi\right)}. \tag{2.46}$$

If the risk allocation is *RORAC-compatible* (see [122]), then $\rho\left(X_i|\Psi\right)$ is uniquely determined by the *Euler's principle*:

$$\rho_{Euler}\left(X_i|\Psi\right) = \lim_{h \downarrow 0} \frac{\rho(\Psi + hX_i) - \rho(\Psi)}{h}.$$

On the other hand, in 2001, M. Denault [38] studied the allocation problem under game-theoretic settings. He proposed the *coherence of allocation principle* and shown that the

Euler principle is a coherent risk allocation scheme. Moreover, based on the works of [14, 90, 113, 114], M. Denault proposed two allocation frameworks, namely the *Shapley* and the *Aumann-Shapley* allocations; while the latter one, was shown to be consistent with the Euler's allocation principle. We will discuss more details of those allocations in Chapter 7.

2.5 Table of Nomenclature

2.5.1 Abbreviation

ODE	*Ordinary Differential Equation*	p. 12
PDE	*Partial Differential Equation*	p. 39
SDE	*Stochastic Differential Equation*	pp. 5, 30
OU	*Ornstein Uhlenbeck Process*	pp. 9, 29
CIR	*Cox-Ingersoll-Ross Process*	pp. 10, 80
BES(n)	*Bessel Process with Order n, Equation* (2.19)	pp. 10, 68
FPT	*First Passage Time (First Hitting Time)*	pp. 7, 29
FPTD	*First Passage Time Density*	pp. 11, 30
BVP	*Boundary Value Problem*	pp. 11, 31
LT	*Laplace Transform*	pp. 11, 30
ILT	*Inverse Laplace Transform*	pp. 14, 37
PnL	*Profit and Loss*	pp. 17, 134
VaR	*Value-at-Risk*	pp. 21, 132
ES	*Expected Shortfall*	pp. 21, 132
FRTB	*Fundamental Review of Trading Book*	pp. 132, 134
RF	*Risk Factor*	pp. 134, 148
LH	*Liquidity Horizon*	pp. 134, 144
CM	*Commodity Asset Class*	pp. 134, 153

to be continued

CR	*Credit Asset Class*	pp. 134, 154
EQ	*Equity Asset Class*	pp. 134, 154
FX	*Foreign Exchange Asset Class*	pp. 134, 153
IR	*Interest Rate Asset Class*	pp. 134, 154
IMA	*Internal Modelling Approach*	pp. 132, 137
IMCC	*Internal Model Capital Charge for Modellable Risk Factors*	pp. 134, 143
F,C	*Full and Current Set*	pp. 136, 137
R,C	*Reduced and Current Set*	pp. 136, 147
R,S	*Reduced and Stress Set*	pp. 137, 136
SE	*Scenario Extraction*	pp. 142, 143
RORAC	*Return on Risk Adjusted Capital*	pp. 22, 132
CAS	*Constrained Aumann-Shapley*	pp. 144, 145
TSI	*Trading Signal Identification*	p. 162
w.l.o.g.	*Without Loss of Generality*	p. 11
a.s.	*Almost Surely*	pp. 8, 31
w.r.t.	*With Respect to*	pp. 32, 33
i.i.d.	*Identically Independent Distribution*	pp. 100, 139

2.5.2 Set and Space

$\mathbb{R}$	*Real Space*	pp. 5, 30
$\mathbb{R}^+$	*Set of Positive Real Numbers*	pp. 10, 35
$\mathbb{N}$	*Set of Natural Numbers*	pp. 17, 34
$\mathbb{N}_0$	$\mathbb{N} \cup \{0\}$	pp. 17, 115

to be continued

$\mathbb{C}$	*Complex Space*	p. 11
$\mathbb{C}^+$	*Positive Half Plane on* $\mathbb{C}$	p. 12
C^2	*Set of Twice Continuously Differentiable Functions*	pp. 6, 12
$C^{2,1}$	*Alternative Notation of* C^2, *See e.g. Equation* (2.27)	p. 12
D	*Domain of SDE; an Open Interval on* $\mathbb{R}$	pp. 5, 30
∂D	*General*[4] *Boundaries of* D, *See e.g. Equation* (2.11)	pp. 8, 37
∂D_a	*Single Side Boundaries of* D, *Equations* (3.2), (3.3)	p. 31
D^c	*Complement Set of* D *on* $\mathbb{R}$	p. 10
I	*Set of Consecutive Finite Integers,* $I \subset \mathbb{N}_0$	p. 17

2.5.3 Probability and Stochastic Process

$\mathbb{P}$	*Probability Measure*	p. 5
$\mathbb{E}$	*Expectation*	p. 6
Cov	*Covariance Matrix*	p. 20
$\mathcal{F}^W$, $\mathcal{F}^B$	*Filtrations Generated by Brownian Motion*	pp. 9, 31
$(\Omega, \mathcal{F}, \mathbb{P})$	*General Probability Space*	p. 21
$\left(\Omega, \mathcal{F}, \{\mathcal{F}_t\}_{t\geq 0}, \mathbb{P}\right)$	*Probability Space Generated by Brownian Filtration*	pp. 5, 30
$\mathbb{P}_x$	*Conditional Probability on* $X_0 = x$ *or* $\mathcal{F}_0$	pp. 7, 31
$\mathbb{E}_x$	*Conditional Expectation on* $X_0 = x$ *or* $\mathcal{F}_0$	p. 6
$\{W_t\}_{t\geq 0}$	*Standard Brownian Motion*	p. 6
$\{X_t\}_{t\geq 0}$	*Time-Homogeneous Diffusion Process, Equation* (2.1)	p. 5

to be continued

[4] In later sections we also use this notation as the simplified version of ∂D_a, with $a = 0$.

$\langle M \rangle_t$	*Quadratic Variation of* $\{M_t\}_{t\geq 0}$ *at time* t	p. 9
τ	*Single Side Constant Barrier FPT*	pp. 10, 31
$\left\{P_t^{(i)},\ i \in I\right\}_{t\geq 0}$	*Normalised Theoretical Price*	p. 18
$\left\{\hat{P}_{t_j}^{(i)},\ i \in I\right\}_{j\in\mathbb{N}_0}$	*Observation of* $P_t^{(i)}$ *at Integer-Indexed Time*	p. 18
$L^\infty,\ L^\infty(\Omega, \mathcal{F}, \mathbb{P})$	*Set of Bounded Random Variables*	p. 21
$X_i,\ i \in I$	*PnL Distribution of Asset* i	p. 19
Ψ	*Portfolio PnL Distribution*	p. 19

2.5.4 Operation and Operator

$\cup, \cap$	*Set Union and Set Intersection*	p. 10
$\setminus$	*Set Subtraction*	p. 10
$\subset, \subseteq$	*Exclusive and Inclusive Subsets*	pp. 8, 22
$\wedge$	*Minimum Between Two Quantities*	p. 35
$\sim$	*Asymptotic Equality of Two Functions*[5]	pp. 47, 73
$⨍$	*Cauchy Principal Value*	p. 81
$o(\cdot)$	*Little-o Notation*	pp. 34, 75
$O(\cdot)$	*Big-O Notation*	pp. 37, 52
$:=$	*Definition Operator*	pp. 6, 31
$'$	*Differentiation Operator*	p. 32
$\partial_\cdot$	*Partial Differentiation Operator*	pp. 6, 35
$\mathcal{G}$	*Standard Brownian Motion Generator*	p. 6
$\mathcal{A}$	*Generator of Time-Homogeneous Diffusion Process*	p. 6
$\mathcal{A}^*$	*Adjoint Operator of* $\mathcal{A}$	p. 7

to be continued

[5]The formal definition should be the ratio of two functions with the limit to be 1. However, in this thesis, as it does not affect our results, we will also use it for the short notation of Big-O: $\cdot = O(\cdot)$.

$\mathcal{L}$	*LT Operator*	p. 14
$\mathcal{L}^{-1}$	*ILT Operator*	p. 14

2.5.5 Function

$p(u)$	*Stationary Distribution Density*	p. 7
$p_x(u,t)$	*Transition Density at Fixed Time t*	p. 7
$s(y)$	*Scale Function, Equation* (2.14)	p. 8
f, $f(x)$, $f(\beta)$, $f(x,\beta)$	*LT of FPTD for General Diffusion Process*	pp. 12, 33
f_0, $f_0(x)$, $f_0(\beta)$, $f_0(x,\beta)$	*LT of Brownian Motion FPTD*	pp. 13, 37
$f_i,\ i \in I$	*i-th Order Perturbed Expansion of f*	pp. 33, 44
$f^{(N)} = \sum_{i=0}^{N} f_i,\ N \in \mathbb{N}_0$	*N-th Order LT Approximation of f*	pp. 35, 46
$p_\tau(t) = \mathcal{L}^{-1}\{f(\beta)\}(t)$	*FPTD of General Diffusion Process*	p. 35
$p_\tau^{(0)}(t)$	*FPTD of Brownian Motion*	p. 13
$p_\tau^{(N)}(t) = \mathcal{L}^{-1}\left\{f^{(N)}(\beta)\right\}(t)$	*N-th Order FPTD Approximation of $p_\tau(t)$*	pp. 35, 46
$q_\tau(t) = p_\tau(t) - p_\tau^{(N)}(t)$	*Perturbed FPTD Error Function*	p. 35
$\eta(x,t) = \mathcal{L}^{-1}\{\partial_x f_N(x,\beta)\}(t)$	*Error Estimation Function*	p. 35
$\rho(\cdot)$	*Risk Measure*	p. 21
$\rho(\cdot\|\cdot)$	*Risk Capital Allocation*	p. 22
$q_u(\cdot)$	*Quantile Function at Confident Level u*	p. 21 p. 21
$\mathbf{1}_{\{\cdot\}}$	*Indicator Function*	p. 36
$\lfloor\cdot\rfloor$, $\lceil\cdot\rceil$	*Floor/Ceiling Functions*	p. 15

to be continued

$Real(\cdot)$	*Real Part of a Function*	p. 12
$\delta_x(u)$	*Dirac Delta Function*	p. 7
$\binom{\cdot}{\cdot}$	*Binomial Coefficient*	p. 15
$\sinh(\cdot)$	*Hyperbolic Sin Function*	pp. 56, 98
$\cosh(\cdot)$	*Hyperbolic Cos Function*	p. 98
$\mathrm{sinc}(\cdot) = \frac{\sin(\pi x)}{\pi x}$	*Sinc Function*	p. 100
$D_\cdot(\cdot)$	*Parabolic Cylinder Function*	pp. 44, 46
$\Gamma(\cdot)$	*Gamma Function*	pp. 48, 101
$IG(x, a, b)$	*Density of Inverse Gamma Distribution with shape parameter a and scale parameter b*	p. 51
$IG(a, b)$	*Inverse Gamma Distribution*	p. 103
$M(\cdot,\cdot,\cdot) = {}_1F_1(\cdot,\cdot,\cdot)$	*Kummer's function (Confluent Hypergeometric Function)*	pp. 48, 105
$K_\cdot(\cdot)$	*Modified Bessel Function of the Second Kind*	p. 69
$I_\cdot(\cdot)$	*Modified Bessel Function of the First Kind*	p. 80
$E_1(\cdot)$	*Exponential Integral Function*	p. 70
$\mathrm{Erfc}(\cdot)$	*Complementary Error Function*	p. 108

Chapter 3

Explicit Asymptotics on the First Passage Times of Diffusion Processes

This chapter presents a unified framework for solving first passage time density asymptotics of time-homogeneous diffusion processes. According to the killed version potential theory and the perturbation theory, we are able to deduce closed-form solutions for probability densities of single-side level crossing problems. The framework is applicable to diffusion processes with continuous drift functions, and a recursive system in the frequency domain has been provided. Besides, we derive a probabilistic representation for error estimation. The representation can be used to evaluate deviations in perturbed density functions. In Chapters 4 and 5 of this thesis, we apply the framework to the OU and Bessel processes to find closed-form approximations for their first passage times; another successful application is given by Chapter 6, where a newly introduced economic bubble model has been discussed. Numerical results are provided at the end of each separate chapter.

3.1 Introduction, Motivation, and Literature Review

The interest of understanding the FPT could be traced back to the early 20th century [6, 109]. Known also as the *first hitting time*, the FPT defines a random time that a stochastic process would visit a predefined state. The phenomenon of uncertainty in time is often observed from

natural or social science. Therefore, within a century the FPT has been actively studied in economics, physics, biology, etc. [32, 93, 103, 106].

Depending on various types of underlying processes and hitting boundaries, the FPT itself consists of a large cluster of different researches. We refer to [4, 16, 94, 118] for a non-conclusive review. Among those researches, especially in the area of mathematical finance and insurance, single-side constant-barrier crossing problem is one of the most commonly studied, e.g. [7, 36]. A general approach of solving such a problem starts with finding the LT of the FPTD. The LT usually comes from a unique solution to a second order non-homogeneous ODE with Dirichlet-type boundary values [39, 60]. For many familiar diffusion processes, the LTs have been solved and are listed in [18]. However, those LTs usually are expressed in terms of special functions and only a few of them have explicit inverse transforms. Therefore, many efforts have been made on the numerical inverse side. We refer to [1] for more details. Alternatively, using spectral theorem on linear operators [62, 70, 71] one can simplify the original LT. Under certain circumstances, closed-form FPTDs could be acquired through series representations [3, 77]. But people may find that the spectral decomposition approach has convergence issues for small t. In this chapter, our object is to apply the perturbation theory and solve explicit asymptotics of FPTDs for general single-side level crossing problems.

Consider a filtered probability space generated by Brownian motion $\left(\Omega, \mathcal{F}, \{\mathcal{F}_t\}_{t\geq 0}, \mathbb{P}\right)$. Let D be an open interval on $\mathbb{R}$ and $h(\cdot)$ be a real-valued continuous function defined on D. Our underlying process is from a class of SDEs in (2.1). We require these SDEs having at least weak solutions and being strong Markov. More precisely, we assume

$$dX_t = \epsilon h(X_t)dt + dW_t,\ X_0 = x \in D. \tag{3.1}$$

Under our settings, ϵ is a real parameter and it should properly define $\{X_t\}_{t\geq 0}$ on the domain. For the convenience of deduction, we set the volatility to be a constant. If a time-homogeneous diffusion coefficient $\sigma(\cdot)$ is given, one may refer to Theorem 2.1.6 or [105, Theorem 1.6], to retrieve an SDE in (3.1) by a stochastic clock. Also, consider a hitting level $a \in \mathbb{R}$, we specify two types of boundaries on D:

$$\partial D_a^u := \{a, +\infty\},\ \partial D_a^l := \{-\infty, a\}, \tag{3.2}$$

namely boundaries for the upper- and lower-regions. For shorthand, we use ∂D_a to represent single sided boundaries without labelling directions. By suppressing x and a, we define the FPT of $\{X_t\}_{t\geq 0}$ from x to a through

$$\tau := \inf\{t > 0 : X_t \in \partial D_a\}. \tag{3.3}$$

Note that the Brownian filtration $\{\mathcal{F}_t\}_{t\geq 0} := \left\{\mathcal{F}_t^W\right\}_{t\geq 0}$ is continuous. According to our discussions in Section 2.2, Chapter 2, τ is regular at the boundary a of the domain. In addition, for $x \in D$, it is guaranteed that $\mathbb{P}_x(\tau > 0) = 1$.

For those FPTs which are finite *a.s.*, we are interested in acquiring their explicit distributions. Clearly, when $h(x) \equiv 0$ (standard Brownian motion), the distribution of τ is given by inverse Gaussian (or inverse Gamma, equivalently) [18]. However, for most of non-trivial drifts, there is no closed-form solution. An example is $h(x) = x$ and which corresponds to the OU process. In this case, the explicit density is only available by restricting $a = 0$ [49].

In this chapter, we apply perturbation technique [57] to solve Dirichlet-type BVPs. By inverting the perturbed LTs from the frequency domain, where those LTs usually have much simpler forms, we then are able to derive closed-form densities in the time domain. The main contribution of our work is to provide a unified recursive framework for solving the single barrier hitting problem. And according to the killed version of potential theory [101], we prove convergence and error estimation results. As illustrations, we show perturbed FPTDs of OU and Bessel processes in Chapters 4 and 5. An application on the economic bubble (exponential-Shiryaev) process is discussed in Chapter 6. Theoretical results in this chapter are confirmed via the following three chapters.

The rest of this chapter[1] is organised as follows. Section 3.2 introduces the perturbed BVP. In Section 3.3, we present the error estimation from the perturbation. Section 3.4 provides a recursive framework for solving the perturbed LTs under the frequency domain. And in appendices of this chapter, we demonstrate further results from our framework. These results may not be closely linked to the work in this thesis, but potentially they could be used in later research.

[1] A conclusion of Chapters 3, 4, and 5 will be given at the end of Chapter 5.

3.2 Perturbed Dirichlet Problem

We follow our settings in Chapter 2, and let $\{X_t\}_{t\geq 0}$ be the solution of SDE (3.1). Consider a function $f \in C^2$, we assume the infinitesimal generator $\mathcal{A}f(x)$ of $\{X_t\}_{t\geq 0}$ exists for all $x \in D$. Then $\mathcal{A}$ is explicitly given by

$$\mathcal{A}f(x) = \epsilon h(x) f^{'}(x) + \mathcal{G}f(x),$$

where $\mathcal{G}$ is the infinitesimal generator of a standard Brownian motion (Example 2.1.1). The notation $^{'}$ in above refers to the derivative *w.r.t.* x, i.e.

$$f^{'} := \partial_x f.$$

Throughout this thesis, we will use these two notations above interchangeably.

Consider $\beta \in \mathbb{C}^+$, and define

$$f(x,\beta) := \mathbb{E}_x \left[e^{-\beta\tau} V\left(X_\tau\right) \right], \tag{3.4}$$

where $V(\cdot)$ is a finite function and τ is given in (3.3). It is clear by our construction that $\{X_t\}_{t\geq 0}$ is continuous over stopping times. On the other hand, by our assumption in Section 3.1, $\{X_t\}_{t\geq 0}$ is a strong Markov process. According to the killed version potential theory [101], $f(x,\beta)$ in (3.4) then is the unique solution to the following Dirichlet problem:

$$\mathcal{A}f(x) = \beta f(x),\ x \in D; \tag{3.5}$$

and the corresponding boundary conditions are given by

$$f(\partial D_a) = \left[V(a), V(\pm\infty)\right]^T, \tag{3.6}$$

where $V(\pm\infty)$ depends on the direction of crossing. Denote by

$$\underline{V} := \left[V(a), V(\pm\infty)\right]^T.$$

Then refer to (3.4), (2.21), (2.22), and Theorem 2.2.1, by setting $V(a) = 1$ and $V(\pm\infty) = 0$,

we immediately find that the solution to BVP (3.5) and (3.6) is the LT for the density function of τ:

$$f(x,\beta) = \mathbb{E}_x\left[e^{-\beta\tau}\right].$$

Following this original BVP, in the next step, we apply perturbations on ϵ and find the perturbed BVPs accordingly. The perturbation approach is a common technique in solving asymptotics for complex systems. It has been successfully applied in quantum physics and mathematical finance [35, 45, 110]. Traditionally, it is required that the perturbation parameter should be small. However, we will show later, this is not necessary in our case.

For abbreviation, we ignore the function arguments in following contents. By default, all implicit operations are *w.r.t.* x.

Consider a sequence of C^2-functions $\{f_i\}_{i\geq 0}$ such that, f can be expressed as

$$f = \sum_{i=0}^{\infty} \epsilon^i f_i. \tag{3.7}$$

Substitute (3.7) into (3.5), and by the linearity of operator $\mathcal{A}$, we have

$$\begin{aligned}
\mathcal{A}f &= \sum_{i=0}^{\infty} \epsilon^i \left(\epsilon h f_i^{'} + \mathcal{G} f_i\right) \\
&= \beta f \\
&= \sum_{i=0}^{\infty} \epsilon^i \beta f_i,
\end{aligned}$$

i.e.

$$\sum_{i=0}^{\infty} \epsilon^i \left(\epsilon h f_i^{'} + \mathcal{G} f_i\right) = \sum_{i=0}^{\infty} \epsilon^i \beta f_i, \ \forall x \in D. \tag{3.8}$$

Move the right-hand side of (3.8) to the left-hand side, and rearrange terms, we further get

$$\begin{aligned}
\sum_{i=0}^{\infty} \epsilon^i \left(\epsilon h f_i^{'} + \mathcal{G} f_i\right) - \sum_{i=0}^{\infty} \epsilon^i \beta f_i &= \mathcal{G} f_0 - \beta f_0 + \sum_{i=0}^{\infty} \epsilon^{i+1} h f_i^{'} + \sum_{i=1}^{\infty} \epsilon^i \mathcal{G} f_i - \sum_{i=1}^{\infty} \epsilon^i \beta f_i \\
&= \mathcal{G} f_0 - \beta f_0 + \sum_{i=1}^{\infty} \epsilon^i h f_{i-1}^{'} + \sum_{i=1}^{\infty} \epsilon^i \mathcal{G} f_i - \sum_{i=1}^{\infty} \epsilon^i \beta f_i \\
&= \mathcal{G} f_0 - \beta f_0 + \sum_{i=1}^{\infty} \epsilon^i \left(h f_{i-1}^{'} + \mathcal{G} f_i - \beta f_i\right).
\end{aligned}$$

And to summarise, (3.8) becomes

$$\mathcal{G}f_0 - \beta f_0 + \sum_{i=1}^{\infty} \epsilon^i \left(h f_{i-1}^{'} + \mathcal{G}f_i - \beta f_i \right) = 0, \ \forall x \in D.$$

Note that by extracting the 0-th order term and assigning proper boundary conditions, we can have the BVP for the standard Brownian motion (where the LT inverse is already known, see Example 2.2.2). Higher order terms can be solved via a recursive system which accumulates information from f_0 and the drift function h.

Denote the BVP with $i = 0$ by $o(1)$ term, by assigning same boundary conditions as in the initial problem, we have

$$\begin{aligned} o(1) : \mathcal{G}f_0 &= \beta f_0, \ x \in D, \\ f_0(\partial D_a) &= [1, 0]^T. \end{aligned}$$

For $i \geq 1$, we use the notation $o(\epsilon^i)$ and define

$$\begin{aligned} o\left(\epsilon^i\right) : \mathcal{G}f_i &= \beta f_i - h \cdot f_{i-1}^{'}, \ x \in D, \\ f_i(\partial D_a) &= [0, 0]^T. \end{aligned}$$

Based on the fact that the solution to the initial BVP is unique, one can check, by solving the recursive system to infinite orders (not necessarily for small ϵ), the sequence $\{f_i\}_{i \geq 0}$ reproduces the initial solution f; *i.e.* Equation (3.7) always holds true. However, in practice, it is not realistic of having infinite order solutions. Therefore we need to decide a truncation order and estimate the corresponding error.

3.3 Truncation Error and Convergence

In this section, we present results about the perturbation convergence and the truncation error estimation. The error estimation below is given by a probabilistic representation, i.e. a formula expressed using the expectation of path integrals. Alternatively, one can also estimate the truncation error via a PDE scheme and which is listed in Appendix 3.A.

Before demonstrating the results, we further introduce some notations. Let $N \in \mathbb{N}$ be a

fixed integer, and for $i = 1, ..., N$, we denote the N-th order truncation of initial LT by

$$f^{(N)} := \sum_{i=0}^{N} \epsilon^i f_i. \tag{3.9}$$

Assume inverse LTs for f, $f^{(N)}$ and $\partial_x f_N(x, \beta)$ exist, and denote by

$$\begin{aligned} p_\tau(t) &= \mathcal{L}^{-1}\left\{f(\beta)\right\}(t), \\ p_\tau^{(N)}(t) &= \sum_{i=0}^{N} \epsilon^i \mathcal{L}^{-1}\left\{f_i(\beta)\right\}(t), \text{ and} \\ \eta(x,t) &= \mathcal{L}^{-1}\left\{\partial_x f_N(x,\beta)\right\}(t), \end{aligned} \tag{3.10}$$

respectively. Define the difference between two FPTDs by

$$q_\tau(t) := p_\tau(t) - p_\tau^{(N)}(t), \tag{3.11}$$

then,

Proposition 3.3.1 (Probabilistic Representation for the Truncation Error)**.** *For all $t \in \mathbb{R}^+$ and all $\beta \in \mathbb{C}^+$, if*

$$\int_0^{+\infty} e^{-\beta t} \mathbb{E}_x \left[\int_0^{\tau \wedge t} \left| h(X_u) \eta\left(X_u, t-u\right) \right| du \right] dt < +\infty, \tag{3.12}$$

then

$$q_\tau(t) = \epsilon^{N+1} \mathbb{E}_x \left[\int_0^{\tau \wedge t} h(X_u) \eta\left(X_u, t-u\right) du \right]. \tag{3.13}$$

Further, if for some constant $M < +\infty$ and

$$\left| \mathbb{E}_x \left[\int_0^{\tau \wedge t} h(X_u) \eta\left(X_u, t-u\right) du \right] \right| \leq M, \tag{3.14}$$

then

$$|q_\tau(t)| \leq \epsilon^{N+1} M. \tag{3.15}$$

Proof. Let $\eta\left(x,t\right)$ be defined as in (3.10), and introduce

$$\tilde{q}_\tau(t) := \epsilon^{N+1} \mathbb{E}_x \left[\int_0^{\tau \wedge t} h(X_u) \eta\left(X_u, t-u\right) du \right].$$

We first show that $\tilde{q}_\tau(t)$ is the inverse LT of $f - f^{(N)}$. Then by the uniqueness of (inverse) LT, $\tilde{q}_\tau(t)$ is the error function in (3.11). Consider the LT of $\tilde{q}_\tau(t)$. By (3.12) and the Fubini's theorem, we have

$$\begin{aligned}
&\int_0^\infty e^{-\beta t}\mathbb{E}_x\left[\int_0^{\tau\wedge t} h(X_u)\eta\left(X_u, t-u\right)du\right]dt \\
=&\mathbb{E}_x\left[\int_0^\infty\int_0^{\tau\wedge t} h(X_u)e^{-\beta t}\eta\left(X_u, t-u\right)dudt\right] \\
=&\mathbb{E}_x\left[\int_0^\tau h(X_u)\int_0^\infty e^{-\beta t}\mathbf{1}_{\{u\le t\}}\eta\left(X_u, t-u\right)dtdu\right] \\
=&\mathbb{E}_x\left[\int_0^\tau h(X_u)\mathcal{L}\left\{\mathbf{1}_{\{u\le t\}}\eta\left(X_u, t-u\right)\right\}(\beta)du\right].
\end{aligned}$$

According to the fact that

$$\mathcal{L}\left\{\mathbf{1}_{\{u\le t\}}\eta(x, t-u)\right\}(\beta) = e^{-\beta u}\mathcal{L}\left\{\eta(x,t)\right\}(\beta),$$

and by the definition of $\eta(x,t)$ in (3.10), we therefore conclude

$$\mathcal{L}\left\{\tilde{q}_\tau(t)\right\}(\beta) = \epsilon^{N+1}\mathbb{E}_x\left[\int_0^\tau h(X_u)e^{-\beta u}\partial_x f_N(X_u,\beta)du\right]. \tag{3.16}$$

Following from above, we show the right-hand side of (3.16) indeed is $f - f^{(N)}$. Let

$$Q(x,\beta) := f(x,\beta) - f^{(N)}(x,\beta).$$

By the linearity of LT and (3.11), we have

$$Q(x,\beta) = \mathcal{L}\left\{p_\tau(t)\right\}(\beta) - \mathcal{L}\left\{p_\tau^{(N)}(t)\right\}(\beta) = \mathcal{L}\left\{q_\tau(t)\right\}(\beta).$$

Since f and $f^{(N)}$ are both in C^2, so is Q. Apply the operator $\mathcal{A}$ on Q, and consider ODEs $o(1)$ and $o(i),\ i \le N$ on p. 34, together they yield

$$\begin{aligned}
\mathcal{A}Q - \beta Q &= \mathcal{A}f - \beta f - \left(\mathcal{A}f^{(N)} - \beta f^{(N)}\right) \\
&= 0 - \left[\mathcal{G}f_0 - \beta f_0 + \sum_{i=1}^N \epsilon^i\left(\mathcal{G}f_0 - \beta f_0 + h\cdot f_{i-1}'\right) + \epsilon^N\cdot\epsilon h f_N'\right] \\
&= -\epsilon^{N+1}h\cdot f_N'.
\end{aligned}$$

Note that f and $f^{(N)}$ share the same boundary conditions, so for $Q(x)$ we have

$$Q\left(\partial D_a\right) = [0,0]^T.$$

According to Theorem 2.2.3, the ODE of $Q(x)$ is the killed version of Dirichlet problem and its solution has the following probabilistic representation:

$$Q(x,\beta) = \epsilon^{N+1}\mathbb{E}_x\left[\int_0^\tau e^{-\beta u}h(X_u)\partial_x f_N(X_u,\beta)du\right].$$

This is indeed the right-hand side of (3.16). By the uniqueness of BVP solution and the uniqueness of the LT/ILT, we conclude that

$$q_\tau(t) = \tilde{q}_\tau(t).$$

In the end, (3.15) is a direct result from assumption (3.14) and (3.13). □

Remark. For small ϵ and under condition (3.14), by Proposition 3.3.1 we see the N-th order perturbed FPTD converges to the true density at $O(\epsilon^{N+1})$. This is the main reason why we use the *little-o* notation on p. 34. On the other hand, even for large ϵ, one can always use (3.13) to check error levels.

3.4 Recursion under Frequency Domain

In this section, we provide a general mechanism for solving recursive BVPs. For simplicity[2] we consider the FPT hitting 0 from above, *i.e.*

$$\tau := \inf\left\{t \geq 0 : X_t = 0 \middle| X_0 = x > 0\right\}. \tag{3.17}$$

Under this treatment, the domain is specified by $D = (0, +\infty)$. We suppress the notation a (note that $a = 0$), and denote the boundaries by $\partial D := \partial D_a = \{0, +\infty\}$.

[2]For an arbitrary hitting level a we can use the affine transformation to retrieve the 0-hitting case. Although not always, for the situation of hitting from below ($x < 0$), we can consider the mirror reflection of $\{X_t\}_{t\geq 0}$ (cf. Section 4.3.1 for the OU process and discussions in Appendices 5.A and 6.D for the Bessel and the Bubble processes).

Lemma 3.4.1 (Laplace Transform for the FPTD of Brownian Motion)**.** *The unique solution to the $o(1)$ BVP is given by*

$$f_0(x,\beta) = e^{-\sqrt{2\beta}x}. \tag{3.18}$$

Proof. The result is directly from Example 2.2.2 by setting $a = 0$. □

Lemma 3.4.2 (Recursive Solution to $o\left(\epsilon^i\right)$)**.** *For $i \geq 1$, let*

$$\gamma := \sqrt{2\beta}. \tag{3.19}$$

The unique solution to the $o\left(\epsilon^i\right)$ BVP, if exists, is given by

$$f_i(x,\beta) = f_0(x,\beta)\left[\int_{A_1}^{x} 2e^{2\gamma y}\left(\int_{A_2}^{y} h(z)k_i(z,\beta)e^{-2\gamma z}dz + C_1\right)dy + C_2\right],$$

where

$$k_i(z,\beta) := \gamma f_0^{-1}(z,\beta)f_{i-1}(z,\beta) - \partial_z\left(f_0^{-1}(z,\beta)f_{i-1}(z,\beta)\right),$$

and $A_1,\ A_2,\ C_1,\ C_2$ are determined subject to conditions $f_i(0,\beta) = 0$, $f_i(+\infty,\beta) = 0$.

Proof. The uniqueness of f_i follows from the Dirichlet-type BVP [101]. Consider that f_i is of the following form

$$f_i := f_0 g_i. \tag{3.20}$$

Then substituting (3.20) into $o\left(\epsilon^i\right)$-ODE yields

$$\frac{1}{2}g_i^{''} - \gamma g_i^{'} = h\left[\gamma g_{i-1} - g_{i-1}^{'}\right]. \tag{3.21}$$

Note g_{i-1} and its derivative are deterministic in the i-th order. We denote by

$$k_i := \gamma g_{i-1} - g_{i-1}^{'}. \tag{3.22}$$

Then Equation (3.21) can be rewritten as

$$\frac{1}{2}g_i^{''} - \gamma g_i^{'} = hk_i. \tag{3.23}$$

Multiply $e^{-2\gamma x}$ and take integrations on both sides of (3.23), we have

$$\int \frac{1}{2} g_i^{''} e^{-2\gamma x} dx - \int \gamma g_i^{'} e^{-2\gamma x} dx = \int h k_i e^{-2\gamma x} dx + C_1. \tag{3.24}$$

Apply integral by parts, for the left-hand side we get

$$\begin{aligned} \int \frac{1}{2} g_i^{''} e^{-2\gamma x} dx - \int \gamma g_i^{'} e^{-2\gamma x} dx &= \frac{1}{2} g_i^{'} e^{-2\gamma x} + \gamma \int g_i^{'} e^{-2\gamma x} dx - \int \gamma g_i^{'} e^{-2\gamma x} dx \\ &= \frac{1}{2} g_i^{'} e^{-2\gamma x}. \end{aligned} \tag{3.25}$$

Use (3.25) and (3.24), further multiply $2e^{2\gamma x}$ and take integrals on both sides,

$$g_i = \int_{A_1}^{x} 2e^{2\gamma y} \left[\int_{A_2}^{y} h k_i e^{-2\gamma z} dz + C_1 \right] dy + C_2. \tag{3.26}$$

Combine (3.20), this concludes our proof. □

Remark. Potentially, using Lemma 3.4.2 we can solve the LT of perturbed FPTD to orders as many as we wish. With the help of symbolic calculation software (e.g. Maple, Python), calculations would become even simpler.

Appendix 3.A Alternative Error Estimation

We consider a PDE representation for solving the error function $q_\tau(t)$ in Proposition 3.3.1. As a counterpart to the probabilistic representation in the previous proposition, the PDE approach below constitutes part of the potential study. Recall in the proof, the LT of the error function, $Q(x, \beta)$, satisfies the following BVP:

$$\frac{1}{2} Q^{''} + \epsilon h Q^{'} = \beta Q - \epsilon^{N+1} h f_N^{'};\ Q(\partial D) = \underline{0}. \tag{3.27}$$

Assume its ILT (denoted by $q_\tau(x, t)$) is bounded, then

$$\partial_x Q(x, \beta) = \int_0^\infty e^{-\beta t} \partial_x q_\tau(x, t) dt, \text{ and}$$

$$\partial_{xx} Q(x, \beta) = \int_0^\infty e^{-\beta t} \partial_{xx} q_\tau(x, t) dt.$$

Therefore,

$$\mathcal{L}^{-1}\left\{\partial_x Q(x,\beta)\right\}(t) = \partial_x q_\tau(x,t), \text{ and}$$

$$\mathcal{L}^{-1}\left\{\partial_{xx} Q(x,\beta)\right\}(t) = \partial_{xx} q_\tau(x,t).$$

For the left-hand side of Equation (3.27), we then have

$$\mathcal{L}^{-1}\left\{\frac{1}{2}\partial_{xx}Q(x,\beta) + \epsilon h(x)\partial_x Q(x,\beta)\right\}(t) = \frac{1}{2}\partial_{xx}q_\tau(x,t) + \epsilon h(x)\partial_x q_\tau(x,t). \tag{3.28}$$

For the right-hand side, consider the fact that

$$\mathcal{L}^{-1}\left\{\beta Q(x,\beta)\right\}(t) = \partial_t q_\tau(x,t) + q_\tau(x,0),$$

where for $x \in D$, we have $q_\tau(x,0) = 0$. Then,

$$\mathcal{L}^{-1}\left\{\beta Q(x,\beta) - \epsilon^{N+1}h(x)\partial_x f_N(x,\beta)\right\}(t) = \partial_t q_\tau(x,t) - \epsilon^{N+1}h(x)\eta(x,t). \tag{3.29}$$

Take the ILT on both sides of (3.27), and consider relations in (3.28) and (3.29), we then get

$$\left(\partial_t - \frac{1}{2}\partial_{xx} - \epsilon h(x)\partial_x\right) q_\tau(x,t) = \epsilon^{N+1}h(x)\eta(x,t).$$

The boundary and initial conditions are given by

$$q_\tau(t,\partial D) = \underline{0},\ t \in \mathbb{R}^+,$$

$$q_\tau(0,x) = 0,\ x \in D.$$

Appendix 3.B Probabilistic Representation of $p_\tau^{(N)}(t)$

From Proposition 3.3.1 and Appendix 3.A, we can see solutions associated with the perturbations can be either interpreted by probabilistic representations or PDEs. On the other hand, note that solutions in Lemma 3.4.2 are deduced from ODEs. Therefore, for the completeness of our study, in this appendix we present the corresponding probabilistic versions of solutions

in Lemma 3.4.2. Let

$$\tau_W := \inf\{t > 0 : W_t \in \partial D_a | W_0 = x \in D\}$$

be the FPT of Brownian motion starting from $W_0 = x$ and hitting the same barrier as $\{X_t\}_{t\geq 0}$. Then, the solution $f_0(x,\beta)$ of $o(1)$ term, in fact is the LT of τ_W (Theorem 2.2.1):

$$f_0(x,\beta) = \mathbb{E}_x\left[e^{-\beta\tau_W}\right].$$

Now we consider higher order $o\left(\epsilon^i\right)$ terms. Define

$$l_i(x,\beta) := h(x)\partial_x f_{i-1}(x,\beta).$$

Note that in recursion i, $f_{i-1}(x,\beta)$ is a known function. Using again Theorem 2.2.3, ODE $o\left(\epsilon^i\right)$ embeds the following representation

$$f_i(x,\beta) = \mathbb{E}_x\left[\int_0^{\tau_W} e^{-\beta s} l_i(W_s,\beta) ds\right].$$

Under L^1-integrable conditions (*w.r.t.* l_i), similar as in the proof of Proposition 3.3.1, we then can rewrite the equation above as

$$f_i(x,\beta) = \int_0^{+\infty} e^{-\beta s}\mathbb{E}_x\left[l_i(W_s,\beta)\mathbf{1}_{\{\tau_W > s\}}\right] ds. \tag{3.30}$$

Note that, the function l_i in above also depends on β. Therefore, f_i in general cannot be simply understood as the killed version of the *resolvent operator*. Equation (3.30) shows f_i, in fact, captures the accumulated effects from the drift function h. And for $|\epsilon| < 1$, with the perturbation order i going further, the effects become less weighted by ϵ^i.

Although we cannot acquire direct ILT from Equation (3.30), the proof of Proposition 3.3.1 inspires us to derive a probabilistic representation for the inverse transform.

Proposition 3.B.1 (Probabilistic Representation for Perturbed FPTD)**.** *For* $1 \leq i \leq N$, $t \in \mathbb{R}^+$, *and* $\beta \in \mathbb{C}^+$, *if*

$$\int_0^{+\infty} e^{-\beta s}\mathbb{E}_x\left[|l_i(W_s,\beta)|\,\mathbf{1}_{\{\tau_W > s\}}\right] ds < +\infty,$$

then

$$p_{\tau}^{(N)}(t) = p_{\tau_W}(t) + \sum_{i=1}^{N} \epsilon^i \mathbb{E}_x \left[\int_0^{t \wedge \tau_W} h(W_u) \eta_i(W_u, t-u) du \right], \tag{3.31}$$

where η_i is the error estimation function defined for order i in (3.10)*.*

Proof. Please refer to the proof of Proposition 3.3.1. □

Proposition 3.B.1 provides us with two ways of evaluating FPTDs. Either, one can use the Monte Carlo approach to simulate Brownian motion paths and their FPTs, or, as an alternative, assume the joint distribution of (W_t, τ_W) (which can be easily solved by using the reflection principle) to be:

$$\xi(y, s|t) := \frac{\mathbb{P}_x \left(W_t \in dy, \tau_W \in ds \right)}{dyds};$$

then the expectation in (3.31) can be further written as

$$\mathbb{E}_x \left[\int_0^{t \wedge \tau_W} h(W_u) \eta_i(W_u, t-u) du \right] = \int_D \int_{\mathbb{R}^+} \int_0^{t \wedge s} h(y) \eta_i(y, t-u) \xi(y, s|u) du ds dy.$$

Chapter 4

First Passage Time of Ornstein-Uhlenbeck Process

The OU process was first introduced to describe the velocity of a particle that follows a Brownian motion movement [124]. Later the process appears widely in neural science [74, 126] and mathematical finance [55, 65, 111, 125], etc. According to our previous settings, the h-function of the OU process is given by

$$h(X_t) = \theta - X_t,\ X_t \in D, \tag{4.1}$$

where θ is the equilibrium parameter in the OU model. Note that the function above is a first order polynomial and which is still a polynomial under operations of integration and differentiation. Since our recursive framework mainly involves those two operations, therefore, we may expect an elegant result from the perturbation method.

Refer to [124, 127], the OU SDE has a unique strong solution. Moreover, as a strong Markov process, it is recurrent and continuous *a.s.* Our framework therefore can be applied. Let $\epsilon > 0$ be the mean-reverting rate, the infinitesimal generator is given by

$$\mathcal{A}f(x) = \frac{1}{2}f^{''}(x) + \epsilon(\theta - x)f^{'}(x),\ x \in D.$$

Consider hitting from above in (3.17). The solution of initial BVP (3.5) and (3.6), is given

by [18]

$$f(x,\beta) = e^{\frac{\epsilon x(x-2\theta)}{2}} \frac{D_{-\frac{\beta}{\epsilon}}\left(\sqrt{2\beta}(\theta - x)\right)}{D_{-\frac{\beta}{\epsilon}}\left(\sqrt{2\beta}\theta\right)}, \tag{4.2}$$

where $\beta \in \mathbb{C}^+$ is the LT parameter, and $D_\cdot(\cdot)$ is the *parabolic cylinder function* (see [2]).

Under a special case that $\theta = 0$, the explicit OU FPTD is given by [3, 49]. However, in general, the explicit inverse of (4.2) seems not available. Instead of acquiring the closed-form solution, one can use numerical schemes (see Section 2.3, Chapter 2); or, many attempts have been made on asymptotic solutions and simulation schemes, see e.g. [59, 71, 77]. In this chapter, we apply our perturbation framework and give explicit asymptotics for the OU FPTD.

This chapter is organised as follows. In Section 4.1, we introduce general results from the N-th order perturbations. Section 4.2 focuses on the error estimation with $N = 1$. Model extensions and numerical results are provided in Section 4.3. In the appendices of this chapter, we summarise supplementary materials.

4.1 N-th Order Perturbed FPTD

Follow Lemma 3.4.2, let

$$\gamma = \sqrt{2\beta}.$$

And for $i = 1$, consider $A_1 = 0$, $A_2 = +\infty$, $C_1 = 0$, and $C_2 = 0$. Then we can immediately find that,

$$f_1(x,\beta) = e^{-\gamma x}\left(\frac{x^2}{2} + \frac{(1-2\theta\gamma)x}{2\gamma}\right), \tag{4.3}$$

which is the solution to the $o(\epsilon^1)$ BVP. For general cases, we have the following proposition.

Proposition 4.1.1 (Recursive Polynomial)**.** *For $i \geq 2$, the solution of $o(\epsilon^i)$-BVP for the OU process is given by*

$$f_i(x,\beta) = f_0(x,\beta) g_i(\gamma x),$$

where

$$g_i(y) := \sum_{j=1}^{2i} p_j^{(i)} y^j. \tag{4.4}$$

The coefficients $\{p_j^{(i)} : i \geq 2, 1 \leq j \leq 2i\}$ *are given by:*

$$\begin{cases} j = 2i: & p_{2i}^{(i)} = \frac{p_{2i-2}^{(i-1)}}{2i\gamma^2} \\ j = 2i-1: & p_{2i-1}^{(i)} = \frac{1}{(2i-1)\gamma^2} p_{2i-3}^{(i-1)} + \left(\frac{1}{2\gamma^2} - \frac{\gamma\theta+(2i-2)}{(2i-1)\gamma^2}\right) p_{2i-2}^{(i-1)} \\ 2 < j < 2i-1: & p_j^{(i)} = \frac{1}{2}(j+1)p_{j+1}^{(i)} + \frac{1}{\gamma^2 j} p_{j-2}^{(i-1)} - \frac{j-1+\gamma\theta}{\gamma^2 j} p_{j-1}^{(i-1)} + \frac{\theta}{\gamma} p_j^{(i-1)} \\ j = 2: & p_2^{(i)} = \frac{3}{2} p_3^{(i)} - \frac{1+\gamma\theta}{2\gamma^2} p_1^{(i-1)} + \frac{\theta}{\gamma} p_2^{(i-1)} \\ j = 1: & p_1^{(i)} = p_2^{(i)} + \frac{\theta}{\gamma} p_1^{(i-1)} \end{cases}.$$

Proof. One can try to solve coefficients from the recursive algorithm in Lemma 3.4.2. Another approach, which is much simpler, is to directly derive solutions of ODE (3.23). We leave details of proof in Appendix 4.A. □

Proposition 4.1.1 enables us to expand perturbed LT to arbitrary orders. However, our final aim is to find its closed-form inverse, while, coefficients in the proposition are functions of the parameter β. In order to avoid unnecessary symbolic calculations, we further decompose the coefficients $\left\{p_j^{(i)} : i \geq 0,\ 1 \leq j \leq 2i\right\}$.

Lemma 4.1.2 (Recursive Polynomial Decomposition)**.** *For each* $p_j^{(i)}$ *in* $\left\{p_j^{(i)} : i \geq 1,\ 1 \leq j \leq 2i\right\}$*, there exists a triple-indexed real sequence*

$$\left\{c_k^{(i,j)} : i \geq 1,\ 1 \leq j \leq 2i,\ 0 \leq k \leq (2i-j) \wedge i\right\},$$

such that

$$p_j^{(i)} = \sum_{k=0}^{(2i-j)\wedge i} c_k^{(i,j)} \left(\frac{1}{\gamma}\right)^{2i-k} \theta^k. \tag{4.5}$$

Proof. Please refer to Appendix 4.B. □

Remark. Note that $\left\{c_k^{(i,j)}\right\}$ is parameter-independent. Therefore we can pre-calculate the

sequence and save it in memory. Later, this will help in enhancing the FPTD computation speed.

Proposition 4.1.3 (N-th Order Perturbed FPTD of OU Process)**.** *Let $N \in \mathbb{N}$, the N-th order perturbed downward FPTD of OU process is*

$$p_\tau^{(N)}(t) = \frac{e^{-\frac{x^2}{4t}}}{\sqrt{2\pi}} \sum_{n=0}^{2N-1} h_n t^{\frac{n}{2}-1} D_{-n+1}\left(\frac{x}{\sqrt{t}}\right),$$

where

$$h_n = \sum_{\substack{i,j,k;\\ 2i-j-k=n}} \epsilon^i c_k^{(i,j)} \theta^k x^j,$$

and $D_\cdot(\cdot)$ is the parabolic cylinder function.

Proof. Express the truncated LT using (3.9) and (3.20). According to Proposition 4.1.1 and Lemma 4.1.2,

$$f^{(N)} = \sum_{i=0}^{N} \epsilon^i e^{-\gamma x} \sum_{j=1}^{2i} \left(\sum_{k=0}^{(2i-j)\wedge i} c_k^{(i,j)} \left(\frac{1}{\gamma}\right)^{2i-k-j} \theta^k \right) x^j. \tag{4.6}$$

For $0 \le n \le 2N-1$, define

$$\hat{h}_n := 2^{-\frac{n}{2}} h_n.$$

Then after standard calculations, we can write (4.6) as

$$f^{(N)} = \sum_{n=0}^{2N-1} \hat{h}_n \cdot e^{-\sqrt{2\beta}x} \beta^{-\frac{n}{2}}. \tag{4.7}$$

Note that $\hat{h}_n$ is independent to β. Referring to [9, Equation (9), Section 5.6], we find for $0 \le n \le 2N-1$,

$$\mathcal{L}^{-1}\left\{e^{-\sqrt{2\beta}x}\beta^{-\frac{n}{2}}\right\}(t) = \frac{2^{\frac{n}{2}} t^{\frac{n}{2}-1}}{\sqrt{2\pi}} e^{-\frac{x^2}{4t}} D_{-n+1}\left(\frac{x}{\sqrt{t}}\right). \tag{4.8}$$

This immediately gives us the result. □

Remark. According to [18], the initial LT of the OU FPTD is given by the ratio of two parabolic cylinder functions. In the end, by applying perturbations we find that the FPTD itself (which is an inverse LT) is expressed as a series of parabolic cylinder functions with the first argument being integers.

The integer-valued D-function is closely related to the Hermite polynomials [81, 12.7 (i)]. Based on the fact [81, 12.7.1] that

$$D_0(z) = e^{-\frac{1}{4}z^2}, \tag{4.9}$$

and according to [81, 12.7.2], we have

$$D_1\left(\frac{x}{\sqrt{t}}\right) = \frac{x}{\sqrt{t}} e^{-\frac{x^2}{4t}}. \tag{4.10}$$

Using the expressions above we can further write

$$p_\tau^{(N)}(t) = (h_0 + \frac{h_1}{x}t)p_\tau^{(0)}(t) + \frac{e^{-\frac{x^2}{4t}}}{\sqrt{2\pi}} \sum_{n=2}^{2N-1} h_n t^{\frac{n}{2}-1} D_{-n+1}\left(\frac{x}{\sqrt{t}}\right), \tag{4.11}$$

where $p_\tau^{(0)}(t)$ is the FPTD of a Brownian motion hitting 0, and which follows the inverse Gamma distribution (see (2.29) in Example 2.2.2 with $a = 0$). From this point of view, the N-th order perturbed OU FPTD is indeed the FPTD of the Brownian motion plus higher order corrections.

Proposition 4.1.4 (Tail Asymptotics of OU Perturbed FPTD)**.** *For $N \geq 1$, tail asymptotics of the N-th order perturbed OU FPTD are given by*[1]

$$p_\tau^{(N)}(t) \sim p_\tau^{(0)}(t), \ \textit{as } t \downarrow 0, \tag{Left Tail}$$

$$p_\tau^{(N)}(t) \sim t^{N-\frac{3}{2}}, \ \textit{as } t \uparrow +\infty. \tag{Right Tail}$$

Proof. We start from the left tail. When $t \downarrow 0$, it is clear from (4.11), that

$$(h_0 + \frac{h_1}{x}t)p_\tau^{(0)}(t) \sim p_\tau^{(0)}(t).$$

We need to further check the asymptotic for the series of D-functions. Denote by $z := \frac{x}{\sqrt{t}}$ and $a = n - \frac{3}{2}$ $(2 \leq n \leq 2N-1)$. Refer to [2, 19.8.1, p. 689] and [81, 12.9.1], when $z \uparrow +\infty$

[1] Please refer to footnote 5 on p. 26, of Section 2.5, Chapter 2, for more details about the symbol $\sim$.

(*i.e.* $t \downarrow 0$), we have

$$D_{-a-\frac{1}{2}}(z) \sim e^{-\frac{1}{4}z^2} z^{-a-\frac{1}{2}} \left(1 + O(\frac{1}{z^2})\right).$$

Therefore

$$\begin{aligned}\frac{1}{\sqrt{2\pi}} \sum_{n=2}^{2N-1} h_n t^{\frac{n}{2}-1} e^{-\frac{x^2}{4t}} D_{-n+1}\left(\frac{x}{\sqrt{t}}\right) &\sim \sum_{n=2}^{2N-1} t^{n-\frac{3}{2}} e^{-\frac{x^2}{2t}} \left(1 + O(t)\right) \\ &\sim p_\tau^{(0)}(t)(t^2 + o(t^2)).\end{aligned}$$

This proves the left tail result.

Now we consider the right tail. Again by (4.11), we immediately have

$$\left(h_0 + \frac{h_1}{x}t\right) p_\tau^{(0)}(t) \sim \frac{h_1}{x} t p_\tau^{(0)}(t) \sim t^{-\frac{1}{2}}, \text{ for } t \uparrow +\infty. \tag{4.12}$$

For the series of D-functions, we use [2, 19.12.3]; and

$$\begin{aligned}D_{-a-\frac{1}{2}}(z) = \sqrt{\pi} 2^{-\frac{1}{2}a} e^{-\frac{1}{4}z^2} \Bigg(&\frac{2^{-\frac{1}{4}}}{\Gamma\left(\frac{3}{4} + \frac{1}{2}a\right)} M\left(\frac{1}{2}a + \frac{1}{4}, \frac{1}{2}, \frac{1}{2}z^2\right) \\ &- \frac{2^{\frac{1}{4}} z}{\Gamma\left(\frac{1}{4} + \frac{1}{2}a\right)} M\left(\frac{1}{2}a + \frac{3}{4}, \frac{3}{2}, \frac{1}{2}z^2\right) \Bigg),\end{aligned}$$

where $M(\cdot,\cdot,\cdot)$ is the *Kummer's function* (*confluent hypergeometric function* ${}_1F_1(\cdot,\cdot,\cdot)$), and $\Gamma(\cdot)$ is the Gamma-function. Introduce the notations

$$\zeta(a,s) := \sqrt{\pi} \frac{2^{-\frac{1}{4}-\frac{1}{2}a}}{\Gamma\left(\frac{3}{4} + \frac{1}{2}a\right)} \frac{(\frac{1}{2}a + \frac{1}{4})_s}{(\frac{1}{2})_s 2^s s!},$$

and

$$\xi(a,s) := -\sqrt{\pi} \frac{2^{\frac{1}{4}-\frac{1}{2}a}}{\Gamma\left(\frac{1}{4} + \frac{1}{2}a\right)} \frac{(\frac{1}{2}a + \frac{3}{4})_s}{(\frac{3}{2})_s 2^s s!},$$

where $(\cdot)_s := \Pi_{k=0}^{s-1}(\cdot + k)$. According to [81, 13.2.2], we can reformulate the D-function as

$$D_{-n+1}\left(\frac{x}{\sqrt{t}}\right) = e^{-\frac{x}{4t}} \left(\sum_{s=0}^{\infty} \zeta(n - \frac{3}{2}, s) \frac{x^{2s}}{t^s} + \sum_{s=0}^{\infty} \xi(n - \frac{3}{2}, s) \frac{x^{2s+1}}{t^{s+\frac{1}{2}}}\right).$$

Now let $t \uparrow +\infty$, it then yields

$$t^{\frac{n}{2}-1}e^{-\frac{x^2}{4t}}D_{-n+1} \sim t^{\frac{n}{2}-1}\left(\sum_{s=0}^{\infty}\zeta(n-\frac{3}{2},s)\frac{x^{2s}}{t^s}+\sum_{s=0}^{\infty}\xi(n-\frac{3}{2},s)\frac{x^{2s+1}}{t^{s+\frac{1}{2}}}\right).$$

Note that for fixed n, the leading term in above is $t^{\frac{n}{2}-1}$. Therefore, by considering the highest order $n = 2N-1$ in the D-function series, we get

$$\frac{1}{\sqrt{2\pi}}\sum_{n=2}^{2N-1}h_n t^{\frac{n}{2}-1}e^{-\frac{x^2}{4t}}D_{-n+1}\left(\frac{x}{\sqrt{t}}\right) \sim t^{N-\frac{3}{2}}. \tag{4.13}$$

This concludes our proof. □

From the right tail asymptotic we find for $N \geq 2$, the perturbed FPTD would diverge at $t = +\infty$. In the case $N = 1$, though $p_\tau^{(1)}(t)$ converges to 0, due to the fat-tail effect of $t^{-\frac{1}{2}}$, we still expect an infinite integral. Therefore the total probability of perturbed FPTD is infinity for all $N \geq 1$. Indeed, the limit value of LT tells, for all $N \geq 1$,

$$\left|\int_0^\infty p_\tau^{(N)}(t)dt\right| = \lim_{\beta\to 0^+}\left|f^{(N)}(\beta)\right| = \infty.$$

On the other hand, the left tail asymptotic shows the equivalence between OU and Brownian motion FPTDs. Opposite to the spectral decomposition [3, 77], our analysis indicates that the perturbation provides smooth densities for small t.

Lemma 4.1.5 (η-Function for OU Process)**.** *For $N \geq 1$, the η-function is given by*

$$\eta(x,t) = \frac{e^{-\frac{x^2}{4t}}}{\sqrt{2\pi}}\sum_{n=0}^{2N-1}t^{\frac{n}{2}-1}\left((\partial_x l_n)D_{-n+1}\left(\frac{x}{\sqrt{t}}\right)-\frac{l_n}{\sqrt{t}}D_{-n+2}\left(\frac{x}{\sqrt{t}}\right)\right), \tag{4.14}$$

where

$$l_n = \sum_{\substack{j,k;\\ j+k=2N-n}} c_k^{(N,j)}\theta^k \cdot x^j. \tag{4.15}$$

Proof. Recall the definition of the η-function in Equation (3.10) and Proposition 3.3.1. The partial derivative of $f_N(x,\beta)$ is given by

$$\partial_x f_N(x,\beta) = e^{-\sqrt{2\beta}x}\sum_{n=0}^{2N-1}\left(2^{-\frac{n}{2}}\partial_x(l_n)\beta^{-\frac{n}{2}}-2^{-\frac{n-1}{2}}l_n\beta^{-\frac{n-1}{2}}\right).$$

The rest of the proof is concluded by using (4.8) again. □

4.2 Error Estimation for $N = 1$

In this section we provide proofs of error estimation and convergence for the case $N = 1$. We begin with the following lemma.

Lemma 4.2.1 (Supplementary Proof of Proposition 4.2.2)**.** *For $N = 1$, let $h(x)$, $\eta(x,t)$ be given as in* (4.1) *and* (4.14)*, respectively. Consider the downward FPT τ of OU process crossing* 0*. For a constant $K > 1$, we have*

$$\mathbb{E}_x\left[\int_0^{\tau\wedge t}\mathbf{1}_{\{X_u>K\}}|h(X_u)\eta(X_u,t-u)|du\right] \le C_0 + C_1\sqrt{t} + C_2 t,$$

where C_0, C_1 and C_2 are positive constants.

Proof. According to (4.14), (4.9), (4.10) and [81, 12.7.2], by setting $N = 1$, we can write

$$h(x)\eta(x,t-u) = \frac{\theta - x}{\sqrt{2\pi}}e^{-\frac{x^2}{2(t-u)}}\left(\frac{x\partial_x l_0}{(t-u)^{\frac{3}{2}}} - \frac{l_0}{(t-u)^{\frac{3}{2}}}\left(\frac{x^2}{t-u} - 1\right) + \frac{\partial_x l_1}{(t-u)^{\frac{1}{2}}} - \frac{x l_1}{(t-u)^{\frac{3}{2}}}\right). \tag{4.16}$$

For $r \in \mathbb{N}$ and $x \ge 0$, we find

$$\left|e^{-\frac{x^2}{2(t-u)}}x^r\right| \le r^{\frac{r}{2}}\cdot(t-u)^{\frac{r}{2}}, \tag{4.17}$$

and $x^* = \sqrt{r(t-u)}$ is the turning point of $e^{-\frac{x^2}{2(t-u)}}x^r$. Based on (4.16), (4.17) and (4.15), for $(x,t) \in D \times [0,+\infty)$ and $u \in [0,t]$, we get

$$\left|h(x)\eta(x,t-u)\mathbf{1}_{\{x>K\}}\right| \le C_0' + C_1'\frac{1}{\sqrt{t-u}} + \left(C_2'\frac{x}{(t-u)^{\frac{3}{2}}} + C_3'\frac{x^3}{(t-u)^{\frac{5}{2}}}\right)e^{-\frac{x^2}{2(t-u)}}\mathbf{1}_{\{x>K\}}, \tag{4.18}$$

where $\left\{C_i' : i = 0,1,...,3\right\}$ are positive constants. Note that, substituting (4.17) into last two terms in (4.18) gives $\frac{1}{t-u}$, which diverges under the integral between 0 and t. Therefore, extra care is required.

For $\alpha > 0$, we consider a more general function:

$$m^{r,\alpha}(x,u,t) := \frac{x^r}{(t-u)^{1+\alpha}}e^{-\frac{x^2}{2(t-u)}}. \tag{4.19}$$

First note that, when $t \leq \frac{K^2}{r}$, for all $u \in [0,t]$, we have $\sqrt{r(t-u)} \leq K < x$. By considering the monotonicity of $m^{r,\alpha}(x,u,t)$ after the turning point, we find

$$m^{r,\alpha}(x,u,t)\mathbf{1}_{\{x>K\}} \leq \frac{K^r}{(t-u)^{1+\alpha}} e^{-\frac{K^2}{2(t-u)}} \mathbf{1}_{\{x>K\}} \tag{4.20}$$

$$= 2^\alpha \Gamma(\alpha) K^{r-2\alpha} IG(t-u,\alpha,\frac{K^2}{2}) \mathbf{1}_{\{x>K\}}, \tag{4.21}$$

where $\Gamma(\cdot)$ is the *Gamma function*, and $IG(t,\alpha,\frac{K^2}{2})$ is the density function of the *inverse Gamma distribution* with shape parameter α and scale parameter $\frac{K^2}{2}$. On the other hand, when $t > \frac{K^2}{r}$, we consider maximums from two separate intervals. If $u \in [t-\frac{K^2}{r}, t]$, by noticing $\sqrt{r(t-u)} < K < x$, we find (4.21) is still valid. If, otherwise, $u \in [0, t-\frac{K^2}{r})$, again, using (4.17) yields

$$m^{r,\alpha}(x,u,t)\mathbf{1}_{\{x>K\}} \leq \frac{r^{\frac{r}{2}}}{(t-u)^{1+\alpha-\frac{r}{2}}} \mathbf{1}_{\{x>K\}}. \tag{4.22}$$

Further, if $1+\alpha-\frac{r}{2} > 0$, then for $u \in [0, t-\frac{K^2}{r})$,

$$m^{r,\alpha}(x,u,t)\mathbf{1}_{\{x>K\}} \leq \frac{r^{1+\alpha}}{K^{2+2\alpha-r}} \mathbf{1}_{\{x>K\}}. \tag{4.23}$$

Follow (4.21) and (4.23), by taking integral of (4.19) and considering the conditional expectation, we get

$$\begin{aligned}
&\mathbb{E}_x\left[\int_0^t m^{r,\alpha}(X_u,u,t)\mathbf{1}_{\{X_u>K\}} du\right] \\
=&\left(\mathbf{1}_{\left\{t\leq\frac{K^2}{r}\right\}} + \mathbf{1}_{\left\{t>\frac{K^2}{r}\right\}}\right) \cdot \int_0^t \mathbb{E}_x\left[m^{r,\alpha}(X_u,u,t)\mathbf{1}_{\{X_u>K\}}\right] du \\
\leq& 2^\alpha\Gamma(\alpha)K^{r-2\alpha}\int_0^t IG(t-u,\alpha,\frac{K^2}{2})\mathbb{P}_x(X_u>K)du \cdot \mathbf{1}_{\left\{t\leq\frac{K^2}{r}\right\}} \\
&+ 2^\alpha\Gamma(\alpha)K^{r-2\alpha}\int_{t-\frac{K^2}{r}}^t IG(t-u,\alpha,\frac{K^2}{2})\mathbb{P}_x(X_u>K)du \cdot \mathbf{1}_{\left\{t>\frac{K^2}{r}\right\}} \\
&+ \int_0^{t-\frac{K^2}{r}} \frac{r^{1+\alpha}}{K^{2+2\alpha-r}}\mathbb{P}_x(X_u>K)du \cdot \mathbf{1}_{\left\{t>\frac{K^2}{r}\right\}} \\
\leq& \left(2^\alpha\Gamma(\alpha)K^{r-2\alpha} - \frac{r^\alpha}{K^{2\alpha-r}}\right) + \frac{r^{1+\alpha}}{K^{2+2\alpha-r}} \cdot t.
\end{aligned}$$

The last inequality is true as $IG(t,\cdot,\cdot)$ is a density function and $\mathbb{P}_x(X_u > K) \leq 1$. Now,

combine the inequality above and (4.18), for the original problem we get

$$\begin{aligned}\mathbb{E}_x\left[\int_0^{\tau\wedge t}\mathbf{1}_{\{X_u>K\}}|h(X_u)\eta(X_u,t-u)|du\right] &\le \mathbb{E}_x\left[\int_0^{t}\mathbf{1}_{\{X_u>K\}}|h(X_u)\eta(X_u,t-u)|du\right]\\ &\le C_0+C_1\sqrt{t}+C_2t.\end{aligned}$$

This concludes our proof. □

Proposition 4.2.2 (First Order Error Estimation and Convergence of OU Process)**.** *For $N=1$ and all $t\in[0,+\infty)$, the error estimation* (3.13) *of perturbed OU FPTD is valid. Moreover, for any $T>0$ and $t\in[0,T]$, the perturbation is $O(\epsilon^2)$-accurate.*

Proof. Recall the h-function in (4.1) and the η-function in (4.14). In the first part of the proof, we show (3.12) in Proposition 3.3.1 is satisfied. As a sufficient condition to (3.12), we need to find a bound

$$\mathbb{E}_x\left[\int_0^{\tau\wedge t}|h(X_u)\eta(X_u,t-u)|du\right]\le M(t)$$

for all $t\in[0,\infty)$, and such that $M(t)$ grows less fast than exponential.

For all fixed $x\in D$, one can check that $h(x)\eta(x,t)\to 0$ as $t\uparrow+\infty$. Let $K>1$ be a large and fixed constant. $h(x)\eta(x,t)$ is continuous, so there exists a constant M_1, (*) *w.l.o.g.*, for all $(x,t)\in[0,K]\times[0,+\infty)$, such that

$$\left|h(x)\eta(x,t)\mathbf{1}_{\{x\le K\}}\right|\le M_1\mathbf{1}_{\{x\le K\}}. \tag{4.24}$$

Note that $\mathbb{P}_x(X_u\le K)\le 1$, therefore (4.24) yields

$$\mathbb{E}_x\left[\int_0^{\tau\wedge t}|h(X_u)\eta(X_u,t-u)|\mathbf{1}_{\{X_u\le K\}}du\right]\le\left[\int_0^t M_1\mathbb{E}_x\left[\mathbf{1}_{\{X_u\le K\}}\right]du\right] \tag{4.25}$$

$$\le M_1\cdot t. \tag{4.26}$$

On the other hand, for $x>K$, by Lemma 4.2.1, we have

$$\mathbb{E}_x\left[\int_0^{\tau\wedge t}|h(X_u)\eta(X_u,t-u)|\mathbf{1}_{\{X_u>K\}}du\right]\le C_0+C_1\sqrt{t}+C_2t. \tag{4.27}$$

Combine (4.26) and (4.27), we get

$$\mathbb{E}_x\left[\int_0^{\tau\wedge t}|h(X_u)\eta(X_u,t-u)|du\right]\leq C_0+C_1\sqrt{t}+(C_2+M_1)t.$$

This concludes the first part proof. The second part of the proof is given by showing, for $t\in[0,T]$,

$$\left|\mathbb{E}_x\left[\int_0^{\tau\wedge t}h(X_u)\eta(X_u,t-u)du\right]\right|\leq C_0+C_1\sqrt{T}+(C_2+M_1)T.$$

□

Remark. In the proof above, the '(*) *w.l.o.g.*' appeared in the second line above the inequality (4.24) should be explained as follows. $h(0)\eta(0,t)$ and $h(x)\eta(x,0)$ are both well-defined for t and x on open intervals. The only singularity is generated by $(x,t)=(0,0)$. However, under the probability space, $X_u=0$ and $t-u=0$ only happens with $t=\tau$, while $P_x(\tau=t)=0$. Therefore, we can define $h(0)\eta(0,0)=0$. Plus $h(x)\eta(x,t)\to 0$ as $t\uparrow+\infty$, this gives us the boundedness of $h(x)\eta(x,t)$ on $[0,K]\times[0,+\infty)$, i.e. (4.24) holds true.

4.3 Model Application

4.3.1 Extension

In this subsection, we summarise a few extensions to our previous work. Let $\sigma>0$ be a constant. For $\sigma>0$, we consider the generalised OU model with a constant volatility:

$$dX_t=\epsilon(\theta-X_t)dt+\sigma dW_t. \tag{4.28}$$

The starting point is $X_0=x\in D$, and the hitting level is denoted by $l<x$, where in this case, l is the lower boundary of D. Consider an affine transformation $Y_t=\frac{X_t-l}{\sigma}$, which is specified by

$$dY_t=\epsilon(\hat{\theta}-Y_t)dt+dW_t,\ Y_0=\frac{x-l}{\sigma},\ \hat{\theta}=\frac{\theta-l}{\sigma}.$$

By choosing a new hitting level $\hat{l}=0$, the initial hitting time for $\{X_t\}_{t\geq 0}$ from x to l, becomes equivalent to the problem for $\{Y_t\}_{t\geq 0}$ from Y_0 to $\hat{l}$, i.e., denote by

$$\hat{\tau}_{\downarrow}:=\inf\{t>0:X_t=l|X_0=x>l\}\ \text{ and }\ \tau_Y:=\inf\left\{t>0:Y_t=0|Y_0=\frac{x-l}{\sigma}\right\},$$

then

$$\mathbb{P}(\hat{\tau}_{\downarrow} = \tau_Y) = 1. \tag{4.29}$$

Let

$$p^{(N)}_{\hat{\tau}_{\downarrow}}(t, l)$$

be the N-th order perturbed FPTD of $\{X_t\}_{t\geq 0}$ in (4.28), hitting from x to l with $x > l$; and denote the N-th order perturbed FPTD of τ_Y (which is given in Section 4.1) by

$$p^{(N)}_{\tau}(t|Y_0, \hat{\theta}),$$

with the starting and mean-reversion levels being specified. Then according to (4.29), we have

$$p^{(N)}_{\hat{\tau}_{\downarrow}}(t, l) = p^{(N)}_{\tau}\left(t \middle| \frac{x-l}{\sigma}, \frac{\theta - l}{\sigma}\right). \tag{4.30}$$

Now we consider the hitting from below case, i.e. $x < l$. Let $Z_t = -X_t$, then

$$dZ_t = \epsilon(\widetilde{\theta} - Z_t)dt + \sigma dB_t,\ Z_0 = -x,\ \widetilde{\theta} = -\theta,\ B_t = -W_t.$$

Define

$$\hat{\tau}_{\uparrow} := \inf\{t > 0 : X_t = l | X_0 = x < l\} \text{ and } \tau_Z := \inf\{t > 0 : Z_t = -l | Z_0 = -x\}.$$

Based on our construction, we further get

$$\mathbb{P}(\hat{\tau}_{\uparrow} = \tau_Z) = 1. \tag{4.31}$$

According to our assumption $x < l$, after the reflection, we have $-x > -l$. This transfers the hitting from below case to the hitting from above problem. And note that, the domain of $\{Z_t\}_{t\geq 0}$ now becomes $(-l, +\infty)$. Therefore[2], our previous work in Section 4.1 is still valid. Combine (4.31), and denote the hitting from below density by $p^{(N)}_{\hat{\tau}_{\uparrow}}(t, l)$, we then have

$$p^{(N)}_{\hat{\tau}_{\uparrow}}(t, l) = p^{(N)}_{\tau}\left(t \middle| \frac{l-x}{\sigma}, \frac{\theta - x}{\sigma}\right). \tag{4.32}$$

[2]We will see in later chapters, this in general is not true, if the process's behaviour is not symmetric about the reflection barrier.

Based on Equations (4.30) and (4.32), we can immediately have the distributions for the running max- and minimum. Define

$$M_T := \max_{0\le t\le T} X_t, \text{ and, } m_T := \min_{0\le t\le T} X_t.$$

For a fixe time T and a given level $l \in \mathbb{R}$, use the facts that

$$\begin{aligned}\{M_T \ge l\} &= \{\hat{\tau}_\uparrow \le T\}, \ x < l, \text{ and,}\\ \{m_T \le l\} &= \{\hat{\tau}_\downarrow \le T\}, \ x > l.\end{aligned}$$

The distributions of M_T and m_T are given by

$$\begin{aligned}\mathbb{P}_x\left(M_T \le l\right) &= 1 - \int_0^T p^{(N)}_{\hat{\tau}_\uparrow}(u,l)du, \text{ and,}\\ \mathbb{P}_x\left(m_T \le l\right) &= \int_0^T p^{(N)}_{\hat{\tau}_\downarrow}(u,l)du.\end{aligned}$$

4.3.2 Alternative Approach for the OU FPTD

We now provide three alternative methods for computing the OU FPTD. These methods will be used as benchmarks in the following subsection.

The first one is the eigenfunction expansion method, by V. Linetsky [77]. For $-\infty < l < x < \infty$, let

$$\bar{x} := \frac{\sqrt{2\epsilon}}{\sigma}(x-\theta), \ \bar{l} := \frac{\sqrt{2\epsilon}}{\sigma}(l-\theta), \ \lambda_n := v_n \cdot \epsilon;$$

where $\{v_n, \ n \ge 1\}$ with $0 < v_1 < ... < v_n \to +\infty$ as $n \to +\infty$, are the positive roots of the following *Hermite equation*:

$$H_v\left(\frac{\bar{l}}{\sqrt{2}}\right) = 0.$$

$H_v(\cdot)$ in above is the *Hermite polynomial* (solution to the *Hermite's differential equation*). Consider another series $\{c_n\}_{n\in\mathbb{N}}$, which is defined by

$$c_n = -\frac{H_{v_n}\left(\frac{\bar{x}}{\sqrt{2}}\right)}{v_n \cdot \frac{\partial}{\partial v}\left\{H_v\left(\frac{\bar{l}}{\sqrt{2}}\right)\right\}\big|_{v=v_n}},$$

then the downward OU FPTD is given by

$$p_\tau(t) = \sum_{n=1}^{\infty} c_n \lambda_n e^{-\lambda_n t}, \text{ for } t > 0. \tag{4.33}$$

This method involves numerical solutions for the zeros of Hermite function and its derivative. And in practice, we cannot compute the infinite sum. As there is no evidence to show c_n converges uniformly with $n \uparrow +\infty$, therefore truncation error is not avoidable for $t \approx 0$.

The second method is proposed by C. Kardaras and T. Ichiba [59]. They use 3-dimensional Brownian bridge simulation to approximate the FPTD of 1-dimensional diffusion. Let $\{X_t\}_{t\geq 0}$ be the OU process starting from x. Consider the hitting level $l < x$, and define $y = \frac{x-l}{\sigma}$ to be the starting point of the affine-transformed process. Also define

$$\psi(y) := \frac{\epsilon^2(\frac{\theta-l}{\sigma} - y)^2 - \epsilon}{2},$$

then under proper conditions [59], the OU FPTD can be expressed as

$$p_\tau(t) = \frac{y}{\sqrt{2\pi t^3}} e^{-\frac{y^2}{2t}} e^{-\int_0^y \epsilon(\frac{\theta-l}{\sigma} - v)dv} \mathbb{E}\left[e^{-t\int_0^1 \psi(|uye_1 + \sqrt{t}b_u|)du}\right] \text{ for } t > 0; \tag{4.34}$$

where $e_1 = [1, 0, 0]^T$, $|\cdot|$ is the Euclidean norm, and $\{b_t : t \geq 0\}$ is a standard 3-dimensional Brownian bridge.

The last method is the well-known explicit solution under a special case, $\theta = l$. Its derivation is based on the time-change method (see Theorem 2.1.6, Chapter 2). For full details of the derivation, please refer to [3, 49]. Here we only list the result:

$$p_\tau(t) = \frac{|x-l|}{\sqrt{2\pi}\sigma} \left(\frac{\epsilon}{\sinh(\epsilon t)}\right)^{\frac{3}{2}} e^{-\frac{\epsilon(x-l)^2 e^{-\epsilon t}}{2\sigma^2 \sinh(\epsilon t)} + \frac{\epsilon t}{2}}, \text{ for } t > 0, \tag{4.35}$$

where $\sinh(\cdot)$ is the *hyperbolic sin function*.

4.3.3 Numerical Example on Downward OU FPTD

In this subsection, we illustrate our results via two sets of exercises. Note that, all discussions in Section 4.3.1 are based on the results from Sections 4.1 and 4.2. Therefore, in this part, we only show the downward OU FPTD results.

We consider a generalised OU process (4.28). Model parameters are selected as follows

$$\epsilon = 0.1,\ \theta = 0.3,\ \sigma = 0.3,\ x = 0.5.$$

We conduct two sets of exercises. In the first one, we choose $l = \theta = 0.3$. And in the second group, we let $l = 0.2$.

Apart from our perturbation method, there are many other studies in finding the FPTD of OU process. For benchmarking purpose we list them below.

i). Talbot method of numerical inverse LT [1] (Theorem 2.3.4, Section 2.3, Chapter 2)

ii). FPTD representation by spectral decomposition [3] (Equation (4.33), Section 4.3.2)

iii). 3-dimensional Brownian bridge simulation [59] (Equation (4.34), Section 4.3.2)

iv). closed-form solution in the special case $l = \theta$ [49] (Equation (4.35), Section 4.3.2)

Method i) has been introduced in Chapter 2. Methods ii)-iv) are discussed in the previous subsection. Among these 4 methods, the closed-form density in iv) does not involve any numerical approximation. But it is only valid for $\theta = l$. Therefore in the first group of test, we treat it as the 'true' density. In general cases where $l \neq \theta$, there is no closed-form solution found yet. As an alternative, we use the Talbot approach to be our benchmark.

Benchmark Comparison for $l = \theta$

In this part, we only compare the Talbot method and our first order perturbation with the closed-form solution. Figures 4.1 and 4.2 show densities and their relative errors (*w.r.t.* approach iv)) in 5 years time.

Green dots in Figure 4.1 indicate 'true' densities. The blue line and orange segment curves plot Talbot inverse and first order perturbation, respectively. By visual observations we find those three densities coincide with each other. This confirms that our method is valid.

In order to check the accurateness and verify our error estimation formulae, we demonstrate relative errors in Figure 4.2. Blue and orange dots depict realised errors, which are calculated from the Talbot inverse and the perturbation density, by benchmarking them on the closed-form solution. Red dots are numerical evaluations from Proposition 3.3.1 and Lemma 4.1.5. We refer them to be theoretical errors. In the computation of $q_\tau(t)$, we simulate

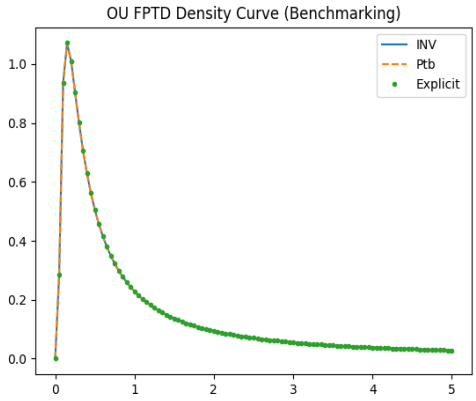

Figure 4.1: FPTD of OU process

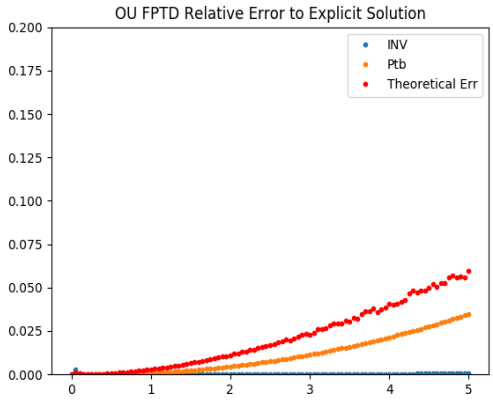

Figure 4.2: Relative errors to iv)

1000 paths with $dt = \frac{t}{1000}$. And the theoretical error is calculated by

$$err = \left| \frac{q_\tau(t)}{p_\tau^{(1)}(t) + q_\tau(t)} \right|.$$

From Figure 4.2 we see, in general, the Talbot inverse is very accurate, apart from that there is a peak for small t. In fact, by checking Figure 4.6 in Appendix 4.C, we find the perturbation approach outperforms the Talbot inverse on the left tail. Considering the fact that the perturbation provides smooth asymptotic on the left tail (Proposition 4.1.4), this result is not surprising. On the other hand, the error function of perturbation diverges when t becomes large. Although this is not very encouraging, it confirms our analysis for the right tail asymptotic.

In Figure 4.2, by further comparing theoretical and realised errors, we find they increase at the same rate. This verifies that Proposition 3.3.1 provides reasonable estimate to the level of error. The spread of them could be explained by limitations from Euler's simulation scheme. By reducing dt to 0, theoretically, we should be able to match red and orange curves. However, in practice we are more interested in the error range rather than exact error values; otherwise, the problem becomes equivalent to solve the FPTD via Monte Carlo simulations.

In terms of the computation speed, we provide the time of evaluating 100 density points. Without considering the initialisation of $\left\{c_k^{(i,j)}\right\}$ sequence[3], the perturbation has the same speed as the explicit density. Both of them spend about 0.001 seconds. The Talbot inverse

[3]The sequence does not involve any parameter in the OU model. Therefore it is only initialised once and pre-saved in memory.

spends about 1.371 seconds - approximately 1371 times slower than other two methods.

General Case Comparison for $l \neq \theta$

In the second exercise, we consider $l \neq \theta$ and illustrate results in the same way as before. Note that for $l \neq \theta$, we do not have any knowledge on the 'true' density. Considering in last section the Talbot inverse is almost the same as the closed-form solution, we therefore use it for benchmarking.

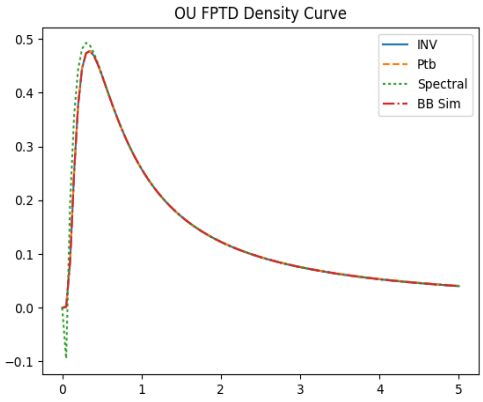

Figure 4.3: FPTD of OU process for general case

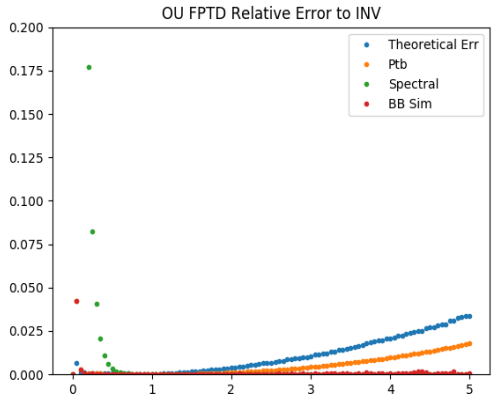

Figure 4.4: Relative error to i) for general case

An immediate observation from Figure 4.3 is that the spectral decomposition does not provide a good estimate on the left tail. By checking [3] one can find this is due to the divergence of spectral series at $t = 0$. Apart from the green curve, the rest three methods provide almost identical results. This confirms that the perturbation method works for general cases.

Results in Figure 4.4 are similar to what we have seen in Figure 4.2. We focus on explaining the spectral approach and the Brownian bridge simulation. Observed from error plots, for large t, those two methods can provide very accurate estimates. However, we have to mention that, their accuracy is based on the cost of requiring extra computational resources. In terms of the perturbation approach, although it is not as accurate as other methods (with a relative error bounded by 2.5%), it maintains an overwhelming advantage in the computation speed (0.001s v.s. 2.19s of the Talbot inverse, 3227.06s of the spectral decomposition, and 1162.11s of the 3-dimensional Brownian bridge simulation).

Appendix 4.A Proof of Proposition 4.1.1

Proof. We write $g_i(y)$ in (4.4) in terms of the *generating function*, i.e.

$$g_i(y) = \sum_{j=1}^{2i} p_j^{(2i)} y^j \leftrightarrow \left\langle 0, p_1^{(i)}, ...p_j^{(i)}, ..., p_{2i}^{(i)} \right\rangle^{2i},$$

where the locations of $\left\{ p_j^{(i)} : 0 \leq j \leq 2i \right\}$ in the brackets correspond to their orders in the polynomial from 0 to the highest order $2i$, and the superscript represents the highest order. Then

$$g_i^{'}(y) \leftrightarrow \left\langle p_1^{(i)}, 2p_2^{(i)}, ..., jp_j^{(i)}, ..., 2ip_{2i}^{(i)}, 0 \right\rangle^{2i},$$

and

$$g_i^{''}(y) \leftrightarrow \left\langle 2p_2^{(i)}, 6p_3^{(i)}, ..., j(j-1)p_j^{(i)}, ..., 2i(2i-1)p_{2i}^{(i)}, 0, 0 \right\rangle^{2i}.$$

Similarly we have the expressions for $g_{i-1}(y)$ and $g_{i-1}^{'}(y)$.

Note that, under our notations, $g_i^{'}$ is the derivative *w.r.t.* y, while in the initial ODE (3.23), the derivative is *w.r.t.* x. For this reason, according to the chain-rules,

$$\frac{1}{2}\partial_{xx} g_i(x) - \gamma \partial_x g_i(x) = (\theta - x)(\gamma g_{i-1}(x) - \partial_x g_{i-1}(x))$$

can be rewritten as

$$\frac{1}{2}\gamma^2 g_i^{''} - \gamma^2 g_i^{'} = (y - \gamma\theta)\left(g_{i-1}^{'} - g_{i-1} \right), \tag{4.36}$$

where $y = \gamma x$.

Substitute the generating function expressions into ODE (4.36), we get

$$\begin{aligned}
&\frac{1}{2}\gamma^2 \left\langle 2p_2^{(i)}, 6p_3^{(i)}, ..., j(j-1)p_j^{(i)}, ..., 2i(2i-1)p_{2i}^{(i)}, 0, 0 \right\rangle^{2i} \\
&\quad -\gamma^2 \left\langle p_1^{(i)}, 2p_2^{(i)}, ..., (j-1)p_{j-1}^{(i)}, ..., 2ip_{2i}^{(i)}, 0 \right\rangle^{2i} \\
&= \left\langle 0, p_1^{(i-1)}, 2p_2^{(i-1)}, ..., (j-2)p_{j-2}^{(i-1)}, ..., (2i-2)p_{2i-2}^{(i-1)} \right\rangle^{2i-2} \\
&\quad - \left\langle 0, 0, p_1^{(i-1)}, ..., p_{j-3}^{(i-1)}, ..., p_{2i-2}^{(i-1)} \right\rangle^{2i-1} \\
&\quad -\gamma\theta \left\langle p_1^{(i-1)}, 2p_2^{(i-1)}, ..., (j-1)p_{j-1}^{(i-1)}, ..., (2i-2)p_{2i-2}^{(i-1)}, 0 \right\rangle^{2i-2} \\
&\quad +\gamma\theta \left\langle 0, p_1^{(i-1)}, ..., p_{j-2}^{(i-1)}, ..., p_{2i-2}^{(i-1)} \right\rangle^{2i-2}.
\end{aligned}$$

Re-arrange the right-hand side, we get

$$\begin{aligned}
&\gamma^2 \cdot \Big\langle p_2^{(i)} - p_1^{(i)}, 3p_3^{(i)} - 2p_2^{(i)}, ..., \frac{1}{2}j(j-1)p_j^{(i)} - (j-1)p_{j-1}^{(i)}, ..., \\
&\qquad i(2i-1)p_{2i}^{(i)} - (2i-1)p_{2i-1}^{(i)}, -2ip_{2i}^{(i)} \Big\rangle^{2i-1} \\
= \; &\Big\langle -\gamma\theta p_1^{(i-1)}, p_1^{(i-1)} - 2\gamma\theta p_2^{(i-1)} + \gamma\theta p_1^{(i-1)}, ..., \\
&\qquad (j-2)p_{j-2}^{(i-1)} - p_{j-3}^{(i-1)} - \gamma\theta(j-1)p_{j-1}^{(i-1)} + \gamma\theta p_{j-2}^{(i-1)}, ..., \\
&\qquad (2i-2)p_{2i-2}^{(i-1)} - p_{2i-3}^{(i-1)} + \gamma\theta p_{2i-2}^{(i-1)}, -p_{2i-2}^{(i-1)} \Big\rangle^{2i-1}.
\end{aligned}$$

Finally, by matching each term in the equation above, from right to left (higher order to lower order), we conclude our proof. □

Appendix 4.B Recursive Polynomial Decomposition and Proof of Lemma 4.1.2

We present the proof of Lemma 4.1.2 at the end of this appendix (cf. p. 66). Before stating the proof, we need the following two corollaries.

Corollary 4.B.1 (Decomposition Structure I)**.** *For $i = 1$ and $i = 2$, $\left\{c_k^{(i,j)}\right\}$ is explicitly given by*

$$\begin{cases}
i = 1: \;\; c_0^{(1,2)} = \frac{1}{2};\; c_0^{(1,1)} = \frac{1}{2};\; c_1^{(1,1)} = -1; \\
\\
i = 2: \;\; \begin{cases} c_0^{(2,4)} = \frac{1}{8};\; c_0^{(2,3)} = \frac{1}{12};\; c_1^{(2,3)} = -\frac{1}{2};\; c_0^{(2,2)} = -\frac{1}{8};\; c_1^{(2,2)} = 0;\; c_2^{(2,2)} = \frac{1}{2}; \\ c_0^{(2,1)} = -\frac{1}{8};\; c_1^{(2,1)} = \frac{1}{2};\; c_2^{(2,1)} = -\frac{1}{2}. \end{cases}
\end{cases}$$

Corollary 4.B.2 (Decomposition Structure II)**.** *For $i \geq 3$, $\left\{c_k^{(i,j)}\right\}$ is recursively determined*

by

$$
\begin{cases}
j = 2i: & c_0^{(i,2i)} = \frac{c_0^{(i-1,2i-2)}}{2i} \\
\\
j = 2i-1: & \begin{cases} c_0^{(i,2i-1)} = \frac{1}{(2i-1)} c_0^{(i-1,2i-3)} - \frac{2i-3}{2(2i-1)} c_0^{(i-1,2i-2)}; \\ c_1^{(i,2i-1)} = \frac{1}{(2i-1)} \left(c_1^{(i-1,2i-3)} - c_0^{(i-1,2i-2)} \right) \end{cases} \\
\\
2 < j < 2i-1: & \begin{cases} k = (2i-j) \wedge i: & \begin{cases} c_{2i-j}^{(i,j)} = \frac{1}{j} \left(c_{2i-j}^{(i-1,j-2)} - c_{2i-j-1}^{(i-1,j-1)} \right), \ j > i \\ c_i^{(i,i)} = -\frac{1}{i} c_{i-1}^{(i-1,i-1)}, \ j = i \\ c_i^{(i,j)} = \frac{1}{2}(j+1) c_i^{(i,j+1)} - \frac{1}{j} c_{i-1}^{(i-1,j-1)} \\ \qquad + c_{i-1}^{(i-1,j)}, \ j < i \end{cases} \\ 0 < k < (2i-j) \wedge i: \ c_k^{(i,j)} = \frac{1}{2}(j+1) c_k^{(i,j+1)} + \frac{1}{j} c_k^{(i-1,j-2)} \\ \qquad - \frac{j-1}{j} c_k^{(i-1,j-1)} - \frac{1}{j} c_{k-1}^{(i-1,j-1)} + c_{k-1}^{(i-1,j)} \\ k = 0: \ c_0^{(i,j)} = \frac{1}{2}(j+1) c_0^{(i,j+1)} + \frac{1}{j} c_0^{(i-1,j-2)} - \frac{j-1}{j} c_0^{(i-1,j-1)} \end{cases} \\
\\
j = 2: & \begin{cases} k = i: & c_i^{(i,2)} = \frac{3}{2} c_i^{(i,3)} - \frac{1}{2} c_{i-1}^{(i-1,1)} + c_{i-1}^{(i-1,2)} \\ 0 < k < i: & c_k^{(i,2)} = \frac{3}{2} c_k^{(i,3)} - \frac{1}{2} c_k^{(i-1,1)} - \frac{1}{2} c_{k-1}^{(i-1,1)} + c_{k-1}^{(i-1,2)} \\ k = 0: & c_0^{(i,2)} = \frac{3}{2} c_0^{(i,3)} - \frac{1}{2} c_0^{(i-1,1)} \end{cases} \\
\\
j = 1: & \begin{cases} k = i: & c_i^{(i,1)} = c_i^{(i,2)} + c_{i-1}^{(i-1,1)} \\ 0 < k < i: & c_k^{(i,1)} = c_k^{(i,2)} + c_{k-1}^{(i-1,1)} \\ k = 0: & c_0^{(i,1)} = c_0^{(i,2)} \end{cases}
\end{cases}.
$$

Proof of Corollaries 4.B.1, 4.B.2. First, consider Corollary 4.B.1. The $i = 1$ case is confirmed by comparing the results with (4.3). Similarly, for $i = 2$, set $A_1 = 0$, $A_2 = +\infty$,

$C_1 = 0$, and $C_2 = 0$. Then by Lemma 3.4.2, we have

$$\begin{aligned} f_2(x) =& e^{-\gamma x}\bigg(\frac{1}{8\gamma^4}(\gamma x)^4 + (\frac{1}{12\gamma^4} - \frac{\theta}{2\gamma^3})(\gamma x)^3 + (-\frac{1}{8\gamma^4} + \frac{\theta^2}{2\gamma^2})(\gamma x)^2 \\ &+ (-\frac{1}{8\gamma^4} + \frac{\theta}{2\gamma^3} - \frac{\theta^2}{2\gamma^2})(\gamma x)\bigg). \end{aligned}$$

The $i = 2$ case in Corollary 4.B.1, is then verified accordingly.

Now we prove Corollary 4.B.2. Note that, $j = i$ is a special case for $0 \le k \le (2i - j) \wedge i$, therefore we need to treat it with an extra care. Denote and split the $2 < j < 2i - 1$ case by,

$$\begin{cases} i < j < 2i - 1 : & \mathcal{G}_{c_k}^{(I)} \\ j = i : & \mathcal{G}_{c_k}^{(II)} \\ 2 < j < i : & \mathcal{G}_{c_k}^{(III)} \end{cases}.$$

Also write the $j = 2$ and $j = 1$ cases as

$$j = 2 : \ \mathcal{S}_{c_k}, \text{ and } j = 1 : \ \mathcal{F}_{c_k},$$

respectively. Recall Proposition 4.1.1 and Lemma 4.1.2. For $i \ge 3$, first consider $j = 2i$. We have $2i - j \wedge i = 0$. Therefore,

$$p_{2i}^{(i)} = c_0^{(i,2i)} \left(\frac{1}{\gamma}\right)^{2i} = \frac{p_{2i-2}^{(i-1)}}{2i\gamma^2} = \frac{1}{2i\gamma^2} \cdot c_0^{(i-1,2i-2)} \left(\frac{1}{\gamma}\right)^{2i-2}.$$

Solving $c_0^{(i,2i)}$ from above, yields

$$c_0^{(i,2i)} = \frac{c_0^{(i-1,2i-2)}}{2i}.$$

Then for $j = 2i - 1$, we have $2i - j \wedge i = 1$. Substitute $\left\{c_k^{(i,j)}\right\}$ in Lemma 4.1.2 into Proposition 4.1.1, we get

$$p_{2i-1}^{(i)} = c_0^{(i,2i-1)} \left(\frac{1}{\gamma}\right)^{2i} + c_1^{(i,2i-1)} \left(\frac{1}{\gamma}\right)^{2i-1} \theta. \tag{4.37}$$

And similarly,

$$p_{2i-3}^{(i-1)} = c_0^{(i-1,2i-3)} \left(\frac{1}{\gamma}\right)^{2i-2} + c_1^{(i-1,2i-3)} \left(\frac{1}{\gamma}\right)^{2i-3} \theta. \tag{4.38}$$

Substitute (4.37) and (4.38) into the recursion formula in Proposition 4.1.1, we further have

$$c_0^{(i,2i-1)}\left(\frac{1}{\gamma}\right)^{2i}+c_1^{(i,2i-1)}\left(\frac{1}{\gamma}\right)^{2i-1}\theta \;=\frac{1}{(2i-1)\gamma^2}\left[c_0^{(i-1,2i-3)}\left(\tfrac{1}{\gamma}\right)^{2i-2}+c_1^{(i-1,2i-3)}\left(\tfrac{1}{\gamma}\right)^{2i-3}\theta\right] + \left(\frac{1}{2\gamma^2}-\frac{\gamma\theta+(2i-2)}{(2i-1)\gamma^2}\right)c_0^{(i-1,2i-2)}\left(\tfrac{1}{\gamma}\right)^{2i-2}.$$

Rearranging the terms in the right-hand side (RHS) gives

$$RHS=\left[\frac{1}{2i-1}c_0^{(i-1,2i-3)}-\frac{2i-3}{2(2i-1)}c_0^{(i-1,2i-2)}\right]\left(\frac{1}{\gamma}\right)^{2i} + \frac{1}{2i-1}\left[c_1^{(i-1,2i-3)}-c_0^{(i-1,2i-2)}\right]\left(\frac{1}{\gamma}\right)^{2i-1}\theta;$$

by matching the coefficients of θ and γ, we get the results for $j=2i-1$ in Lemma 4.1.2.

Now we consider the cases for general j. The calculation involves $p_j^{(i)}$, $p_{j+1}^{(i)}$, $p_{j-2}^{(i-1)}$, $p_{j-1}^{(i-1)}$ and $p_j^{(i-1)}$. First consider when $i<j<2i-1$, in this case we have

$$\begin{cases} 2i-j\wedge i=2i-j \\ 2i-j-1\wedge i=2i-j-1 \\ 2i-j\wedge i-1=2i-j \\ 2i-j-1\wedge i-1=2i-j-1 \\ 2i-j-2\wedge i-1=2i-j-2 \end{cases}.$$

The recursion formula in Proposition 4.1.1 can be written as

$$\sum_{k=0}^{2i-j}c_k^{(i,j)}\left(\frac{1}{\gamma}\right)^{2i-k}\theta^k=\frac{1}{2}(j+1)\sum_{k=0}^{2i-j-1}c_k^{(i,j+1)}\left(\frac{1}{\gamma}\right)^{2i-k}\theta^k + \frac{1}{\gamma^2 j}\sum_{k=0}^{2i-j}c_k^{(i-1,j-2)}\left(\frac{1}{\gamma}\right)^{2i-k-2}\theta^k+\frac{\theta}{\gamma}\sum_{k=0}^{2i-j-2}c_k^{(i-1,j)}\left(\frac{1}{\gamma}\right)^{2i-k-2}\theta^k - \frac{j-1+\gamma\theta}{\gamma^2 j}\sum_{k=0}^{2i-j-1}c_k^{(i-1,j-1)}\left(\frac{1}{\gamma}\right)^{2i-k-2}\theta^k.$$

Rearrange the terms, and use the expression of generating function (w.r.t. $\left(\frac{1}{\gamma}\right)^{2i-k}\theta^k$) again,

we have the following equation

$$\begin{aligned}\left\langle c_0^{(i,j)},...,c_k^{(i,j)},...,c_{2i-j}^{(i,j)}\right\rangle^{2i-j} &= \frac{1}{2}(j+1)\left\langle c_0^{(i,j+1)},...,c_k^{(i,j+1)},...,0\right\rangle^{2i-j}\\ &+ \frac{1}{j}\left\langle c_0^{(i-1,j-2)},...,c_k^{(i-1,j-2)},...,c_{2i-j}^{(i-1,j-2)}\right\rangle^{2i-j}\\ &- \frac{j-1}{j}\left\langle c_0^{(i-1,j-1)},...,c_k^{(i-1,j-1)},...,0\right\rangle^{2i-j}\\ &- \frac{1}{j}\left\langle 0,...,c_{k-1}^{(i-1,j-1)},...,c_{2i-j-1}^{(i-1,j-1)}\right\rangle^{2i-j}\\ &+ \left\langle 0,...,c_{k-1}^{(i-1,j)},...,0\right\rangle^{2i-j}.\end{aligned}$$

By matching the coefficients, we get the expression of $\mathcal{G}_{c_k}^{(I)}$.

For $\mathcal{G}_{c_k}^{(II)}$, consider $i=j$, we have

$$\begin{cases}2i-j\wedge i=i\\ 2i-j-1\wedge i=i-1\\ 2i-j\wedge i-1=i-1\\ 2i-j-1\wedge i-1=i-1\\ 2i-j-2\wedge i-1=i-2\end{cases}.$$

By using the same method as in solving $\mathcal{G}_{c_k}^{(I)}$, we find $\mathcal{G}_{c_k}^{(II)}$. Similarly, $\mathcal{G}_{c_k}^{(III)}$ is acquired by repeating again the calculations.

Now for $j=2$, different recursion equation is considered. The calculation requires

$$\begin{cases}p_2^{(i)}=\sum_{k=0}^{i}c_k^{(i,2)}\left(\frac{1}{\gamma}\right)^{2i-k}\theta^k\\ p_3^{(i)}=\sum_{k=0}^{i}c_k^{(i,3)}\left(\frac{1}{\gamma}\right)^{2i-k}\theta^k\\ p_2^{(i-1)}=\sum_{k=0}^{i-1}c_k^{(i-1,2)}\left(\frac{1}{\gamma}\right)^{2i-k-2}\theta^k\end{cases}.$$

Write in terms of generating coefficients, we get

$$\begin{aligned}\left\langle c_0^{(i,2)},...,c_k^{(i,2)},...,c_i^{(i,2)}\right\rangle^{i} &= \frac{3}{2}\left\langle c_0^{(i,3)},...,c_k^{(i,3)},...,c_i^{(i,3)}\right\rangle^{i}-\frac{1}{2}\left\langle c_0^{(i-1,1)},...,c_k^{(i-1,1)},...,0\right\rangle^{i}\\ &- \frac{1}{2}\left\langle 0,...,c_{k-1}^{(i-1,1)},...,c_{i-1}^{(i-1,1)}\right\rangle^{i}+\left\langle 0,...,c_{k-1}^{(i-1,2)},...,c_{i-1}^{(i-1,2)}\right\rangle^{i}.\end{aligned}$$

Again, by comparing orders, we have the expression of $\mathcal{S}_{c_k}$.

In the end, consider $j = 1$, we need

$$\begin{cases} p_1^{(i)} = \sum_{k=0}^{i} c_k^{(i,1)} \left(\frac{1}{\gamma}\right)^{2i-k} \theta^k \\ p_2^{(i)} = \sum_{k=0}^{i} c_k^{(i,2)} \left(\frac{1}{\gamma}\right)^{2i-k} \theta^k \\ p_1^{(i-1)} = \sum_{k=0}^{i-1} c_k^{(i-1,1)} \left(\frac{1}{\gamma}\right)^{2i-k-2} \theta^k \end{cases} .$$

The equation of generating coefficients is given by

$$\left\langle c_0^{(i,1)}, ..., c_k^{(i,1)}, ..., c_i^{(i,1)} \right\rangle^i = \left\langle c_0^{(i,2)}, ..., c_k^{(i,2)}, ..., c_i^{(i,2)} \right\rangle^i + \left\langle 0, ..., c_{k-1}^{(i-1,1)}, ..., c_{i-1}^{(i-1,1)} \right\rangle^i .$$

This solves $\mathcal{F}_{c_k}$, and concludes the proof.

□

Proof of Lemma 4.1.2. The existence and structures of $\left\{c_k^{(i,j)}\right\}$, which satisfies Equation (4.5), are proved by Corollaries 4.B.1 and 4.B.2 above. □

Appendix 4.C Further Numerical Result

In this appendix, we provide the left tail zoom-in of FPTDs/errors shown in Section 4.3.3. Figures 4.5 and 4.6 correspond to the density/error plots in Figures 4.1 and 4.2. Similarly, Figures 4.7 and 4.8 are the left tails of FPTDs/errors in Figures 4.3 and 4.4. The purpose of this appendix is to show the accurateness of the perturbation for the left tails.

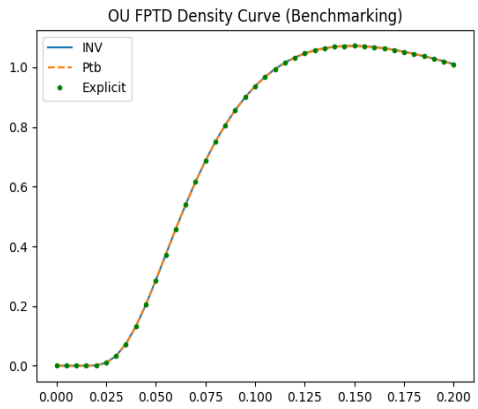

Figure 4.5: OU left tail density for $l = \theta$

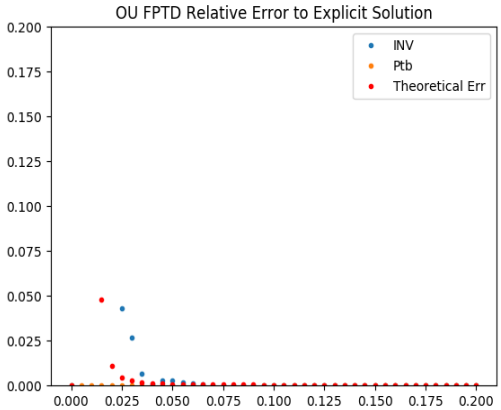

Figure 4.6: OU left tail error for $l = \theta$

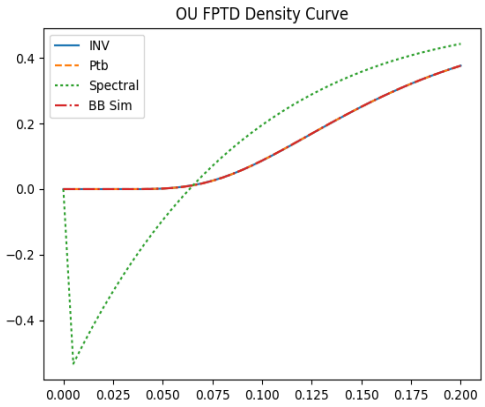

Figure 4.7: OU left tail density for $l \neq \theta$

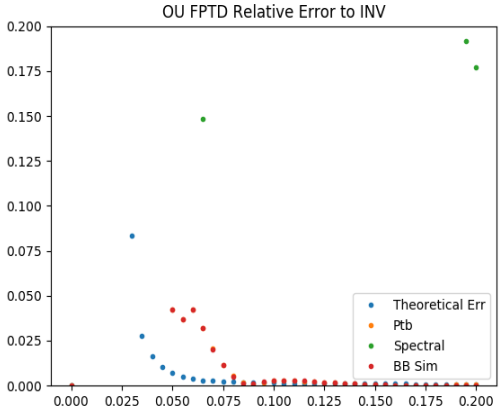

Figure 4.8: OU left tail error for $l \neq \theta$

Chapter 5

First Passage Time of Bessel Process

The Bessel process was introduced in [87] as the norm of an n-dimensional Brownian motion. Denote by BES(n) (sometimes by BES(ν) with $\nu = \frac{n-2}{2}$), the Bessel process has been studied extensively in [105, Chapter XI]. In mathematical finance, the family of Bessel processes is closely[1] related to models in short rates and stochastic volatilities [22, 24, 27, 34, 55].

In this chapter, we consider the class of Bessel processes with orders $n = 1 + \epsilon$, where $-1 < \epsilon < 1$. The SDE of BES(n) is specified in (2.19), Chapter 2. Based on our previous notations, for BES($1 + \epsilon$), the h-function is given by

$$h(X_t) = \frac{1}{2X_t},\ X_t \in D, \tag{5.1}$$

where $D = (0, +\infty)$. According to [62, 69], $\{\infty\}$ is a natural boundary for all $\epsilon \in \mathbb{R}$; for $-1 < \epsilon < 1$ ($0 < n < 2$), $\{0\}$ is a regular boundary with both types of exit and entrance. We assume the process makes instantaneous reflection at 0. Refer to [69], the infinitesimal generator then is well defined for all C^2-functions on D. Denote it by

$$\mathcal{A}f(x) = \frac{1}{2}f^{''}(x) + \frac{\epsilon}{2x}f^{'}(x),\ x \in D.$$

We consider a general hitting level $0 < a < X_0 = x$ rather than $a = 0$. The domain D

[1] Squared Bessel process appears in the Constant Elasticity of Variance (CEV) model and the Cox-Ingersoll-Ross (CIR) process (or Heston model), see also Example 2.1.7, Chapter 2.

then is reduced to $D = (a, +\infty)$. Follow our definition in (3.3), by suppressing a, we denote the downward FPT of $\{X_t\}_{t\geq 0}$ by

$$\tau = \inf\{t > 0 : X_t = a\}, \ X_0 = x > a.$$

According to [105], BES$(1+\epsilon)$ is recurrent on D for all $\epsilon \in (-1, 1)$. This guarantees that τ is finite *a.s.* Therefore the corresponding BVP exists. The BVP boundary in (3.6) is specified by $f(a) = 1$. And refer to [18, 69], the initial LT is given by the ratio of *modified Bessel functions of the second kind*:

$$f(x, \beta) = \left(\frac{a}{x}\right)^{\frac{\epsilon-1}{2}} \frac{K_{\frac{\epsilon-1}{2}}(\sqrt{2\beta}x)}{K_{\frac{\epsilon-1}{2}}(\sqrt{2\beta}a)}. \tag{5.2}$$

Similar as in the OU process, the ILT can be computed numerically via [1] (Section 2.3, Chapter 2) or using spectral decompositions [71]. In this chapter, we apply our previous work and solve the downward FPTD via perturbation. Note that, the h-function for BES$(1+\epsilon)$ is no more closed under integration. Similar recursion formulae (as what we have seen in Chapter 4) may not be found easily for the FPTD of $\{X_t\}_{t\geq 0}$. Therefore, in this chapter, we focus on the analysis of the first order perturbation.

The rest of this chapter is organised as follows. In Section 5.1, we solve the first order FPTD. Section 5.2 provides further technical discussions on tail asymptotics and the error estimation. Numerical results are demonstrated in Section 5.3. Section 5.4 is a short conclusion for the work from Chapters 3, 4, and 5. In the appendices of this chapter, we summarise a few extensions of our model. Those results will be referred to later in Chapter 8.

5.1 First Order Perturbed FPTD

Throughout this chapter, again we use the notation $\gamma = \sqrt{2\beta}$. For $x > a$, let f_0 be defined as in (2.28), Example 2.2.2:

$$f_0(x, \beta) = e^{-\gamma(x-a)}.$$

And as we did before, we use f_0, $f_0(x)$, $f_0(x, \beta)$ (the same for f_1, g_1) interchangeably.

Lemma 5.1.1 (First Order BVP Solution)**.** *The first order perturbed LT is given by*

$$f_1(x,\beta) = f_0(x,\beta)\frac{\ln(\frac{a}{x}) + e^{2\gamma a}E_1(2\gamma a) - e^{2\gamma x}E_1(2\gamma x)}{2},$$

where $E_1(\cdot)$ *is the* exponential integral function.

Proof. Follow Lemma 3.4.2, the h-function and k_1 are specified by (5.1) and $k_1 = \gamma$, respectively. According to (3.26), by assigning $A_0 = 0$, $A_2 = +\infty$, we get

$$g_1 = \int_0^x 2e^{2\gamma y}\left[\gamma\int_{+\infty}^{y}\frac{1}{2z}e^{-2\gamma z}dz + C_1\right]dy + C_2. \tag{5.3}$$

After standard calculations, the inner integral yields

$$\frac{\gamma}{2}\int_{+\infty}^{y}\frac{1}{z}e^{-2\gamma z}dz = -\frac{\gamma}{2}E_1(2\gamma y).$$

Simplify (5.3) using the equation above, we have

$$g_1 = \int_0^x -\gamma e^{2\gamma y}E_1(2\gamma y)dy + C_1\frac{e^{2\gamma x}-1}{\gamma} + C_2. \tag{5.4}$$

Refer to [48, Equation (5), 4.2.], for the integral in (5.4), we further have

$$\int_0^x -\gamma e^{2\gamma y}E_1(2\gamma y)dy = -\frac{\ln(x) + e^{2\gamma x}E_1(2\gamma x)}{2} + C_3.$$

Combine C_3 and C_2, based on (5.4), (5.3) then becomes

$$g_1 = -\frac{\ln(x) + e^{2\gamma x}E_1(2\gamma x)}{2} + C_1\frac{e^{2\gamma x}-1}{\gamma} + C_2. \tag{5.5}$$

C_1 and C_2 are determined through boundary conditions in the $o(\epsilon^1)$-problem. We start with the upper boundary $\{+\infty\}$. By L'Hôpital's rule, $f_0(x)\ln(x) \to 0$ as $x \uparrow +\infty$. And refer to [48, Equation (5), 3.3], for the E_1-term, we find

$$\lim_{x\uparrow+\infty} f_0(x)e^{2\gamma x}E_1(2\gamma x) = 0.$$

Therefore,

$$\lim_{x\uparrow+\infty} f_1 = \lim_{x\uparrow+\infty} f_0 g_1 = \lim_{x\uparrow+\infty} C_1\frac{e^{2\gamma x}-1}{\gamma};$$

and the only C_1 which satisfies the condition $f_1(+\infty) = 0$ is 0. Similarly, substitute $C_1 = 0$ into (5.5) and solve $f_1(a) = 0$, we get

$$C_2 = \frac{\ln(a) + e^{2\gamma a} E_1(2\gamma a)}{2}.$$

The rest of the proof is then concluded by Lemma 3.4.2. □

Corollary 5.1.2 (Full Integrability)**.** *The first order perturbed FPTD of BES*$(1+\epsilon)$ *is fully integrable, i.e.*

$$\int_0^{+\infty} \mathcal{L}^{-1}\left\{f^{(1)}(\beta)\right\}(t)dt = 1.$$

Proof. The corollary is proved by showing

$$\lim_{\beta \to 0^+} f^{(1)}(x, \beta) = 1.$$

Since $\lim_{\beta\to 0^+} f_0(x, \beta) = 1$, therefore it is sufficient to only justify

$$\lim_{\beta \to 0^+} g_1(x, \beta) = 0.$$

Indeed, by considering [48, Equation (1), 3.3] that

$$E_1(x) = -c_\gamma - \ln(x) + \int_0^x \frac{1 - e^{-u}}{u} du,$$

where $c_\gamma = 0.5772$ is the Euler's constant; and note that

$$\lim_{x \downarrow 0} \int_0^x \frac{1 - e^{-u}}{u} du = 0,$$

we immediately prove the result. □

Proposition 5.1.3 (First Order Perturbed FPTD of BES$(1+\epsilon)$)**.** *The first order perturbed downward FPTD of BES*$(1+\epsilon)$ *is given by*

$$p_\tau^{(1)}(t) = \left(1 + \frac{\epsilon}{2}\ln(\frac{a}{x})\right) p_{\tau,x,a}^{(0)}(t) + \frac{\epsilon(x-a)}{\sqrt{2\pi t}} \int_{(x-a)^2}^{\infty} \frac{p_\Gamma(y, 1, \frac{1}{2t})dy}{(\sqrt{y} - x + 3a)(\sqrt{y} + x + a)} dy, \quad (5.6)$$

where

$$p^{(0)}_{\tau,x,a}(t) := \frac{x-a}{\sqrt{2\pi}} t^{-\frac{3}{2}} e^{-\frac{(x-a)^2}{2t}}, \tag{5.7}$$

and

$$p_{\Gamma}(y, 1, \frac{1}{2t}) := \frac{1}{2t} e^{-\frac{y}{2t}} \tag{5.8}$$

are density functions of inverse Gamma and Gamma distributions, respectively.

Proof. Rearrange terms in the first order LT,

$$f^{(1)}(x,\beta) = f_0(x,\beta)\left(1 + \frac{\epsilon}{2}\ln(\frac{a}{x})\right) + \epsilon f_0(x,\beta)\frac{e^{2\gamma a}E_1(2\gamma a) - e^{2\gamma x}E_1(2\gamma x)}{2}. \tag{5.9}$$

The inverse of the first term in (5.9) is given by (2.29), Example 2.2.2. Now consider the second term. Recall the definition of $E_1(z)$:

$$E_1(z) := \int_z^{+\infty} \frac{e^{-u}}{u} du.$$

By multiplying e^z we have

$$e^z E_1(z) = \int_0^{\infty} \frac{e^{-uz}}{u+1} du. \tag{5.10}$$

Assume we can change the order of integrals, then substituting (5.10) into the second term of (5.9) yields

$$\mathcal{L}^{-1}\left\{e^{-\sqrt{2\beta}(x-a)} e^{z\sqrt{2\beta}} E_1(z\sqrt{2\beta})\right\}(t) = \int_0^{\infty} \frac{\mathcal{L}^{-1}\left\{e^{-\sqrt{2\beta}(x-a+uz)}\right\}(t)}{u+1} du \tag{5.11}$$

$$= \int_0^{\infty} \frac{p^{(0)}_{\tau,x-a+uz,0}(t)}{u+1} du, \tag{5.12}$$

where $p^{(0)}_{\tau,x-a+uz,0}(t)$ is defined by (5.7); more specifically, let

$$y := (x-a+uz)^2, \tag{5.13}$$

(5.12) further gives

$$\begin{aligned}\int_0^\infty \frac{p^{(0)}_{\tau,x-a+uz,0}(t)}{u+1}du =& \frac{1}{\sqrt{2\pi}t^{\frac{3}{2}}}\int_0^\infty \frac{(x-a+uz)e^{-\frac{(x-a+uz)^2}{2t}}}{u+1}du \\ =& \frac{1}{\sqrt{2\pi t}}\int_{(x-a)^2}^\infty \frac{\frac{1}{2t}e^{-\frac{y}{2t}}}{\sqrt{y}+a-x+z}dy.\end{aligned}$$

According to the definition in (5.8), we then get

$$\mathcal{L}^{-1}\left\{e^{-\sqrt{2\beta}(x-a)}e^{z\sqrt{2\beta}}E_1(z\sqrt{2\beta})\right\}(t) = \frac{1}{\sqrt{2\pi t}}\int_{(x-a)^2}^\infty \frac{p_\Gamma(y,1,\frac{1}{2t})}{\sqrt{y}-(x-a)+z}dy, \tag{5.14}$$

where $p_\Gamma(y,1,\frac{1}{2t})$ is the density function of Gamma distribution with shape parameter 1 and rate parameter $\frac{1}{2t}$. The rest of the proof is concluded by substituting $z=2a$ and $z=2x$ into (5.14), respectively. □

Remark. The perturbed density for BES$(1+\epsilon)$ is continuous on $(0,+\infty)$. As a sufficient but not necessary condition, as long as[2]

$$1+\frac{\epsilon}{2}\ln(\frac{a}{x}) \geq 0,$$

the function $p^{(1)}_\tau(t)$ then is guaranteed to be positive. Therefore, combine Corollary 5.1.2, the first order perturbed FPTD is a valid probability density function. On the other hand, by using properties of integer Bessel functions in [128, Chapter III], potentially one can derive FPTDs of BES$(n+\epsilon)$ with $n \in \mathbb{N}$.

5.2 Tail Asymptotic and Error Estimation

Proposition 5.2.1 (Tail Asymptotics of BES$(1+\epsilon)$ Perturbed FPTD)**.** *Tail asymptotics of the first order perturbed BES$(1+\epsilon)$ FPTD are given by*[3]

$$p^{(1)}_\tau(t) \sim p^{(0)}_{\tau,x,a}(t), \ \text{as } t \downarrow 0, \tag{Left Tail}$$

$$p^{(1)}_\tau(t) \sim t^{-1-\alpha}, \ \text{as } t \uparrow +\infty, \tag{Right Tail}$$

[2]In fact, in the case $\epsilon < 0$ (this gives a Bessel process of an order between 0 and 1), the inequality holds true for any $a \leq x$.

[3]Please refer to footnote 5 on p. 26, of Section 2.5, Chapter 2, for more details of the symbol $\sim$.

where $0 < \alpha < \frac{1}{2}$.

Proof. We start from the left tail. The first term in $p_\tau^{(1)}(t)$ has the same order as the FPTD of Brownian motion. We only need to check the second term, which involves the expectation of functionals on a Gamma variable.

We rewrite the integral term in (5.6) as a convolution. From (5.11), by applying the convolution rule on $\mathcal{L}^{-1}\left\{e^{-\sqrt{2\beta}(x-a)}e^{-\sqrt{2\beta}uz)}\right\}(t)$, we can write

$$\begin{aligned}&\frac{1}{\sqrt{2\pi t}}\int_{(x-a)^2}^{\infty}\frac{p_\Gamma(y,1,\frac{1}{2t})dy}{(\sqrt{y}-x+3a)(\sqrt{y}+x+a)}dy\\&=\int_0^t p_{\tau,x,a}^{(0)}(v)\int_0^\infty\frac{p_{\tau,2ua,0}^{(0)}(t-v)-p_{\tau,2ux,0}^{(0)}(t-v)}{2(u+1)}dudv.\end{aligned}\tag{5.15}$$

Denote by

$$\lambda(t):=t^{-\frac{3}{2}}e^{-\frac{(x-a)^2}{2t}},\tag{5.16}$$

and

$$\mu(t):=\int_0^t\lambda(v)\int_0^\infty\frac{p_{\tau,2ua,0}^{(0)}(t-v)-p_{\tau,2ux,0}^{(0)}(t-v)}{2(u+1)}dudv,\tag{5.17}$$

to be the asymptotics of the inverse Gamma density and the convolution, respectively. Let $t\downarrow 0$, then (5.17) yields

$$\mu(t)\sim\int_0^t\lambda(v)\int_0^\infty\frac{p_{\tau,2ua,0}^{(0)}(v)-p_{\tau,2ux,0}^{(0)}(v)}{2(u+1)}dudv.\tag{5.18}$$

Define

$$r(t):=\frac{\mu(t)}{\lambda(t)}.$$

An immediate observation is that the limit of $r(t)$ at 0 is a $\frac{0}{0}$-type. To see this, consider the LT of $\mu(t)$. Based on the initial value theorem (Equation (2.37), Fact 2.3.1, Section 2.3), we have

$$\lim_{t\downarrow 0}\mu(t)=\lim_{\beta\to+\infty}\left(\beta e^{-\sqrt{2\beta}(x-a)}\left(e^{2a\sqrt{2\beta}}E_1(2a\sqrt{2\beta})-e^{2x\sqrt{2\beta}}E_1(2x\sqrt{2\beta})\right)\right).$$

According to [81, 6.12.1], we further have

$$\lim_{t\downarrow 0}\mu(t)=\lim_{\beta\to+\infty}\left(\beta e^{-\sqrt{2\beta}(x-a)}\left(\frac{1}{2a\sqrt{2\beta}}-\frac{1}{2x\sqrt{2\beta}}\right)\right)=0.\tag{5.19}$$

Now apply L'Hôpital's rule on $r(t)$. Follow the asymptotic in (5.18), the limit of $r(t)$ is given by

$$\begin{aligned}\lim_{t\downarrow 0}\frac{\mu(t)}{\lambda(t)} =& \lim_{t\downarrow 0}\frac{\lambda(t)\int_0^\infty \frac{p^{(0)}_{\tau,2ua,0}(t)-p^{(0)}_{\tau,2ux,0}(t)}{2(u+1)}du}{\lambda'(t)}\\ =& \lim_{t\downarrow 0}\frac{t^{-\frac{6}{2}}\int_0^\infty\left(\frac{ua}{u+1}e^{-\frac{2u^2a^2}{t}}-\frac{ux}{u+1}e^{-\frac{2x^2a^2}{t}}\right)du}{t^{-\frac{7}{2}}}\\ =&0.\end{aligned}$$

Therefore $\mu(t)=o(\lambda(t))$, and the left tail asymptotic is then given by

$$\left(1+\frac{\epsilon}{2}\ln(\frac{a}{x})\right)p^{(0)}_{\tau,x,a}(t).$$

For the right tail, consider (5.15). Let $w:=\frac{2ua}{\sqrt{t-v}}$ and $w:=\frac{2ux}{\sqrt{t-v}}$, respectively. Then the inner integral can be further written as

$$\begin{aligned}\int_0^\infty \frac{p^{(0)}_{\tau,2ua,0}(t-v)-p^{(0)}_{\tau,2ux,0}(t-v)}{2(u+1)}du =& \int_0^\infty \frac{\frac{2ua}{\sqrt{2\pi}(t-v)^{\frac{3}{2}}}e^{-\frac{(2ua)^2}{2(t-v)}}-\frac{2ux}{\sqrt{2\pi}(t-v)^{\frac{3}{2}}}e^{-\frac{(2ux)^2}{2(t-v)}}}{2(u+1)}du\\ =&\frac{x-a}{(t-v)^{\frac{3}{2}}}\int_0^\infty\frac{w\phi(w)}{(w+\frac{2a}{\sqrt{t-v}})(w+\frac{2x}{\sqrt{t-v}})}dw, \qquad (5.20)\end{aligned}$$

where $\phi(w)$ is the density of a standard normal distribution. Since $x>a$, therefore,

$$\lambda(v)\int_0^\infty\frac{p^{(0)}_{\tau,2ua,0}(t-v)-p^{(0)}_{\tau,2ux,0}(t-v)}{2(u+1)}du\geq 0,\ \forall v\in(0,t).$$

Let $K<<t$ be a fixed constant, then

$$\mu(t)\geq\int_0^K\lambda(v)\int_0^\infty\frac{p^{(0)}_{\tau,2ua,0}(t-v)-p^{(0)}_{\tau,2ux,0}(t-v)}{2(u+1)}dudv. \qquad (5.21)$$

Denote the right-hand side of (5.21) by $\mu_K(t)$. For $0\leq v\leq K<<t$, combine (5.20), we further have

$$\mu_K(t)\sim\int_0^K\lambda(v)dv\cdot\int_0^\infty\frac{p^{(0)}_{\tau,2ua,0}(t)-p^{(0)}_{\tau,2ux,0}(t)}{2(u+1)}du\sim t^{-\frac{3}{2}}\int_0^\infty\frac{w\phi(w)}{(w+\frac{1}{\sqrt{t}})^2}dw. \qquad (5.22)$$

Since $t^{-\frac{3}{2}}$ is the asymptotic of $\lambda(t)$ for large t, and

$$\lim_{t\uparrow+\infty}\frac{\mu_K(t)}{t^{-\frac{3}{2}}}\geq\int_0^1\frac{\phi(w)}{w}dw=+\infty,$$

so according to (5.21), we find

$$\lim_{t\uparrow+\infty}\frac{\mu(t)}{\lambda(t)}\geq\lim_{t\uparrow+\infty}\frac{\mu_K(t)}{\lambda(t)}\geq+\infty. \tag{5.23}$$

This yields

$$p_\tau^{(1)}(t)\sim\mu(t).$$

The next step is to confirm that $\mu(t)$ is a valid asymptotic, *i.e.* itself does not diverge. Indeed, apply the final value theorem (Equation (2.38), Fact 2.3.1, Section 2.3), one immediately has

$$\lim_{t\uparrow+\infty}\mu(t)=0.$$

In addition, note that previously in Corollary 5.1.2, we have shown

$$\lim_{\beta\to0^+}f_1(x,\beta)=\lim_{\beta\to0^+}f_0(x,\beta)g_1(x,\beta)=0,$$

which further yields

$$\int_0^\infty\mathcal{L}^{-1}\left\{f_1(x,\beta)\right\}(t)dt=0. \tag{5.24}$$

Since the inverse in (5.24) is given by

$$\mathcal{L}^{-1}\left\{f_1(x,\beta)\right\}(t)=\epsilon\left(\frac{1}{2}\ln(\frac{a}{x})p_{\tau,x,a}^{(0)}(t)+\frac{(x-a)^2}{\sqrt{2\pi}}\mu(t)\right), \tag{5.25}$$

therefore, substitute (5.25) into (5.24), we further get

$$\begin{aligned}\int_0^\infty\mu(t)dt=&\frac{\sqrt{2\pi}}{2(x-a)^2}\ln(\frac{x}{a})\int_0^\infty p_{\tau,x,a}^{(0)}(t)dt &(5.26)\\ =&\frac{\sqrt{2\pi}}{2(x-a)^2}\ln(\frac{x}{a}). &(5.27)\end{aligned}$$

The equality in (5.27) comes from the fact that $p_{\tau,x,a}^{(0)}(t)$ is the *p.d.f.* of the inverse Gamma distribution. As a necessary condition for (5.26), (5.27) to hold true, the convergence rate of

$\mu(t)$ must be

$$\mu(t) = O(t^{-1-\alpha}),$$

for some $\alpha > 0$. Combine (5.23), we further require $0 < \alpha < \frac{1}{2}$. This concludes our proof. $\square$

Proposition 5.2.2 (Error Estimation and Convergence of BES$(1+\epsilon)$)**.** *The η-function for the error estimation is given by*

$$\eta(x,t) = \frac{1}{2}\ln(\frac{x}{a})\rho(x,a,t) - \frac{1}{4t}\int_{(x-a)^2}^{\infty}\left(\frac{p_\Gamma(y,\frac{3}{2},\frac{1}{2t}) - p_\Gamma(y,\frac{1}{2},\frac{1}{2t})}{\sqrt{y}-x+3a} + \frac{p_\Gamma(y,\frac{3}{2},\frac{1}{2t}) - p_\Gamma(y,\frac{1}{2},\frac{1}{2t})}{\sqrt{y}+x+a}\right)dy, \tag{5.28}$$

where

$$\rho(x,a,t) := \frac{1}{\sqrt{2\pi}}t^{-\frac{5}{2}}\left((x-a)^2 - t\right)e^{-\frac{(x-a)^2}{2t}};$$

and $p_\Gamma(y,\alpha,s)$ is the density of Gamma distribution with the shape parameter α and the rate parameter s (see Equation (5.8)*).*

Besides, for all $t \in [0,+\infty)$, the probabilistic representation in Equation (3.13)*, Proposition 3.3.1, is valid. And for $t \in [0,T]$ with fixed $T > 0$, the first order perturbed FPTD of BES$(1+\epsilon)$ converges at rate $O(\epsilon^2)$.*

Proof. Taking the partial derivative on x from $f_1(x,\beta)$ (Lemma 5.1.1) yields

$$\begin{aligned}\partial_x f_1(x,\beta) =& \partial_x\left(f_0(x,\beta)\frac{\ln(\frac{a}{x}) + e^{2\gamma a}E_1(2\gamma a) - e^{2\gamma x}E_1(2\gamma x)}{2}\right)\\ =& f_0(x,\beta)\left(-\gamma\frac{\ln(\frac{a}{x}) + e^{2\gamma a}E_1(2\gamma a) - e^{2\gamma x}E_1(2\gamma x)}{2} + \frac{-\frac{1}{x}+\frac{1}{x} - 2\gamma e^{2\gamma x}E_1(2\gamma x)}{2}\right)\\ =& -\gamma f_0(x,\beta)\frac{\ln(\frac{x}{a}) + e^{2\gamma a}E_1(2\gamma a) + e^{2\gamma x}E_1(2\gamma x)}{2}.\end{aligned}$$

According to [9], for some positive z, we have

$$\mathcal{L}^{-1}\left\{\sqrt{2\beta}e^{-\sqrt{2\beta}z}\right\}(t) = \frac{1}{\sqrt{2\pi}}t^{-\frac{5}{2}}\left(z^2 - t\right)e^{-\frac{z^2}{2t}}. \tag{5.29}$$

Then by repeating the same trick as in between (5.12) and (5.14), we prove the result for the η-function.

Now we verify conditions of Proposition 3.3.1. The idea of the proof is similar to that

in Proposition 4.2.2. Let the η-function be given in (5.1). For the first part proof, when $x \in [a, K]$ for some large K, please refer to the proof of Proposition 4.2.2.

Here we show the second part. When $x > K$ and K is large enough, we have $\ln(\frac{x}{a}) \leq (x-a)$. Therefore,

$$\left|\frac{1}{2x} \cdot \frac{1}{2} \ln(\frac{x}{a}) \rho(x, a, t)\right| \leq \frac{1}{4K} \frac{1}{\sqrt{2\pi}} t^{-\frac{5}{2}} \left((x-a)^3 + t(x-a)\right) e^{-\frac{(x-a)^2}{2t}}. \tag{5.30}$$

And the boundedness of (5.30) is given in the proof of Lemma 4.2.1. The only thing left then, is to show the Gamma-density part in (5.28) satisfies (3.12) and (3.14). First note that,

$$y \geq (x-a)^2 > 0, \text{ and } x > a;$$

therefore,

$$\max\left\{\frac{1}{\sqrt{y} - x + 3a}, \frac{1}{\sqrt{y} + x + a}\right\} \leq \frac{1}{2a}.$$

For the rest of the integral, consider a shape parameter $\alpha > 0$. Then for $x > K$ and such that $x - a > 1$, given $y > (x-a)^2 > 1$, we have

$$\begin{aligned}
\frac{1}{4t} \int_{(x-a)^2}^{\infty} p_\Gamma(y, \alpha, \frac{1}{2t}) dy &= \frac{1}{2\Gamma(\alpha)} \int_{(x-a)^2}^{\infty} \frac{1}{(2t)^{\alpha+1}} y^{\alpha-1} e^{-\frac{y}{2\alpha}} dy \\
&\leq \frac{\Gamma(\alpha+1)}{2\Gamma(\alpha)} \int_{(x-a)^2}^{\infty} \frac{y^\alpha}{\Gamma(\alpha+1)(2t)^{\alpha+1}} e^{-\frac{y}{2\alpha}} dy \\
&\leq \frac{\Gamma(\alpha+1)}{2\Gamma(\alpha)}.
\end{aligned}$$

The last inequality is due to the fact that the integral is the *cumulative distribution function* of the Gamma distribution. In the end, substitute $\alpha = \frac{3}{2}$ and $\alpha = \frac{1}{2}$ into the inequality above, we then conclude the proof. □

5.3 Numerical Example on Downward BES$(1+\epsilon)$ FPTD

In this section we demonstrate numerical results similarly to which in Section 4.3.3. The comparison is between the first order perturbed FPTD and the Talbot numerical inverse. Both the density curve and the relative error plots are provided (additionally with their

left-tail zoom-in plots). *W.l.o.g.*, we choose model parameters as follows:

$$\epsilon = 0.1,\ x = 0.7,\ l = 0.1.$$

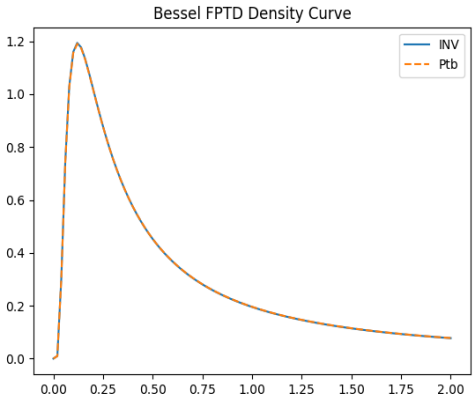

Figure 5.1: Bessel density with $\epsilon = 0.1,\ x = 0.7,\ l = 0.1$

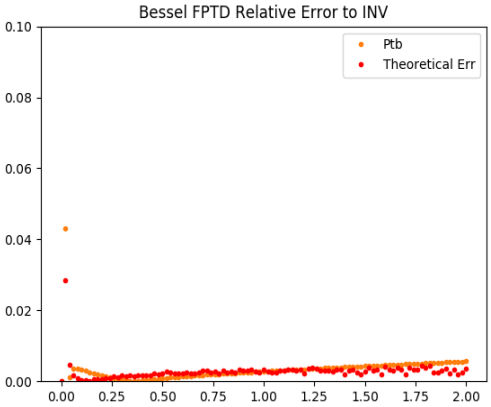

Figure 5.2: Bessel density error with $\epsilon = 0.1,\ x = 0.7,\ l = 0.1$

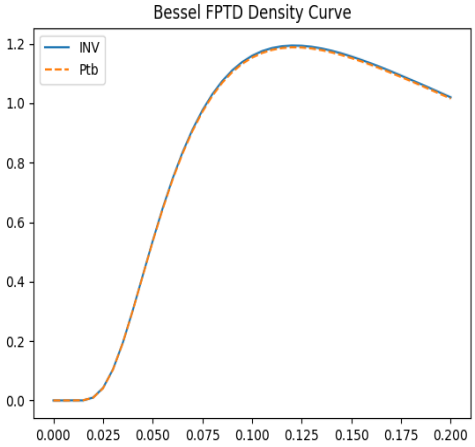

Figure 5.3: Bessel left tail density

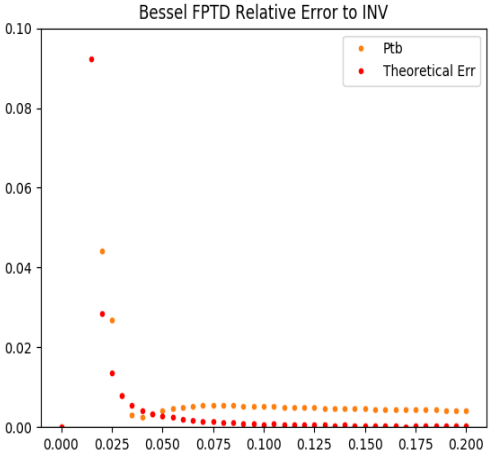

Figure 5.4: Bessel left tail relative error

Results in Figures 5.1 to 5.4 are similar to what we have seen in Chapter 4. From the density plot (Figure 5.1), we find the first order perturbation provides a good estimate on the FPTD. Figure 5.2 shows the consistency between theoretical and realised errors, and which verifies our convergence conclusions (Propositions 5.2.2 and 3.3.1). In general, this example indicates that the perturbation works well for the Bessel process.

5.4 Conclusion

Chapters 3 to 5 are splits from one of our working paper [31]. In this paper, we provide a systematic approach to solve closed-form asymptotics on diffusion FPTDs; besides, we demonstrate the convergence of perturbation and derive a probabilistic representation for the error estimate (see Chapter 3).

The perturbation resulted closed-form solution does not only increase the computational efficiency; but also provides an analytical tractability in understanding FPTs at extreme times (see e.g. Propositions 4.1.4 and 5.2.1). Using the framework we find valid approximations for the OU (Chapter 4) and the Bessel (Chapter 5) FPTDs. The theoretical work in these three chapters has also been verified by numerical exercises in Chapters 4 and 5.

Additionally, by taking the stochastic clock into account, results in this chapter could also be extended to the CIR process (see Appendix 5.C). Another example of applying our framework is given in Chapter 6. In practice, potential applications of the perturbed FPTD could be found in survival analysis, bond option pricing, etc. Later, in Chapter 8, we will study the possibility of identifying trading signals via level crossing probabilities.

Appendix 5.A Upward FPTD of BES$(1+\epsilon)$

According to [18], the LT for the upcrossing ($0 < x < a$) density of BES$(1+\epsilon)$ is given by

$$f(x,\beta) = \left(\frac{a}{x}\right)^{\frac{\epsilon-1}{2}} \frac{I_{\frac{\epsilon-1}{2}}(\sqrt{2\beta}x)}{I_{\frac{\epsilon-1}{2}}(\sqrt{2\beta}a)},$$

where $I_{\cdot}(\cdot)$ is the *modified Bessel function of the first kind*. Note that, in the case of hitting from below, we are dealing with a reflecting boundary $\{0\}$. And according to [62, page 108], the boundary value of the Dirichlet problem is the limit of functionals of $f(x)$, $k(x)$ and $m(x)$ at 0, where $k(x)$ and $m(x)$ are the killing and speed measure functions of BES$(1+\epsilon)$, respectively. In fact, by checking [81, 10.30 (i)], we find

$$f(0) = \left(\frac{\sqrt{2\beta}a}{2}\right)^{\frac{\epsilon-1}{2}} \cdot \frac{1}{\Gamma(\frac{\epsilon+1}{2}) I_{\frac{\epsilon-1}{2}}(\sqrt{2\beta}a)}. \tag{5.31}$$

Similar to Section 4.3.1, we solve the upward asymptotic FPTD using the reflected process. However, different to the OU process, after reflection, the new domain of BES$(1+\epsilon)$ becomes

$D = \{-a, 0\}$. And in this case, the boundary $\{0\}$ is ill-posed. If we force the perturbed ODEs to match (5.31), in the end we could possibly get a solution in terms of modified Bessel functions again. This does not simplify the solution at all. On the other hand, the perturbation is based on the philosophy that the process locally behaves like the Brownian motion; while, at $\{0\}$, the reflected process has an negatively infinite instantaneous drift. Therefore, by forcing to match the boundary condition at $\{0\}$ we may not even find a solution from the perturbation. We then decide to match the boundary condition at $-a$ only, and assign the condition on $\{0\}$ according to our need. In practice, this causes no harm if we start from $0 << x$ and which is close to the hitting level a.

Repeat the calculations in Lemma 5.1.1 and Proposition 5.1.3, we find that the results for the upward FPT are the same as in the downward case, apart from by replacing $\hat{x} = -x$ and $\hat{a} = -a$. However, the exponential integral function, as mentioned in Lemma 5.1.1, should be redefined via the *Cauchy principal value*[4]:

$$E_1(z) = \fint_z^{+\infty} \frac{e^{-y}}{y} dy.$$

To summarise, we list the LT and the FPTD of the upward BES$(1+\epsilon)$ in below:

$$f_1(x, \beta) = f_0(-x, \beta) \frac{\ln(\frac{a}{x}) + e^{-2\gamma a} E_1(-2\gamma a) - e^{-2\gamma x} E_1(-2\gamma x)}{2},$$

and

$$p_\tau^{(1)}(t) = \left(1 + \frac{\epsilon}{2} \ln(\frac{a}{x})\right) p^{(0)}_{\tau,-x,-a}(t) - \frac{\epsilon(x-a)}{\sqrt{2\pi t}} \int_{(x-a)^2}^{\infty} \frac{p_\Gamma(y, 1, \frac{1}{2t}) dy}{(\sqrt{y} + x - 3a)(\sqrt{y} - x - a)} dy. \quad (5.32)$$

Note that, for $x < a$, two singularity points are involved in the denominator of the integrand; that is why the Cauchy principal value is used again. For more details of derivations, please refer to the proofs of Lemma 5.1.1 and Proposition 5.1.3.

As a quick numerical test, we demonstrate 4 figures on the next page. From the results we can see, the perturbation works well if x is close to a. And our framework provides much better estimate of the left tail than the right tail. This could be explained by the Cauchy principal values in both the LT and the FPTD.

[4]This is due to the fact that $Real(2\gamma\hat{a}) \leq 0$ and $Real(2\gamma\hat{x}) \leq 0$.

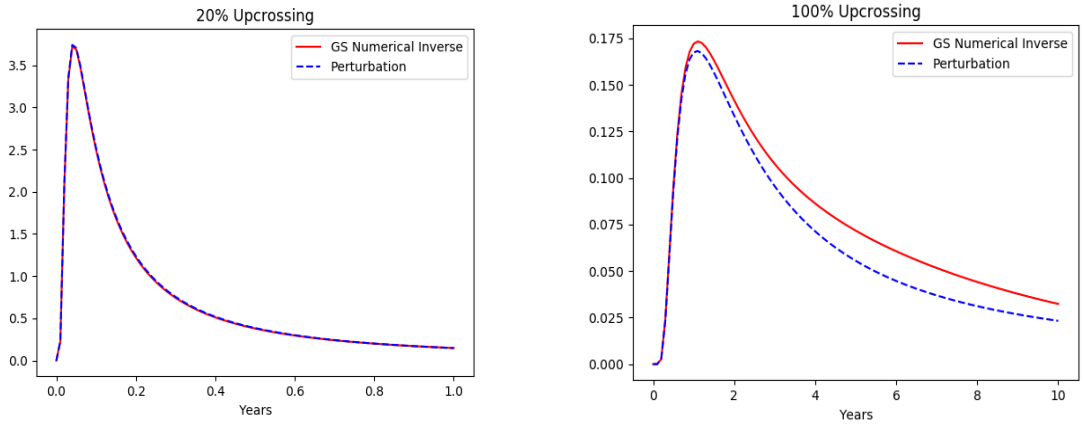

Figure 5.5: Upcrossing FPTD of BES(1.5). $\epsilon = 0.5$, $x = 1.8$. Left figure, 20% upcrossing ($a = 2.16$); right figure, 100% upcrossing ($a = 3.6$)

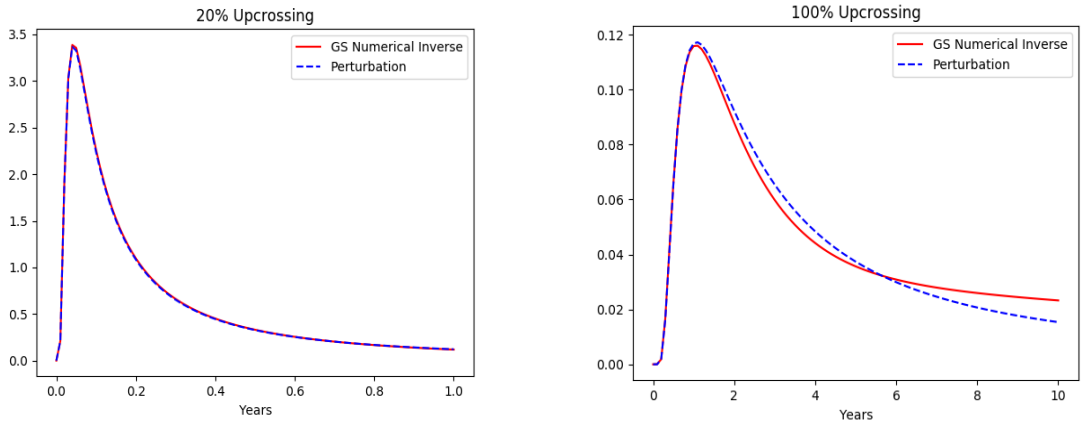

Figure 5.6: Upcrossing FPTD of BES(0.5). $\epsilon = -0.5$, $x = 1.8$. Left figure, 20% upcrossing ($a = 2.16$); right figure, 100% upcrossing ($a = 3.6$)

Appendix 5.B Extension to BES(n)

We already mentioned in Chapter 3, that the perturbation parameter ϵ is not necessary to be small. In this appendix, we illustrate this point.

Consider a general $n \geq 0$, a natural way of thinking, on finding the FPTD of BES(n), is to perturb those integer orders which have explicit densities. We call these orders the 'anchor points'. For example, when $n = 3$ (which corresponds to $\nu = \frac{1}{2}$), refer to [18], we know the

LT of hitting from below[5] is given by

$$f(x,\beta) = \frac{a\sinh(\sqrt{2\beta}x)}{x\sinh(\sqrt{2\beta}a)}.$$

And according to [9], its inverse is given by the derivative of θ-function:

$$\mathcal{L}^{-1}\left\{f(x,\beta)\right\}(t) = \frac{1}{\sqrt{2}x}\partial_x\theta_4\left(\frac{x}{2a}\middle|\frac{i\pi t}{2a^2}\right).$$

Unfortunately, if we take $n = 3$ as an anchor point, after tedious calculations, we find the first order perturbed LT consists of *Shi*- and *Chi*-functions:

$$Shi(z) = \int_0^z \frac{\sinh(y)}{y}dy,$$

and

$$Chi(z) = c_\gamma + \ln(z) + \int_0^z \frac{\cosh(y)-1}{y}dy,$$

where as it is mentioned in Corollary 5.1.2, c_γ is the Euler's constant. Based on our research, we find it is very difficult to find the explicit inverse of f_1. As an alternative, we therefore consider to use the anchor point $n = 1$ and a large $\epsilon > 1$, to approximate the FPTD of BES(n).

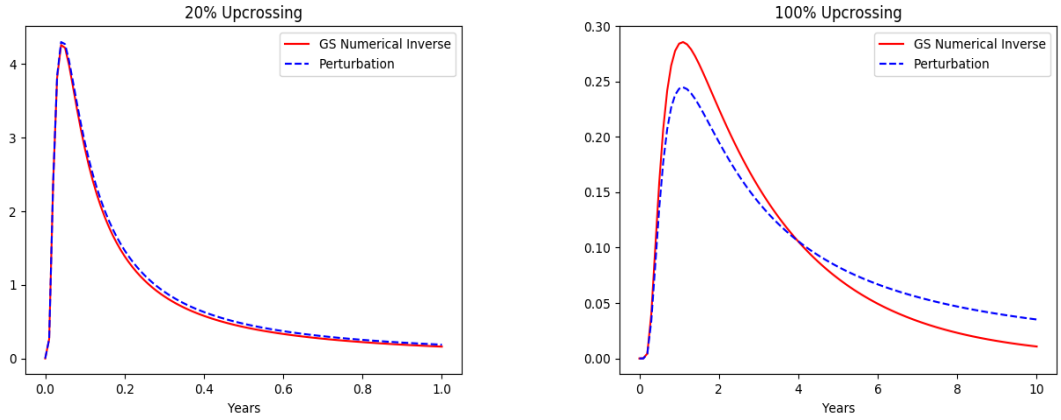

Figure 5.7: Upcrossing probability of BES(3). $\epsilon = 2$, $x = 1.8$. Left figure, 20% upcrossing ($a = 2.16$); right figure, 100% upcrossing ($a = 3.6$)

[5] In this case, hitting from above is not guaranteed to be finite.

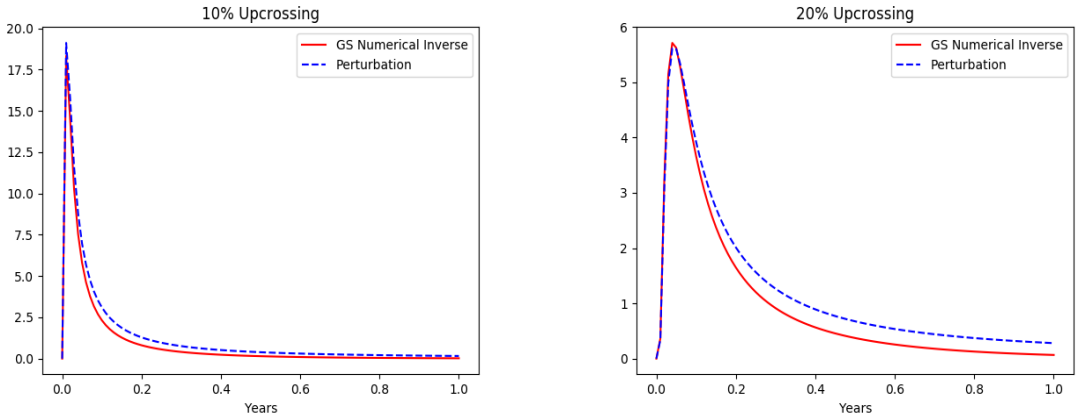

Figure 5.8: Upcrossing probability of BES(6.5). $\epsilon = 5.5$, $x = 1.8$. Left figure, 10% upcrossing ($a = 1.98$); right figure, 20% upcrossing ($a = 2.16$)

From these examples, we find that the perturbation still works well for $\epsilon > 1$, as long as t is not large, and x is close to a (e.g., below 20%).

Appendix 5.C Lower Boundary of CIR FPTD

In the last appendix of this chapter, we provide a lower boundary of the FPT probability for the CIR process[6]. Consider a CIR process as introduced in Example 2.1.7, Chapter 2:

$$dX_t = \epsilon(\theta - X_t)dt + \sigma\sqrt{X_t}dW_t, \ X_0 = x > 0. \tag{5.33}$$

And let $\{Y_t\}_{t\geq 0}$, $\{Z_s\}_{s\geq 0}$ be the time-changed squared Bessel process, and the Bessel process, as defined in (2.18) and (2.19), respectively.

For $x > a$, define

$$\tau^* = \inf\{t \geq 0 : X_t = a | X_0 = x > a\}.$$

Then according to (2.17), we have

$$\tau^* = \inf\left\{t \geq 0 : Y_{\frac{\sigma^2}{4\epsilon}(e^{\epsilon t}-1)} = ae^{\epsilon t} \middle| Y_0 = x > a\right\}.$$

[6]Note that the exactly perturbed FPTD of the CIR process can be solved by considering the radial OU process.

Note that, since $\epsilon > 0$, so for $t > 0$, $ae^{\epsilon t} > a$. If we define

$$\tau^{**} = \inf\left\{t \geq 0 : Y_{\frac{\sigma^2}{4\epsilon}(e^{\epsilon t}-1)} = a \middle| Y_0 = x > a\right\},$$

then $\tau^* < \tau^{**}$, and which further gives

$$\mathbb{P}_x\left(\tau^{**} \leq t\right) \leq \mathbb{P}_x\left(\tau^* \leq t\right). \tag{5.34}$$

On the other hand, define

$$\tau = \inf\left\{s \geq 0 : Z_s = \sqrt{a} \middle| Z_0 = \sqrt{x} > \sqrt{a}\right\};$$

then according to the stochastic clock,

$$\tau^{**} = \frac{1}{\epsilon}\ln(\frac{4\epsilon}{\sigma^2}\tau + 1).$$

This leads to

$$\mathbb{P}_x\left(\tau^{**} \leq t\right) = \mathbb{P}_x\left(\tau \leq \frac{\sigma^2}{4\epsilon}(e^{\epsilon t} - 1)\right).$$

Therefore, the lower boundary for the initial τ^* is given by

$$\mathbb{P}_x\left(\tau^* \leq t\right) \geq \int_0^{\frac{\sigma^2}{4\epsilon}(e^{\epsilon t}-1)} p_\tau^{(1)}(u)du, \tag{5.35}$$

where $p_\tau^{(1)}(u)$ is introduced in (5.6). For the hitting from below case, the problem may not be well defined (it depends on the choice of ϵ). But in general, consider a fixed time $t > 0$, then for $0 \leq u \leq t$, redefine

$$\tau^{**} = \inf\left\{0 \leq u \leq t : Y_{\frac{\sigma^2}{4\epsilon}(e^{\epsilon u}-1)} = ae^{\epsilon t} \middle| Y_0 = x < ae^{\epsilon t}\right\},$$

then by (5.34) again, the lower boundary is given by τ^{**}. And define

$$\tau_t = \inf\left\{0 \leq s \leq \frac{\sigma^2}{4\epsilon}(e^{\epsilon t} - 1) : Z_s = \sqrt{a}e^{\frac{\epsilon}{2}t} \middle| Z_0 = \sqrt{x} > \sqrt{a}e^{\frac{\epsilon}{2}t}\right\}, \tag{5.36}$$

in the end, we find

$$\mathbb{P}_x\left(\tau^* \leq t\right) \geq \int_0^{\frac{\sigma^2}{4\epsilon}\left(e^{\epsilon t}-1\right)} p_{\tau_t}^{(1)}(u)du, \tag{5.37}$$

where $p_{\tau_t}^{(1)}(u)$ is given by (5.32).

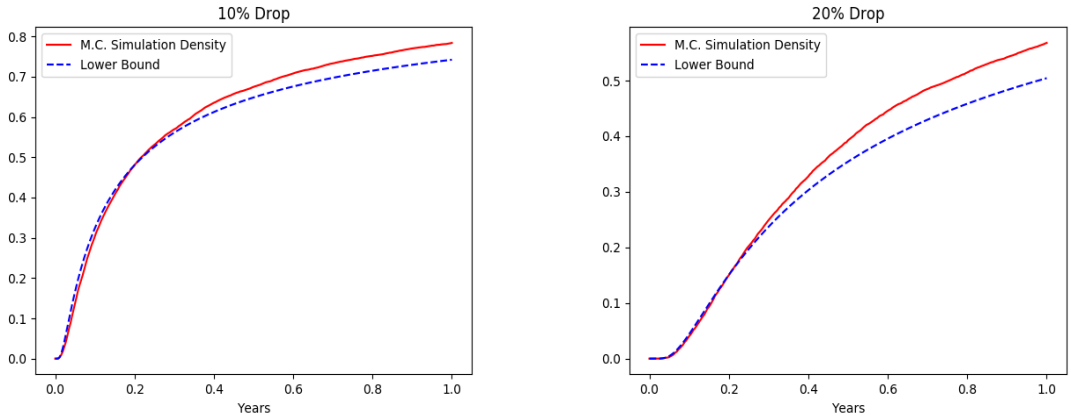

Figure 5.9: Downcrossing probability of CIR. $\epsilon = 0.1,\ \theta = 0.5,\ \sigma = 0.3,\ x = 0.8$. Left figure, 10% downcrossing ($a = 0.72$); right figure, 20% downcrossing ($a = 0.64$)

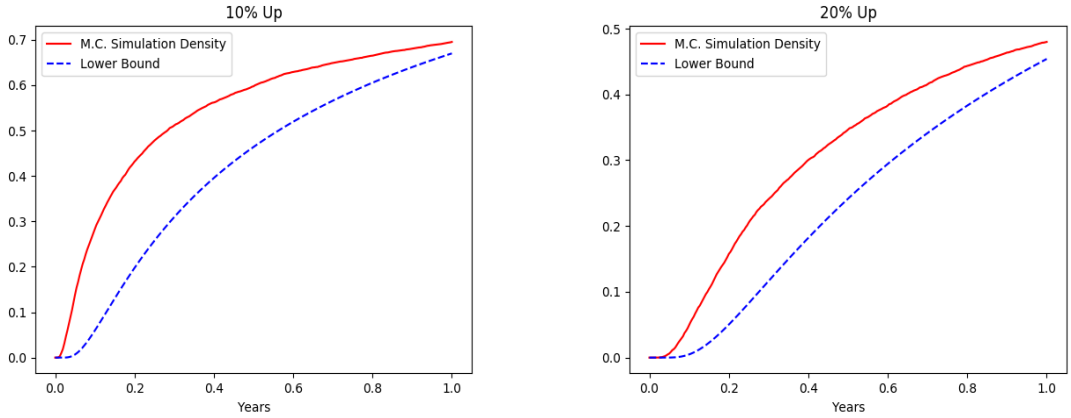

Figure 5.10: Upcrossing probability of CIR. $\epsilon = 0.1,\ \theta = 0.5,\ \sigma = 0.3,\ x = 0.8$. Left figure, 10% upcrossing ($a = 0.88$); right figure, 20% upcrossing ($a = 0.96$)

In Figures 5.9 and 5.10, we plot numerical examples for the CIR FPT probabilities. The benchmark curve (red) is given by Monte Carlo simulation. From these figures, we see the upcrossing boundary is less sharp than that from the downcrossing. In fact, refer to (5.36), for simplicity, in this example we choose the final value T as the terminal point rather than evaluating the integral with the actual t at each point.

Chapter 6

An Economic Bubble Model and Its First Passage Time

In this chapter, we introduce a new diffusion process to describe economic bubble dynamics. The process can be treated as a scaled version of log-transform on the Shiryaev process [117]; our study shows that the new scaling parameter is crucial for modelling economic bubbles. We conduct fundamental analysis and prove that the process and its first passage time are well-defined. Besides, a series of closed-form solutions on the process and its distribution functions are given. Especially, by solving the Fokker-Planck equation we show that the process follows an exponential-Gamma distribution at infinity time. Moreover, by employing the perturbation technique, we deduce the closed-form asymptotic for the downward first passage time density. Therefore, based on the model, the burst time of an economic bubble can be estimated accordingly. The object of this study is to understand asset price dynamics when a financial bubble is believed to form, and correspondingly provide estimates of the bubble's crash time. Calibration examples on the US dot-com bubble and the 2007 Chinese stock market crash verify the effectiveness of the new model. The example on BitCoin prediction confirms that we can provide meaningful estimate of the downward probability of asset prices.

Contents in this chapter can be split into two parts. In the first part, we demonstrate various properties of the model itself. And the second part can be seen as an application to our perturbation framework in Chapter 3.

6.1 Introduction, Motivation, and Literature Review

An *economic bubble* usually refers to the economic phenomenon that asset prices extremely deviate from their fundamental values [115]. One of the most famous bubbles in history, known as the Dutch Tulip Bubble [29, 46], could be traced back to the 1630s. According to P.M. Garber [46], from November 1636 to February 1637, the price of tulip bulbs had increased about 20 times. At the peak of the bubble, by selling a few bulbs people could even buy a luxury house in Amsterdam. However, only three months later, the bulbs became worthless. The rapid rise and sudden drop in asset prices form to be a common feature reflected by a bubble cycle. More modern examples can be found in [23, 58, 129].

The *burst* of an economic bubble sometimes follows with financial crisis, or even economic depression. In modern history, the most devastating crisis would be the 2007-2009 Financial Crisis [104], where people believe the crash of the US real estate market is one of the causes. And the crash itself, is usually referred to as the burst of the US Housing Bubble [58]. Although it is believed that a bubble cannot be predicted before it is formed, by knowing the burst time in advance, governments and market participants can manage the potential risk accordingly. Therefore, an effective estimate before the crash will help in preventing the systematic risk. The object of this study is to understand asset price dynamics for an economic bubble and provide estimates to the probability distribution of the collapse time.

The financial bubbles have been studied extensively in econometrics and statistics. As a non-conclusive review, we refer to [102] and the literatures it mentioned for the econometric approach; agent-based models in statistics can be found in [44, 51, 52]. In financial mathematics, local martingale models have been considered in option pricing problems, see R.A. Jarrow and P. Protter et al. [63, 64, 98]. A. Cox and D.G. Hobson [26] included a wide branch of stochastic diffusions in their work. S. Heston et al. [56] enriched the discussions by introducing the CIR process and the Heston stochastic volatility model. Apart from above, most recently, in the work by M. Schatz and D. Sornette [107], they propose a unified framework to mathematically describe economic bubbles. In terms of the burst time prediction, C. Brooks and A. Katsaris [19, 20] forecasted the collapse of speculative bubbles in S&P 500 index using a three-regime model. To the best of our knowledge, there is limited research in modelling economic bubble dynamics via a pure time-homogeneous diffusion process. The research on finding the explicit probability density of bubble crash time is even less. One paper related

to our work is contributed by A. Kiselev and L. Ryzhik [73], where a mean-reversion process with an exogenous functional drift has been considered.

In this chapter, we introduce a new time-homogeneous diffusion model. Within the framework of [107], the new process can be seen as a continuous-time bubble model which takes market failures into account. Our motivation is to provide an alternative approach, with the mathematical form to be as simple and tractable as possible, to probabilistically describe asset price dynamics within an economic bubble cycle. The new model is closely linked to the Shiryaev process [116, 117], which is derived by A.N. Shiryaev in the context of sequential analysis. Our model involves three independent parameters, where two of them provide mean-reversion effects as in the OU process. As the crucial part of our model, the third parameter controls the speed of exponential decay in the drift function. Consequently, the dependence structure among the return, asset price, equilibrium level, and the mean-reversion rate, has been mitigated. Without introducing extra functionals, our model provides sufficient degree of freedom for calibrations, while on the other hand, avoids over-fitting. Due to the simple structure of the model, we are able to find the closed-form asymptotic density of the bubble crash time[1].

The main contribution in this chapter is that we provide a self-contained material for modelling bubble dynamic and predicting its burst time. On the theoretical side, we prove that the new model is a well-defined diffusion process. To be more specific, the process is a semimartingale with a unique strong solution. As a recurrent strong Markov process, the model embeds an *a.s.* finite FPT; moreover, its stationary distribution is shown as an exponential-Gamma or exponential-Inverse Gamma distribution. On the practical side, a calibration algorithm based on economic features has been considered. We give explicit distribution of the process at fixed time. And the LT of the FPTD is found. Since in practice, we are more interested in the burst time rather than predicting how record-high the bubble would visit, so based on the perturbation technique, we solve the closed-form density for the downward FPT. In the end, the effectiveness of the model and its FPTD is verified by three numerical examples.

The rest of this chapter is organised as follows. Section 6.2 introduces the SDE of our new model and its connection with economic bubbles. Section 6.3 discusses the theoretical result from the new process itself. The closed-form FPTD is given by Section 6.4. In Section

[1]In the current work, the crash time is defined as the first passage time.

6.5, we demonstrate the calibration algorithm and illustrate the model application via three examples, among which, a prediction on the BitCoin burst time has been given. Section 6.6 concludes. In the end, extra relevant materials are provided in appendices of this chapter.

6.2 Stochastic Dynamic, Economic Bubble, and Burst Time

Consider a filtered Brownian probability space $\left(\Omega, \mathcal{F}, \{\mathcal{F}_t\}_{t\geq 0}, \mathbb{P}\right)$. We introduce the following three-parameter SDE

$$dX_t = \epsilon\left(e^{-2\alpha X_t} - c\right)dt + dW_t,\ X_0 = x \in \mathbb{R}, \tag{6.1}$$

where $\epsilon \in \mathbb{R}$, $\alpha \in \mathbb{R}$, and $0 \leq c \leq 1$. The dynamic describes a process with an exponentially decayed mean-reversion drift. It can be used in modelling log-prices or short rates. By considering the level where the drift is 0, in a long run, the process $\{X_t\}_{t\geq 0}$ oscillates around its equilibrium $X^R = -\frac{\ln(c)}{2\alpha}$.

In terms of the link between SDE (6.1) and a financial bubble, we refer to the discussions in [107]. Based on the *Financial Instability Hypothesis (FIH)* of H.P. Minsky [89] and observations from [21, 72], M. Schatz and D. Sornette [107] propose three minimal criteria for a well-defined bubble process. By summarising [107, Definitions 2.1, 2.2, 2.3, and 2.4], we define a bubble as follows:

Definition 6.2.1 (Economic Bubble)**.** Let $\{P_t\}_{t\geq 0}$, $\left\{\tilde{S}_t\right\}_{t\geq 0}$, $\{Z_t\}_{t\geq 0}$ be adapted to the filtered Brownian probability space $\left(\Omega, \mathcal{F}, \{\mathcal{F}_t\}_{t\geq 0}, \mathbb{P}\right)$, and where $\left\{\tilde{S}_t\right\}_{t\geq 0}$ is a semimartingale. Consider a finite stopping time τ_J, given which we have

$$P_t = \tilde{S}_t \mathbf{1}_{\{t\leq \tau_J\}} + Z_t \mathbf{1}_{\{t>\tau_J\}}. \tag{6.2}$$

If

1. $\mathbb{E}\left[P_t \mathbf{1}_{\{t\geq\tau_J\}}\right] < \mathbb{E}\left[\tilde{S}_t \mathbf{1}_{\{t\geq\tau_J\}}\right],\ t \geq 0,$
2. there does not exist a local-martingale measure $\mathbb{Q}$ for $\left\{\tilde{S}_t\right\}_{t\geq 0}$,
3. there exists a local-martingale measure $\mathbb{Q}$ for $\{P_t\}_{t\geq 0}$,

then we say $\{P_t\}_{t\geq 0}$ is a well-defined bubble process. And $\left\{\tilde{S}_t\right\}_{t\geq 0}$, $\{Z_t\}_{t\geq 0}$ are referred to as the pre-drawdown and the drawdown processes, respectively.

The definition above intuitively explains a bubble's behaviour and its components from a mathematical standpoint. From condition 3, it firstly says, in terms of the lifetime of an asset, the efficient market hypothesis should be valid for all tradable assets. But on the other hand, within a specific time period, a bubble may form due to the failure of market efficiency (conditions 1 & 2). In the original work [107], the pre-drawdown process is allowed (but not necessary) to be an explosive process. It explains the price dynamic which reflects the 'fundamental instability of a capitalist economy'; according to H.P. Minsky [89], such an 'instability' indeed refers to the 'tendency of explosion'. On the other hand, after the boom stage of a bubble, due to market capital limits or aversions of risk, the market expectations become negative. Therefore, the asset price drops towards its fundamental value. This is then captured by the drawdown process, $\{Z_t\}_{t\geq 0}$. For more details on the bubble definition and its financial justifications, please refer to [107].

Proposition 6.2.2 (An Economic Bubble Model)**.** *Let* $\{X_t\}_{t\geq 0}$ *in SDE* (6.1) *be the log-price of* $\{P_t\}_{t\geq 0}$*, i.e.,*

$$P_t = e^{X_t},\ P_0 = e^{X_0}.$$

Then under Definition 6.2.1, $\{P_t\}_{t\geq 0}$ *is a valid bubble process.*

Proof. The crucial part of the proof is to find a proper stopping time τ_J. Later in Proposition 6.3.6, we will show that $\{X_t\}_{t\geq 0}$ is a recurrent process on $\mathbb{R}$. Therefore, for any $0 < a < +\infty$, define

$$\tau_J = \inf\{t \geq 0 : P_t = a | P_0 < a\},$$

and $\tau_J < +\infty$ *a.s.* By considering an explosion after τ_J, the pre-drawdown process can be given as

$$\tilde{S}_t = P_t \mathbf{1}_{\{t\leq \tau_J\}} + \infty \mathbf{1}_{\{t>\tau_J\}}. \tag{6.3}$$

And define

$$Z_t = P_t \mathbf{1}_{\{t>\tau_J\}},$$

then by our construction, P_t embeds the decomposition as in (6.2).

The next step is to show those three conditions in Definition 6.2.1 are fulfilled. Indeed,

according to (6.3), and combine our discussions in Section 6.3 that $\{X_t\}_{t\geq 0}$ is continuous and does not explode, we immediately see condition 1 is satisfied. Also from (6.3), since $\left\{\tilde{S}_t\right\}_{t\geq 0}$ is an explosive process, so the equivalent measure under the Girsanov theorem does not exist. Hence, condition 2 is satisfied. In the end, consider the SDE of P_t, that

$$dP_t = P_t\left[\epsilon\left(\frac{1}{P_t^{2\alpha}} - c + \frac{1}{2\epsilon}\right)dt + dW_t\right],$$

the Radon-Nikodym derivative is given by

$$\left.\frac{d\mathbb{Q}}{d\mathbb{P}}\right|_{\mathcal{F}_t} = \exp\left\{-\int_0^t \epsilon\left(\frac{1}{P_s^{2\alpha}} - c + \frac{1}{2\epsilon}\right)dW_s - \frac{1}{2}\int_0^t \epsilon^2\left(\frac{1}{P_s^{2\alpha}} - c + \frac{1}{2\epsilon}\right)^2 ds\right\}.$$

Under mild conditions (e.g. the Novikov's condition for $-\epsilon\left(\frac{1}{P_t^{2\alpha}} - c + \frac{1}{2\epsilon}\right)$), the martingale-measure exists for $\{P_t\}_{t\geq 0}$. This proves condition 3, and we therefore conclude that $\{P_t\}_{t\geq 0}$ is a well-defined bubble process. □

Based on Definition 6.2.1 and Proposition 6.2.2, we define the *burst time* of an economic bubble via the first passage time:

Definition 6.2.3 (Burst Time and Imminent Risk)**.** Let $\{P_t\}_{t\geq 0}$ be a bubble process. For a fixed observation time $t_0 \geq 0$, consider a real parameter $0 \leq b \leq 1$. Define

$$\tau(t_0, b) = \inf\left\{t \geq t_0 : P_t \leq (1-b)\max_{0\leq s\leq t_0} P_s\right\}.$$

If $\tau(t_0, b) < +\infty$ *a.s.*, then we say $\tau(t_0, b)$ is the *burst time* of an economic bubble at the level of b%-drop. Moreover, for $T > t_0$, we refer to the probability

$$\mathbb{P}\left(\tau(t_0, b) \leq T\right)$$

as the *imminent risk* of the burst.

Remark. In the definition above, the burst time is associated with the percentage drop of the asset price from its peak. For example, in our later numerical exercises, we find that when the bubbles began to burst in the NASDAQ and China Shanghai Stock indices, within a month, they suffered more than 30% drops from their historical peaks.

Further Discussion

To illustrate our new process and its connection with a financial bubble, we plot the simulated asset price in Figure 6.2, together with the drift function explanation in Figure 6.1.

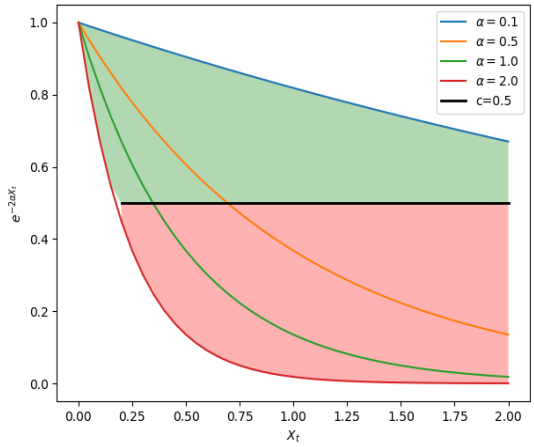

Figure 6.1: Function plots of $e^{-2\alpha X_t}$ with $\alpha = 0.1, 0.5, 1, 2$. Green zone: positive drift; red zone: negative drift

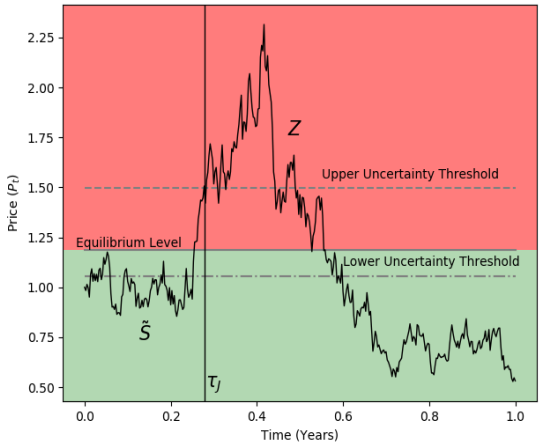

Figure 6.2: Sample path of e^{X_t} in 1 year time. Parameters are chosen as $\alpha = 2$, $\epsilon = 0.1$, $c = 0.5$, $X_0 = 0$ and $dt = \frac{1}{260}$

[**Skewed Drift Function**] As the most important parameter in our model, α controls the skewness (speed, curvature, and higher order information) of the drift term. From Figure 6.1, we observe that small α produces mildly linear decays in the drift, and this extends the range of the process where positive return is maintained; on the other hand, large α generates evident exponential decays, in this case, the drift sign is sensitive to the values of X_t, and the range of positive drift is compressed.

[**Three Regimes**] We plot the simulated sample path of $P_t = e^{X_t}$ in Figure 6.2, with $\alpha = 2$ and which corresponds to the red curve in Figure 6.1. From SDE (6.1), we can roughly split the sample path of P_t into three regimes: I) when X_t is negative or near 0, the diffusion process embeds a strongly positive trend; II) when the log-price oscillates around its equilibrium level, i.e. $X_t \approx X^R$, the price has an unstable trend (could be positive or negative), and it is dominated by the Brownian motion; III) when $X_t >> X^R$, the process is forced to drop back due to the strongly negative trend. Those three regimes are correspondingly described by the areas below the dash line of *Lower Uncertainty Threshold*, between the *Lower Uncertainty Threshold* and the *Upper Uncertainty Threshold*, and above the *Upper Uncertainty Threshold*, respectively.

[**Asymmetricity and Pro-cyclicality**] The lower and upper uncertainty thresholds are

chosen such that the bubble P_t has a $+30\%$ and a -30% log-returns (drift value of dX_t), respectively. From the relative positions between those two thresholds and the equilibrium level (the grey line between the red and green zones), we find that given the same amount of return changes, the distance (on the y-axis) of the price drop is much smaller than that of the price increase. This asymmetric feature is indeed a reflection of the skewness in the exponential drift function (see Figure 6.1). From the agent behaviour point of view, during the boom stage of a bubble, investors are confident in a persistent increase of the asset price. As such, a slight drop in the asset price will be regarded as a timing of investment, and the investor would have a higher expectation of returns than which are embedded in the pre-drop price. Moreover, different to a rational market[2], within a euphoria, the market may not immediately react to the deviations in asset prices. Therefore, only after a period, where the market price attains a higher position[3], the asset then accumulates a significant amount of negatively expected returns. This mechanism above is similar to the concept of *pro-cyclicality*, and which is often observed in a bubble cycle (cf. [17, 120]). Mathematically, such an asymmetric behaviour essentially differentiates our new model from the OU type mean-reversion processes.

[**Realisation under Definition 6.2.1**] Additionally, we also accommodate our model to the settings in Definition 6.2.1. In the example of Figure 6.2, we choose τ_J to be the FPT to a level P_t^*, where the log-return at P_t^* is -30%. The pre-drawdown process $\left\{\tilde{S}_t\right\}_{t\geq 0}$ and the drawdown process $\{Z_t\}_{t\geq 0}$ can be identified from the graph accordingly.

[**Parameter Dependency**] In the end, from the calibration point of view, α mitigates the dependence structure among the instantaneous return, the (log-) price, the equilibrium level, and the mean-reversion rate. Consider the drift function where α is suppressed:

$$\mu(X_t) := \epsilon\left(e^{-X_t} - c\right).$$

In this model, once c is determined, the equilibrium level $X_t = -\ln(c)$ becomes a fixed number. If a large rate of c is calibrated, then we simultaneously have a small equilibrium level $-\ln(c)$. Therefore when X_t is small, where $e^{-X_t} - c$ is close to 0, in order to fit a large

[2]Hereby we assume, investors are exposed to complete information and market is efficient in correcting prices. More precisely, we assume that the magnitude of returns is purely determined by the relative positions between the current price and the fundamental value (equilibrium level).

[3]The 'higher position' is in comparison with the position below the equilibrium level and where the asset embeds the same magnitude but positive returns.

instantaneous return[4], the mean-reversion rate ϵ should be adjusted highly as well. But we know that usually a bubble spends years to finish its whole cycle; so large reversion rate is not desired for a bubble model. This simple analysis shows that the α-suppressed model is not capable for calibrating a bubble dynamic. As a complement, extra functional term is required (cf. [73]). However, without introducing extra functions, our three-parameter model extends the freedom in model calibration.

6.3 Theoretical Result

6.3.1 Existence, Uniqueness and the Strong Markov Property

Proposition 6.3.1 (Solution of SDE (6.1))**.** *There exists a unique strong solution* $\{X_t\}_{t\geq 0}$ *to SDE* (6.1) *and which has the following explicit form*

$$X_t = x + W_t - c\epsilon t + \frac{1}{2\alpha}\ln\left(1 + 2\epsilon\alpha e^{-2\alpha x}\int_0^t e^{-2\alpha(W_s - c\epsilon s)}ds\right); \tag{6.4}$$

moreover, $\{X_t\}_{t\geq 0}$ *is a strong Markov process.*

Proof. We consider the exponential transform of X_t. Define

$$Y_t = e^{2\alpha X_t} \text{ with } Y_0 = e^{2\alpha x}.$$

By the Itô's lemma, we show Y_t satisfies the global Lipschitz continuity and the linear growth conditions:

$$dY_t = 2\alpha\left[\epsilon + (\alpha - c\epsilon)Y_t\right]dt + 2\alpha Y_t dW_t. \tag{6.5}$$

According to Theorem 2.1.2, we conclude that $\{Y_t\}_{t\geq 0}$ is the unique strong solution to SDE (6.5). Therefore, $\{X_t\}_{t\geq 0}$ is the unique strong solution to SDE (6.1). The strong Markov property is then proved by Theorem 2.1.3. On the other hand, refer to [121, Section 4.4], $\{Y_t\}_{t\geq 0}$ has the following explicit form:

$$Y_t = e^{2\alpha(W_t - c\epsilon t)}\left[Y_0 + 2\alpha\epsilon\int_0^t e^{-2\alpha(W_s - c\epsilon s)}ds\right].$$

[4]Otherwise the process will take a long period to visit regime III), where $e^{-X_t} \approx 0$ and $-c$ becomes dominating.

Replace Y_t by $e^{2\alpha X_t}$, and solve X_t, we get the explicit solution of $\{X_t\}_{t\geq 0}$. This concludes the proof. □

Remark. The proof depicts $\{X_t\}_{t\geq 0}$ from another aspect. SDE (6.5) shows $\{Y_t\}_{t\geq 0}$ is a geometric Brownian motion with a mean-reversion drift. Refer to [117, Equation (9)], this is indeed a Shiryaev process. Therefore, $\{X_t\}_{t\geq 0}$ is the logarithm of the Shiryaev process. We denote it by the *exponential-Shiryaev process*.

From (6.4) we clearly see $\{X_t\}_{t\geq 0}$ is a semimartingale, where the *bounded variation (BV)* part consists of a strictly decreasing function and a strictly increasing function. Depending on the Brownian motion path in the exponential integral, for different $t > 0$, the BV part could be either positive or negative. However, if $c = 0$, then only the increasing function is retained. This indicates that under special circumstance, $\{X_t\}_{t\geq 0}$ could be a submartingale.

Corollary 6.3.2 (Submartingale)**.** *If $c = 0$, then $\{X_t\}_{t\geq 0}$ is a strict submartingale.*

Proof. When c is suppressed, the solution of $\{X_t\}_{t\geq 0}$ becomes

$$X_t = x + W_t + \frac{1}{2\alpha} \ln\left(1 + 2\epsilon\alpha e^{-2\alpha x} \int_0^t e^{-2\alpha W_s} ds\right). \tag{6.6}$$

The adaptability is clear from definition. We consider the L^1-integrability of X_t. Note that, by applying the Jensen's inequality for a concave function $\ln(\cdot)$, we have

$$\mathbb{E}\left[\ln\left(1 + 2\epsilon\alpha e^{-2\alpha x} \int_0^t e^{-2\alpha W_s} ds\right)\right] \leq \ln\left(\mathbb{E}\left[1 + 2\epsilon\alpha e^{-2\alpha x} \int_0^t e^{-2\alpha W_s} ds\right]\right). \tag{6.7}$$

Change the order of integral and expectation,

$$\mathbb{E}\left[\int_0^t e^{-2\alpha W_s} ds\right] = \frac{1}{2\alpha^2}\left(e^{2\alpha^2 t} - 1\right). \tag{6.8}$$

On the other hand, when $\alpha,\ \epsilon \in \mathbb{R}^+$,

$$1 + 2\epsilon\alpha e^{-2\alpha x} \int_0^t e^{-2\alpha W_s} ds \geq 1,\ \forall t \geq 0. \tag{6.9}$$

Therefore

$$\left|\ln\left(1 + 2\epsilon\alpha e^{-2\alpha x} \int_0^t e^{-2\alpha W_s} ds\right)\right| = \ln\left(1 + 2\epsilon\alpha e^{-2\alpha x} \int_0^t e^{-2\alpha W_s} ds\right). \tag{6.10}$$

Combine (6.8), (6.10), and (6.7), we further have

$$\frac{1}{2\alpha}\mathbb{E}\left[\left|\ln\left(1+2\epsilon\alpha e^{-2\alpha x}\int_0^t e^{-2\alpha W_s}ds\right)\right|\right] \leq \frac{1}{2\alpha}\ln\left(1+\frac{\epsilon}{\alpha}e^{-2\alpha x}\left(e^{2\alpha^2 t}-1\right)\right). \tag{6.11}$$

Note that,

$$\mathbb{E}\left[|W_t|\right] = \sqrt{\frac{2t}{\pi}}. \tag{6.12}$$

According to the triangle inequality, combine (6.11) and (6.12), we then show the L^1-integrability of X_t:

$$\mathbb{E}\left[|X_t|\right] \leq x + \sqrt{\frac{2t}{\pi}} + \frac{1}{2\alpha}\ln\left(1+\frac{\epsilon}{\alpha}e^{-2\alpha x}\left(e^{2\alpha^2 t}-1\right)\right) < +\infty.$$

In the end, the non-decreasing conditional expectation of $\mathbb{E}\left[X_t\middle|\mathcal{F}_s\right]$, for $0 \leq s < t < +\infty$, is given by again using (6.9), that

$$\ln\left(1+2\epsilon\alpha e^{-2\alpha x}\int_0^t e^{-2\alpha W_s}ds\right) > 0.$$

This concludes our proof. □

6.3.2 Probability Distribution of $\{X_t\}_{t\geq 0}$

In this subsection, we consider the distributions of $\{X_t\}_{t\geq 0}$ at fixed and infinite times, respectively. From Proposition 6.3.1, we find that the solution of X_t involves a Brownian motion and its exponential integral. Similar problem has been studied by A. Dassios and J. Nagaradjasarma [33] for the square-root process. G. Peskir [100] deduced the fixed time distribution of the Shiryaev process in a special case; but for general cases, only the LT has been given. Here we refer to the results about the Brownian motion and its exponential integral by H. Matsumoto and M. Yor [86, 131]. And we first show the following proposition.

Proposition 6.3.3 (Transition Density at Fixed Time)**.** *For fixed $t > 0$ and $u \in \mathbb{R}$, the probability density of X_t is given by*

$$\mathbb{P}_x\left(X_t \in du\right) = \alpha du \cdot \left[\int_0^\infty \zeta(u;\frac{c\epsilon}{\alpha},y)\theta\left(\zeta(u;1,y),\alpha^2 t\right)e^{-\frac{c^2\epsilon^2 t+1/y+\zeta(u;2,y)}{2}}dy\right], \tag{6.13}$$

where

$$\theta(r,s)=\frac{r}{\sqrt{2\pi^3 s}}e^{\frac{\pi^2}{2s}}\int_0^\infty e^{-\frac{v^2}{2s}-r\cosh(v)}\sinh(v)\sin\left(\frac{\pi v}{s}\right)dv, \tag{6.14}$$

and

$$\zeta(u;\mu,y)=\frac{\left(1+2\frac{\epsilon}{\alpha}e^{-2\alpha x}y\right)^{\frac{\mu}{2}}e^{-\mu\alpha(u-x)}}{y}. \tag{6.15}$$

Proof. Let $s=\alpha^2 t$, then for another standard Brownian motion B_s, with probability 1 the following equation holds true

$$B_s+\frac{c\epsilon}{\alpha}s=-\alpha\left(W_t-c\epsilon t\right).$$

Denote by

$$\mu:=\frac{c\epsilon}{\alpha},\ B_s^{(\mu)}:=B_s+\mu s,\ A_s^{(\mu)}:=\int_0^s e^{2B_v^{(\mu)}}dv. \tag{6.16}$$

Refer to [86, 131], we have

$$\mathbb{P}\left(A_s^{(\mu)}\in dy,B_s^{(\mu)}\in dz\right)=\frac{1}{y}\theta\left(\frac{e^z}{y},s\right)\exp\left\{\mu z-\frac{\mu^2 s}{2}-\frac{1+e^{2z}}{2y}\right\}dydz, \tag{6.17}$$

where $\theta(\cdot,\cdot)$ is defined by (6.14).

Next, we reexpress X_t using $B_s^{(\mu)}$ and $A_s^{(\mu)}$. Note that,

$$A_s^{(\mu)}=\int_0^{\alpha^2 t}\exp\left\{-2\alpha\left(W_{\frac{v}{\alpha^2}}-c\epsilon\frac{v}{\alpha^2}\right)\right\}dv.$$

Let $w=\frac{v}{\alpha^2}$, we further have

$$A_s^{(\mu)}=\alpha^2\int_0^t e^{-2\alpha(W_w-c\epsilon w)}dw. \tag{6.18}$$

Rewrite $\{X_t\}_{t\geq 0}$ in (6.6) using (6.16) and (6.18), we get

$$X_t=x-\frac{B_s^{(\mu)}}{\alpha}+\frac{1}{2\alpha}\ln\left(1+2\frac{\epsilon}{\alpha}e^{-2\alpha x}A_s^{(\mu)}\right). \tag{6.19}$$

Now we consider the density function of X_t. For a fixed $u\in\mathbb{R}$, (6.19) and $X_t\leq u$ together yield

$$\alpha(x-u)+\frac{1}{2}\ln\left(1+2\frac{\epsilon}{\alpha}e^{-2\alpha x}A_s^{(\mu)}\right)\leq B_s^{(\mu)}.$$

Denote by

$$g\left(u, A_s^{(\mu)}\right) := \alpha(x-u) + \frac{1}{2}\ln\left(1 + 2\frac{\epsilon}{\alpha}e^{-2\alpha x}A_s^{(\mu)}\right).$$

Then according to (6.17), we can write[5]

$$\mathbb{P}_x\left(X_t \le u\right) = \int_{y\in(0,\infty)}\int_{z\ge g(u,y)} \mathbb{P}\left(A_s^{(\mu)} \in dy, B_s^{(\mu)} \in dz\right). \tag{6.20}$$

Take the partial derivative on u, we further get

$$\mathbb{P}_x\left(X_t \in du\right) = -\int_{y\in(0,\infty)} \frac{1}{y}\theta\left(\frac{e^{g(u,y)}}{y}, s\right) e^{\mu g(u,y) - \frac{\mu^2 s}{2} - \frac{1+e^{2g(u,y)}}{2y}} dy \cdot \partial_u g(u,y) du \tag{6.21}$$

$$= \alpha du \cdot \int_{y\in(0,\infty)} \frac{1}{y}\theta\left(\frac{e^{g(u,y)}}{y}, s\right) e^{\mu g(u,y) - \frac{\mu^2 s}{2} - \frac{1+e^{2g(u,y)}}{2y}} dy. \tag{6.22}$$

Introduce the function $\zeta(u;\mu,y)$ as in (6.15). We can show

$$\zeta(u;\mu,y) = \frac{e^{\mu g(u,y)}}{y}.$$

Substitute the equation above into (6.22), and rearrange the terms, we get

$$\frac{1}{y}\theta\left(\frac{e^{g(u,y)}}{y}, s\right) e^{\mu g(u,y) - \frac{\mu^2 s}{2} - \frac{1+e^{2g(u,y)}}{2y}} = \zeta(u;\mu,y)\theta\left(\zeta(u;1,y), s\right) e^{-\frac{\mu^2 s}{2} - \frac{1/y+\zeta(u;2,y)}{2}}.$$

In the end, the proof is concluded by substituting $\mu = \frac{c\epsilon}{\alpha}$ and $s = \alpha^2 t$ into the equation above. □

Remark. The function $\theta(r,s)$ is closely related to the study of the Hartman-Watson distribution [54]. As it is noticed by H. Matsumoto, M. Yor [86], and many others [8, 61], $\theta(r,s)$ is highly oscillating, especially for small s. Therefore it is not easy to calculate accurate values of the density. Although, this is not the objective of the present chapter.

In practice, it is more meaningful to provide the probability distribution function instead of the density function. This requires an extra integral on $\mathbb{P}(X_t \in du)$. Consider one integral involved in $\theta(r,s)$, one integral in the density itself, and plus the one taken on the density function; in total we need to calculate three integrals for the distribution function $\mathbb{P}(X_t \le du)$.

[5]Note that, the right-hand side of (6.20) depends on $X_0 = x$, where x is implicitly embedded in the $g(\cdot,\cdot)$ function.

A direct finite-difference scheme would therefore have computational efficiency issue. Instead, we consider calculating the probability via the Monte Carlo simulation.

Refer to (6.20) and (6.13), respectively, we have two choices in developing the simulation algorithm. According to (6.20), we could follow the acceptance-rejection approach by considering the relative positions between z and $g(u, y)$. But in this chapter, we follow (6.13) and concentrate on the direct sampling scheme.

Proposition 6.3.4 (Probability Distribution at Fixed Time)**.** *For fixed $t > 0$ and $z \in \mathbb{R}$, define*

$$m(z, y) := \alpha\zeta(z; \frac{c\epsilon}{\alpha}, y)\hat{\theta}\left(\zeta(z; 1, y), \alpha^2 t\right) \exp\left\{-\frac{c^2\epsilon^2 t + 1/y + \zeta(z; 2, y)}{2}\right\}, \tag{6.23}$$

where

$$\hat{\theta}(r, s) := \frac{r}{2s} e^{\frac{\pi^2}{2s}} \mathbb{E}\left[V e^{-r\cosh(V)} \sinh(V) \operatorname{sinc}\left(\frac{V}{s}\right)\right]$$

with $\operatorname{sinc}(w) := \frac{\sin(w\pi)}{w\pi}$ *and* $V \sim N(0, \sqrt{s})$ *(normal distribution with mean* 0 *and standard deviation* $\sqrt{s}$*). Then for* $u \in \mathbb{R}$ *and for two* i.i.d. *uniformly distributed random variables* U *and* Y*, the probability distribution of* X_t *is given by*

$$\mathbb{P}_x\left(X_t \leq u\right) = \mathbb{E}\left[\frac{m\left(-\frac{1}{U} + u + 1, \frac{1}{Y} - 1\right)}{U^2 Y^2}\right].$$

Proof. First we show the identity between $\hat{\theta}(r, s)$ and $\theta(r, s)$. Recall in Proposition 6.3.3 that

$$\theta(r, s) = \frac{r}{\sqrt{2\pi^3 s}} e^{\frac{\pi^2}{2s}} \int_0^\infty e^{-\frac{v^2}{2s} - r\cosh(v)} \sinh(v) \sin\left(\frac{\pi v}{s}\right) dv.$$

Reorganise the function, we get

$$\begin{aligned}
\theta(r, s) &= \frac{r}{s} e^{\frac{\pi^2}{2s}} \int_0^\infty v e^{-r\cosh(v)} \sinh(v) \operatorname{sinc}\left(\frac{v}{s}\right) \cdot \frac{1}{\sqrt{2\pi s}} e^{-\frac{v^2}{2s}} dv \\
&= \frac{r}{2s} e^{\frac{\pi^2}{2s}} \mathbb{E}\left[V e^{-r\cosh(V)} \sinh(V) \operatorname{sinc}\left(\frac{V}{s}\right)\right] \\
&=: \hat{\theta}(r, s).
\end{aligned}$$

The second equation in above holds true is due to the fact that,

$$(v\sinh(v))\cdot e^{-r\cosh(v)}\cdot \operatorname{sinc}\left(\frac{v}{s}\right)$$

is an even function.

Now let $m(z,y)$ be defined in (6.23). Based on the identity between $\theta(r,s)$ and $\hat{\theta}(r,s)$, and refer to Proposition 6.3.3, we can write the probability distribution of X_t as

$$\mathbb{P}_x\left(X_t \le u\right) = \int_{-\infty}^{u}\int_{0}^{\infty} m(z,y)dydz. \tag{6.24}$$

Consider the following changes of variables,

$$U = -\frac{1}{z-u-1},\ Y = \frac{1}{1+y}.$$

Solve z, y in terms of U, Y, and substitute them into (6.24), we get

$$\mathbb{P}_x\left(X_t \le u\right) = -\int_{0}^{1}\int_{1}^{0} m\left(-\frac{1}{U}+u+1, \frac{1}{Y}-1\right)\frac{dUdY}{U^2Y^2}.$$

In the end, by noticing the fact that the uniform distribution has constant probability density ($dU = dY = 1$), we then conclude the proof. □

Remark. The main consideration of involving $\operatorname{sinc}(\cdot)$ is to reduce the oscillation effects from the function $\sin(\cdot)$. From the numerical point of view, the sinc-function, though cannot totally solve the oscillating issue, could mitigate the chaos to some extent.

Proposition 6.3.5 (Stationary Distribution)**.** *Let $t \uparrow +\infty$, the stationary distribution of $X_\infty := \lim_{t\uparrow+\infty} X_t$ is given by*

$$\mathbb{P}(X_\infty \in dx) = \frac{2\alpha\left(\frac{\nu}{c}\right)^{\nu}}{\Gamma(\nu)}\cdot\exp\left\{-\frac{\nu}{c}e^{-2\alpha x} - 2\alpha\nu x\right\}dx,$$

where $\nu := \frac{\epsilon c}{\alpha}$ and $\Gamma(\cdot)$ is the Gamma function.

Proof. Consider the Fokker-Planck equation at $t = +\infty$ (see (2.10)). From (6.1), the stationary density $p(x)$ solves

$$\frac{1}{2}p^{''}(x) - \epsilon(e^{-2\alpha x} - c)p^{'}(x) + 2\alpha\epsilon e^{-2\alpha x}p(x) = 0. \tag{6.25}$$

Define

$$w(x) := \exp\left\{\frac{\nu}{c}e^{-2\alpha x} + 2\nu\alpha x\right\}, \tag{6.26}$$

where $\nu := \frac{\epsilon c}{\alpha}$. Then ODE (6.25) has the following general solution:

$$p(x) = \frac{C_1 \int_{-\infty}^{x} w(y)dy + C_2}{w(x)}. \tag{6.27}$$

When $y \downarrow -\infty$, note that $w(y) \uparrow +\infty$, and it is dominated by a double-exponential function. Since $w(y) \geq 0$, so for $\forall y \in \mathbb{R}$ and $x \neq -\infty$,

$$\int_{-\infty}^{x} w(y)dy = +\infty.$$

Therefore, in order to get a valid density function, we set $C_1 = 0$. On the other hand, the full integrability condition yields

$$C_2 = \left[\int_{\mathbb{R}} w^{-1}(x)dx\right]^{-1}. \tag{6.28}$$

Consider the substitution that

$$u := \frac{\nu}{c}e^{-2\alpha x},$$

then combine (6.26), (6.28) can be rewritten as

$$\begin{aligned} C_2 &= \left[\int_0^{\infty} \frac{\exp\left\{-u + \nu \ln\left(\frac{cu}{\nu}\right)\right\}}{2\alpha u}du\right]^{-1} \\ &= \frac{2\alpha\left(\frac{\nu}{c}\right)^{\nu}}{\int_0^{\infty} e^{-u}u^{\nu-1}du}. \end{aligned}$$

Note that, by our definition, ϵ, c, and α are all bigger than 0. Therefore $\nu > 0$, and the denominator of C_2 is indeed $\Gamma(\nu)$. This concludes our proof. □

Remark. The stationary distribution of X_∞ is right-skewed and closely related to the Gamma distribution family. In fact, consider the exponential transform

$$Z_t := e^{-2\alpha X_t},$$

it is easy to show that

$$Z_\infty \sim \Gamma\left(\nu, \frac{\nu}{c}\right),$$

where $\Gamma(a, b)$ is the Gamma distribution with density function

$$p(z) = \frac{b^a}{\Gamma(a)} z^{a-1} e^{-bz}.$$

Therefore, the Shiryaev process, as mentioned in the remark under Proposition 6.3.1, that

$$Y_t = e^{2\alpha X_t} = \frac{1}{Z_t},$$

has the corresponding inverse Gamma distribution $IG\left(\nu, \frac{\nu}{c}\right)$. This coincides with the analysis from [100].

6.3.3 Finiteness of the First Passage Time

In the later section we will deduce the FPTD of $\{X_t\}_{t\geq 0}$. Before conducting the calculations, we first show the existence of the FPT for any constant level $a \in \mathbb{R}$.

Proposition 6.3.6. *(Recurrence)* $\{X_t\}_{t\geq 0}$ *is a recurrent process on* $\mathbb{R}$.

Proof. Let

$$Z_t := e^{-2\alpha X_t},\ Z_0 = e^{-2\alpha x}. \tag{6.29}$$

Then,

$$dZ_t = 2\alpha Z_t(-\epsilon Z_t + c\epsilon + \alpha)dt - 2\alpha Z_t dW_t. \tag{6.30}$$

According to Proposition 6.3.1, we know $\{Z_t\}_{t\geq 0}$ is a diffusion process with the unique strong solution; moreover the strong Markov property holds as well[6]. Therefore, if we can show $\{Z_t\}_{t\geq 0}$ satisfies the non-degeneracy and the local-integrability conditions in (2.12) and (2.13), respectively, further if we show that the conditions for the scale function in Theorem 2.1.4 hold, then we prove $\{Z_t\}_{t\geq 0}$ is recurrent. Correspondingly, the recurrence of $\{X_t\}_{t\geq 0}$ is given by the 1-1 mapping in (6.29).

From our construction, we see $\{Z_t\}_{t\geq 0}$ only takes values on the positive half-plane. Be-

[6] In fact one can even find the explicit solution of Z_t by referring to the stochastic Verhulst equation in [121].

sides, by checking (6.30), we find $Z_t = 0$ is an absorbing bound. Consider

$$I = (0, +\infty)$$

to be the domain of $\{Z_t\}_{t\geq 0}$. Refer to SDE (6.30), for any $z \in I$, the non-degeneracy condition for $\{Z_t\}_{t\geq 0}$

$$4\alpha^2 z^2 > 0$$

holds. In addition, consider $\delta > 0$ and which is small enough, such that $z - \delta \in I$. Then the local-integrability condition is satisfied by demonstrating

$$\int_{z-\delta}^{z+\delta} \frac{1 + 2\alpha\zeta \left|(-\epsilon\zeta + c\epsilon + \alpha)\right|}{4\alpha^2\zeta^2} d\zeta \leq \frac{\delta}{2\alpha^2\left(z^2 - \delta^2\right)} + \frac{\epsilon}{\alpha}\delta + \frac{c\epsilon + \alpha}{2\alpha} \ln\left(\frac{z+\delta}{z-\delta}\right) < +\infty.$$

Therefore, for any fixed parameter $A \in I$, refer to SDE (6.30) and Equation (2.14), the scale function of $\{Z_t\}_{t\geq 0}$,

$$s(z) := \int_A^z \exp\left\{-\int_A^\xi \frac{(-\epsilon\zeta + c\epsilon + \alpha)}{\alpha\zeta} d\zeta\right\} d\xi, \ z \in I, \tag{6.31}$$

is well-defined.

We now check the limit conditions in Theorem 2.1.4. After standard calculations, (6.31) further yields

$$s(z) = A^{1+\frac{c\epsilon}{\alpha}} e^{-\frac{A\epsilon}{\alpha}} \int_A^z \frac{e^{\frac{\epsilon}{\alpha}\xi}}{\xi^{1+\frac{c\epsilon}{\alpha}}} d\xi. \tag{6.32}$$

Substitute the boundary values into (6.32), we have

$$s(0^+) = -A^{1+\frac{c\epsilon}{\alpha}} e^{-\frac{A\epsilon}{\alpha}} \int_{0^+}^A \frac{e^{\frac{\epsilon}{\alpha}\xi}}{\xi^{1+\frac{c\epsilon}{\alpha}}} d\xi = -\infty,$$

and

$$s(+\infty) = A^{1+\frac{c\epsilon}{\alpha}} e^{-\frac{A\epsilon}{\alpha}} \int_A^{+\infty} \frac{e^{\frac{\epsilon}{\alpha}\xi}}{\xi^{1+\frac{c\epsilon}{\alpha}}} d\xi = +\infty.$$

The rest of the proof is then concluded by Theorem 2.1.4. □

Corollary 6.3.7 (Finiteness of the FPT)**.** *For any $a \in \mathbb{R}$ and $X_0 = x \in \mathbb{R}$, the first hitting time of $\{X_t\}_{t\geq 0}$ from x to a is finite* a.s.

Proof. This directly follows from Proposition 6.3.6. □

6.4 First Passage Time of $\{X_t\}_{t\geq 0}$

Here we prove the main results of this chapter. Our previous analysis in Section 6.3 shows that $\{X_t\}_{t\geq 0}$ is a well-defined diffusion process. More precisely, various technical assumptions in Section 2.2 are satisfied. Therefore, we can solve the FPTD via the BVP in Section 2.2 and our perturbation framework in Chapter 3.

6.4.1 Solution of the Initial Dirichlet Problem

Let $f \in C^2$, the infinitesimal generator of $\{X_t\}_{t\geq 0}$ is given by[7]

$$\mathcal{A}f(x) = \frac{1}{2}f^{''}(x) + \epsilon(e^{-2\alpha x} - c)f^{'}(x),\ x \in \mathbb{R}. \tag{6.33}$$

In addition, consider a constant barrier $a \in \mathbb{R}$, we further restrict $D = (a, +\infty)$ or $D = (-\infty, a)$, depending on whether $x > a$ or $x < a$, respectively. Then we define the single side FPT (τ) of $\{X_t\}_{t\geq 0}$ through Equation (3.3). The LT of τ, denoted by $f(x, \beta)$, is given by solving the initial BVP in Equations (3.5) and (3.6). Let

$$\begin{cases} m := \frac{\sqrt{c^2\epsilon^2+2\beta}-\epsilon c}{2\alpha} \\ n := \frac{\sqrt{c^2\epsilon^2+2\beta}+\alpha}{\alpha} \\ \psi := \frac{\epsilon e^{-2\alpha x}}{\alpha} \\ \lambda := x(\epsilon c - \sqrt{c^2\epsilon^2 + 2\beta}) \end{cases}. \tag{6.34}$$

Then refer to [2], the general solution of (3.5) is

$$f(x, \beta) = C_1 e^{\lambda} M\left(m, n, \psi\right) + C_2 e^{\lambda} U\left(m, n, \psi\right), \tag{6.35}$$

where $M(m, n, \psi)$ and $U(m, n, \psi)$ are solutions to the following Kummer's equation [28]

$$\psi u^{''}(\psi) + (n - \psi)u^{'}(\psi) = mu(\psi).$$

Now we need to determine the constants C_1 and C_2. Start with the hitting from above

[7]The domain in below is $\mathbb{R}$ is due to the fact from Proposition 6.3.6 that $\{X_t\}_{t\geq 0}$ is recurrent on $\mathbb{R}$.

case, i.e. $x > a$. Substitute $x = +\infty$ into (6.34), we get

$$\psi = 0 \text{ and } Real(\lambda) = -\infty.$$

Refer to [81, Section 13.2 (iii)], we find that depending on the choices of β, the limit of $U(m, n, \psi)$ at $\psi = 0^+$ has various versions. In order to guarantee the uniqueness of the solution[8], we set $C_2 = 0$. And for the limit of $M(m, n, \psi)$, [81] gives

$$M(m, n, \psi) = 1 + O(\psi),\ \psi \downarrow 0.$$

So C_1 is retained, and (6.35) becomes

$$f(x, \beta) = C_1 e^{\lambda} M(m, n, \psi). \tag{6.36}$$

Further let

$$\begin{cases} \hat{\psi} := \frac{\epsilon e^{-2\alpha a}}{\alpha} \\ \hat{\lambda} := a(\epsilon c - \sqrt{c^2\epsilon^2 + 2\beta}) \end{cases}. \tag{6.37}$$

Then substitute (6.36) into $f(a, \beta) = 1$, we solve the LT of τ:

$$f(x, \beta) = \frac{e^{\lambda} M(m, n, \psi)}{e^{\hat{\lambda}} M\left(m, n, \hat{\psi}\right)},\ x > a. \tag{6.38}$$

Next, consider hitting from below with $x < a$. In this case, the boundary $\{-\infty\}$ should be taken extra cares. From SDE (6.1), we can see $X_t = -\infty$ generates an infinite instantaneous drift. In fact, according to [100], $\{-\infty\}$ is an entry but not exit boundary. Further refer to [62, page 108], $f(-\infty, \beta)$ exists but is not necessarily to be 0. Let $x = -\infty$, from (6.34), we find

$$\psi = +\infty,\ \text{and},\ Real(\lambda) = +\infty.$$

Refer to [81], the asymptotics of $U(m, n, \psi)$ and $M(m, n, \psi)$, for large ψ, are given by

$$U(m, n, \psi) \sim \psi^{-m},\ \psi \uparrow +\infty, \tag{6.39}$$

[8]The parameter β is involved in the LT. We want a function of solution $f(x)$ that is unique in functional forms to all $\beta \in \mathbb{C}^+$.

and

$$M\left(m,n,\psi\right)\sim\frac{e^{\psi}\psi^{m-n}}{\Gamma(m)},\ \psi\uparrow+\infty, \tag{6.40}$$

respectively. An immediate observation from (6.40) is that,

$$\lim_{x\downarrow-\infty}e^{\lambda}M\left(m,n,\psi\right)=+\infty.$$

Therefore, we set $C_1=0$. And for the U-function part, substitute (6.39) into the limit of (6.35), we find

$$\begin{aligned}\lim_{x\downarrow-\infty}e^{\lambda}U\left(m,n,\psi\right)&=\lim_{x\downarrow-\infty}e^{\lambda}\psi^{-m}\\&=\left(\frac{\epsilon}{\alpha}\right)^{-m}\lim_{x\downarrow-\infty}\exp\left\{x(\epsilon c-\sqrt{c^2\epsilon^2+2\beta})+2\alpha x(\frac{\sqrt{c^2\epsilon^2+2\beta}-\epsilon c}{2\alpha})\right\}\\&=\left(\frac{\epsilon}{\alpha}\right)^{-m}.\end{aligned}$$

So in the hitting from below case, C_2 is retained. In the end, use again notations in (6.37), and by solving $f(a,\beta)=1$, we have

$$f(x,\beta)=\frac{e^{\lambda}U(m,n,\phi)}{e^{\hat{\lambda}}U(m,n,\hat{\phi})},\ x<a. \tag{6.41}$$

The boundary condition at $x=-\infty$ is correspondingly given by

$$f(-\infty,\beta)=\frac{(\epsilon/\alpha)^{-m}}{e^{\hat{\lambda}}U(m,n,\hat{\phi})}. \tag{6.42}$$

Equation (6.38) shows the LT for the downward FPT. Due to the special function, it is difficult to find the explicit inverse transform. In the following subsection, by employing the perturbation technique, we provide a closed-form asymptotic for the downward FPTD. And based on Definition 6.2.3, the asymptotic density function can be used in evaluating the imminent risk of a bubble burst.

6.4.2 Perturbed Downward FPTD

As we have seen in previous chapters, the LTs of τ for $\{X_t\}_{t\geq0}$ are given again by the ratios of special functions. We may infer that the direct inverse is not easy to be found. Numerical

methods in Section 2.3 therefore can be applied. Besides, in this subsection, we follow our perturbation framework and give the first order asymptotic FPTD of $\{X_t\}_{t\geq 0}$.

The h-function of the bubble process is specified by

$$h(X_t) = e^{-2\alpha X_t} - c,\ X_t \in D. \tag{6.43}$$

In the following content, we solve the recursive system up to $i = 1$ for the downward FPT.

W.l.o.g., we further let $a = 0$, and consider the τ defined by (3.17). Follow Lemma 3.4.2, set $A_1 = 0$, $A_2 = +\infty$, $C_1 = 0$, and $C_2 = 0$, we find

$$f_1(x,\beta) = f_0(x,\beta)\left(\frac{\gamma\left(e^{-2\alpha x}-1\right)}{2\alpha\left(\gamma+\alpha\right)} + cx\right), \tag{6.44}$$

where $\gamma = \sqrt{2\beta}$ and $f_0(x,\beta)$ is given by (3.18). Based on (6.44), we have the following proposition.

Proposition 6.4.1 (First Order Perturbed FPTD of the Bubble Process)**.** *The first order perturbed downward FPTD of* $\{X_t\}_{t\geq 0}$ *is given by*

$$\begin{aligned} p_\tau^{(1)}(t) = &\left(1+\epsilon\left(cx + \frac{\left(1-e^{-2\alpha x}\right)(\alpha t - x)}{2\alpha x}\right)\right) p_\tau^{(0)}(t) \\ &- \epsilon\frac{\alpha}{4}\left(1-e^{-2\alpha x}\right) e^{\alpha x\left(\frac{\alpha t}{2x}+1\right)} Erfc\left(\frac{x}{\sqrt{2t}} + \alpha\sqrt{\frac{t}{2}}\right), \end{aligned} \tag{6.45}$$

where $p_\tau^{(0)}(t)$ *is the downward FPTD for Brownian motion with* $a = 0$ *(Equation* (2.29)*), and* $Erfc(\cdot)$ *is the* complementary error function*.*

Proof. Combine (3.9), (3.18), and (6.44), the first order perturbed LT of τ is given by

$$f^{(1)}(x,\beta) = f_0(x,\beta)\left(1+\epsilon cx\right) + \epsilon f_0(x,\beta)\frac{\gamma\left(e^{-2\alpha x}-1\right)}{2\alpha(\alpha+\gamma)}. \tag{6.46}$$

According to Example 2.2.2, the inverse of $f_0(x,\beta)$ is given by $p_\tau^{(0)}(t)$.

Now we consider the ILT of the second term in (6.46). Define

$$\tilde{l}_1(\beta) := \frac{\sqrt{\beta}e^{-\sqrt{\beta}}}{\alpha x + \sqrt{\beta}}. \tag{6.47}$$

Then the second term can be rewritten as

$$\epsilon f_0(x,\beta)\frac{\gamma\left(e^{-2\alpha x}-1\right)}{2\alpha(\alpha+\gamma)} = \epsilon\frac{e^{-2\alpha x}-1}{2\alpha}\cdot\tilde{l}_1(2x^2\beta). \tag{6.48}$$

Refer to [9], the inverse of (6.47) is given by

$$\mathcal{L}^{-1}\left\{\tilde{l}_1(\beta)\right\}(t) = \alpha^2x^2e^{\alpha x(\alpha xt+1)}\text{Erfc}\left(\frac{1}{2\sqrt{t}}+\alpha x\sqrt{t}\right) - \frac{2\alpha xt-1}{2\sqrt{\pi}}t^{-\frac{3}{2}}e^{-\frac{1}{4t}}. \tag{6.49}$$

Also consider the fact [95] that, for a constant b,

$$\mathcal{L}^{-1}\left\{\frac{1}{b}\tilde{l}_1\left(\frac{\beta}{b}\right)\right\}(t) = \mathcal{L}^{-1}\left\{\tilde{l}_1(\beta)\right\}(bt).$$

So let $b=\frac{1}{2x^2}$, and by the linearity of ILT, we further have

$$\mathcal{L}^{-1}\left\{\tilde{l}_1(2x^2\beta)\right\}(t) = \frac{1}{2x^2}\mathcal{L}^{-1}\left\{\tilde{l}_1(\beta)\right\}\left(\frac{t}{2x^2}\right). \tag{6.50}$$

Summarise (6.48), (6.49), (6.50), and substitute the results into $\mathcal{L}^{-1}\left\{f^{(1)}(x,\beta)\right\}(t)$, where $f^{(1)}(x,\beta)$ is given in (6.46), we then conclude the proof. □

Remark. As an approximation, the first order perturbation provides a continuous function, but which is not necessarily a valid probability density function. In fact, one can check,

$$\int_0^{+\infty} p_\tau^{(1)}(t)dt = \lim_{\beta\to 0^+} f^{(1)}(x,\beta) = 1+\epsilon cx.$$

In the case $c>0$, the first order perturbation provides an extra tiny probability of ϵcx. We will discuss the accuracy issue in a later proposition.

Proposition 6.4.2 (Tail Asymptotics)**.** *For $i=1$, the tail asymptotics of $p_\tau^{(1)}$ are given by*

$$p_\tau^{(1)} \sim \left(1+\epsilon\left(cx-\frac{1-e^{-2\alpha x}}{2\alpha}\right)\right)p_\tau^{(0)}(t),\ t\downarrow 0, \tag{Left Tail}$$

and

$$p_\tau^{(1)} \sim \left(1+\epsilon\left(cx+\frac{(1-\alpha x)\left(1-e^{-2\alpha x}\right)}{2\alpha^2x}\right)\right)p_\tau^{(0)}(t),\ t\uparrow+\infty. \tag{Right Tail}$$

Proof. The left tail asymptotic is given, by considering the fact [25] that

$$\text{Erfc}\left(\frac{x}{\sqrt{2t}}+\alpha\sqrt{\frac{t}{2}}\right)\sim\exp\left\{-\left(\frac{x}{\sqrt{2t}}+\alpha\sqrt{\frac{t}{2}}\right)^2\right\},\ t\downarrow 0. \tag{6.51}$$

Now we consider the right tail. Note that, if we repeat using (6.51), the second term of $p_\tau^{(1)}$ will remain as a constant while the first term vanishes. This leads to a constant tail asymptotic for $t\uparrow+\infty$. But $p_\tau^{(1)}\downarrow 0$ indeed. Refer to another fact [96], that

$$\text{Erfc}(y)\sim\frac{e^{-y^2}}{y\sqrt{\pi}}\left(1-\frac{1}{2y^2}\right),\ y\uparrow+\infty. \tag{6.52}$$

And rewrite the first term of $p_\tau^{(1)}$ as

$$\begin{aligned}&\left(1+\epsilon\left(cx+\frac{\left(1-e^{-2\alpha x}\right)(\alpha t-x)}{2\alpha x}\right)\right)p_\tau^{(0)}(t)\\ =&\left(1+\epsilon\left(cx-\frac{\left(1-e^{-2\alpha x}\right)}{2\alpha}\right)\right)p_\tau^{(0)}(t)+\epsilon\frac{\left(1-e^{-2\alpha x}\right)t}{2x}p_\tau^{(0)}(t).\end{aligned} \tag{6.53}$$

Then substitute (6.52) and (6.53) into (6.45), we find as $t\uparrow+\infty$,

$$\begin{aligned}p_\tau^{(1)}(t)\sim&\left(1+\epsilon\left(cx-\frac{\left(1-e^{-2\alpha x}\right)}{2\alpha}\right)\right)p_\tau^{(0)}(t)+\epsilon\frac{\left(1-e^{-2\alpha x}\right)e^{-\frac{x^2}{2t}}}{2\sqrt{2\pi t}}\\ &-\epsilon\frac{\alpha\left(1-e^{-2\alpha x}\right)}{4}\cdot\frac{\sqrt{2}e^{-\frac{x^2}{2t}}}{\sqrt{\pi t}\alpha}+\epsilon\frac{\alpha\left(1-e^{-2\alpha x}\right)}{4}\cdot\frac{2\sqrt{2}e^{-\frac{x^2}{2t}}}{2\sqrt{\pi}\alpha^3t^{\frac{3}{2}}}\\ =&\left(1+\epsilon\left(cx-\frac{\left(1-e^{-2\alpha x}\right)}{2\alpha}\right)\right)p_\tau^{(0)}(t)+0+\epsilon\frac{1-e^{-2\alpha x}}{2x\alpha^2}p_\tau^{(0)}(t).\end{aligned}$$

This completes our proof. □

Remark. Proposition 6.4.2 indicates that the asymptotic FPTD of $\{X_t\}_{t\geq 0}$ has the same right tail as the one for the Brownian motion. Since we know the Brownian motion is a null-recurrent Markov process, therefore we may infer $\mathbb{E}_x[\tau]=+\infty$. Indeed, according to the first moment rule, and by (6.46), we can show

$$\mathbb{E}_x[\tau]\approx-\partial_\beta f^{(1)}(x,0^+)=+\infty.$$

Proposition 6.4.3 (Error Estimation and Convergence)**.** *The η-function for the perturbation error of $p_\tau^{(1)}(t)$ is given by*

$$\eta(x,t) = -\frac{\alpha^2\cosh(\alpha x)}{2}M_1(x,t) + \frac{1-e^{-2\alpha x}}{2\sqrt{2\pi}\alpha}M_2(x,t) + \frac{e^{-2\alpha x}}{\sqrt{2\pi}}M_3(x,t) + c\left(2-\frac{x^2}{t}\right)p_\tau^{(0)}(t), \tag{6.54}$$

where

$$\begin{cases} M_1(x,t) = Erfc\left(\frac{x}{\sqrt{2t}} + \alpha\sqrt{\frac{t}{2}}\right)e^{\frac{\alpha^2}{2}t} \\ M_2(x,t) = e^{-\frac{x^2}{2t}}\left[\alpha^2t^2 - (\alpha x+1)t + x^2\right]t^{-\frac{5}{2}} \\ M_3(x,t) = e^{-\frac{x^2}{2t}}(\alpha t - x)\,t^{-\frac{3}{2}} \end{cases}. \tag{6.55}$$

Moreover, the error estimation and the convergence results in Proposition 3.3.1 hold true for the perturbed FPTD of the bubble process.

Proof. Let $\eta(x,t) = \mathcal{L}^{-1}\left\{\partial_x f_1(x,\beta)\right\}(t)$ be defined as in (3.10). The partial derivative of f_1 on x is given by

$$\begin{aligned}\partial_x f_1(x,\beta) =& -\gamma e^{-\gamma x}\left(\frac{\gamma\left(e^{-2\alpha x}-1\right)}{2\alpha(\gamma+\alpha)} + cx\right) + e^{-\gamma x}\left(-\frac{\gamma e^{-2\alpha x}}{\gamma+\alpha} + c\right) \\ =& ce^{-\gamma x} - cx\gamma e^{-\gamma x} - e^{-2\alpha x}\frac{\gamma e^{-\gamma x}}{\gamma+\alpha} - \left(e^{-2\alpha x}-1\right)\frac{\gamma^2 e^{-\gamma x}}{2\alpha(\gamma+\alpha)}.\end{aligned}$$

The inverse of the first term is $cp_\tau^{(0)}(t)$; the second term is given by (5.29); the ILT of the third term can be found in the proof of Proposition 6.4.1; and the last term is given by another fact in [9], that

$$\begin{aligned}\mathcal{L}^{-1}\left\{\frac{\gamma^2 e^{-\gamma x}}{2\alpha(\gamma+\alpha)}\right\}(t) =& \mathcal{L}^{-1}\left\{\frac{\beta e^{-\sqrt{\beta}\sqrt{2}x}}{\sqrt{2}\alpha\left(\sqrt{\beta}+\alpha/\sqrt{2}\right)}\right\}(t) \\ =& \frac{t^{-\frac{5}{2}}(x^2 - t - x\alpha t + \alpha^2t^2)e^{-\frac{x^2}{2t}}}{2\sqrt{2\pi}\alpha} - \frac{\alpha^2}{4}e^{x\alpha}e^{\frac{\alpha^2}{2}t}\mathrm{Erfc}\left(\frac{x}{\sqrt{2t}} + \alpha\sqrt{\frac{t}{2}}\right).\end{aligned}$$

Then consider the substitutions in (6.55), and after standard calculations, one can get (6.54).

Now we prove that the conclusion from Proposition 3.3.1 is valid for our bubble process. Note that, apart from the first term of the η-function, $-\frac{\alpha^2\cosh(\alpha x)}{2}M_1(x,t)$, the boundedness of the rest terms can be shown by repeating the proofs in Lemma 4.2.1 and Proposition 4.2.2. Let

$$z = \alpha x + \frac{\alpha^2 t}{2}.$$

Then for the first term, we have

$$\begin{aligned}\left|-\frac{\alpha^2\cosh(\alpha x)}{2}M_1(x,t)\right| =& \frac{\alpha^2(e^{-\alpha x}+e^{\alpha x})}{4}\text{Erfc}\left(\frac{x}{\sqrt{2t}}+\alpha\sqrt{\frac{t}{2}}\right)e^{\frac{\alpha^2}{2}t} \\ =& \frac{\alpha^2(e^{-2\alpha x+z}+e^{z})}{4}\text{Erfc}\left(\sqrt{z+\frac{x^2}{2t}}\right). \end{aligned} \tag{6.56}$$

Note that, both $e^{-2\alpha x}$ and $\text{Erfc}\left(\sqrt{z+\frac{x^2}{2t}}\right)$ are positive and are decreasing functions of x. Therefore, for $x>0$ and $t>0$, from (6.56), we further have

$$\left|-\frac{\alpha^2\cosh(\alpha x)}{2}M_1(x,t)\right| \leq \frac{\alpha^2 e^z}{2}\text{Erfc}\left(\sqrt{z}\right).$$

In the end, let $z\uparrow+\infty$, by considering the asymptotic in (6.51), we show the first term in (6.54) is bounded by $\frac{\alpha^2}{2}$. And this boundedness is uniform on t and x. Therefore, combine our previous discussions on the rest three terms, we show that the η-function satisfies the conditions in Proposition 3.3.1, and we conclude the proof by here. □

6.5 Model Implementation

In this section, we consider the SDE with a constant volatility $\sigma>0$:

$$dX_t=\epsilon(e^{-2\alpha X_t}-c)dt+\sigma dW_t,\ X_0=x\in\mathbb{R}. \tag{6.57}$$

Similar as in Section 4.3.1, by taking the affine transformation into account, one can have the corresponding FPTD for $\{X_t\}_{t\geq 0}$. More precisely, denote the perturbed FPTD in Section 6.4.2 by

$$p_\tau^{(1)}(t|\epsilon,\alpha,c,x).$$

Then for a hitting level $a\neq 0$ and $a<x$, define

$$\tau^*:=\inf\left\{t>0:X_t=a|X_0=x\right\}, \tag{6.58}$$

the first order perturbed FPTD of τ^* is given by (please see Appendix 6.B).

$$p_{\tau^*}^{(1)}(t)=p_\tau^{(1)}\left(t\middle|\frac{\epsilon}{\sigma}e^{-2\alpha a},\alpha\sigma,ce^{2\alpha a},\frac{x-a}{\sigma}\right). \tag{6.59}$$

6.5.1 Model Calibration

In this subsection, we provide a calibration scheme for the extended SDE (6.57). Recall the notations in Section 2.4, we denote the observed asset prices $\{P_t\}_{t=0,1,...,N}$ by

$$P_t = P_0 e^{\hat{X}_t},\ t = 0, 1, ..., N. \tag{6.60}$$

Therefore, $\left\{\hat{X}_t\right\}_{t=0,...,N}$ represents the normalised log-price with $\hat{X}_0 = 0$. Let $\{\hat{r}_t\}_{t=1,...,N}$ be the log-return of $\{P_t\}_{t=0,1,...,N}$. By definition,

$$\hat{r}_t = \hat{X}_t - \hat{X}_{t-1},\ t = 1, ..., N. \tag{6.61}$$

We consider the calibration based on $\{\hat{r}_t\}_{t=1,...,N}$. Mathematically, there are 4 parameters to be decided, so at least 4 different statistical quantities should be provided. A natural candidate is the first four moments of $\{\hat{r}_t\}_{t=1,...,N}$. However, on the one hand, as we have shown in Section 6.2, the bubble dynamic in different regimes could have different statistical behaviours; so global moments on the whole time-series may not be representative. On the other hand, from Proposition 6.3.3, $\{X_t\}_{t\geq 0}$ has a very complicated probability density. Follow the proposition, even for the first moment, we cannot easily get the explicit expression. Therefore, instead of using the moment calibration, we provide an alternative scheme by splitting the time-series according to different bubble regimes.

Recall those three regimes of $\{X_t\}_{t\geq 0}$ as we have discussed in Section 6.2 (Figure 6.2), and by which, we make the following assumptions:

- Regime I) During this period, we assume $X_t \approx 0$. SDE (6.57) then can be simplified as

$$dX_t \approx \epsilon(1 - c)dt + \sigma dW_t. \tag{6.62}$$

- Regime II) In this stage, the dynamic follows SDE (6.57) but will visit the equilibrium level. Denote the level by X^R, we have

$$e^{-2\alpha X^R} = c. \tag{6.63}$$

- Regime III) Within this regime, X_t hits the record-high level. Assume $e^{-2\alpha X_t} \approx 0$, then

SDE (6.57) degenerates to

$$dX_t \approx -c\epsilon dt + \sigma dW_t. \tag{6.64}$$

Moreover, we assume that each regime could be recognised from the data. Let $\{0, 1, ..., t_1\}$, $\{t_1, ..., t_2\}$, $\{t_2, ..., t_3\}$ be the time periods for regimes I, II, and III. Denote the normalised log-price and log-return in each regime, by

$$\hat{X}^I := \left\{\hat{X}_t\right\}_{t=0,...,t_1},\ \hat{X}^{II} := \left\{\hat{X}_t\right\}_{t=t_1,...,t_2},\ \hat{X}^{III} := \left\{\hat{X}_t\right\}_{t=t_2,...,t_3},\ \text{and,}$$
$$\hat{r}^I := \{\hat{r}_t\}_{t=1,...,t_1},\ \hat{r}^{II} := \{\hat{r}_t\}_{t=t_1+1,...,t_2},\ \hat{r}^{III} := \{\hat{r}_t\}_{t=t_2+1,...,t_3},$$

respectively. Also we assume that the equilibrium level is observable, and which is given by

$$\hat{X}^R.$$

Now we consider the model calibration. Start with $\hat{\epsilon}$ and $\hat{c}$. The general idea is to take log-returns from regimes I and III in to account. Let

$$\bar{r}^I := \text{Mean}\left(\hat{r}^I\right),\ \text{and,}\ \bar{r}^{III} := \text{Mean}\left(\hat{r}^{III}\right)$$

be annualised sample means of returns. Then by matching $\bar{r}^I$ and $\bar{r}^{III}$ with their theoretical expectations from (6.62) and (6.64), we have

$$\begin{cases} \hat{\epsilon}(1-\hat{c}) = \bar{r}^I \\ -\hat{\epsilon}\hat{c} = \bar{r}^{III} \end{cases}.$$

Solve $\hat{\epsilon}$ and $\hat{c}$, we get

$$\begin{cases} \hat{\epsilon} = \bar{r}^I - \bar{r}^{III} \\ \hat{c} = -\frac{\bar{r}^{III}}{\bar{r}^I - \bar{r}^{III}} \end{cases}. \tag{6.65}$$

Remark. Note that, according to our assumptions, regime I should provide positive trend ($\bar{r}^I \geq 0$) while regime III generates negative moves ($\bar{r}^{III} \leq 0$). Therefore $\hat{\epsilon}$ and $\hat{c}$ are guaranteed to be positive. Moreover, since

$$0 \leq -\bar{r}^{III} \leq \bar{r}^I - \bar{r}^{III},$$

so $0 \leq \hat{c} \leq 1$.

Remark. In order to have a more effective calibration, we can (*) calculate the average of positive returns from regime I and the average of negative returns from regime III. Also, we are more interested in the longer term trend rather than the daily trend. So (**) using monthly rolling returns would help in enhancing the estimation stability. We add (*) and (**) as special data cleaning treatments in our algorithm.

Consider $\hat{\sigma}$. Observe from (6.62) and (6.64), we see volatilities of $\hat{r}^I$ and $\hat{r}^{III}$ are provided by the Brownian motion part only. Let $\hat{r}^{I\&III} := \hat{r}^I \cup \hat{r}^{III}$. Then we can calculate $\hat{\sigma}$ by

$$\hat{\sigma} = StdDev\left(\hat{r}^{I\&III}\right).$$

As an alternative plan, note that usually the time-series in regime III is more volatile, therefore, in order to have a more significant volatility, we can use $\hat{r}^{III}$ only:

$$\hat{\sigma} = StdDev\left(\hat{r}^{III}\right). \tag{6.66}$$

Given $\hat{c}$ as shown in (6.65), the last parameter $\hat{\alpha}$ is easy to be determined. From (6.63), we immediately have

$$\hat{\alpha} = -\frac{\ln(\hat{c})}{2\hat{X}^R}. \tag{6.67}$$

We summarise our calibration algorithm on the next page.

Remark. Algorithm 1 relies on two judgmental decisions: 1) time ranges for different regimes, and 2) the equilibrium level. For the first item, during an asset price increasing period, from the economical point of view, it is not difficult to differentiate each regime. Even though there is no clear economical signal, we can still split the time-series equally into three pieces. However, for $\hat{X}^R$, without a significant price drop, mathematically it is very challenging to decide the equilibrium level. Therefore fundamental analysis from economics may be required. The enhancement of Algorithm 1 will be remained in the future work.

6.5.2 Numerical Example

We provide three numerical exercises. The first two are similar in nature, where based on historical data, we verify the effectiveness of $\{X_t\}_{t\geq 0}$ in capturing bubble dynamics. In the third exercise, we provide drop-down probabilities (imminent risk) of the BitCoin.

Algorithm 1 $\{X_t\}_{t\geq 0}$ Model Calibration

1. Determine the time ranges for regimes I-III, and correspondingly compute the normalised log-price $\hat{X}^I,\ \hat{X}^{II},\ \hat{X}^{III}$ by (6.60). Identify the equilibrium level $\hat{X}^R$.

2. Compute monthly rolling log-returns $\hat{r}_m^I$ and $\hat{r}_m^{III}$ from $\hat{X}^I$ and $\hat{X}^{III}$, respectively. Find $\bar{r}^I$ and $\bar{r}^{III}$ via
$$\begin{cases} \bar{r}^I = Mean\left(\hat{r}_m^I \middle| \hat{r}_m^I \geq 0\right) \times 12 \\ \bar{r}^{III} = Mean\left(\hat{r}_m^{III} \middle| \hat{r}_m^{III} \leq 0\right) \times 12 \end{cases}.$$
Then use Equation (6.65) to calibrate $\hat{\epsilon},\ \hat{c}$.

3. Compute the daily log-return $\hat{r}_d^{III}$ from $\hat{X}^{III}$. Then compute the annualised return $\hat{r}^{III}$ via
$$\hat{r}^{III} = \hat{r}_d^{III} \times \sqrt{260},$$
and calibrate $\hat{\sigma}$ using (6.66).

4. Substitute $\hat{X}^R$ from Step 1 and $\hat{c}$ from Step 2 into (6.67) to calibrate $\hat{\alpha}$.

1997-01-02 to 2003-12-30 NASDAQ Composite Index

The US dot-com bubble [23] could be observed from the technology-dominated NASDAQ Composite Index (US ticker symbol ^IXIC). From the mid-90's, ^IXIC grew exponentially from below 1,000 USD to about 5,000 USD. The index hit its historical maximum in 2000-03-10, and at which date the total trading amount exceeded 10 Trillion USD (according to Yahoo Finance). After then, the market collapsed rapidly and dropped back to about 1,000 USD in 2002.

In this exercise, we use the adjusted daily closing price of ^IXIC from 1997-01-02 to 2003-12-30. The data is from Yahoo Finance. Note that, for the purpose of burst time prediction, there is no sense to calibrate the model using the full-cycle data. Therefore, only a truncated time-series is used in this model calibration. To be more specific, we choose calibration regimes as follows

$$\begin{cases} \hat{X}^I:\ \text{1997-01-02 } (P_0 = 1,280) \text{ to 1997-06-26 } (P_{t_1} = 1,436) \\ \hat{X}^{II}:\ \text{1997-06-26 } (P_{t_1} = 1,436) \text{ to 1999-02-10 } (P_{t_2} = 2,309) \\ \hat{X}^{III}:\ \text{1999-02-10 } (P_{t_2} = 2,309) \text{ to 2000-10-18 } (P_{t_3} = 3,171) \end{cases}. \tag{6.68}$$

The red curve in Figure 6.3 plots the full series of $\left\{\hat{X}_t\right\}_{t=0,1,\ldots,N}$. By observation, we set the equilibrium level to be $\hat{X}^R = 0.67$ ($P_R = 2,502$).

In order to compare our new model with existing models, we include the OU process and the drifted Brownian motion (DBM) as well. The time-series used for calibrating these two models are the same as in the $\{X_t\}_{t\geq 0}$ calibration, i.e. from 1997-01-02 to 2000-10-18. For the OU calibration algorithm, we refer to [119]. And we directly estimate the mean and volatility in the DBM. 1,000 paths between 1997-01-02 and 2003-12-30 are simulated using those three models. In Figure 6.3, apart from the historical price of ^IXIC, we demonstrate the best path among 1,000 simulations for each model. It is clear by the graph that our new model provides better fit than existing models. In order to measure the closeness of different paths to the historical dynamic, the correlations for each model are calculated:

$$\{X_t\}_{t\geq 0}:\ 91.20\%,\ OU:\ 81.01\%,\ DBM:\ 72.03\%.$$

As expected, $\{X_t\}_{t\geq 0}$ provides the highest correlation while DBM is the worst among three models.

To further explain our calibration algorithm, we plot three regimes in Figure 6.4. We also show 10,000 onward simulation paths for $\{X_t\}_{t\geq 0}$ with $X_0 = \hat{X}_{t_3}$. From the figure, we see that the historical prices are fully covered by the simulated paths. This indicates that our model is effective.

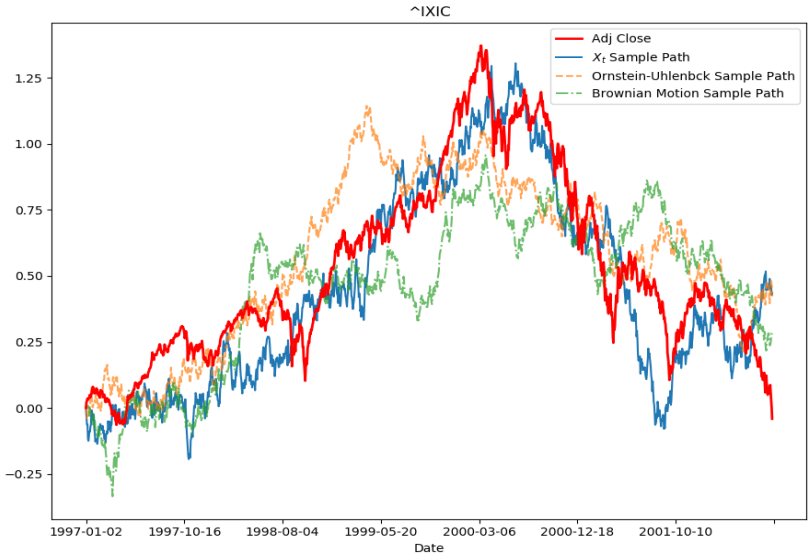

Figure 6.3: Model calibration comparisons for NASDAQ index (US ticker symbol ˆIXIC) from 1997-01-02 to 2003-12-30. Red curve: historical adjusted log-price; blue curve: the best of 1,000 simulations from $\{X_t\}_{t\geq 0}$; orange curve: the best of 1,000 simulations from OU process; green curve: the best of 1,000 simulations from DBM. Calibration parameters, $\{X_t\}_{t\geq 0}$: $(\hat{\epsilon}, \hat{\alpha}, \hat{\sigma}, \hat{c}) = (0.39, 0.23, 0.43, 0.73)$; OU : $(\hat{\kappa}, \hat{\mu}, \hat{\sigma}) = (0.47, 1.09, 0.31)$; BM : $(\hat{\mu}, \hat{\sigma}) = (0.25, 0.31)$. The data source is from Yahoo Finance

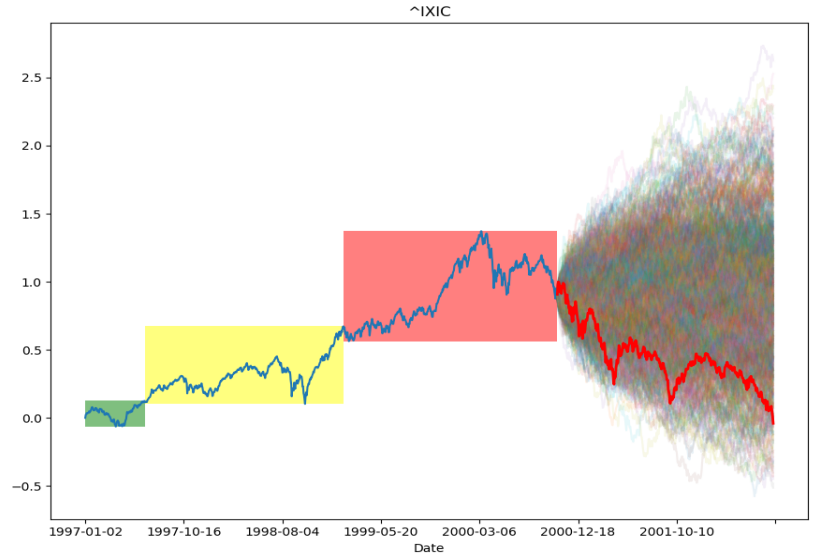

Figure 6.4: Algorithm 1 illustration based on ˆIXIC and 10,000 paths simulation starting from $X_0 = \hat{X}_{t_3}$. Green zone indicates regime I, the displacement stage; yellow zone indicates regime II, the boom stage; red zone indicates regime III, the euphoria & profit taking stages. Blue curve shows the historical data used for calibration. Red curve, covered by shadowed region, shows the historical data after t_3. The shadowed region plots 10,000 simulation paths

2006-01-04 to 2008-12-31 Shanghai Stock Exchange Composite Index

We use a second example to confirm our observations from the last exercise. The 2007 Chinese stock market crash [67] just happened before the 2008 global financial crisis. Started in early 2006, the Shanghai Stock Exchange Composite Index (US ticker symbol SSEC, China ticker symbol 000001.SS) increased from about 1,000 CNY to 6,092 CNY (mid-October, 2007). And within one year's time, from October 2007 to October 2008, the price dropped below 1,800 CNY. Similar to the pattern in ^IXIC, the historical log-price of SSEC dropped rapidly after the sudden peak, and before which there was a sharp increase.

Settings are the same as in the previous one. We only mention the regime choices and make comments wherever necessary.

$$\begin{cases} \hat{X}^I: \text{ 2006-01-04 } (P_0 = 1,180) \text{ to 2006-03-06 } (P_{t_1} = 1,288) \\ \hat{X}^{II}: \text{ 2006-03-06 } (P_{t_1} = 1,288) \text{ to 2007-05-30 } (P_{t_2} = 4,053) \\ \hat{X}^{III}: \text{ 2007-05-30 } (P_{t_2} = 4,053) \text{ to 2008-04-21 } (P_{t_3} = 3,116) \\ \text{equilibrium level}: \hat{X}^R = 1.23 \ (P_R = 4,040) \end{cases} . \tag{6.69}$$

Figure 6.5 demonstrates comparisons between the best simulated path and the historical log-price. We can immediately see that the OU process provides a much faster mean-reversion rate than which is reflected from the price dynamic. This shows the OU process cannot provide enough degree of freedom in calibrating bubble dynamics.

Correlations for different models to the actual data are given by:

$$\{X_t\}_{t\geq 0}: 96.11\%, \ OU: 88.00\%, \ DBM: 84.42\%.$$

Similar plot for the calibration illustration is given in Figure 6.6. Through this exercise, we can further confirm that our new model is a good candidate for describing economic bubbles.

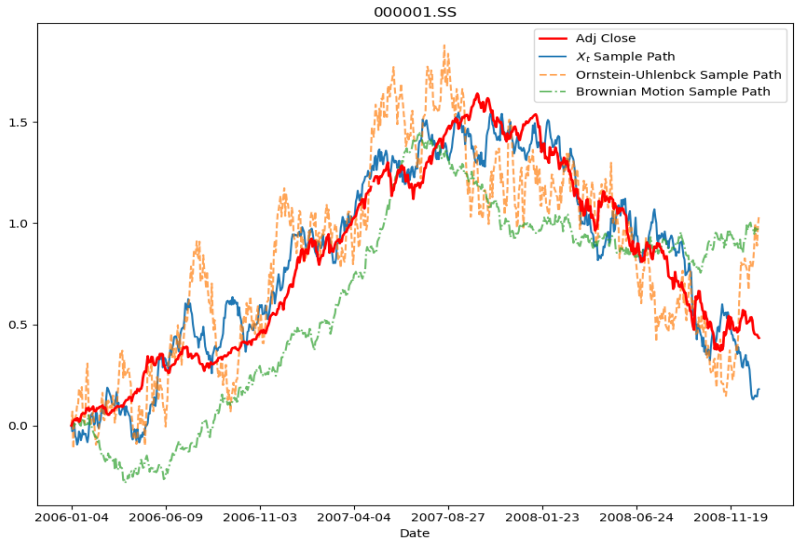

Figure 6.5: Model calibration comparisons for Shanghai Stock Exchange Composite index (US ticker symbol SSEC, China ticker symbol 000001.SS) from 2006-01-04 to 2008-12-31. Red curve: historical adjusted log-price; blue curve: the best of 1,000 simulations from $\{X_t\}_{t\geq 0}$; orange curve: the best of 1,000 simulations from OU process; green curve: the best of 1,000 simulations from DBM. Calibration parameters, $\{X_t\}_{t\geq 0}$: $(\hat{\epsilon}, \hat{\alpha}, \hat{\sigma}, \hat{c}) = (0.32, 0.14, 0.56, 0.70)$; OU : $(\hat{\kappa}, \hat{\mu}, \hat{\sigma}) = (3.30, 0.97, 1.20)$; BM : $(\hat{\mu}, \hat{\sigma}) = (0.44, 0.33)$. The data source is from Yahoo Finance

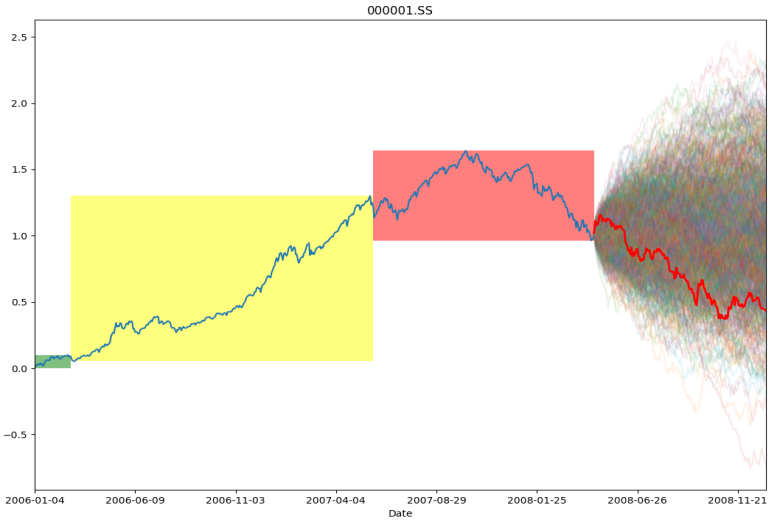

Figure 6.6: Algorithm 1 illustration based on 000001.SS and 10,000 paths simulation starting from $X_0 = \hat{X}_{t_3}$. Green zone indicates regime I, the displacement stage; yellow zone indicates regime II, the boom stage; red zone indicates regime III, the euphoria & profit taking stages. Blue curve shows the historical data used for calibration. Red curve, covered by shadowed region, shows the following historical data after t_3. The shadowed region plots 10,000 simulation paths

BitCoin Downward Probability Estimation

2017 is a year of BitCoin. At the first trading day of 2017, the price of 1 BitCoin was 995.44 USD. Although at then spending 1,000 dollars to buy one cryptocurrency was unbelievable to people, within 1 year's time, the price hit 19,345.49 USD. Figure 6.7 illustrates patterns for the price and trading volume between 2016-01-01 and 2017-12-10. There are many potential reasons that drive the nearly 20 times increase, for example, the increasing investments from institutional investors, more open mind from lawmakers, etc. In this exercise, we are interested in knowing whether the price would drop significantly in the near future. We conduct analysis in predicting the minimum of BitCoin price in the following month, effectively from 2017-12-10 to 2018-01-12.

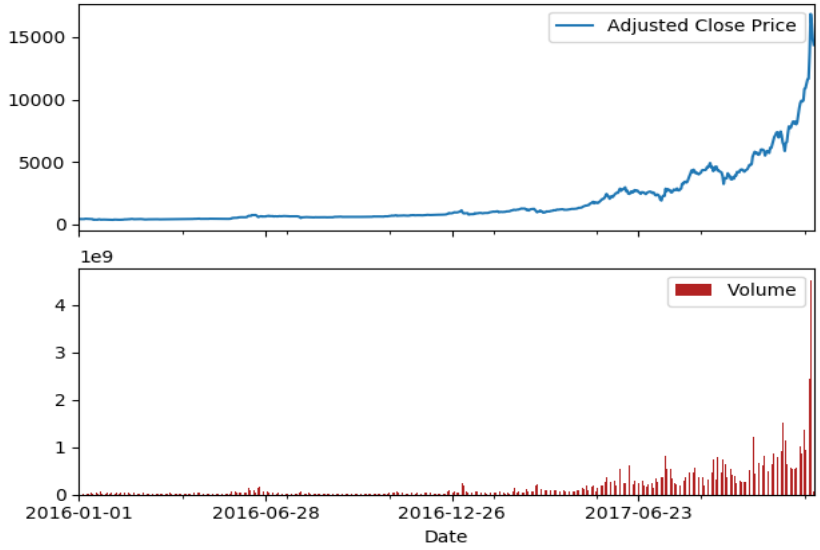

Figure 6.7: Bitcoin daily price and trading volume from 2016-01-01 to 2017-12-10. The data source is from Yahoo Finance

The model calibration is based on the time-series between 2016-01-01 and 2017-12-10:

$$\begin{cases} \hat{X}^I: \text{ 2016-01-01 } (P_0 = 433) \text{ to 2016-05-30 } (P_{t_1} = 528) \\ \hat{X}^{II}: \text{ 2016-05-30 } (P_{t_1} = 528) \text{ to 2017-08-13 } (P_{t_2} = 4,327) \\ \hat{X}^{III}: \text{ 2017-08-13 } (P_{t_2} = 4,327) \text{ to 2017-12-10 } (P_{t_3} = 14,371) \\ \text{equilibrium level}: \ \hat{X}^R = 2.30 \ (P_R = 4,327) \end{cases} . \tag{6.70}$$

Without mentioning too much detail, we summarise outputs from algorithm 1 in below:

$$\hat{\epsilon} = 0.51;\ \hat{\alpha} = 0.08; \hat{\sigma} = 0.91; \hat{c} = 0.69. \tag{6.71}$$

The prediction was made on 2017-12-10 with the price at $P_{t_3} = 14,371$[9]. We consider 0% to 60% drops from P_{t_3}. We compute the dropdown probabilities within a month via (6.79), i.e. the imminent risk[10]

$$\mathbb{P}\left(\tau(t_3, b) \leq 1/12\right),\ 0 \leq b \leq 0.6.$$

Furthermore, in order to evaluate the perturbation error, we refer to Proposition 6.4.3 and provide the relative error of density functions. Using the probabilistic representation in Proposition 3.3.1, we estimate $q_\tau(t)$ via 10,000 paths simulation. It should be noticed that, the relative error generally is high at tails as densities converge to 0. Therefore, it is not necessary to compute the relative error at each point. In fact, we are more concerned that whether the peak of the distribution would be changed by perturbations; so only relative errors on the density peak are computed. Table 6.1 summarises the results.

Percentage of Drop	Price P_l (USD)	Probability $\mathbb{P}\left(P_t^* \leq P_l\right)$	Peak Relative Error
0%	14,371.62	100.00%	0.00%
5%	13,653.05	84.85%	4.97%
10%	12,934.47	69.38%	1.48%
20%	11,497.30	40.19%	0.04%
30%	10,060.14	17.87%	0.86%
40%	8,622.98	5.35%	0.68%
50%	7,185.81	0.86%	1.45%
60%	5,748.65	0.05%	1.78%

Table 6.1: BitCoin imminent risk prediction between 2017-12-10 and 2018-01-12. Columns 1-4 correspond to the percentage of price drop, dropped price P_l, probability of the lowest price P_t^* ($\min_{0 \leq s \leq t} P_s$), and the relative error in density peaks

First by checking the last column (relative errors), we see in general the perturbation

[9]Note that, the data in our record does not correspond to the closing price of 2017-12-10. In fact, the data was downloaded when the market was still under trading.

[10]In our case, $P_{t_3} \approx \max_{0 \leq s \leq t_3} P_s$, therefore there is no harm to use P_{t_3} as the benchmark of the pre-drop price.

model is accurate. The largest error was in the 5% drop. In this case the hitting level is very close to the initial price P_{t_3}. As a result, the density curve will shrink to the y-axis. Therefore a larger error is expected. Analogously, large errors might also exist in the case that hitting levels are far to the initial price. For more details of the error analysis, please refer to Appendix 6.D.

We now consider the possibility of market collapse. Refer to the scenarios in ˆIXIC and 000001.SS, we find their largest drops in a month were about 30%, and which happened in the spring of 2000 and the autumn of 2008, respectively. Then check the probability of 30% drop for BitCoin, from Table 6.1, we only see about 17.87%. In fact, even for a 20% drop, the probability is about 40.19%. This means there is more than half chance that the price would remain above 11,497.30. Therefore, we conclude that the market is unlikely to collapse in the next month (2017-12-10 to 2018-01-12).

As a kind of backtest, we collect the one month data from 2017-12-10 to 2018-01-12 and plot the time-series in Figure 6.8. From the graph we see the lowest closing price was 12,531.52 on 2017-12-30. This verifies our conclusion that the market would not collapse immediately. On the other hand, compare the probabilities in Table 6.1 with the thresholds in Figure 6.8. The price on 2017-12-30 broke the 10% drop threshold, where the probability given by our prediction was 69.38%. This further confirms that our model is effective.

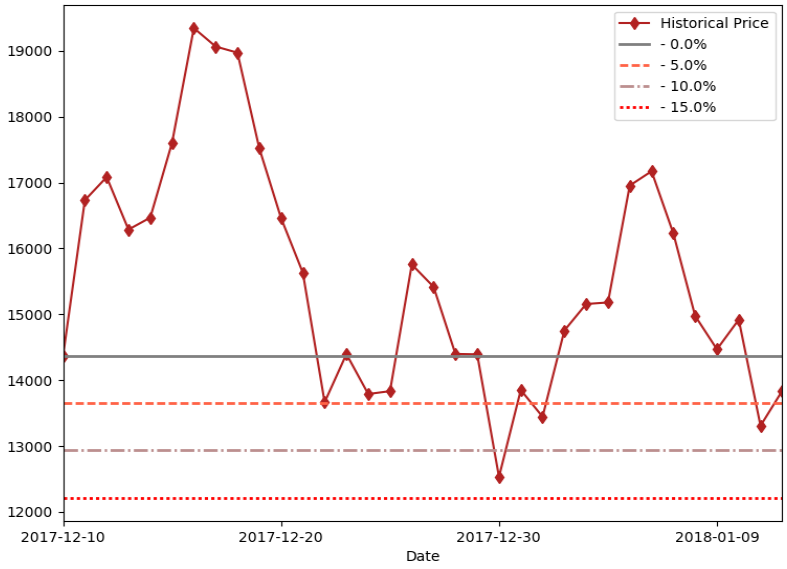

Figure 6.8: BitCoin closing price between 2017-12-10 and 2018-01-12. The probabilities of different thresholds are reported in Table 6.1

6.6 Conclusion

In this chapter, we provide a new diffusion process which can be used in modelling economic bubbles. The simple form of the model enables us to deduce its downward FPTD explicitly. Therefore, the new process can be seen as a good candidate in estimating the burst time of an economic bubble. Numerical examples in Section 6.5 consistently confirm that the model and its prediction are effective. Results in Section 6.3 show that the process has desirable properties, and which potentially can be employed in the future option pricing work. One remaining issue is the exact simulation of the process. This requires further understandings on the $\theta(r,s)$ function in (6.14), and itself is closely linked to the Hartman-Watson distribution. We leave this for the future work.

Appendix 6.A Recursive Solution for $c = 0$

Under $c = 0$, the h-function of the bubble process becomes a purely exponential function, i.e. $h(y) = e^{-2\alpha y}$. Similar as in the OU case, the exponential function is also closed under operations of integration and differentiation. Therefore, recursive solutions of arbitrary order N should exist. In this appendix, we summarise conclusions for $f^{(N)}$ and its inverse.

Consider the hitting level $a = 0$, and let τ be the downward FPT in (3.17). Then,

Proposition 6.A.1 (Recursive Structure of $f_i(x,\beta)$)**.** *Let $i \in \mathbb{N}$, $\beta \in \mathbb{C}^+$, and $\gamma = \sqrt{2\beta}$, the solution of the $o\left(\epsilon^i\right)$ BVP is given by*

$$f_i(x,\beta) = f_0(x,\beta)\sum_{k=0}^{i} p_{i,k}(\beta)e^{-2k\alpha x},$$

where $p_{i,k}(\beta)$ is given by

$$\begin{cases} p_{i,k}(\beta) = \frac{2^{\frac{\gamma}{\alpha}}\gamma/\alpha}{2\sqrt{\pi}\alpha^k\Gamma(k+1)} \cdot \frac{\Gamma\left(\frac{1}{2}+\frac{1}{2}\frac{\gamma}{\alpha}\right)\Gamma\left(k+\frac{1}{2}\frac{\gamma}{\alpha}\right)}{\Gamma\left(k+1+\frac{\gamma}{\alpha}\right)} \cdot p_{i-k,0}(\beta),\ 0 < k \le i, \\ p_{i,0}(\beta) = -\sum_{k=1}^{i} p_{i,k}(\beta),\ k = 0, \end{cases}$$

with $p_{0,0}(\beta) = 1$.

Proof. For $i \geq 0$, we assume the g_i in (3.20) has the following structure:

$$g_i = \sum_{k=0}^{i} p_{i,k} e^{-2k\alpha x},$$

where $p_{i,k}$ is independent of x and to be determined. To verify the assumption, for $i = 0$, we find

$$1 = g_0 = p_{0,0} \cdot e^{-0},$$

and which implies $p_{0,0} = 1$. Then for $i \geq 1$, substitute g_i into the left-hand side of Equation (3.21), we have

$$\begin{aligned} \frac{1}{2} g_i^{''} - \gamma g_i^{'} &= 2 \sum_{k=0}^{i} p_{i,k} k^2 \alpha^2 e^{-2k\alpha x} + 2\gamma \sum_{k=0}^{i} p_{i,k} k\alpha e^{-2k\alpha x} \\ &= 2 \sum_{k=0}^{i} p_{i,k} k\alpha(k\alpha + \gamma) e^{-2k\alpha x}. \end{aligned} \tag{6.72}$$

For the right-hand side, by substituting g_{i-1} into (3.21), we get

$$\begin{aligned} h\left(\gamma g_{i-1} - g_{i-1}^{'}\right) &= e^{-2\alpha x} \left(\gamma \sum_{k=0}^{i-1} p_{i-1,k} e^{-2k\alpha x} + 2 \sum_{k=0}^{i-1} p_{i-1,k} k\alpha e^{-2k\alpha x} \right) \\ &= \sum_{k=1}^{i} p_{i-1,k-1} \left[\gamma + 2(k-1)\alpha\right] e^{-2k\alpha x}. \end{aligned} \tag{6.73}$$

Match the coefficients between (6.72) and (6.73), we have

$$p_{i,k} = \frac{\gamma + 2(k-1)\alpha}{2k\alpha(k\alpha + \gamma)} p_{i-1,k-1}. \tag{6.74}$$

Further simplify (6.74) by multiplying up-to $p_{i-k,0}$, we get

$$p_{i,k} = p_{i-k,0} \cdot \prod_{m=1}^{k} \left[\frac{\gamma + 2\alpha(m-1)}{2m\alpha\left(m\alpha + \gamma\right)} \right], \; i > 0, \; 0 < k \leq i.$$

Consider definition and properties of Gamma functions, we can rewrite $p_{i,k}$ as

$$p_{i,k} = \frac{2^{\frac{\gamma}{\alpha}} \gamma/\alpha}{2\sqrt{\pi}\alpha^k \Gamma\left(k+1\right)} \cdot \frac{\Gamma\left(\frac{1}{2} + \frac{1}{2}\frac{\gamma}{\alpha}\right) \Gamma\left(k + \frac{1}{2}\frac{\gamma}{\alpha}\right)}{\Gamma\left(k + 1 + \frac{\gamma}{\alpha}\right)} \cdot p_{i-k,0}. \tag{6.75}$$

Note that, the $p_{i,0}$ term is not included in (6.75) above, but according to the condition that $g_i(0) = 0$ for $i > 1$, we can find

$$p_{i,0} = -\sum_{k=1}^{i} p_{i,k}. \tag{6.76}$$

This concludes our proof. □

Proposition 6.A.2 (Existence, Continuity and Full Integrability of $p_\tau^{(N)}$)**.** *For any $N \in \mathbb{N}_0$, the ILT of $f^{(N)}(\beta)$ exists:*

$$p_\tau^{(N)}(t) = \mathcal{L}^{-1}\left\{f^{(N)}(\beta)\right\}(t).$$

Moreover, $p_\tau^{(N)}(t)$ is continuous on $t > 0$, and

$$\int_0^\infty p_\tau^{(N)}(t)dt = 1.$$

Proof. Before stating the proof, it is worthy to be mentioned that not all functions can be inverted; and for those which can be inverted, even though the frequency function is continuous, it is not necessarily true that the time-domain function is also continuous.

In the following proof, we first show the existence of the inverse transform for $f^{(N)}$. For $\beta \in \mathbb{C}^+$, we assume that $f^N(\beta)$ does not contain any pools on the right of K, for some real number K to be large enough. Later we will show this condition is satisfied by $f^{(N)}$.

Let $0 \le i \le N$, recall Equation (6.74) in the proof of Proposition 6.A.1. Since $p_{i,k}$ is a function with at most polynomial growth on β, so for $\beta \in \mathbb{C}^+$, we have

$$\lim_{\beta \to +\infty} e^{-\sqrt{2\beta}x} p_{i,k}(\beta) e^{-2k\alpha x} = 0.$$

According to the recursion structure in Proposition 6.A.1, this leads to

$$\lim_{\beta \to +\infty} f_i(\beta) = 0.$$

For $i \ge 1$, based on the Jordan's lemma and (2.36), we can rewrite the inverse of f_i as

$$\mathcal{L}^{-1}\left\{f_i(\beta)\right\}(t) := \sum_{\hat{\beta} \in \mathcal{P}_i} Res\left(f_i(\hat{\beta})e^{\hat{\beta}t}\right), \tag{6.77}$$

where $\mathcal{P}_i$ is the collection of all pools of f_i (see (2.35)). Note that, by checking with (6.75),

we find that the pools of $f_i(\beta)$ are the same as pools of $\Gamma\left(\frac{1}{2}+\frac{1}{2}\frac{\gamma}{\alpha}\right)\Gamma\left(k+\frac{1}{2}\frac{\gamma}{\alpha}\right)$. Consider the fact that, the Γ-function has only pools at $\mathbb{N}_0$. We then have

$$\mathcal{P}_i=\left\{\beta:\sqrt{2\beta}=-\alpha(2m+1),\ m\in\mathbb{N}_0\right\}\cup\left\{\beta:\sqrt{2\beta}=-2\alpha(n+k),\ n\in\mathbb{N}_0,\ 1\leq k\leq i\right\}. \tag{6.78}$$

On the other hand, recall the *De Moivre's formula*:

$$\sqrt{z}=\pm\sqrt{r}\left(\cos\left(\frac{\theta}{2}\right)+i\sin\left(\frac{\theta}{2}\right)\right),\ z\in\mathbb{C}^+,\ r\in\mathbb{R}^+,\ \theta\in\mathbb{R}.$$

Then by choosing $\theta\in\{0,2\pi\}$, we immediately see that the β in (6.78) has two real solutions on the positive and the negative planes, respectively. As we require that $f_i(\beta)$ does not have any pool when $|\beta|\uparrow+\infty$, so the only possible pools are on the negative plane. This concludes the first part proof, that for any $N\in\mathbb{N}_0$, the inverse of $f^{(N)}(\beta)$ exists.

Now we consider the continuity and the full-integrability. Substitute negative-pools into (6.77), and based on Proposition 6.A.1, we have

$$\mathcal{L}^{-1}\left\{f_i(\beta)\right\}(t)=\sum_{k=0}^{i}\sum_{\hat{\beta}\in\mathcal{P}_i}p_{i,k}\left(\hat{\beta}\right)e^{-2k\alpha x-\sqrt{2\hat{\beta}}x+\hat{\beta}t}.$$

From the equation above, for $t>0$ and $i\in\mathbb{N}_0$, we can see the inverse is continuous on t, and therefore is

$$p_\tau^{(N)}(t)=\frac{xt^{-\frac{3}{2}}}{\sqrt{2\pi}}e^{-\frac{x^2}{2t}}+\sum_{i=1}^{N}\epsilon^i\mathcal{L}^{-1}\left\{f_i(\beta)\right\}(t).$$

For the probability integral, recall (6.76); we find $\lim_{\beta\to0^+}p_{i,k}(\beta)=0$ for all $i\geq1$ and $0\leq k\leq i$. Combine the fact that $\lim_{\beta\to0^+}f_0(x,\beta)=1$, we can show

$$\lim_{\beta\to0^+}f^{(N)}(x,\beta)=\lim_{\beta\to0^+}f_0(x,\beta)+\sum_{i=1}^{N}\epsilon^N\lim_{\beta\to0^+}f_i(x,\beta)=1+0=1.$$

So according to the moment rule, we further have

$$\int_0^{+\infty}p_\tau^{(N)}(t)dt=1.$$

And this concludes our proof. □

Appendix 6.B Generalised FPTD with $\sigma > 0$ and $a \neq 0$

Consider a generalised SDE (6.57), and a hitting level $a \neq 0$ with $a < x$. Define the affine transformation of $\{X_t\}_{t\geq 0}$ by $\{Y_t\}_{t\geq 0}$, where

$$Y_t = \frac{X_t - a}{\sigma},\ Y_0 = \frac{x-a}{\sigma}.$$

Then Y_t embeds the following SDE

$$\begin{aligned} dY_t &= \frac{\epsilon}{\sigma}\left(e^{-2\alpha X_t} - c\right)dt + dW_t \\ &= \frac{\epsilon e^{-2\alpha}}{\sigma}\left(e^{-2\alpha\sigma Y_t} - ce^{2\alpha}\right)dt + dW_t \\ &=: \tilde{\epsilon}\left(e^{-2\tilde{\alpha}Y_t} - \tilde{c}\right)dt + dW_t,\ Y_0 = y, \end{aligned}$$

with

$$\tilde{\epsilon} = \frac{\epsilon e^{-2\alpha}}{\sigma},\ \tilde{\alpha} = \alpha\sigma,\ \tilde{c} = ce^{2\alpha},\ y = \frac{x-a}{\sigma}.$$

Let τ be the downward FPT of hitting 0, as it has been discussed in Section 6.4. Further define τ^* to be the downward FPT of $\{X_t\}_{t\geq 0}$ (see (6.58)). Based on the equivalence between $\{X_t\}_{t\geq 0}$ and $\{Y_t\}_{t\geq 0}$ (which also implies $\tau^* = \tau$ *a.s.*), we then can express the perturbed density of τ^* as given in (6.59).

Further consider the relation between the running minimum and the downward FPT (cf. 4.3.1). Define

$$X_t^* := \min_{0\leq s\leq t} X_s.$$

Then for a fixed $t > 0$ and $a < x$, the perturbed distribution of X_t^* is given by

$$\mathbb{P}_x\left(X_t^* \leq a\right) = \int_0^t p_\tau^{(1)}\left(s|\tilde{\epsilon},\tilde{\alpha},\tilde{c},y\right)ds. \tag{6.79}$$

Appendix 6.C Further Numerical Analysis for $\{X_t\}_{t\geq 0}$

We repeat the analysis that we have done in Section 4.3.3 and Section 5.3. We benchmark the first order downward FPTD with the Talbot inverse. Full density curve and its error are provided in Figures 6.9 and 6.10. Figures 6.11 and 6.12 focus on the left tail.

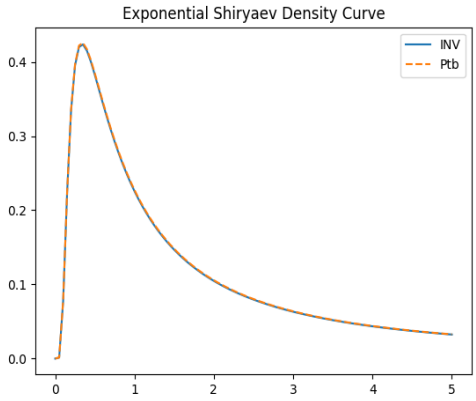

Figure 6.9: Density plot with $\epsilon = 0.1,\ \alpha = 0.5,\ c = 0.2,\ \sigma = 0.5,\ x = 0.7,\ l = 0.2$

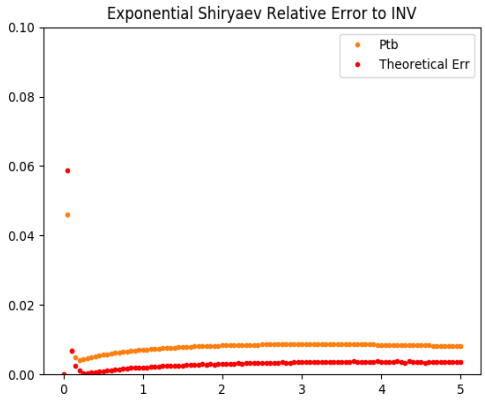

Figure 6.10: Error plot with $\epsilon = 0.1,\ \alpha = 0.5,\ c = 0.2,\ \sigma = 0.5,\ x = 0.7,\ l = 0.2$

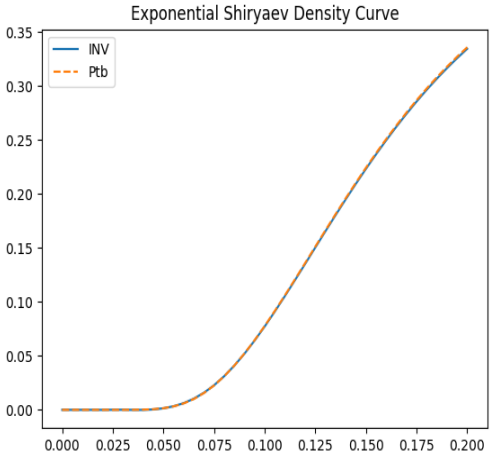

Figure 6.11: Left tail density

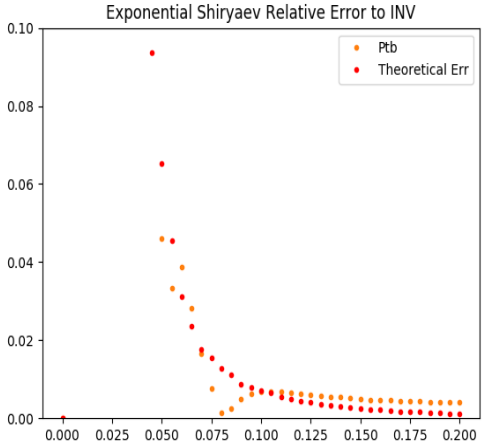

Figure 6.12: Left tail density error

Appendix 6.D First Order Perturbed Upward FPTD

In this appendix, we provide the analysis of the upward FPTD. First recall Section 6.4.1, when $x < a$, we have mentioned that the lower boundary $\{-\infty\}$ is ill-posed. The boundary value for the original BVP is given in (6.42). Similar as in the case of BES(n), if we force the perturbed ODEs to match (6.42), in the end we could possibly get a solution in terms of confluent hypergeometric functions, or, we may even not get a valid solution. Therefore, we repeat the technique that we used in Appendix 5.A, where we simply solve the upward FPT by reflecting the process with $Y_t = -X_t$.

Denote the downward perturbed FPTD of $\{X_t\}_{t\geq 0}$ by

$$p^{(1)}_{\tau_\downarrow} = p^{(1)}_{\tau}\left(t|\epsilon,\alpha,c,x\right), x>0.$$

Then by considering the reflection, the upward FPTD of $\{X_t\}_{t\geq 0}$ is given by

$$p^{(1)}_{\tau_\uparrow} = p^{(1)}_{\tau}\left(t|-\epsilon,-\alpha,c,-x\right), x<0. \tag{6.80}$$

We emphasise again, as we have highlighted in Appendix 5.A, (6.80) is only valid if x is not too far from 0. Besides, by repeating the calculations in Proposition 6.4.2, we find the left-tail has the same asymptotic as in the downward FPTD. But the right-tail asymptotic of (6.80) is given by[11] $e^{\frac{\alpha^2}{2}t}$. Therefore, from the time dimension, (6.80) only works for small t.

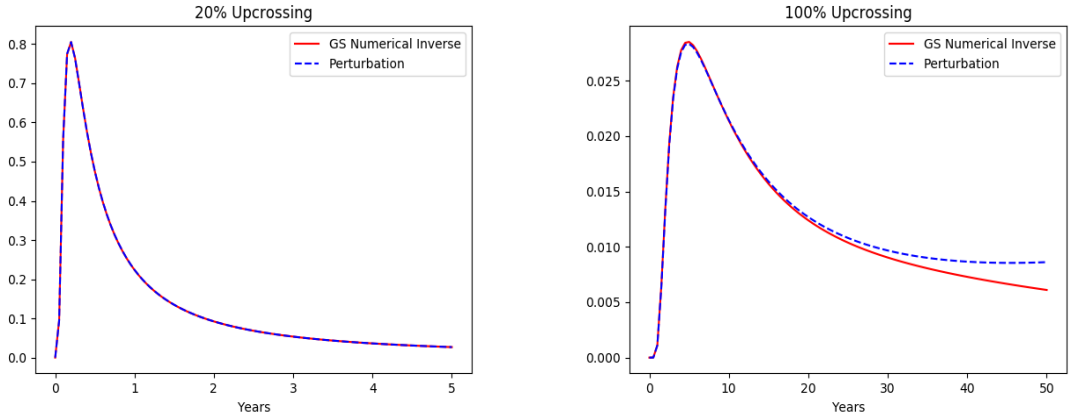

Figure 6.13: Upcrossing FPTD of the bubble process. $\epsilon = 0.1,\ \alpha = 0.5,\ c = 0.3, \sigma = 0.4,\ x = 1.5$. Left figure, 20% upcrossing ($a = 1.8$); right figure, 100% upcrossing ($a = 3$).

[11] This is due to $\lim_{t\uparrow+\infty} \text{Erfc}(-\alpha\sqrt{\frac{t}{2}}) = 2$. And from the LT, for the upward case, the f_1-function exists only if $\beta \geq \frac{\alpha^2}{2}$.

Chapter 7

Capital Allocation under the Fundamental Review of Trading Book

In January 2016[1], the Basel Committee on Banking Supervision finalised the next stage regulatory framework for market risk. Formally known as the Fundamental Review of Trading Book (FRTB), the new document overhauls minimum capital requirements in both the *standardised approach* and the *internal model approach (IMA)*. Under the FRTB IMA, banks need to report aggregated expected shortfalls (ES) as capital charges. Besides, the predefined Liquidity Horizons (LH) and Risk Factor Categories (RF) restrict capital reduction effects from cross-hedging. Facing the tightened regulation, in order to reevaluate the capital efficiency under their strategies, banks need to develop corresponding capital allocation methodologies. In this chapter, we provide two allocation schemes under the FRTB IMA, which could effectively reflect the capital structure that is required by the new regulation. Meanwhile, both schemes are guaranteed to be no more computationally complex than allocations under the current VaR-based regulatory framework. At the end of this chapter, numerical results show that our allocation schemes are more stable than allocations under the traditional ES.

For a table of acronyms appeared in this chapter, please refer to Section 2.5.1 on p. 23.

[1]The newest version of the FRTB is released on 14$^{\text{th}}$-January-2019 by the Basel Committee on Banking Supervision. It does not affect our results in this chapter.

7.1 Introduction, Motivation, and Literature Review

FRTB [12] is the newest version of the regulatory guidance for the global banking industry. It aims to address the shortcomings of the Basel II and its current amendments [10]. Firstly published in 2016, the new document specifies calculations of minimum capital requirements for market risk. Later in March 2018, a consultative document of FRTB [13] has been released and which modifies requirements in the standardised approach and the *profit and loss analysis* for IMA. But in general, the IMA calculation in the original FRTB document does not change. On 7$^{\text{th}}$ December 2017, the Basel Committee oversight body, *Group of Central Bank Governors and Heads of Supervision*, announced that the implementation date of the FRTB will be extended to January 2022.

In the FRTB IMA, the risk reporting metric shifts from VaR to an aggregation of traditional ES measure. Besides, the new regulation also takes the liquidity risk into account and the capital-reducing effect of cross-hedging is constrained. As a result, bank's cost is facing significant increases[2], although, this was not the intention from the Basel Committee. Facing the new regulation, banks may need to reevaluate their capital efficiency and reposition their resources strategically to business units with high RORAC (see Equation (2.46)), where the RORAC itself should be calculated in the manner of allocated capitals under the FRTB. These bring forward the needs of finding new allocation schemes; especially, such allocations should be able to reflect the capital structure that is required by the FRTB IMA. On the other hand, the aggregated ES based capital charge is computationally more demanding than which under the current practice. Thus, in order to meet various risk management needs, new allocation methodologies should also be developed in a computationally efficient way.

In this chapter, we propose two allocation methods for the capital charge under the FRTB IMA, namely the Euler approach and the constrained Aumann-Shapley (CAS) allocation. Both allocations consist of two stages. In the first stage, the FRTB capital charge is allocated to each predefined RF and LH bucket. In the second stage, allocations in different buckets are decomposed, realigned, and then aggregated. These allocation schemes can be applied when one treats the *stress scaling factor* [12, Paragraph 181 (d)] as a constant. Alternatively, in Section 7.3.4 of this chapter, we also extend our methods to the situation where the impact

[2]In the 2014 industry *Quantitative Impact Study (QIS)* [11], 44 banks have reported an average of 54% increase on capital charges under the new IMA. And the increased cost margin from the standardised approach is even more significant.

of risk factors from the stress scenarios is incorporated.

The Euler allocation principle has been studied extensively. Tasche [122] has shown that it can be employed in optimising the firm's RORAC. While later in 2001, Denault [38] established axiomatic characterisations for the Euler allocation. When the Euler allocation principle is applied under the FRTB IMA, we show that the allocation to each RF and LH bucket is a scaled version of the Euler allocation to the standard ES. And the scaling factor reflects the relative weight of the standalone ES for the bucket to the total *FRTB-ES* [12, Paragraph 181 (c)] from the same RF category. Our second allocation method is motivated by the CAS allocation by Li et al. [76]. Similar to the Euler allocation, we find the CAS allocation is also a scaled version of the traditional ES allocation. In this case, the scaling factor becomes the average of incremental FRTB-ES ratios under different LH permutations. Reducing the new allocation methods to the traditional ES allocation ensures computational efficiency. In the end, the *scenario extraction* technique [41] for the traditional ES allocation can be used accordingly. This avoids any revaluation on the capital charge.

At the end of this chapter, we illustrate the FRTB allocations via three groups of simulation analysis. Results show that, for risk factors with longer liquidity horizons, they are correspondingly allocated larger portions of the total capital. Meanwhile, negative allocations, resulting from either independent risk factors or hedged positions among different RF and LH buckets, are disappeared from the FRTB allocations. These observations, on the one hand, confirm that our allocations are more stable than that in the regular ES (VaR); on the other hand, the FRTB features, including the LH scaling and the constraint on the cross-hedging, are correctly reflected by our schemes. In addition, the example in Section 7.4.2 indicates that, if the hedging is within the same RF and LH bucket, then negative allocations can still happen under FRTB. But their magnitudes are significantly smaller than traditional allocations. This further confirms the stability of the FRTB allocations. More importantly, in the third simulation analysis, we find that the allocation under the FRTB is sensitive to the choice of the *reduced set* [12, Paragraph 181 (d)]. Inspired by this test, we realise that by comparing the allocations with/without decomposing the stress scaling factor, banks can identify those risk positions which have fewer risk contributions in the current calibration period but embed significant loss during the stress period. As a result, as long as the *75% rule* [12, Paragraph 181 (d)] is satisfied, banks could decrease their total capital charges by simply removing those identified positions from the reduced set.

The rest of this chapter is organised as follows. Section 7.2 introduces the internal model capital charge under the FRTB and investigates its homogeneity and sub-additivity properties. Allocation methods and their extensions are introduced in Section 7.3, followed by the simulation analysis in Section 7.4. Section 7.5 concludes. All proofs are provided separately in the appendices of this chapter.

7.2 Internal Model Capital Charge under FRTB

The original document [12] of FRTB includes 3 major chapters. In each of them, the definition of the trading book, the standardised approach, and the IMA are respectively discussed. And within [12, Chapter C], the final capital charge of IMA is further split into *default risk charge*, *internal model capital charge for modellable risk factors (IMCC)*, and *non-modellable risk factor add-ons*. Among those three parts, the default risk charge and non-modellable risk factor add-ons are calculated either using the traditional VaR-model or according to a sensitivity-based approach. Mathematically, the only fundamental change is from the IMCC calculation. Therefore, more precisely, our allocation methods in this chapter refer to the IMCC allocation. In this section, we review [12, Sections C.2, C.7, C.9] and introduce corresponding mathematical notations for major concepts. Those notations later will be used in Section 7.3.

7.2.1 Risk Factor and Liquidity Horizon Bucketing

According to the FRTB IMA, the PnL of a risk position is attributed to risk factors of five different categories

$$\{\mathrm{RF}_i : 1 \leq i \leq 5\} := \{\mathrm{CM}, \mathrm{CR}, \mathrm{EQ}, \mathrm{FX}, \mathrm{IR}\}.$$

Further, within each RF category, the risk factor is assigned with a liquidity horizon with lengths (in terms of days)

$$\{\mathrm{LH}_j : 1 \leq j \leq 5\} := \{10, 20, 40, 60, 120\}. \tag{7.1}$$

For more details of definitions on each RF_i and LH_j, one can refer to [12, Paragraphs 185, 181 (k), 188].

For the convenience of mathematical derivations, throughout this chapter, we refer the

negative value of the PnL to the *loss* of a risk position; i.e., recall (2.42), the loss of position n is given by $-X_n(T)$.

Consider a portfolio with $N \in \mathbb{N}$ risk positions. For each risk position n, $1 \leq n \leq N$, its loss is further classified into RF_i and LH_j bucket. Denote the loss[3] of position n in RF_i-and-LH_j-bucket by

$$\tilde{X}_n(i,j),\ 1 \leq n \leq N,\ 1 \leq i,j \leq 5.$$

Then $\sum_{i,j} \tilde{X}_n(i,j)$ is the loss from the original risk position n. For each position n, there are in total 5×5 RF and LH buckets. By considering each bucket, we write the loss of each position as a 5×5 matrix, and denote it by

$$\tilde{X}_n := \{\tilde{X}_n(i,j)\}_{1 \leq i,j \leq 5},\ 1 \leq n \leq N.$$

In order to align with the ES definition in [12, Paragraph 181 (c)], now we define the *liquidity-horizon-adjusted* loss as

$$X_n(i,j) := \sqrt{\frac{\mathrm{LH}_j - \mathrm{LH}_{j-1}}{10}} \sum_{k=j}^{5} \tilde{X}_n(i,k),\ 1 \leq n \leq N,\ 1 \leq i,j \leq 5, \tag{7.2}$$

where $\mathrm{LH}_0 = 0$. By our definition, for a fixed n and i, $X_n(i,j)$ is the the sum of scaled losses with liquidity horizons at least as long as LH_j, and the scaling factors are the square-roots of the differences between two LHs (adjusted by 10 days).

Similarly, we record the liquidity-horizon-adjusted loss of risk position n by a 5×5 matrix

$$X_n := \{X_n(i,j)\}_{1 \leq i,j \leq 5},\ 1 \leq n \leq N.$$

And we refer to the matrix X_n as the *risk-profile of the position* n. Then consider a component-wise sum across $1 \leq i,j \leq 5$ on $1 \leq n \leq N$, we denote the *risk-profile of the portfolio* by

$$X := \sum_n X_n,\ 1 \leq n \leq N, \tag{7.3}$$

where note that, $X = \{X(i,j)\}_{1 \leq i,j \leq 5}$ is also a 5×5 matrix.

Based on our notations above, we follow [12, Paragraph 181 (c)] and define the *FRTB-ES*

[3] According to FRTB IMA, the sample loss is defined by 10-day observations.

of RF_i as

$$\mathrm{ES}(X(i)) := \sqrt{\sum_{j=1}^{5} \mathrm{ES}(X(i,j))^2}, \ 1 \leq i \leq 5, \tag{7.4}$$

where each $\mathrm{ES}(X(i,j))$ is the regular expected shortfall (see Example 2.4.3) of $X(i,j)$ (the (i,j)-th element in the matrix X) calculated at the 97.5% quantile.

Remark. It is not explicitly required in [12, Paragraph 181] to ceiling each $\mathrm{ES}(i,j)$ at zero. This means that profit in $X(i,j)$ (i.e., negative $X(i,j)$) would lead to increase in the risk measure $\mathrm{ES}(X(i))$. To avoid this counter intuitive behavior, we suggest to ceiling each $\mathrm{ES}(X(i,j))$ at zero, and introduce

$$\mathrm{ES}^+(X(i)) := \sqrt{\sum_{j=1}^{5} \mathrm{ES}^+(X(i,j))^2}, \tag{7.5}$$

where $\mathrm{ES}^+(X(i,j)) = \max\{\mathrm{ES}(X(i,j)), 0\}$. This modification introduces better properties to the FRTB-ES (see Section 7.2.3 later), but still retains its positive homogeneity property. Hence the allocation methods that we introduce later can be applied to both $\mathrm{ES}(X(i))$ and $\mathrm{ES}^+(X(i))$.

7.2.2 Stress Period Scaling and IMCC

In [12, Paragraph 181 (d)], FRTB also requires banks to calibrate their risk models to a stress period. For each RF_i, the $\mathrm{ES}(X(i))$ in (7.4) should be calculated under three different scenarios:

- the *current* (most recent) 12-month observation period with a *full set* of risk factors which are relevant to all modellable risk positions; we denote the corresponding FRTB-ES as $\mathrm{ES}^{\mathrm{F,C}}(X(i))$
- banks should identify a *reduced set* of risk factors, and calculate its associated $\mathrm{ES}(X(i))$ over the same *current* period; we denote such a FRTB-ES by $\mathrm{ES}^{\mathrm{R,C}}(X(i))$; besides, it is required that the reduced set of risk factors should be large enough so that $\mathrm{ES}^{\mathrm{R,C}}(X(i)) \geq 75\%$ of $\mathrm{ES}^{\mathrm{F,C}}(X(i))$
- subsequently, banks also need to identify a 12-month *stress period* in which the portfolio experiences the largest loss, and then calculate $\mathrm{ES}(X(i))$ with the *reduced set* of risk factors based on the stress scenarios; we denote this risk measure as $\mathrm{ES}^{\mathrm{R,S}}(X(i))$

Then follow [12, Paragraph 181 (d)], we introduce the following *expected-shortfall-capital-charge* for RF_i:

$$\mathrm{IMCC}(X(i)) := \frac{\mathrm{ES}^{\mathrm{R,S}}(X(i))}{\mathrm{ES}^{\mathrm{R,C}}(X(i))}\mathrm{ES}^{\mathrm{F,C}}(X(i)), \quad 1 \leq i \leq 5. \tag{7.6}$$

Before we define the final IMCC of the portfolio X, there is one last concept to be considered: the *constrained* and the *unconstrained* portfolios. According to [12, Paragraph 188], banks need to calculate $IMCC(X(i))$ for $1 \leq i \leq 5$, and these are referred to as the expected-shortfall-capital-charge for the constrained portfolios. On the other hand, we extend the risk-profile for each position by adding another row:

$$X_n(6, j) := \sum_{i=1}^{5} X_n(i, j), \quad 1 \leq j \leq 5,$$

which records the loss aggregated across all RFs but in the same LH_j. We denote by $X_n(6, \cdot)$ the *unconstrained risk-profile* of the risk position n, and correspondingly extend the risk-profile of the portfolio by adding this row. Then $IMCC(X(6))$ can be calculated via (7.6), and it is referred to as the expected-shortfall-capital-charge for the unconstrained portfolio.

Now follow [12, Paragraph 189], the IMCC of modellable risk factors under the FRTB IMA is defined by:

Definition 7.2.1 (Internal Model Capital Charge for Modellable Risk Factors (IMCC))**.** The aggregated capital charge for modellable risk factors is a weighted sum of the constrained and unconstrained expected-shortfall-capital-charges:

$$\mathrm{IMCC}(X) := \rho\,\mathrm{IMCC}(X(6)) + (1-\rho)\sum_{i=1}^{5}\mathrm{IMCC}(X(i)), \tag{7.7}$$

where the relative weight ρ is set to be 0.5.

Remark. From the massive discussions above (starting from Section 7.2.1 up until Equation (7.7)), we can see that the complexity of calculating the IMCC arises from both the conceptual and the technical aspects. In general, banks first need to follow (7.2) and organise risk profiles into 3 different sets (cf. Section 7.2.2); then within each set, the risk profiles should be further classified into 6 different RFs (constrained and unconstrained) and 5 different LHs. Under each of these classifications, the 97.5% ES is calculated. In total, banks therefore need to

compute 3 (sets) $\times$ 6 (RFs) $\times$ 5 (LHs) = 90 (ESs). And this is only the first step; after which, banks should then follow (7.4), (7.6), and (7.7) to aggregate those 90 ESs gradually to acquire the final IMCC.

7.2.3 Property of IMCC

Lemma 7.2.2 (Homogeneity and Sub-additivity)**.** *For any constant $a \geq 0$ and risk profiles X and Y, the following statements hold:*

(i) (Positive homogeneity) IMCC(aX) = a IMCC(X).

(ii) (Sub-additivity of FRTB-ES) For $i = 1, \ldots, 6$, if $ES((X+Y)(i,j)) \geq 0$ for any j, then

$$ES((X+Y)(i)) \leq ES(X(i)) + ES(Y(i)). \tag{7.8}$$

(iii) (Sub-additivity of expected-shortfall-capital-charge) For any $i = 1, \ldots, 6$, if

$$\frac{ES^{R,S}((X+Y)(i))}{ES^{R,C}((X+Y)(i))} \leq \min\left\{\frac{ES^{R,S}(X(i))}{ES^{R,C}(X(i))}, \frac{ES^{R,S}(Y(i))}{ES^{R,C}(Y(i))}\right\}, \tag{7.9}$$

and $ES^{F,C}((X+Y)(i,j)) \geq 0$ for any j, then

$$IMCC((X+Y)(i)) \leq IMCC(X(i)) + IMCC(Y(i)). \tag{7.10}$$

The previous lemma shows the sub-additivity properties for the FRTB-ES and the expected-shortfall-capital-charge do not hold naturally. In fact, without conditions $\mathrm{ES}((X+Y)(i,j)) \geq 0$ and (7.9), the following examples show that the sub-additivity may fail.

Example 7.2.3 (Counter Example of Item (ii))**.** For fixed RF_i and LH_j, consider two risk positions. Assume that $X(i,j)$ has a Bernoulli distribution with $\mathbb{P}(X(i,j) = -1) = \mathbb{P}(X(i,j) = 0) = 0.5$, and let $Y(i,j) = -1 - X(i,j)$. Hence $\mathbb{P}((X+Y)(i,j) = -1) = 1$. And by definition,

$$\mathrm{ES}((X+Y)(i)) = \left|\mathrm{ES}((X+Y)(i,j))\right| = |-1| = 1 > \mathrm{ES}(X(i)) + \mathrm{ES}(Y(i)) = 0 + 0.$$

However, if the expected shortfall is ceiling at zero as in our previous remark, then the sub-additivity for FRTB-ES and IMCC holds without the positivity assumption $\mathrm{ES}((X+$

$Y)(i,j)) \geq 0$ for all j.

Example 7.2.4 (Counter Example of Item (iii))**.** Fix RF_i and LH_j, assume that $X(i,j)$ and $Y(i,j)$ are *i.i.d.* standard normal. Moreover, for their reduced sets, we assume

$$\mathrm{ES}^{\mathrm{R,C}}(X(i)) = 0.75\mathrm{ES}^{\mathrm{F,C}}(X(i)),\ \mathrm{ES}^{\mathrm{R,C}}(Y(i)) = \mathrm{ES}^{\mathrm{F,C}}(Y(i)).$$

Under stress scenarios, we consider that $X(i,j)$ and $Y(i,j)$ have independent normal distributions, but their standard deviations are scaled up by 1.2 and 9 times, respectively, of their standard deviations under the current period. Then

$$\min\left\{\frac{\mathrm{ES}^{\mathrm{R,S}}(X(i))}{\mathrm{ES}^{\mathrm{R,C}}(X(i))}, \frac{\mathrm{ES}^{\mathrm{R,S}}(Y(i))}{\mathrm{ES}^{\mathrm{R,C}}(Y(i))}\right\} = \min\Big\{1.2, 9\Big\} = 1.2.$$

Now consider the aggregated portfolio, the standard deviation of $X(i,j)+Y(i,j)$ in the full current set is $\sqrt{2}$. And for the reduced current set, $StdDev(X(i,j)+Y(i,j)) = \sqrt{0.75^2+1} = 1.25$. Under the stress scenario, the standard deviation of the portfolio in the reduced set becomes $\sqrt{(0.75\times 1.2)^2+9^2} \approx 9.04$. Hence

$$\frac{\mathrm{ES}^{\mathrm{R,S}}((X+Y)(i))}{\mathrm{ES}^{\mathrm{R,C}}((X+Y)(i))} = \frac{9.04}{1.25} = 7.23 > 1.2.$$

Therefore, the condition (7.9) is violated. Now we have

$$\begin{aligned}\mathrm{IMCC}((X+Y)(i)) &= \frac{\mathrm{ES}^{\mathrm{R,S}}((X+Y)(i))}{\mathrm{ES}^{\mathrm{R,C}}((X+Y)(i))}\mathrm{ES}^{\mathrm{F,C}}((X+Y)(i)) \\ &= 7.23\times\sqrt{2}ES(N(0,1)).\end{aligned}$$

On the other hand, compare the number above with the sum of two expected-shortfall-capital-charges:

$$\begin{aligned}\mathrm{IMCC}(X(i)) + \mathrm{IMCC}(Y(i)) &= \frac{\mathrm{ES}^{\mathrm{R,S}}(X(i))}{\mathrm{ES}^{\mathrm{R,C}}(X(i))}\mathrm{ES}^{\mathrm{F,C}}(X(i)) + \frac{\mathrm{ES}^{\mathrm{R,S}}(Y(i))}{\mathrm{ES}^{\mathrm{R,C}}(Y(i))}\mathrm{ES}^{\mathrm{F,C}}(Y(i)) \\ &= (1.2+9)ES(N(0,1)),\end{aligned}$$

we find

$$7.23\times\sqrt{2} = 10.22 > 10.20.$$

Hence (7.10) fails.

Remark. Combine the discussions above with Definition 2.4.2 on p. 21, we show that the IMCC is not a coherent risk measure[4]. Note that, in practice, any break of the coherent properties could potentially lead to risk capital arbitrage; but this is not our purpose of demonstrating it here.

7.3 Capital Allocation

We introduce in this section two methods of allocating the IMCC (see Definition 7.2.1). All allocations have two steps. Consider a risk-profile X of a portfolio (including the 6^{th} row) and a risk measure ρ. In the first step, we allocate the capital to the liquidity-horizon-adjusted loss, $\{X_n(i,j)\}_{1\leq n\leq N, 1\leq i\leq 6, 1\leq j\leq 5}$. We denote the first step allocation by

$$\rho(X_n(i,j)|X).$$

On the other hand, recall from (7.2) that $X_n(i,j)$ is aggregated from $\tilde{X}_n(i,k)$ with $k \geq j$. Therefore, in the second step, we further allocate $\rho(X_n(i,j)|X)$ to $\tilde{X}_n(i,k)$. Consider a further allocation on $X_n(i,j)$:

$$\rho(\tilde{X}_n(i,k)|X_n(i,j)), \quad k \geq j.$$

Then in order to obtain the allocation of $\tilde{X}_n(i,k)$ from X, we sum up all their contributions from $X_n(i,j)$ with $j \leq k$:

$$\rho(\tilde{X}_n(i,k)|X) = \sum_{j=1}^{k} \rho(X_n(i,k)|X_n(i,j)).$$

The second step is independent to the choices of allocation methods, so we focus on the first step allocation in what follows.

[4]Even though we did not mention, it is very easy for the reader to find counterexamples to disprove the monotonicity and the translation invariance properties of the IMCC.

7.3.1 Euler Allocation

The Euler allocation has been studied extensively; see [38, 78, 122, 123], and many others. We introduce in this subsection a computationally efficient scheme for the Euler allocation of the IMCC.

For each RF_i, we first allocate $\mathrm{ES}(X(i))$ in (7.4) to $X_n(i,j)$ with $1 \le j \le 5$. To this end, we further introduce some notations. Let $v = (v_n)_{1\le n\le N}$ be a sequence of real numbers. Given a collection of risk-profiles $\{X_n\}_{1\le n\le N}$, we denote by

$$X^{v,j}(i) := \sum_n X_n^{v_n,j}(i), \tag{7.11}$$

where the sum is computed component-wise and

$$X_n^{v_n,j}(i) := \big(X_n(i,1), \cdots, X_n(i,j-1), v_n X_n(i,j), X_n(i,j+1), \cdots, X_n(i,5)\big).$$

We define the allocation to each $X_n(i,j)$ as follows.

Definition 7.3.1 (Euler Allocation of FRTB-ES)**.** For $1 \le n \le N, 1 \le i \le 6, 1 \le j \le 5$, let

$$\mathrm{ES}(X_n(i,j) \,|\, X(i)) := \partial_{v_n} \mathrm{ES}(X^{v,j}(i))\Big|_{v=1}, \tag{7.12}$$

where $\mathrm{ES}(X^{v,j}(i))$ is the FRTB-ES of the row $X^{v,j}(i)$, and $v = 1$ represents $v_n = 1$ for all n. We call $\mathrm{ES}(X_n(i,j) \,|\, X(i))$ the Euler allocation of the FRTB-ES.

The chain rule in differentiation yields the following representation.

Lemma 7.3.2 (Representation for Euler Allocation)**.** *For $1 \le n \le N, 1 \le i \le 6, 1 \le j \le 5$,*

$$ES(X_n(i,j) \,|\, X(i)) = \frac{ES(X(i,j))}{ES(X(i))}\, \partial_{v_n} ES\big(X^v(i,j)\big)\Big|_{v=1}, \tag{7.13}$$

where $X^v(i,j) = \sum_n v_n X_n(i,j)$.

Remark. Note that, $\partial_{v_n}\mathrm{ES}(X^v(i,j))\big|_{v=1}$ on the right-hand side of (7.13) is the standard Euler allocation of $\mathrm{ES}(X(i,j))$. Therefore, the Euler allocation under FRTB-ES is the weighted version of the standard Euler allocation. The scaling factor $\mathrm{ES}(X(i,j))/\mathrm{ES}(X(i))$ reflects the ratio between the standalone ES of $X(i,j)$ and the FRTB-ES of $X(i)$. This scaling factor is applied to all risk positions with the same liquidity horizon.

When the distribution of $X(i,j)$ satisfies certain regularity conditions (cf. [122, Assumption (S)]), the standard Euler allocation can be written as a conditional expectation (cf. [122]):

$$\partial_{v_n}\mathrm{ES}\big(X^v(i,j)\big)\Big|_{v=1} = \mathbb{E}\big[X_n(i,j)\,|\,X(i,j)\geq \mathrm{VaR}(X(i,j))\big] =: \mathrm{SE}\big(X_n(i,j)\,|\,X(i,j)\big), \quad (7.14)$$

where $\mathrm{VaR}(X(i,j))$ is the Value-at-Risk of $X(i,j)$ calculated at the 97.5% quantile. The conditional expectation above can be calculated by the *scenario-extraction* method and hence is denoted by $\mathrm{SE}\big(X_n(i,j)\,|\,X(i,j)\big)$.

After applying the Euler allocation to the FRTB-ES under the full set of risk factors, and by treating the scaling factor as a constant, we have the following allocation to the IMCC.

Definition 7.3.3 (Euler Allocation of IMCC)**.** For $1\leq n\leq N, 1\leq i\leq 6, 1\leq j\leq 5$, let

$$\mathrm{IMCC}^E(X_n(i,j)\,|\,X(i)) := 0.5\,\frac{\mathrm{ES}^{\mathrm{R,S}}(X(i))}{\mathrm{ES}^{\mathrm{R,C}}(X(i))}\,\mathrm{ES}^{\mathrm{F,C}}\big(X_n(i,j)\,|\,X(i)\big). \quad (7.15)$$

We call $\mathrm{IMCC}^E(X_n(i,j)\,|\,X(i))$ the Euler allocation of the expected-shortfall-capital-charge. For the risk-profile X_n, we define its Euler allocation of the IMCC as

$$\mathrm{IMCC}^E(X_n\,|\,X) = \sum_{i,j}\mathrm{IMCC}^E\big(X_n(i,j)\,|\,X(i)\big).$$

Remark. In the definition above, $\mathrm{IMCC}^E(X_n\,|\,X)$ should be differentiated with X_n, where the former one is a real number and which refers to the capital allocation to risk position n in the sense of liquidity-horizon-adjusted loss, while the latter one refers to a 6×5 matrix.

Proposition 7.3.4 (Full Allocation of the Euler Scheme)**.** *The Euler allocation of IMCC is a full allocation, i.e.,*

$$\sum_n IMCC^E(X_n\,|\,X) = \sum_{n,i,j} IMCC^E\big(X_n(i,j)\,|\,X(i)\big) = IMCC(X).$$

Remark. If the expected shortfall of $X^v(i,j)$ is ceiling at zero, then (7.13) can be replaced by

$$\mathrm{ES}^+(X_n(i,j)\,|\,X(i)) = \begin{cases} \frac{\mathrm{ES}^+(X(i,j))}{\mathrm{ES}^+(X(i))}\,\mathrm{SE}\big(X_n(i,j)\,|\,X(i,j)\big) & \text{if } \mathrm{ES}(X(i,j)) > 0 \\ 0 & \text{otherwise} \end{cases}. \quad (7.16)$$

The resulting Euler allocation of IMCC is still a full allocation, since ES^+ is still homogeneous of degree 1.

When a portfolio contains hedging positions, the Euler allocation on regular ES could produce negative allocations. However, since the FRTB-ES discourages hedging across different RF-and-LH-buckets, negative allocations could be reduced or disappeared under FRTB. The following example illustrates this point.

Example 7.3.5 (Mitigated Negative Allocations in the FRTB Euler Scheme)**.** Consider a portfolio with two risk positions whose risk-profiles are denoted by Y and Z respectively. We assume that Y concentrates on RF_i and LH_j, and Z concentrates on RF_k and LH_j, with $1 \le i \ne k \le 5$. Therefore, $Y = Y(i,j)$ and $Z = Z(k,j)$. We assume that $Y = -Z$ and both of them follow standard normal distributions. Then the net loss of the portfolio $X = Y + Z = 0$, and the standard Euler allocation of regular ES would be negative for either Y or Z, say $\mathrm{SE}(Y|X) < 0$.

However, under FRTB framework, $X(i) = Y(i,j) = Y$. Then

$$\mathrm{IMCC}^E\big(Y(i,j)\,|\,X(i)\big) = 0.5\frac{\mathrm{ES}^{\mathrm{R,S}}(Y)}{\mathrm{ES}^{\mathrm{R,C}}(Y)}\mathrm{ES}^{\mathrm{F,C}}(Y|X(i)) = 0.5\frac{\mathrm{ES}^{\mathrm{R,S}}(Y)}{\mathrm{ES}^{\mathrm{R,C}}(Y)}\mathrm{ES}^{\mathrm{F,C}}(Y) > 0.$$

Therefore, this positive allocation could compensate the negative allocation from

$$\mathrm{IMCC}^E\big(Y(6,j)\,|\,X(6)\big).$$

In the end, $\mathrm{IMCC}^E(Y|X)$ could be less negative, or even positive, comparing to $\mathrm{SE}(Y|X)$.

7.3.2 Constrained Aumann-Shapley Allocation

The Shapley and Aumann-Shapley allocations were introduced in [38], where the results of [112] and [5] on coalitional games were applied to capital allocation problems. The concepts in those two allocations were combined in [76] to introduce the constrained Aumann-Shapley

allocation, where permutations of different risk positions are restricted to each business unit. In the FRTB IMA framework, the risk factor bucketing rule produces a natural constraint on risk profile organisations. Therefore, motivated by [76], we constrain the Shapley-type permutations by different LHs.

We introduce the following *full liquidity horizon permutation matrix*:

$$\mathcal{L} := \begin{bmatrix} 10 & 20 & 40 & 60 & 120 \\ 10 & 20 & 40 & 120 & 60 \\ \vdots & \vdots & \ddots & \vdots & \vdots \\ 120 & 60 & 40 & 20 & 10 \end{bmatrix}_{5!\times 5}.$$

Each row of $\mathcal{L}$ records a permutation of liquidity horizons $\{10, 20, 40, 60, 120\}$. There are $5! = 120$ permutations in total. For a given row r and a liquidity horizon LH_j, we denote by $\mathcal{L}^{-1}(r, j)$ the column of $\mathcal{L}$ in which LH_j locates. For example, $\mathcal{L}^{-1}(2, 5) = 4$, or equivalently, $\mathcal{L}(2, 4) = \mathrm{LH}_5 = 120$.

Given a risk-profile X_n, a risk factor category RF_i, a liquidity horizon LH_j, and a permutation of liquidity horizons (say r-th row in $\mathcal{L}$). We want to first allocate $\mathrm{ES}(X(i))$ to $X_n(i, j)$. We call this allocation the CAS allocation of the FRTB-ES, and denote it by

$$\mathrm{CAS}(r, X_n(i, j)).$$

To introduce the value of $\mathrm{CAS}(r, X_n(i, j))$, let $v = (v_n)_{1\le n\le N}$ be a sequence of real numbers, $q \in [0, 1]$, and

$$X^{v,r,j}(i) = \sum_n X_n^{v,r,j}(i), \tag{7.17}$$

where $X_n^{v,r,j}(i)$ is a row with entries $X_n(i, \ell)$ at the ℓ-th column if $\mathcal{L}^{-1}(i, \ell) < \mathcal{L}^{-1}(i, j)$ (i.e., LH_ℓ appears before LH_j in the permutation r); the entry $v_n X_n(i, j)$ at the j-th column; and zero in all other columns. Take the second row in matrix $\mathcal{L}$ as an example, for $j = 5$, we have

$$X_n^{v,2,5}(i) = \big(X_n(i, 1), X_n(i, 2), X_n(i, 3), 0, v_n X_n(i, 5)\big).$$

Then the CAS value of the FRTB-ES is given by

$$\mathrm{CAS}(r, X_n(i,j)) := \int_0^1 \partial_{v_n} \mathrm{ES}(X^{v,r,j}(i))\Big|_{v=q} dq,$$

where $v = q$ means $v_n = q$ for all n. Intuitively, $\partial_{v_n} \mathrm{ES}(X^{v,r,j}(i))|_{v=q}$ is the marginal contribution, in the direction of $X_n(i,j)$, of the FRTB-ES given the portfolio's risk-profile consisting of $qX(i,j)$ and all $X(i,\ell)$, if LH_ℓ appears before LH_j in the permutation r.

Lemma 7.3.6 (CAS Value under FRTB-ES)**.** *For $1 \le n \le N$, $1 \le i \le 6$, $1 \le j \le 5$, and $1 \le r \le 5!$,*

$$CAS(r, X_n(i,j)) = \eta(r,i,j)\, \partial_{v_n} ES\big(X^v(i,j)\big)\Big|_{v=1}, \tag{7.18}$$

where

$$\eta(r,i,j) = \frac{\sqrt{\sum_{1\le s\le \mathcal{L}^{-1}(r,j)} ES\big(X(i,\mathcal{L}(r,s))\big)^2} - \sqrt{\sum_{1\le s< \mathcal{L}^{-1}(r,j)} ES\big(X(i,\mathcal{L}(r,s))\big)^2}}{ES\big(X(i,j)\big)}. \tag{7.19}$$

When the distribution of $X(i,j)$ satisfies [122, Assumption (S)], the derivative on the right-hand side of (7.18) *can be replaced by $SE\big(X_n(i,j)\,|\,X(i,j)\big)$.*

Remark. Similar to the Euler allocation under the FRTB-ES, the CAS allocation is also a weighted version of the standard Euler allocation. The scaling factor $\eta(r,i,j)$ is the ratio between the $X(i,j)$ induced increment of FRTB-ES in the permutation r and the standalone ES of $X(i,j)$.

After averaging over all permutations, we introduce the final version of the CAS allocation to the IMCC.

Definition 7.3.7 (CAS Allocation of IMCC)**.** For $1 \le n \le N$, $1 \le i \le 6$, $1 \le j \le 5$,

$$\mathrm{IMCC}^C(X_n(i,j)\,|\,X(i)) := 0.5\,\frac{\mathrm{ES}^{\mathrm{R,S}}(X(i))}{\mathrm{ES}^{\mathrm{R,C}}(X(i))}\,\frac{1}{5!}\sum_{r=1}^{5!}\mathrm{CAS}^{\mathrm{F,C}}(r, X_n(i,j)),$$

where $\mathrm{CAS}^{\mathrm{F,C}}$ is the CAS value of FRTB-$ES^{\mathrm{F,C}}$. We call $\mathrm{IMCC}^C(X_n(i,j)\,|\,X(i))$ the CAS allocation of the IMCC.

Proposition 7.3.8 (Full Allocation of the CAS Scheme)**.** *The CAS allocation of IMCC is a full allocation.*

If the ES for $X^v(i,j)$ is ceiling at zero, then the CAS allocation can be adjusted similarly as in (7.16). The adjusted CAS allocation is still a full allocation.

Remark. An important concept for capital allocation is the *associativity* property (see Definition 2.4.4). Consider a subportfolio Y in X, where Y is aggregated from risk-profiles $\{Y_m\}_{1\leq m\leq M}$. We want to know whether the allocation to the portfolio Y equals to the sum of allocations to all $\{Y_m\}$, i.e. whether $\rho(Y|X) = \sum_m \rho(Y_m|X)$ is true. The answer to this question is positive for both Euler and CAS allocations. This is due to the fact that both of them are scaled versions of the Euler allocation for the regular ES, which is associative itself.

7.3.3 The Second Step Allocation

After the first step of both allocation methods, capital is allocated to each liquidity-horizon-adjusted loss $X_n(i,j)$. For the unconstrained part $i=6$, we consider $X_n(6,j) = \sum_{i=1}^{5} X_n(i,j)$ and use the standard Euler allocation to find $\mathrm{IMCC}(X_n(i,j)\,|\,X(6))$.

Now for each $1 \leq i \leq 6$, since $X_n(i,j)$ is aggregated from $\tilde{X}_n(i,k)$ with $k \geq j$ (see (7.2)), it therefore becomes natural to extract the capital associated to each $\tilde{X}(i,k)$ from the capital allocated to $X(i,j)$. Recall from (7.2). We can treat $X_n(i,j)$ as a portfolio of $\sqrt{\frac{\mathrm{LH}_j-\mathrm{LH}_{j-1}}{10}}\tilde{X}_n(i,k)$ with $k \geq j$. Hence we use the Euler method to allocate capital from $X_n(i,j)$ further down to each $\sqrt{\frac{\mathrm{LH}_j-\mathrm{LH}_{j-1}}{10}}\tilde{X}_n(i,k)$. We denote the resulting allocations by

$$\mathrm{IMCC}\left(\sqrt{\frac{\mathrm{LH}_j-\mathrm{LH}_{j-1}}{10}}\tilde{X}_n(i,k)\middle|X_n(i,j)\right), \quad k \geq j.$$

Now use the associativity property in Definition 2.4.4, we can sum all capital from $X_n(i,j)$ with $j \leq k$ to get the contribution of $\tilde{X}_n(i,k)$:

$$\mathrm{IMCC}\left(\tilde{X}_n(i,k)|X(i)\right) = \sum_{j\leq k}\mathrm{IMCC}\left(\sqrt{\frac{\mathrm{LH}_j-\mathrm{LH}_{j-1}}{10}}\tilde{X}_n(i,k)\middle|X_n(i,j)\right). \tag{7.20}$$

In the end, combine the constrained and the unconstrained allocations, the allocation for the natural position $\tilde{X}_n(i,j)$, with $1 \leq n \leq N$, $1 \leq i \leq 5$ and $1 \leq j \leq 5$, is given by

$$\mathrm{IMCC}^{Total}\left(\tilde{X}_n(i,k)|X(i)\right) := \mathrm{IMCC}\left(\tilde{X}_n(i,k)|X(i)\right) + \mathrm{IMCC}\left(\tilde{X}_n(i,k)|X(6)\right). \tag{7.21}$$

7.3.4 Extension

In the previous two subsections, the Euler and the CAS allocations of the IMCC are applied to FRTB-ES for the full set under regular scenarios; and the stress scaling factor $\mathrm{ES}^{\mathrm{R,S}}(X(i))/\mathrm{ES}^{\mathrm{R,C}}(X(i))$ is treated as a constant for each RF_i. In this subsection, we consider the impact of $X_n(i,j)$ from the stress scaling factors and introduce the associated modifications to the Euler and the CAS allocations. The second step allocation is the same as in Section 7.3.3.

Definition 7.3.9 (Euler Allocation of IMCC with Stress Scaling Adjustment)**.** For $1 \le n \le N$, $1 \le i \le 6$, $1 \le j \le 5$, we define

$$\mathrm{IMCC}^{\mathrm{E,S}}\big(X_n(i,j)\,|\,X(i)\big) := 0.5 \cdot \partial_{v_n}\Big[\frac{\mathrm{ES}^{\mathrm{R,S}}\big(X^{v,j}(i)\big)}{\mathrm{ES}^{\mathrm{R,C}}\big(X^{v,j}(i)\big)}\mathrm{ES}^{\mathrm{F,C}}\big(X^{v,j}(i)\big)\Big]\Big|_{v=1}.$$

Taking differentiations to each FRTB-ESs, we obtain

Proposition 7.3.10 (Euler Allocation of IMCC with Stress Scaling Adjustment, Continued)**.** *For* $1 \le n \le N$, $1 \le i \le 6$, $1 \le j \le 5$,

$$\begin{aligned} IMCC^{E,S}\big(X_n(i,j)\,|\,X(i)\big) = 0.5\Big[&\frac{ES^{R,S}(X(i))}{ES^{R,C}(X(i))}\,ES^{F,C}\big(X_n(i,j)\,|\,X(i)\big) \\ &+\frac{ES^{F,C}(X(i))}{ES^{R,C}(X(i))}\,ES^{R,S}\big(X_n(i,j)\,|\,X(i)\big) \\ &-\frac{ES^{R,S}(X(i))ES^{F,C}(X(i))}{ES^{R,C}(X(i))^2}\,ES^{R,C}\big(X_n(i,j)\,|\,X(i)\big)\Big]. \end{aligned} \tag{7.22}$$

The previous expression for $\mathrm{IMCC}^{\mathrm{E,S}}$ motivates us to define the following CAS allocation with the scaling adjustment.

Definition 7.3.11 (CAS Allocation of IMCC with Stress Scaling Adjustment)**.** For $1 \le n \le N$, $1 \le i \le 6$, $1 \le j \le 5$, we define

$$\begin{aligned} \mathrm{IMCC}^{\mathrm{C,S}}\big(X_n(i,j)\,|\,X(i)\big) := \frac{0.5}{5!}\sum_{r=1}^{5!}\Big[&\frac{\mathrm{ES}^{\mathrm{R,S}}(X(i))}{\mathrm{ES}^{\mathrm{R,C}}(X(i))}\,\mathrm{CAS}^{\mathrm{F,C}}\big(r, X_n(i,j)\big) \\ &+\frac{\mathrm{ES}^{\mathrm{F,C}}(X(i))}{\mathrm{ES}^{\mathrm{R,C}}(X(i))}\,\mathrm{CAS}^{\mathrm{R,S}}\big(r, X_n(i,j)\big) \\ &-\frac{\mathrm{ES}^{\mathrm{R,S}}(X(i))\mathrm{ES}^{\mathrm{F,C}}(X(i))}{\mathrm{ES}^{\mathrm{R,C}}(X(i))^2}\,\mathrm{CAS}^{\mathrm{R,C}}\big(r, X_n(i,j)\big)\Big]. \end{aligned}$$

Proposition 7.3.12 (Full Allocation and Associativity under Stress Scaling Adjustment)**.** *Both Euler and CAS allocations of IMCC with scaling adjustment are full allocations and satisfy the additivity property.*

7.4 Simulation Analysis

7.4.1 Positive Correlation

This simulation exercise illustrates the difference of allocations among different RF-and-LH-buckets. We assume that there is only one risk position, and all $\tilde{X}(i,j)$ have identical normal distributions with zero mean and 30% annual volatility. We consider the following four scenarios of correlation structures:

(i) Independence: all $\tilde{X}(i,j)$ are mutually independent;

(ii) Uniform positive correlation: each pair of $\tilde{X}(i,j)$ and $\tilde{X}(k,l)$ have correlation 0.99;

(iii) Positive correlation among RFs and zero correlation among LHs: $\text{corr}(\tilde{X}(i,j), \tilde{X}(k,j)) = 0.99$ and $\text{corr}(\tilde{X}(i,j), \tilde{X}(i,k)) = 0$ for any $i \neq k$;

(iv) Positive correlation among LHs and zero correlation among RFs: $\text{corr}(\tilde{X}(i,j), \tilde{X}(k,j)) = 0$ and $\text{corr}(\tilde{X}(i,j), \tilde{X}(i,k)) = 0.99$ for any $i \neq k$.

We simulate risk-profiles for 250 days, risk-profiles are independent across different days, and risk-profiles in the same day follow the correlation scenarios above. The stress period scalings are assumed to be 1 for all RFs. First, we report and compare the IMCC and the regular 97.5% ES values in the following table.

Scenario	IMCC	Regular ES
(i) Independent	12.48	3.28
(ii) Uniform Positive Corr	28.57	16.70
(iii) Zero-LH-Corr	18.28	7.81
(iv) Zero-RF-Corr	21.00	7.59

Table 7.1: FRTB IMCC v.s. regular ES

We can see from Table 7.1 that the IMCC values are between 1.7 and 3.8 times of the regular ES. Moreover, strong positive correlations among different liquidity horizons (scenario

(iv)) increase the capital more than the scenario with strong positive correlations among different risk factor categories (scenario (iii)). This reflects the FRTB liquidity horizon bucketing rule.

Figure 7.1 illustrates the Euler allocation of IMCC, the CAS allocation of IMCC, and the Euler allocation of regular ES, respectively. It reports allocations to different $\tilde{X}(i,j)$, after combining the constrained and the unconstrained allocations (see Equation (7.21)).

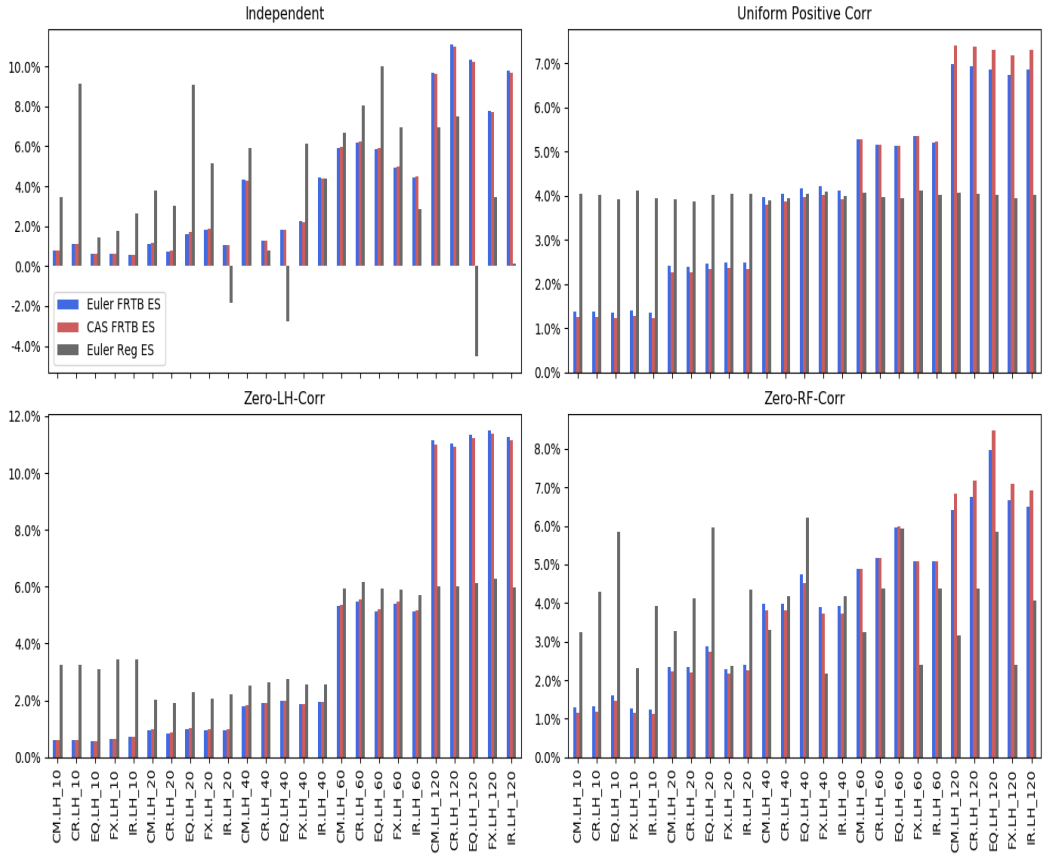

Figure 7.1: Euler allocation of IMCC (Euler FRTB ES), CAS allocation of IMCC (CAS FRTB ES), and Euler allocation of regular ES (Euler Reg ES). Upper-left panel: scenario (i); upper-right panel: scenario (ii); bottom-left panel: scenario (iii); bottom-right panel: scenario (iv). Each panel presents the percentage of allocation to different $\tilde{X}(i,j)$. The total capital charges are reported in Table 7.1

Figure 7.1 shows that both FRTB allocations typically allocate more capital to risk factors with longer liquidity horizons. This feature is due to the facts that 1) longer liquidity horizon has bigger scalings (see Equation (7.2)); and 2) longer liquidity horizon has more allocation contributions from shorter liquidity horizon allocations (see Equation (7.20)). On the other hand, due to allocations from the unconstrained part, when there is no strong

positive correlation among RFs, allocations to each LH vary within the same RF category.

The upper-left panel of Figure 7.1 shows that the Euler allocation for regular ES present large variations and negative allocations, even when there is no negative correlation. These features are due to the instability of the Euler allocation for regular ES or VaR, which has been documented in [130]. The kernel smoothing technique (see [41]) can improve the stability of the Euler allocation. Figure 7.2 presents the allocations when the kernel smoothing technique is applied to each method. Compare Figures 7.1 and 7.2, we find that the kernel smoothing significantly improves the stability of the Euler allocation for the regular ES, but it is less effective on FRTB allocations.

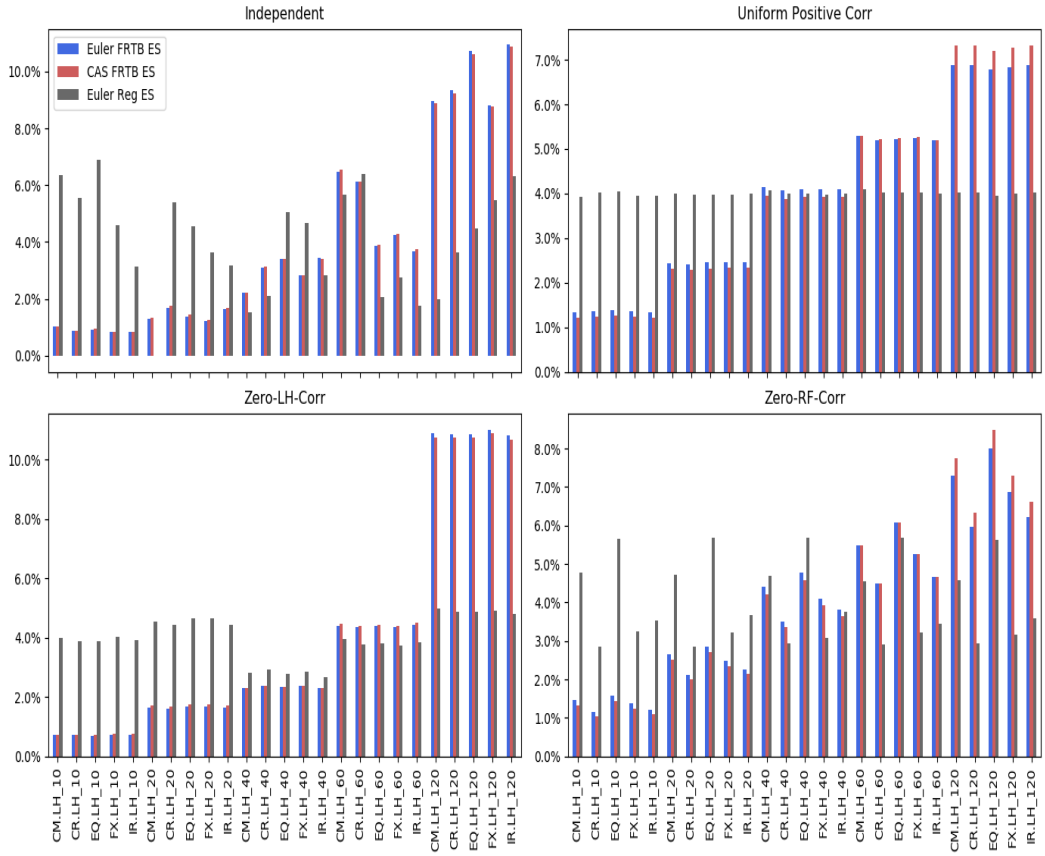

Figure 7.2: Kernel smoothed allocations

7.4.2 Hedging

In the second simulation exercise, we analyse three scenarios of hedging relations: hedging between 2 RFs; hedging between 2 LHs; and hedging between two risk positions within the same bucket. We treat different buckets as different risk positions. In this way, $X_n(i,j) =$

$\sqrt{\frac{LH_j - LH_{j-1}}{10}}\tilde{X}_n(i,j)$, and the correlations between different $\tilde{X}_n(i,j)$ are the same as the correlations between different $X_n(i,j)$. This allows us to focus on the impact of FRTB allocations with hedging positions.

We consider the following three correlation structures:

(i) Strong hedging between EQ and IR: $\text{corr}(\tilde{X}(3,j), \tilde{X}(5,j)) = -0.99$ for any j and zero correlation between all other pairs;

(ii) Strong hedging between LH_1 and LH_2: $\text{corr}(\tilde{X}(i,1), \tilde{X}(i,2)) = -0.99$ for all i and zero correlation between all other pairs;

(iii) Strong hedging between 2 risk positions within the same bucket: $\text{corr}(\tilde{X}_1(i,j), \tilde{X}_2(i,j)) = -0.99$ for all i, j, and zero correlation between all other pairs.

Simulation settings remain the same as in the previous exercise. The IMCC and the regular ES are reported in Table 7.2 below. Because FRTB restricts hedging among different buckets, so the ratios between IMCC and ES in scenario (i) and (ii) are larger than the ratio in scenario (iii), where hedging within the same bucket is not restricted by FRTB.

Scenario	IMCC	Regular ES
(i) RF Hedging	7.90	2.17
(ii) LH Hedging	8.43	2.55
(iii) Position Hedging	0.84	0.33

Table 7.2: FRTB IMCC v.s. Regular ES

Figure 7.3 illustrates allocations of the IMCC and the regular ES. The left and middle panels show that, even though there are negative correlations between different RF or LH buckets, the Euler and CAS allocations of IMCC are still positive. This confirms our analysis in Example 7.3.5.

When hedging appears in the same bucket, the right panel in Figure 7.3 shows that there could be negative allocations for both Euler and CAS allocations of the IMCC. But their magnitudes are smaller than the Euler allocations to the regular ES. Consider the facts that, for the Euler allocation of the regular ES, one scenario extraction is applied to each loss simulation of 250 days; however, in both Euler and CAS allocations of IMCC, one scenario extraction is applied to each bucket, therefore, there are in total $30 = 6 \times 5$ scenario extractions

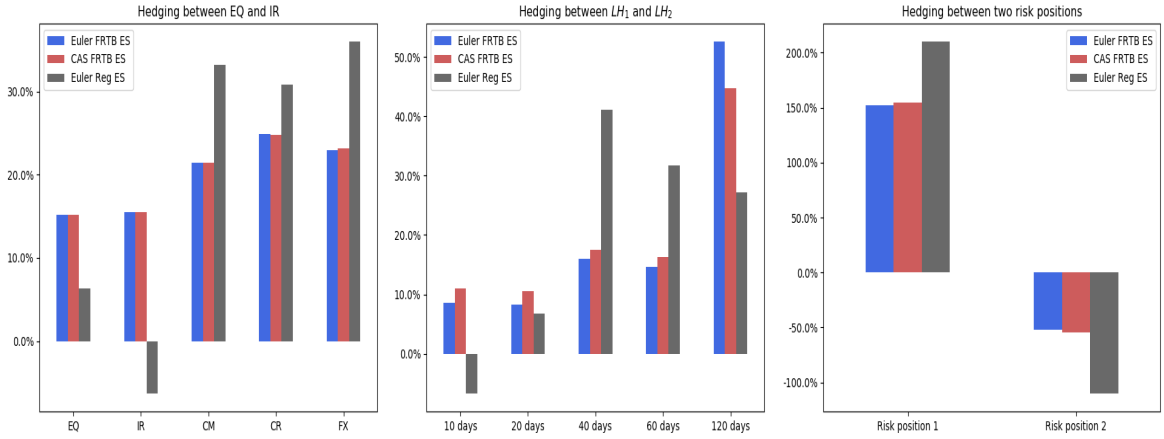

Figure 7.3: Allocations of IMCC and regular ES for portfolios with hedging components. Left panel: hedging structure (i); middle panel: hedging structure (ii); right panel: hedging structure (iii). Each panel presents the percentage of allocation to different $\tilde{X}(i,j)$. The total capital charges are reported in Table 7.2

applied to each loss simulation of 250 days. Since the final allocation of a risk position is a weighted sum of 30 scenario extraction results, hence the FRTB allocations produce more stable results comparing to regular ES allocations.

In order to further analyse negativity and stability of different allocations, we extend the hedging scenario (iii) from 2 risk positions to 20 risk positions. Each pair of risk positions follows the hedging scenario (iii). Figure 7.4 illustrates histograms and kernel densities of different allocations. Even without aggregations among different RF and LH classes, Figure 7.4 shows that the Euler and CAS allocations of IMCC still produce tighter histograms comparing to the Euler allocation of regular ES. Moreover, comparing to the Euler allocation of IMCC, we observe that the CAS allocation produces slightly more stable results with less extreme allocations. This is due to the fact that the CAS allocation is an average of 5! permutations.

7.4.3 Allocation with Scaling Adjustment

In the third simulation exercise, we illustrate the impact of the choice of reduced sets on the IMCC allocations, by taking the scaling adjustment in Section 7.3.4 into account. Consider the situation where the reduced factor set is chosen so that all $X_n(i,j)$ have similar distributions in both the stressed period and the current period, then $\mathrm{ES}^{\mathrm{R,S}}(X(i))$ is similar to $\mathrm{ES}^{\mathrm{R,C}}(X(i))$, and the allocations $\mathrm{ES}^{\mathrm{R,S}}\big(X_n(i,j)\,|\,X(i)\big)$ and $\mathrm{ES}^{\mathrm{R,C}}\big(X_n(i,j)\,|\,X(i)\big)$ are simi-

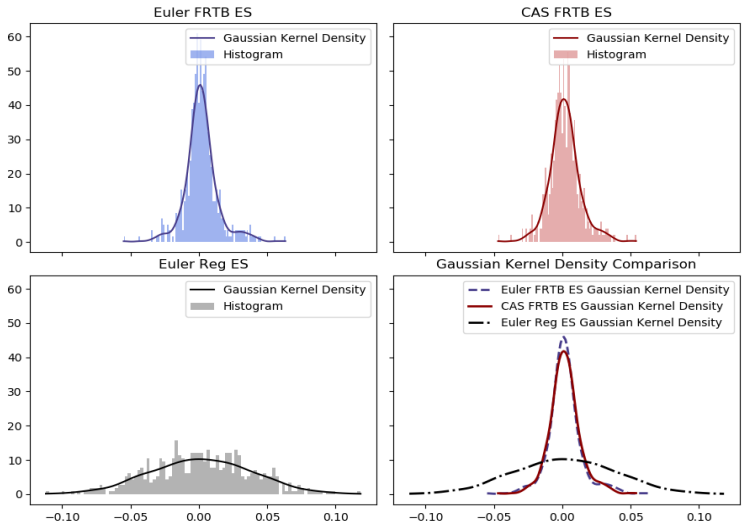

Figure 7.4: Histograms and kernel densities for FRTB allocations and regular ES allocation. Extreme allocations: i) Euler FRTB ES: left end, -5.50%; right end: 6.32%; ii) CAS FRTB ES: left end, -4.69%; right end: 5.39%; iii) Euler Regular ES: left end, -11.19%; right end: 11.83%

lar as well. Therefore, the second and the third terms on the right-hand side of (7.22) are similar, so

$$\mathrm{IMCC}^{\mathrm{E,S}}\big(X_n(i,j)\,|\,X(i)\big) \approx 0.5\frac{\mathrm{ES}^{\mathrm{R,S}}\big(X(i)\big)}{\mathrm{ES}^{\mathrm{R,C}}\big(X(i)\big)}\mathrm{ES}^{\mathrm{F,C}}\big(X_n(i,j)\,|\,X(i)\big). \tag{7.23}$$

This allocation will be significantly different from the case where risk factors have distinct distributions in the stress period and the current period.

We follow the convention of the previous exercise where different buckets are treated as different risk positions. We consider a portfolio with two risk positions. During the current period, all $\tilde{X}_n(i,j)$ are independent and have the same distribution. During the stress period, the correlations between any pairs of $\tilde{X}_n(i,j)$ become 0.7. The standard deviations of $\tilde{X}_1(3,3)$ and $\tilde{X}_2(1,4)$ during the stress period become 9 times of the standard deviations during the current period. Distributions of all other $\tilde{X}_n(i,j)$ in the stress period are assumed to be the same as in the current period.

We consider two reduced sets:

- Set A: all risk factors except 60-days EQ and 120-days CM
- Set B: all risk factors except 40-days EQ and 60-days CM

Note that, Set B excludes risk factors which have distinct distributions in the stress period. Table 7.3 shows that both reduced sets satisfy the requirement that $\mathrm{ES}^{\mathrm{R,C}}(X(i)) \geq 75\%\mathrm{ES}^{\mathrm{F,C}}(X(i))$ for all RFs.

	CM	CR	EQ	FX	IR	Unconstrained
Set A	80%	100%	97%	100%	100%	95%
Set B	97%	100%	94%	100%	100%	98%

Table 7.3: Ratios between the FRTB-ES using the reduced set and the full set

Table 7.4 shows different allocations with/without stress-scaling adjustment using different reduced sets. We can see from results associated to the Set A that, when distributions of risk factors in the reduced set are different between the stress and current periods, allocations with stress-scaling adjustment increases the percentages of allocations on stress positions. However, when distributions of risk factors in the reduced set are similar between the stress and current periods, results associated to Set B indicate that allocations are the same with/without stress-scaling adjustment. Moreover the total IMCC is much lower using Set B than Set A.

	Set A (Adjustment)	Set A (Without adj)	Set B (Adjustment)	Set B (Without adj)
CM.60 days.Position 2	4.00%	2.24%	1.43%	1.43%
EQ.40 days.Position 1	5.04%	3.26%	2.11%	2.11%

Table 7.4: Percentages of allocations with and without stress-scaling adjustment using different reduced factor sets. Columns labeled adjustment report allocations using (7.22), columns labeled without adj report allocation using (7.15). The total IMCC are the same in both methods: IMCC(Set A)=11.55; IMCC(Set B)=3.14

7.5 Conclusion

The FRTB IMA introduces higher standards on the calculations of bank's regulatory capital. As a result, corresponding capital allocation methods should be considered to reflect the new capital structure feature, meanwhile, new methods should also be efficient for implementation.

Our main contribution in this chapter is to solve the issues above. Theoretical analy-

sis and numerical results show, compared to the traditional ES allocation, the Euler and CAS allocations for FRTB could correctly reflect the non-cross hedging requirements among different RF-and-LH-buckets. The extended case in Section 7.3.4 takes the stress scenario allocation into account as well. In terms of the computational complexity, given the close connection between our new methods and traditional ES allocations, apart from organising the components from the FRTB IMA calculation, there is no extra complex computation required. Therefore, the computational efficiency of our methods should be the same as in the traditional ES and VaR allocations.

One future work is to apply and analyse our models in real-life trading book portfolios; besides, the portfolio optimisation problem (RORAC optimisation) under the FRTB forms another branch of potential research.

Appendix 7.A Proof of Lemma 7.2.2

The expected shortfall is positive homogeneous, then $\mathrm{ES}(aX(i,j)) = a\mathrm{ES}(X(i,j))$. All operations in (7.4), (7.6), and (7.7) are positive homogeneous. Hence the statement in (i) holds.

For (ii), recall that the expected shortfall is sub-additive, i.e.,

$$\mathrm{ES}((X+Y)(i,j)) \leq \mathrm{ES}(X(i,j)) + \mathrm{ES}(Y(i,j)).$$

When $\mathrm{ES}((X+Y)(i,j)) \geq 0$ for all j, then

$$\begin{aligned}\mathrm{ES}((X+Y)(i)) &= \sqrt{\sum_{j=1}^{5} \mathrm{ES}((X+Y)(i,j))^2} \leq \sqrt{\sum_{j=1}^{5} \left[\mathrm{ES}(X(i,j)) + \mathrm{ES}(Y(i,j))\right]^2} \\ &\leq \sqrt{\sum_{j=1}^{5} \mathrm{ES}(X(i,j))^2} + \sqrt{\sum_{j=1}^{5} \mathrm{ES}(Y(i,j))^2} = \mathrm{ES}(X(i)) + \mathrm{ES}(Y(i)),\end{aligned}$$

where the second inequality follows from the Minkowski inequality.

For (iii), it follows from the sub-additivity for $\mathrm{ES}^{\mathrm{F,C}}$ that

$$\mathrm{ES}^{\mathrm{F,C}}((X+Y)(i)) \leq \mathrm{ES}^{\mathrm{F,C}}(X(i)) + \mathrm{ES}^{\mathrm{F,C}}(Y(i)).$$

Then, when (7.9) is satisfied, we have

$$\begin{aligned}\mathrm{IMCC}((X+Y)(i)) =& \mathrm{ES}^{\mathrm{F,C}}((X+Y)(i))\frac{\mathrm{ES}^{\mathrm{R,S}}((X+Y)(i))}{\mathrm{ES}^{\mathrm{R,C}}((X+Y)(i))}\\ \leq& \frac{\mathrm{ES}^{\mathrm{R,S}}((X+Y)(i))}{\mathrm{ES}^{\mathrm{R,C}}((X+Y)(i))}\Big[\mathrm{ES}^{\mathrm{F,C}}(X(i))+\mathrm{ES}^{\mathrm{F,C}}(Y(i))\Big]\\ \leq& \frac{\mathrm{ES}^{\mathrm{R,S}}(X(i))}{\mathrm{ES}^{\mathrm{R,C}}(X(i))}\mathrm{ES}^{\mathrm{F,C}}(X(i))+\frac{\mathrm{ES}^{\mathrm{R,S}}(Y(i))}{\mathrm{ES}^{\mathrm{R,C}}(Y(i))}\mathrm{ES}^{\mathrm{F,C}}(Y(i))\\ =& \mathrm{IMCC}(X(i))+\mathrm{IMCC}(Y(i)).\end{aligned}$$

Appendix 7.B Proof of Proposition 7.3.4

Since the FRTB-ES, defined in (7.4), is a risk measure homogeneous of degree 1. It then follows from Euler's theorem on homogeneous functions (see [123, Theorem A.1]) that the Euler allocation on FRTB-ES is a full allocation, i.e.,

$$\sum_{n,j}\mathrm{ES}^{\mathrm{F,C}}\big(X_n(i,j)\,|\,X(i)\big)=\mathrm{ES}^{\mathrm{F,C}}(X(i)).$$

This identity, combined with (7.6) and (7.7), yields

$$\begin{aligned}\sum_{n,i,j}\mathrm{IMCC}\big(X_n(i,j)\,|\,X(i)\big) =& 0.5\sum_{i=1}^{6}\frac{\mathrm{ES}^{\mathrm{R,S}}(X(i))}{\mathrm{ES}^{\mathrm{R,C}}(X(i))}\Big(\sum_{n,j}\mathrm{ES}^{\mathrm{F,C}}\big(X_n(i,j)\,|\,X(i)\big)\Big)\\ =& 0.5\sum_{i=1}^{6}\frac{\mathrm{ES}^{\mathrm{R,S}}(X(i))}{\mathrm{ES}^{\mathrm{R,C}}(X(i))}\mathrm{ES}^{\mathrm{F,C}}(X(i))=\mathrm{IMCC}(X).\end{aligned}$$

Appendix 7.C Proof of Lemma 7.3.6

When LH_j is in the first column of the permutation r, i.e., $\mathcal{L}^{-1}(r,j)=1$, the row $X^{v,r,j}(i)$ has only one nonzero entry $\sum_n v_n X_n(i,j)$ at the j-th column. Then

$$\mathrm{ES}\big(X^{v,r,j}(i)\big)=\big|\mathrm{ES}\big(\sum_n v_n X_n(i,j)\big)\big|.$$

Since the expected shortfall is homogeneous of degree 1, then

$$\begin{aligned}\partial_{v_n}\mathrm{ES}\big(X^{v,r,j}(i)\big)\Big|_{v=q} =& \mathrm{sign}\big(\mathrm{ES}(qX(i,j))\big)\,\partial_{v_n}\mathrm{ES}\big(\sum_n v_n X_n(i,j)\big)\Big|_{v=q}\\ =& \mathrm{sign}\big(\mathrm{ES}(X(i,j))\big)\,\partial_{v_n}\mathrm{ES}\big(\sum_n v_n X_n(i,j)\big)\Big|_{v=1}.\end{aligned}$$

As a result,

$$\begin{aligned}\mathrm{CAS}(r,X_n(i,j)) = \int_0^1 \partial_{v_n}\mathrm{ES}\big(X^{v,r,j}(i)\big)\big|_{v=q}\,dq &= \int_0^1 \partial_{v_n}\mathrm{ES}\big(X^{v}(i,j)\big)\big|_{v=1}\,dq\\ &= \partial_{v_n}\mathrm{ES}\big(X^{v}(i,j)\big)\big|_{v=1}.\end{aligned}$$

Note that $\eta(r,i,j) = \mathrm{sign}\big(\mathrm{ES}(qX(i,j))\big)$ in this case. Therefore the previous expression of $\mathrm{CAS}(r,X_n(i,j))$ agrees with (7.18).

When LH_j is not in the first column, i.e., $\mathcal{L}^{-1}(r,j) > 1$,

$$\mathrm{ES}\big(X^{v,r,j}(i)\big) = \sqrt{\mathrm{ES}\big(\sum_n v_n X_n(i,j)\big)^2 + \sum_{1\le s<\mathcal{L}^{-1}(r,j)} \mathrm{ES}\big(i,\mathcal{L}(r,s)\big)^2}.$$

Denote

$$\mathrm{ES}\big(X^{q,r,j}(i)\big) = \sqrt{\mathrm{ES}\big(qX(i,j)\big)^2 + \sum_{1\le s<\mathcal{L}^{-1}(r,j)} \mathrm{ES}\big(i,\mathcal{L}(r,s)\big)^2}.$$

It follows from the homogeneous property of the expected shortfall that

$$\begin{aligned}\partial_{v_n}\mathrm{ES}\big(X^{v,r,j}(i)\big)\Big|_{v=q} =& \frac{\mathrm{ES}\big(qX(i,j)\big)\,\partial_{v_n}\mathrm{ES}\big(\sum_n v_n X_n(i,j)\big)\big|_{v=q}}{\mathrm{ES}\big(X^{q,r,j}(i)\big)}\\ =& \frac{q\mathrm{ES}\big(X(i,j)\big)\,\partial_{v_n}\mathrm{ES}\big(\sum_n v_n X_n(i,j)\big)\big|_{v=1}}{\mathrm{ES}\big(X^{q,r,j}(i)\big)}.\end{aligned}$$

Integrate the derivative with respect to q, we obtain

$$\begin{aligned}\int_0^1 \partial_{v_n}\mathrm{ES}\big(X^{v,r,j}(i)\big)\Big|_{v=q}\,dq &= \partial_{v_n}\mathrm{ES}\big(X^{v}(i,j)\big)\big|_{v=1}\int_0^1 \frac{q\mathrm{ES}\big(X(i,j)\big)}{\mathrm{ES}\big(X^{q,r,j}(i)\big)}dq\\ &= \frac{\partial_{v_n}\mathrm{ES}\big(X^{v,r,j}(i)\big)\Big|_{v=1}}{\mathrm{ES}\big(X(i,j)\big)}\int_0^1 \frac{q\mathrm{ES}\big(X(i,j)\big)^2}{\mathrm{ES}\big(X^{q,r,j}(i)\big)}dq\\ &= \frac{\partial_{v_n}\mathrm{ES}\big(X^{v,r,j}(i)\big)\Big|_{v=1}}{2\,\mathrm{ES}\big(X(i,j)\big)}\int_0^1 \frac{d\big(q^2\mathrm{ES}\big(X(i,j)\big)^2\big)}{\mathrm{ES}\big(X^{q,r,j}(i)\big)}dq\\ &= \eta(r,i,j)\,\partial_{v_n}\mathrm{ES}\big(X^{v,r,j}(i)\big)\Big|_{v=1}.\end{aligned}$$

Appendix 7.D Proof of Proposition 7.3.8

From Lemma 7.3.6 and the fact that the standard Euler allocation is a full allocation, we have

$$\begin{aligned}\sum_n \mathrm{CAS}(r,X_n(i,j)) &= \eta(r,i,j)\sum_n \partial_{v_n}\mathrm{ES}\big(X^{v}(i,j)\big)\big|_{v=1} = \eta(r,i,j)\mathrm{ES}\big(X(i,j)\big)\\ &= \sqrt{\sum_{1\le s\le \mathcal{L}^{-1}(r,j)}\mathrm{ES}\big(X(i,\mathcal{L}(r,s))\big)^2} - \sqrt{\sum_{1\le s< \mathcal{L}^{-1}(r,j)}\mathrm{ES}\big(X(i,\mathcal{L}(r,s))\big)^2}.\end{aligned}$$

Therefore

$$\sum_{n,j}\mathrm{CAS}(r,X_n(i,j)) = \mathrm{ES}(X(i)).$$

The rest proof is similar to the proof of Proposition 7.3.4.

Appendix 7.E Proof of Proposition 7.3.12

Recall that

$$\sum_{n,j}\mathrm{ES}\big(X_n(i,j)\,|\,X(i)\big) = \mathrm{ES}\big(X(i)\big).$$

Then by applying the previous identity to the Euler allocation for $\mathrm{ES}^{\mathrm{F,C}}, \mathrm{ES}^{\mathrm{R,S}}$, and $\mathrm{ES}^{\mathrm{R,C}}$, respectively, we obtain

$$\begin{aligned}\sum_{n,j} \mathrm{IMCC}^{\mathrm{E,S}}\big(X_n(i,j) \,|\, X(i)\big) = 0.5\Big[&\frac{\mathrm{ES}^{\mathrm{R,S}}(X(i))}{\mathrm{ES}^{\mathrm{R,C}}(X(i))}\,\mathrm{ES}^{\mathrm{F,C}}\big(X(i)\big) + \frac{\mathrm{ES}^{\mathrm{F,C}}(X(i))}{\mathrm{ES}^{\mathrm{R,C}}(X(i))}\,\mathrm{ES}^{\mathrm{R,S}}\big(X(i)\big) \\ &- \frac{\mathrm{ES}^{\mathrm{R,S}}(X(i))\mathrm{ES}^{\mathrm{F,C}}(X(i))}{\mathrm{ES}^{\mathrm{R,C}}(X(i))^2}\,\mathrm{ES}^{\mathrm{R,C}}\big(X(i)\big)\Big] \\ = 0.5\,&\frac{\mathrm{ES}^{\mathrm{R,S}}(X(i))}{\mathrm{ES}^{\mathrm{R,C}}(X(i))}\,\mathrm{ES}^{\mathrm{F,C}}\big(X(i)\big) = \mathrm{IMCC}\big(X(i)\big).\end{aligned}$$

The proof for $\mathrm{IMCC}^{\mathrm{C,S}}$ is similar.

Chapter 8

Application in Systematic Trading

In this chapter, we study the application of FPTs in systematic trading. Under certain market environments, and for a universe set of underlying assets, not all of them might generate desirable returns within a specified period; therefore, by effectively identifying and ruling out those assets with less returns, an investor could have a better performance in the market. In view of this, we propose a new trading strategy which selects investment assets according to their probabilities of attaining a predefined trading target. Before illustrating the FPT-based trading strategy, in this chapter we first introduce a mathematical framework for defining trading signal identification strategies and demonstrate how existing strategies can be accommodated to our definition; followed by which, the FPT trading signal identification strategy is discussed. By considering various diffusion models, the new strategy enables us to select underlying assets across different markets and taking different price patterns into account. At the end of this chapter, we use simulated portfolios to examine our strategy. Numerical analysis shows, in comparison with the Markowitz optimal portfolio on the universe set, the FPT strategy could evidently enhance the investment performance. Additionally, as an illustration to Chapter 7, we calculate and allocate the FRTB capital charges of the simulated portfolios. In the appendices of this chapter, real data backtest of the FPT strategy on the China stock market is provided.

8.1 Introduction, Motivation, and Literature Review

Broadly speaking, *systematic trading* refers to trading activities which are fully or partially automated by employing computers. Usually, it is not easy to precisely define what spe-

cific activities are within or without the range of systematic trading. However, as long as an executable algorithm is properly defined and which is implemented by the computer to participate in daily trading, we can treat such a system as a systematic trading machine.

The idea of systematic trading has been widely brought into practice since the 1990s. One of the most famous examples would be the story of the *Long-Term Capital Management (LTCM)* [40]. Founded in 1994 by the star trader at the Wall Street, J. Meriwether, and with the help of two future Nobel Prize winners, M.S. Scholes and R.C. Merton, the fund had nearly tripled its investors' money in the first 3 years. However, in the summer of 1998, due to the wrong-direction bet on the Russian Ruble and followed by the margin call caused liquidity crisis, the fund suffered severe losses in its 5^{th} year, and in the end, accepted the rescue package from the Federal Reserve. Even though this is not a story with a happy ending, still, the LTCM has initiated a revolution in the financial industry - both from the way of trading and the attention on risk management.

One major trading strategy employed by the LTCM is the long-short strategy based on arbitrage (*convergence trade*). Believing in the *efficient market hypothesis*, and by figuring out the assets which are mispriced[1], the LTCM would buy or sell those assets to attain higher excess returns. Such a strategy relies highly on computers and introduces the new concept of systematic trading. When time passed through the new millennial, computers are playing more and more important roles in trading. While on the other hand, the development in technology facilitates experiments in new trading strategies. Nowadays, no matter in high- or low-frequency tradings, it is difficult to imagine banks or other investment institutions who do not use automated processes in their trading decisions. And even for individual investors, it becomes very common to use algorithms to identify trading opportunities. Against this context, we want to verify the feasibility of applying the FPT to the area of systematic trading.

In general, a systematic trading platform is a complex system, which, roughly speaking, involves data processing, signal generation, trade execution, and risk control, etc. In this chapter, we focus on the signal generation part. This is sometimes also referred to as the *portfolio selection problem*. We believe that such a selection problem should contain two stages. In the first stage, an investor selects desired components of a portfolio and determines

[1]The mispricing is not necessarily to be the arbitrage price on financial derivatives. It can also refer to cash products whose prices deviating from their fundamental values.

their long-short positions; and in the next step, he or she allocates the weights for each of the components. The second step has been answered by the *modern portfolio theory (MPT)* from H. Markowitz [83, 84], which we have introduced in Section 2.4. The first stage then, of how to choose a proper portfolio according to certain criteria, forms the major consideration of this chapter. Throughout this chapter, we denote the first stage by the *trading signal identification (TSI)*.

Within the range of the TSI, there are many well-explored strategies. For example, the simplest momentum strategy [80] selects portfolios based on historical returns of each component. As an extension to the momentum strategy, statistical indicators [92] like the *moving average convergence/divergence (MACD)*, the *exponentially weighted moving average (EWMA)*, etc., are widely used in price forecasting. Today, with the fast development in data science and machine learning, more strategies based on data mining [99] and factor analysis [53] have been studied. Apart from the statistical analysis, another branch of strategies is built on by practicing financial or economic theories. The *Capital Asset Pricing Model (CAPM)* [66] is one of such. And later, the *Fama-French Three Factor Model* [42, 43] has extended the CAPM framework by introducing market caps and book values into.

In this chapter, we introduce a new concept of the *executable TSI strategy* and discuss desired properties such a strategy should hold. Based on the new definition, we demonstrate how the FPT, together with other well-developed strategies, could be mathematically described in the TSI problem. A major part of this chapter is to illustrate and test the trading system built from our FPT studies. The present research is motivated by the *pairs trading* strategy [47] (known also as the *statistical arbitrage*). Traditionally, by selecting strongly correlated pairs of assets, people assume that their spreads follow the OU process. Given this model assumption, and by ranking the FPT probabilities of each asset, investors then can select desired portfolio. We generalise this mechanism to different diffusion models. The fundamental assumption of our approach is that, within a specific period, due to different economic or financial reasons, each asset price has a unique and recognisable stochastic dynamic. According to our extension, the implementation of the statistical arbitrage is no more constrained on constructing trading pairs. Instead, even for a single underlying asset, as long as a proper SDE can be identified, we can calculate its FPT probability and correspondingly provide a trading decision metric.

The main contribution of this chapter comes from two aspects. On the one hand, we

propose that the portfolio selection problem should consist of two steps and we provide a mathematical framework for defining valid strategies of the first step, i.e. the executable TSI strategy. On the other hand, we propose the so-called FPT-TSI strategy. The new strategy extends the application of the traditional pairs trading strategy; and with the help of our closed-form FPTD work, the FPT-TSI enables investors to efficiently select underlyings from a large set global portfolio. Additionally, our new strategy also takes the liquidity risk into account, which to some extent, could help in preventing the investment failure due to liquidity crisis (cf. the example of the LTCM). We will address more about this point in Section 8.2.3 later. At the end of this chapter, numerical examples show that the TSI is crucial to the investment optimisation and our FPT-TSI is a successful strategy in enhancing the investment performance.

One special remark is that, this chapter only provides a prototype for the concept verification. The numerical analysis is based on simulations rather than the real data. For the latter one, an extra statistical module is required. And the strategy performance is sensitive to the choices of statistical parameters (e.g. calibration window, p-value, etc.). While without digging too much into the statistical side, at least, the analysis in this chapter confirms that the concepts of TSI/FPT-TSI are reasonable. And in turn, the conclusion from this study further proves that our previous FPT asymptotics are effective.

The rest of this chapter is organised as follows. In Section 8.2, we first define a valid TSI strategy and then illustrate how the FPT framework accommodates under the definition. Section 8.3 is the numerical verification based on simulation; risk management and capital allocation are included as well. Section 8.4 concludes. 11 years China stock market backtest is provided in the appendices of this chapter.

8.2 Trading Signal Identification via the First Passage Time

We follow the notations introduced in Section 2.4. Let I defined in (2.39) be the index set of all tradable assets. Such assets could be stocks, bonds, or even sub-portfolios (e.g. ETF index). Assume[2] there is no transaction cost and assets in the market are fractionally tradable. Consider a Brownian filtration $\left(\Omega, \mathcal{F}, \{\mathcal{F}_t\}_{t\geq 0}, \mathbb{P}\right)$ and denote a portfolio value

[2]These two assumptions do not restrict the application of our framework. It is only for the convenience of mathematical derivations.

process (self-financing) by

$$V_t = C_t + P_t,\ t \geq 0, \tag{8.1}$$

where $\{C_t\}_{t\geq 0}$ is $\mathcal{F}_t$-adapted and represents the cash amount. In addition,

$$P_t := \sum_{i\in I} w_t^{(i)} P_t^{(i)},\ P_t^{(i)} \in \mathcal{F}_t,\ \forall i \in I, \tag{8.2}$$

is the total price of tradable assets under a strategy $\underline{w} := \underline{w}(\infty)$, where

$$\underline{w}(\infty) = \left\{ w_t^{(i)} \in \mathcal{F}_{t^-} : i \in I,\ t > 0 \right\}. \tag{8.3}$$

In the following contents, we first define a TSI strategy. Based on the definition, we then demonstrate the application of FPT in the TSI.

8.2.1 Executable Strategy and the TSI

In general, a TSI can be regarded as a map from the full set I to its subset S, where $S \in \mathcal{P}(I)$ and $\mathcal{P}(I)$ is the power set of I. However, following this definition, there could be infinitely many strategies. For example, we can always choose the i-th asset, i.e. $S = \{i\}$, to be the candidate portfolio. But apparently, such a selection does not have any economic explanation nor quantitative criteria. In view of this, we therefore propose that a meaningful TSI in the systematic trading should, at least, consist of two components: a valid trading strategy, and quantitative criteria which can be used to evaluate the output from the strategy.

We first define an executable strategy by the following.

Definition 8.2.1 (Executable Strategy)**.** Let $\{V_t\}_{t\geq 0}$, $\{C_t\}_{t\geq 0}$, $\{P_t\}_{t\geq 0}$, and $\underline{w} := \underline{w}(\infty)$ be defined as in (8.1), (8.2), and (8.3). We say $\underline{w}$ is an *executable strategy*, if for all $t \geq 0$, the following conditions are satisfied:

1. given any fixed $0 \leq b$, there exists a finite stopping time $\tau_b > t$, such that

$$\begin{cases} C_{\tau_b} - C_{\tau_b^-} = -bC_{\tau_b^-} \\ P_{\tau_b} - P_{\tau_b^-} = bC_{\tau_b^-} \end{cases},$$

2. given any fixed $0 \leq s$, there also exists a finite stopping time $\tau_s > t$, such that

$$\begin{cases} C_{\tau_s} - C_{\tau_s^-} = sP_{\tau_s^-} \\ P_{\tau_s} - P_{\tau_s^-} = -sP_{\tau_s^-} \end{cases}.$$

Remark. Though the definition reads slightly mathematical, it speaks that an executable strategy should be able to achieve all targeting buying and selling (in terms of proportion of b and s) within a finite time. Moreover, by summing up two equations in conditions 1 and 2, respectively, the definition further requires that the executable strategy should not break the self-financing condition, i.e. $V_{\tau_b} - V_{\tau_b^-} = 0$ and $V_{\tau_s} - V_{\tau_s^-} = 0$.

Remark. Besides, note that we do not restrict $b \leq 1$ and $s \leq 1$. This enables the definition to be applicable under short positions. More precisely, $b > 1$ means borrowing assets and $s > 1$ refers to short selling.

Example 8.2.2 (Periodically Rebalanced MPT is Executable)**.** The periodically rebalanced MPT weights form an executable strategy. To see this, consider $t_1 < t_2$, and correspondingly let the optimal weights be given by $\underline{w}_{t_1} := \left\{ w_{t_1}^{(i)} : i \in I \right\}$ and $\underline{w}_{t_2} := \left\{ w_{t_2}^{(i)} : i \in I \right\}$. Assume $\tau_s = \tau_b = t_2$ and there is no interest rate, then

$$s = \sum_{i \in I} \left(w_{t_1}^{(i)} - w_{t_2}^{(i)} \right)^+ P_{t_2}^{(i)} / P_{t_2}, \text{ and } b = \sum_{i \in I} \left(w_{t_2}^{(i)} - w_{t_1}^{(i)} \right)^+ P_{t_2}^{(i)} / (C_{t_1} + sP_{t_2}).$$

Example 8.2.3 (Non-Executable Strategies)**.** Obviously, not all strategies are executable. According to Definition 8.2.1, a non-executable strategy could come from one or combinations of the following scenarios:

1. The trading decision is not a well-defined stopping time. For example, the selling point is the time that the current asset price attains its maximum in comparison with prices in the near future, i.e.

$$\tau_s = \inf \left\{ u \geq t : P_u^{(i)} \geq \max_{u \leq v \leq u + \Delta T} P_v^{(i)} \right\}.$$

2. The trading decision induced stopping time could be infinite. An example would be, considering

$$\tau_s = \inf \left\{ u \geq t : P_u^{(i)} \geq 100 | P_t^{(i)} = 90 \right\};$$

if $\{i\}$ is the stock of Lehman Brothers Holdings Inc (former NYSE code LEH) and t is the time just before the 2008 crisis, then such a strategy would never be executed.

3. The stopping time is properly defined and finite, but the self-financing condition is broken. For instance, when selling $sP_{\tau_s^-}$ amount of assets, an extra c amount of cash is added to the cash account. In this case, if there is no PnL adjustment, the investor would lose the tracking on the performance of the strategy. Moreover, if it is an institutional investor and the cash c is raised from public investors, then it cannot be guaranteed that every time the financing would be successful.

Based on the previous definition, we now introduce the concept of trading signal identification (TSI).

Definition 8.2.4 (Trading Signal Identification)**.** Let $\mathcal{I}$, $\mathcal{W}$, and $\mathcal{M}$ be the sets of asset index collections, executable strategies, and metric spaces, respectively. Then a *trading signal identification*, denoted by $\mathcal{T}$, is a map from $\mathcal{I} \times \mathcal{W} \times \mathcal{M}$ to $\mathcal{P}(\mathcal{I})$, such that for $I \in \mathcal{I}$, $\underline{w} \in \mathcal{W}$, and $\underline{m} \in \mathcal{M}$,

$$\mathcal{T}(I, \underline{w}, \underline{m}) =: S \in \mathcal{P}(I).$$

And the triple, $(I, \underline{w}, \underline{m})$, is referred to as the *characteristic of the TSI*.

A new element introduced by the definition is the set of metric spaces, $\mathcal{M}$. A metric vector $\underline{m} \in \mathcal{M}$, could be either qualitative (e.g. investors' belief of asset price rises) or quantitative (e.g. measures of asset returns). But in general, we want the metric $\underline{m}$ to be quantified. As such, the whole system, $\mathcal{T}(I, \underline{w}, \underline{m})$, can be implemented by assigning proper algorithms. We provide two TSI examples below.

Example 8.2.5 (MPT-TSI)**.** Again, we use Markowitz's MPT as an example. The index set is I (with $n+1$ assets), and the strategy is chosen as the optimal weights (denoted by $\underline{w}^*$). At time $t > 0$, consider the following vector of metrics:

$$\underline{m}^{(*)} := [\underline{m}^{(*)}(0), ..., \underline{m}^{(*)}(n)]^T = \left[|w_t^{*,(0)}|, ..., |w_t^{*,(n)}|\right]^T,$$

which represents absolute values of the optimal MPT weights for each asset. Then for a

critical value[3] $0 \leq p \leq 1$, the MPT-TSI can be specified as

$$\mathcal{T}^{MPT}(I, \underline{w}^*, \underline{m}^{(*)}) = \left\{ i \in I : \underline{m}^{(*)}(i) \geq p \right\}.$$

This TSI strategy selects those assets which have significant representatives (weights larger than p) from the global basket.

Example 8.2.6 (Momentum-TSI)**.** In the second example, we consider a simple momentum strategy based on the asset returns. For the same global portfolio set I with $n+1$ elements, we let

$$\underline{w}^{(**)} = \left[\frac{1}{n+1}, ..., \frac{1}{n+1} \right]^T,$$

i.e. each asset is assigned with equal weights. The stopping times of buying and selling are chosen to be at discrete time, e.g., for $t \geq 0$, $\tau_s = \tau_b = t + \Delta T$, and ΔT could be 1 month or 1 week, etc. Then by properly determining b and s, one can check that $\underline{w}^{(**)}$ is an executable strategy. Now consider a metric vector which calculates the weighted historical returns of each asset:

$$\underline{m}^{(**)} := [\underline{m}^{(**)}(0), ..., \underline{m}^{(**)}(n)]^T = \left[\frac{r_0}{n+1}, ..., \frac{r_n}{n+1} \right]^T.$$

Then either by setting a constant threshold or by selecting the ranked returns, we can correspondingly define the Momentum-TSI as

$$\mathcal{T}^{Threshold}(I, \underline{w}^{**}, \underline{m}^{(**)}) = \left\{ i \in I : \underline{m}^{(**)}(i) \geq p \right\}, \ p \in \mathbb{R}, \text{ or}$$
$$\mathcal{T}^{Rank}(I, \underline{w}^{**}, \underline{m}^{(**)}) = \left\{ i \in I : \underline{m}^{(**)}(i) \geq \underline{m}^{(l),(**)} \right\}, \ l \in I,$$

where $\underline{m}^{(l),(**)}$ is the ordered statistic from large to small.

From Example 8.2.6, we find that by having different weights in $\underline{w}^{**}$, the outputs of the TSI may be totally different. This reveals the fact that some TSI problems depend on the choices of executable strategies. While on the other hand, given a strategy and an output of TSI, say S; by optimising the strategy (e.g. applying MPT) on the sub-portfolio S, we may end up with different weights in comparison with the original strategy. And those new weights in turn can be applied again in determining a new TSI. Therefore, under certain circumstances, there is a conjugate relationship between the strategy and the TSI.

[3] *W.l.o.g.*, assuming there is no short-selling allowed.

8.2.2 Long-Short Strategy by FPT

Following the discussion at the end of the previous subsection, we introduce in this subsection a new TSI strategy. Our TSI is based on the FPT of asset price dynamics and we will show that it is independent of the strategy weights.

Proposition 8.2.7 (FPT Executable Strategy)**.** *Consider a discrete time vector* $T^{\Delta} = \{t_0, t_1, ..., t_J\}$, $J \in \mathbb{N}_0$. *For constants* $u \geq 0$ *and* $l \geq 0$, *and for each* $i \in I$, *define the* take-profit *and the* stop-loss *times as*

$$\tau_u^{(i)} = \inf\left\{t \geq t_j : P_t^{(i)} \geq (1+u)P_{t_j}^{(i)}\right\},\ t_j \in T^{\Delta}, \text{ and}$$
$$\tau_l^{(i)} = \inf\left\{t \geq t_j : P_t^{(i)} \leq (1-l)P_{t_j}^{(i)}\right\},\ t_j \in T^{\Delta}.$$

Further, for each $t_j < t \leq t_{j+1}$ *where* $j \in \{0, ..., J-1\}$, *and for each* $i \in I$, *define the buying and the selling times as*

$$\tau_b = t_j,\ \text{and}\ , \tau_s = \tau_u^{(i)} \wedge \tau_l^{(i)} \wedge t_{j+1},$$

respectively; and let $\underline{w}$ *be a trading strategy as defined in* (8.3) *such that*

$$w_t^{(i)} = w_{\tau_b}^{(i)} \mathbf{1}_{\{t \leq \tau_s\}}. \tag{8.4}$$

Then such a strategy $\underline{w}$, *together with its associated stopping times* τ_b *and* τ_s, *form an executable strategy.*

Proof. The crucial part of the proof is to show that $\underline{w}$ is a well-defined trading strategy; especially, it is $\mathcal{F}_{t^-}$-measurable. Indeed, by our construction, the filtration generated by $\mathbf{1}_{\{t \leq \tau_s\}}$ is left continuous with right limits. And plus that $t > \tau_b = t_j$, therefore, $w_t^{(i)}$ is predictable. The rest of the proof then is concluded by checking that the conditions in Definition 8.2.1 are satisfied. □

The philosophy behind Proposition 8.2.7 is very straightforward. At the beginning of a trading cycle, we decide and fix (during the whole cycle) the weight of each position. Then between t_j and t_{j+1}, if either the take-profit or the stop-loss threshold is touched by the asset price, we close such a position at the given threshold; however, if neither of them is attained, we hold the asset until the end of the period and close the position at the current market

price. We will explain later, that the reason of not rebalancing (reinvesting) the portfolio within the trading cycle, is to avoid risk concentrations.

Proposition 8.2.8 (FPT-TSI)**.** *Let I be the index set of $n+1$ tradable assets and $\underline{w}$ be the FPT executable strategy. For all $j \in \{1, ..., J\}$, $J \in \mathbb{N}$, denote the total length of each trading cycle by $\Delta t_j := t_j - t_{j-1}$, and let*

$$\underline{m}^u := [\underline{m}^u(0), ..., \underline{m}^u(n)]^T = \left[\mathbb{P}(\tau_u^{(0)} \leq \Delta t_j), ..., \mathbb{P}(\tau_u^{(n)} \leq \Delta t_j)\right]^T, \text{ and,}$$
$$\underline{m}^l := [\underline{m}^l(0), ..., \underline{m}^l(n)]^T = \left[\mathbb{P}(\tau_l^{(0)} \leq \Delta t_j), ..., \mathbb{P}(\tau_l^{(n)} \leq \Delta t_j)\right]^T$$

be vectors of probabilities for the upward- and the downward-crossings, respectively. Introduce the notation

$$\underline{m} = \left\{\underline{m}^u, \underline{m}^l\right\}.$$

Then $(I, \underline{w}, \underline{m})$ consists of a FPT-TSI characteristic. Further consider two critical values in evaluating the upward- and the downward-probabilities, $0 \leq \alpha^u \leq 1$ and $0 \leq \alpha^l \leq 1$, then the FPT-TSI for long-only positions is given by

$$\mathcal{T}(I, \underline{w}, \underline{m}) = \left\{i \in I : \underline{m}^u(i) \geq \alpha^u \text{ and } \underline{m}^l(i) \leq \alpha^l\right\}. \tag{8.5}$$

Proof. The proof directly follows from Definition 8.2.4. □

The selection in Proposition 8.2.8 is based on the possibilities of each asset price that would attain a predefined level. Note that, since we are choosing long positions, we want the upper critical value to be as large as possible, while the lower critical value to be as small as possible, i.e. $\alpha^u >> \alpha^l$. This ensures that asset prices in our TSI portfolio will have much more significant probabilities of increasing during the period Δt_j, rather than which of decreasing.

Follow Proposition 8.2.8, the FPT-TSI for short-only and long-short portfolios can be introduced accordingly. For the former one, we can define

$$\mathcal{T}^{Short}(I, \underline{w}, \underline{m}) = \left\{i \in I : \underline{m}^l(i) \geq \alpha^l \text{ and } \underline{m}^u(i) \leq \alpha^u\right\}, \text{ with } \alpha^u << \alpha^l.$$

And for the latter one, denote (8.5) by $\mathcal{T}^{Long}(I, \underline{w}, \underline{m})$ with $\alpha^u >> \alpha^l$, then

$$\mathcal{T}^{Long-Short}(I, \underline{w}, \underline{m}) = \mathcal{T}^{Long}(I, \underline{w}, \underline{m}) \cup \mathcal{T}^{Short}(I, \underline{w}, \underline{m}).$$

Corollary 8.2.9 (Weight Independence of FPT-TSI)**.** *For all FPT executable strategies and $i \in I$, as long as the initial weights $w_{\tau_b}^{(i)}$ in* (8.4) *are not zero (null), then the FPT-TSI does not dependent on the weight selections.*

Proof. For all non-null weights, the FPT-TSI only relies on the crossing probabilities of each underlying asset. And such probabilities are invariant under weight-scalings (see Proposition 8.2.7). Therefore we conclude the proof. □

8.2.3 Discussion

Feature of FPT-TSI

Different from most TSI strategies, where the selection of portfolios is based on either the return or the risk, the FPT-TSI focuses on the level-crossing probability. In practice, the key parameters which determine whether a strategy is successful, are the win-loss ratio and the win-loss probabilities. Consider a simple scenario, that the portfolio has a 70% chance of achieving a 20% increase in the following year; and a 40% chance that will lose 20% of its current value. Then without too much thinking[4], the expected return of the portfolio would be

$$70\% \times 20\% - 40\% \times 20\% = 6\%.$$

In this case, the win-loss ratio is given by $\frac{20\%}{20\%} = 1$, and the win-loss probabilities are given by 70% and 40%, respectively. In order to have a higher return, we want the win-loss ratio to be as high as possible, while on the other hand, we want a higher probability in the win and a lower in the loss. And those quantities are indeed reflected by our FPT-TSI strategy. More precisely, the win-loss ratio in our strategy is controlled by $\frac{u}{l}$ (or $\frac{l}{u}$ for short positions), and the probabilities are controlled by the thresholds α^u and α^l.

Apart from those two quantities, the length of a trading cycle also affects the portfolio's performance. Using the example above, if the win-loss ratio and the probabilities are valid

[4]Of course, the actual return should also take the scenarios where the complementary happened into account, but the number below gives a quick indication of the portfolio's performance.

for a bi-monthly cycle, then the annualised return becomes

$$(1 + 6\%)^6 \approx 142\%.$$

Besides, recall the example of the LTCM. If the investor believes that the market environment is getting deteriorated, then he or she can choose a smaller trading cycle to reduce his or her exposures to the potential liquidity crisis. In our FPT-TSI, the trading cycle parameter is controlled by Δt_j.

In short, the FPT-TSI enables the investor to choose portfolios according to his or her anticipations, where these anticipations are translated into the crucial parameters discussed above.

Absence of Weight Rebalancing

Recall the comment under Proposition 8.2.7, where we have mentioned that during one trading cycle, there is no rebalancing on the portfolio's weights. The reason comes from two major considerations.

First, in contrast to the traditional MPT portfolios (in which an investor seeks for absolute returns by hedging risk out in a diversified portfolio), the output from the FPT-TSI would be a portfolio with a relatively small size. With time passing, where assets under our FPT strategy are gradually sold out, the number of remaining assets becomes even less. While, according to the modern financial theory, the reduction in asset numbers, itself, indicates that the portfolio has become more and more risky.

Secondly, even though the asset prices in the FPT-TSI portfolio are of significant probabilities in increasing (assuming in a long-only scenario), those probabilities cannot be 100%. The risk in our portfolio, indeed, comes from the failures in the probability. After $\tau_u^{(i)}$ or $\tau_l^{(i)}$, where the targeted assets have been sold, if we reinvest (rebalance weights) into the unattained underlyings, then the $1-\alpha^u$ or the $1-\alpha^l$ scenarios may happen to them; and this will cause a risk concentration because we have more money in the positions which conditionally have a larger failure probability. Therefore, it would rather be better of not reinvesting into the remaining assets.

Metric $\underline{m}$ in the FPT-TSI

In practice, a technical difficulty from the FPT-TSI strategy is to effectively evaluate the FPT probabilities, i.e. the metric $\underline{m}$. Here we discuss three potential methods, together with their pros and cons.

[**Model-Independent Approach**] In this approach, we do not make any assumption on the price dynamics. The estimates of the FPT probabilities are from historical scenarios. For example, by fixing a 5 years observation window and counting the proportions of successful hittings within a 2 months window, one can have an estimate to the probability of each asset. This method does not require any model assumption and can be easily implemented. However, similar as in the momentum strategy, this approach relies on the historical information and can mislead investors, if, say, a procyclicality feature is embedded in the asset price.

[**Model-Dependent Approach**] Alternatively, we can assume a few asset (log-) price dynamics which could be observed from the market, e.g. the OU process, our bubble process, the CIR process, drifted Brownian motion, etc. Based on these candidate processes, we can calibrate the market data into a proper model, and by our FPTD results, we are able to calculate the $\underline{m}$-metric. In comparison with the model-independent approach, this approach has a more meaningful economic explanation for asset prices. And the situation in the previous procyclicality example can be avoided to some extent. But a practical challenge of this method is to accurately identify different SDEs and calibrate model parameters. The discussions of this approach form the main content in the next section.

[**Hybrid Approach**] The third approach is a potential research topic and it combines the pros from the previous two methods. The basic idea is to find a proper functional basis, e.g. $\sin(\cdot)$ and $\cos(\cdot)$ functions; and using our FPT framework from Chapter 3, we can try to deduce closed-form FPTDs for the functional basis. Then by employing the functional regression, we can construct featured price dynamics for each asset and calculate their $\underline{m}$-metric. But in practice, a special care should be taken to avoid the overfitting issue.

8.3 Numerical Verification

In this section, we check the feasibility of the FPT-TSI in trading decisions. The $\underline{m}$-metric is calculated by the model-dependent approach and the results in this section are based on simulations. Real data backtest is provided separately in Appendix 8.A.

Before continuing the following contents, we highlight a few assumptions where we have made to conduct the analysis.

1. There is no transaction cost nor interest rate, the market assets are fractionally tradable.

2. Each asset has a unique price dynamic and which can be exactly identified.

3. Model parameters for each asset can be accurately calibrated.

Note that, the first assumption is not critical as the test settings can be modified to accommodate those requirements. It is only for the convenience of coding and presentation. But the rest two assumptions are very restrictive. They require that the model identification and calibration are 100% accurate. Apparently this is not realistic in practice. However, we have mentioned at the beginning that the purpose of this chapter is to verify the concept of the FPT-TSI, and we want to avoid any contamination from bad data quality or inefficiency of statistical modules, therefore, the second and the third items still constitute the main assumptions of this section.

8.3.1 Setting

We assume 4 types of SDEs to form our candidate model pool, namely the OU process (cf. (4.28)), the bubble process (cf. (6.57)), the CIR process (cf. (5.33)), and the drifted Brownian motion (DBM) with mean $\mu \in \mathbb{R}$ and volatility $\sigma \in \mathbb{R}^+$. These 4 stochastic models represent log-price dynamics of different assets.

For the reasons of choosing those 4 models, first, they are the most commonly observed dynamics from market: in the commodity and the foreign exchange markets, the seasonality and the application of pairs trading usually lead to an OU pattern in the log-prices; while in the credit market, our bubble process can be employed in modelling the credit spreads[5]; and for the CIR process, it is used for the short rates of the fixed income market; in the end, the log-prices of equities are often described by the DBM. Secondly, apart from the DBM (where the closed-form FPTD is known), the closed-form FPTDs of other processes have been given in Chapters 4 - 6 of this thesis. Therefore, by choosing those SDEs, we can further verify the

[5]We have not conducted the empirical study on this point, however, considering that a financial bubble usually comes with the increase in credit spreads (e.g. the rise of CDS rates during the 2008 crisis), it causes no harm to assume that our bubble model can be adapted.

effectiveness of our perturbation framework. And conversely, those perturbation results help us to compute the $\underline{m}$-metric in a fast manner.

A further note to be added is that, even though we will assign each asset class with a unique SDE, it does not mean that each class can only have one stochastic pattern. For example, in Chapter 6, we have shown that the bubble model can be applied in the equity market; and the CIR process is also used in modelling the credit spreads, etc. The point here we want to make is that, in practice, the candidate model pool is generic across different asset classes; and within one asset class, there might be different SDEs applicable to different assets. But in this section, for the convenience of illustration, we give each asset class a unique stochastic model. And these asset classes later will be referred to in the capital allocation part (cf. Section 8.3.4).

After understanding the candidate models, the next step is to choose proper model parameters. Based on our analysis on the China stock market (cf. Figure 8.9, Appendix 8.A), in general, there are at least 20% of stocks (out of about 3000) which could attain a 20% increase during a bi-monthly moving window. Therefore, we consider one regime of the model parameters that could generate significant probabilities in the upward moving. For the DBM, this could be achieved by choosing higher values in μ and σ; and for the OU model, we can adjust a higher mean-reversion rate, a higher volatility, a lower starting level, and a higher equilibrium level, etc. Parallel to the real market data, we set 20% amount of model parameters that are in the upward moving regime. And symmetrically, we choose 20% amount of parameters in the downward moving regime. The rest 60% parameters are set in a neutral regime, i.e. no significant upward or downward trends. For the illustration of regime settings, visualised by hitting probabilities, please refer to Appendix 8.A.

We summarise the simulation information into Table 8.1 below.

	Stochastic Process	Upward Regime	Neutral Regime	Downward Regime
CM	OU	20	60	20
CR	Bubble	20	60	20
FX	OU	20	60	20
IR	CIR	20	60	20
EQ	DBM	20	60	20

Table 8.1: Model choices and numbers of simulated paths in different regimes

Our testing data is simulated as follows. There are in total 1,000 simulated portfolios. In each portfolio, there are 500 assets equally distributed across those 5 asset classes above. Each asset price is simulated for 2 years time. And in each simulation, not only the sample path, but also the model parameters are randomly generated. The model parameters follow uniform distributions with the intervals being specified in different regimes[6]. Figure 8.1 below presents the normalised values of three simulated portfolios with equal weights between year 1 and year 2.

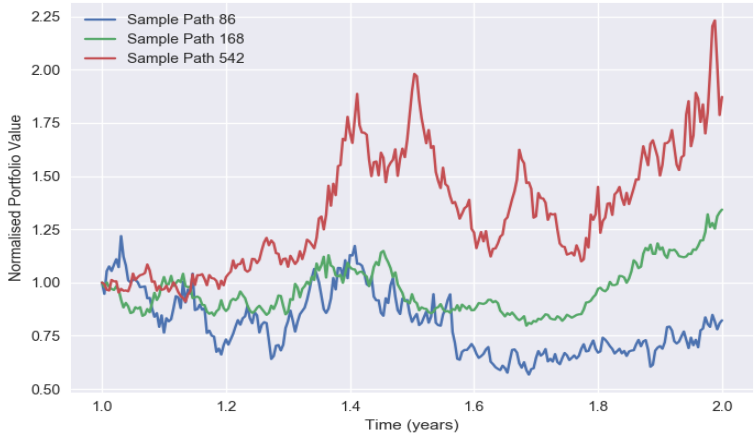

Figure 8.1: Simulated portfolio paths (normalised) with equal weights across different assets

8.3.2 Trading Strategy Illustration

In this part, we use portfolio #542 (red curve in Figure 8.1) to illustrate crucial steps and main statistics involved in the FPT-TSI strategy. Note that, our simulation starts from time $t = 0$. In order to have relatively stable (stationary) paths, we apply the FPT-TSI between $t = 1$ and $t = 2$. Also, in the following exercises, we do not allow short-selling in our model[7].

Recall Propositions 8.2.7 and 8.2.8, the basic parameters in our strategy are chosen as

$$w_t^{(i)} = 1/500,\ \Delta t_j = 2/12,\ u = 0.2,\ l = 0.2,$$

i.e. we consider an equally weighted strategy on a portfolio consisting of 500 assets; the

[6]Since among those 4 models, plus by considering 3 regimes in each model, we have 60 different intervals. So for the convenience of presentation, we do not list them in this chapter. But the test code, where parameter settings are included, can be provided upon request.

[7]This avoids the complexity of choosing proper limits in the leverage ratio.

win-loss ratio is given by $20\%/20\% = 1$ and the trading cycle is set to be 2 months. For the critical values of hitting probabilities, we let[8]

$$\begin{cases} \alpha^u = 0.7,\ \alpha^l = 0.4, \text{ if } \left\{\ln(P_t^{(i)})\right\}_{t\geq 0} \text{ is an OU process or a DBM} \\ \alpha^u = 0.8,\ \alpha^l = 0.4, \text{ if } \left\{\ln(P_t^{(i)})\right\}_{t\geq 0} \text{ is a Bubble process} \\ \alpha^u = 0.65,\ \alpha^l = 0.35, \text{ if } \left\{\ln(P_t^{(i)})\right\}_{t\geq 0} \text{ is a CIR process} \end{cases} . \tag{8.6}$$

And the formulae of perturbed FPTDs for each model are summarised in Table 8.2 below.

Stochastic Process	Upward Hitting ($p_{\tau_u}(t)$)	Downward Hitting ($p_{\tau_l}(t)$)
OU	cf. Equation (4.32) on p. 54	cf. Equation (4.30) on p. 54
CIR	cf. Equation (5.37) on p. 86	cf. Equation (5.35) on p. 85
Bubble	cf. Equation (6.80) on p. 130	cf. Equation (6.59) on p. 112
DBM	cf. [18, Equation (2.0.2), p. 295]	cf. [18, Equation (2.0.2), p. 295]

Table 8.2: Formulae of perturbed FPTDs for each model

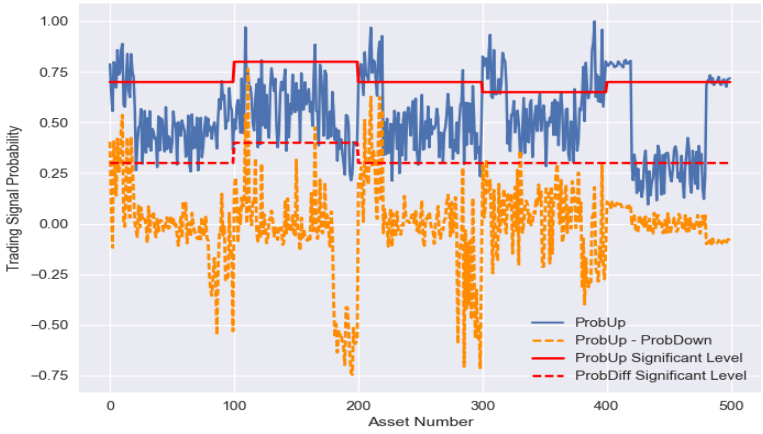

Figure 8.2: First stage signal illustration of portfolio #542. Blue and orange curves refer to the upcrossing probability and the difference between upcrossing and downcrossing probabilities. Red solid line indicates α^u and red dashed line plots $\alpha^u - \alpha^l$

With parameters in (8.6) and FPTDs in Table 8.2 being specified, we apply the long-only FPT-TSI (cf. (8.5)). As an illustration, we consider the trading opportunities between $t = 1$

[8]The choices below are based on the effectiveness of the perturbed FPTDs. For more details please refer to Chapters 4 - 6.

and $t = 1+2/12$. The original signals under (8.5) for the first trading cycle is given in Figure 8.13 of Appendix 8.B. However, those signals are a bit messy for presenting. In view of this, instead of showing $\underline{m}^l$ and α^l, we plot $\underline{m}^u - \underline{m}^l$ (orange curve) and $\alpha^u - \alpha^l$ (red dashed line) in Figure 8.2 above.

According to Figure 8.2, though not strictly equivalent, those assets where both the blue and the orange curves are above the solid and the dashed red curves, respectively, are selected to form our portfolio. In this scenario, there are in total 9 assets being chosen, with asset index numbers

$$\mathcal{T}_{t=1}^{Long}(I, \underline{w}, \underline{m}) := \{0,\ 3,\ 9,\ 10,\ 205,\ 209,\ 210,\ 217,\ 219\}\,. \tag{8.7}$$

Now, given the selected portfolio in (8.7), we conduct a one stage backtest. More specifically, we apply the FPT executable strategy as introduced in Proposition 8.2.7 and demonstrate its realisation between $t = 1$ and $t = 1 + 2/12$.

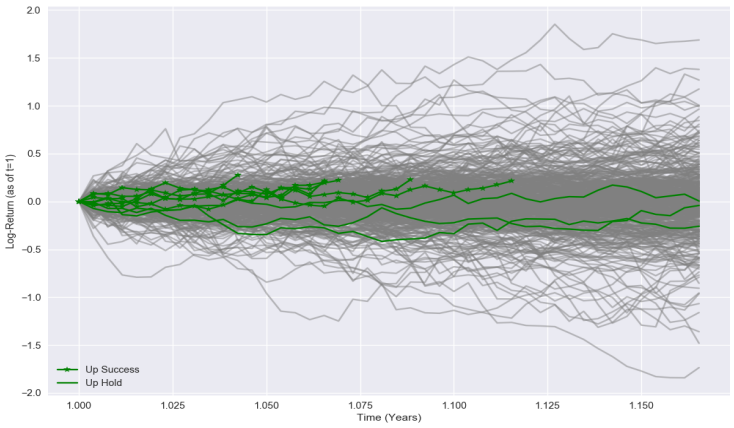

Figure 8.3: One stage backtest of portfolio #542 between $t = 1$ and $t = 1+2/12$. Green curves marked by star symbols demonstrate the selected paths that attain the 20% target increase; green curves with no marks show the selected paths but which are held until t=1+2/12. Grey paths are for unchosen assets

In Figure 8.3, we plot the paths of log-returns (*w.r.t.* $t = 1$) for each asset. The selected assets in (8.7) are highlighted by green while those unselected ones are marked by grey. In addition, we make extra star marks on those assets where the 20% target are achieved within the 2 months period, i.e. for those $i \in \mathcal{T}_{t=1}^{Long}(I, \underline{w}, \underline{m})$ and $\tau_u^{(i)} < 1 + 2/12$. Another point to mention is that, in the strategy implementation, we set the 2-month 99% VaR as the stop-loss

threshold instead of the 20% drop of the price; although, the portfolio is selected based on the 20% loss in the FPT-TSI[9].

From Figure 8.3, we can see that there are 6 assets which attain 20% returns, accounting $6/9 \approx 66\%$ of the total number of selected assets. And three assets are held until the end of 2 months. In this example, there is no asset touching the 2-month 99% VaR barrier. As a simple statistic, the success rate (accuracy) of our strategy is 66%. And if we compare this number with our critical value settings in (8.6), we can conclude that our FPT-TSI could effectively select the assets according to the investor's need. Besides, if we assign equal weights to those 9 assets, then at the end of the 2 months time, the return of our portfolio is

$$6/9 \times 0.2 + (0.0048 - 0.2590 - 0.0414)/9 \approx 10.05\%.$$

In order to further confirm the effectiveness of our FPT-TSI strategy, we repeat such a one stage backtest on 1,000 simulated portfolios and calculate the success rate, the hold-to-maturity rate, and the failure rate (attains the stop-loss threshold) in each run. The data from each simulation is shown in Figure 8.14 of Appendix 8.B. And here, we report major statistics from those 1,000 simulations. Results in Table 8.3 below support that the FPT-TSI strategy is effective and reasonable.

	Mean	StdDev
Success Rate	69.71%	14.29%
Hold-to-Maturity Rate	30.19%	14.25%
Failure Rate	0.09%	1.00%

Table 8.3: Statistics of one step backtest through 1,000 simulations

8.3.3 Backtest on Simulated Portfolio

In this subsection, we provide the full 1-year backtest of our strategy. Similar as before, we will first use portfolio #542 as an illustration. Then, a statistical summary of 1,000 simulated portfolios will be provided.

[9]About the stop-loss selection, itself is another topic to be discussed: a stricter value would be easily triggered and leads to the cumulative loss in the portfolio; while a looser threshold would introduce extreme event risk into the portfolio. Here, we will not dig into too many details of it and we will use the 99% VaR metric throughout this chapter.

Note that, the FPT-TSI is a weight-independent strategy. After acquiring the sub-portfolios (see e.g. (8.7)), we also need to decide the weight of each asset, i.e. to finish the second step of the portfolio selection problem. In this part, we consider two schemes of weight allocations, namely the equally weighted scheme and the Markowitz variance-minimised weights with a constraint on short selling[10]. On the other hand, we choose the global portfolio (with a total number of 500 assets) as our benchmarks: for the equally weighted scheme, we assign equal weights across assets in the global portfolio; and for the Markowitz scheme, we apply the same optimisation to the global portfolio.

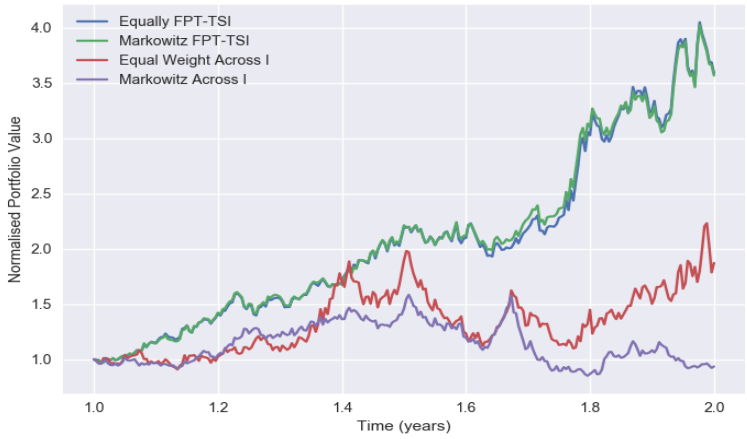

Figure 8.4: One-year backtest of portfolio #542 between $t = 1$ and $t = 2$. Green and blue curves refer to two schemes of the FPT-TSI; red and purple curves plot the performances of global portfolios

Figure 8.4 shows the backtest results based on portfolio #542. There are a few interesting observations. First, there is a big difference between those two benchmark portfolios. The Markowitz global portfolio is more stable than the equally weighted one (this is expected as our target is to minimise the portfolio variance), but its end-of-year return is negative; while in contrast, the equally weighted benchmark has a nearly 80% increase. Secondly, consider the FPT-TSI portfolios, the picture shows that they outperform the benchmarks in either scheme (this is not surprising, especially by noticing that we have an outstanding success rate as shown by Table 8.3). And there is a weak pattern that the FPT-TSI under the Markowitz optimisation is more stable than the equally weighted FPT-TSI. This test,

[10]Recall (2.44), the scheme mentioned here refers to the settings that $\lambda = 1$ and $\underline{r} = \underline{0}$, plus the short selling constraint. The covariance matrix is estimated by a 1-year rolling window.

from the numerical point of view, confirms our argument in the preamble that by effectively identifying and ruling out those assets with less desirable returns, the investor would have a better performance in the market.

In Table 8.4 below, based on the daily log-returns, we provide major statistics associated with each portfolio and their annualised *Sharpe Ratios (SRs)/Information Ratios (IRs)*. In general, by comparing the mean and the standard deviation, we can conclude that the daily performances of two FPT-TSI portfolios dominate that of the benchmarks. And this observation is further verified by checking the Sharpe ratios. Besides, the skewness indicates two FPT-TSI portfolios have more positive returns than those of negative, while the returns of global portfolios are skewed to the loss side. Combine that all those four portfolios have evident kurtosis, we can say that the tails of FPT-TSI portfolios are driven by positively extreme returns, while the opposite happens to benchmark portfolios. In the end, the information ratio helps us to understand the relative performances between each FPT-TSI portfolio and their benchmarks. Both the IRs are positive, this again, confirms that the FPT-TSI outperforms the global portfolio. However, we need to emphasise that the situation where the Markowitz FPT-TSI has a much higher IR than that of the equally weighted FPT-TSI, does not mean that the former is better, as these two portfolios have different benchmarks.

	Mean	StdDev	Skewness	Kurtoris
Equally FPT-TSI	0.0049	0.0260	0.2447	3.5367
Equally Global (Benchmark)	0.0024	0.0445	-0.1195	3.5460
Markowitz FPT-TSI	0.0049	0.0249	0.2706	3.7786
Markowitz Global (Benchmark)	-0.0003	0.0293	-0.2383	3.5522
	SR	IR		
Equally FPT-TSI	3.0503	0.7570		
Equally Global (Benchmark)	0.8742	NA		
Markowitz FPT-TSI	3.1663	2.0690		
Markowitz Global (Benchmark)	-0.1387	NA		

Table 8.4: Statistics of one-year backtest on portfolio #542

Further, in Figure 8.5 below, we provide the histograms of annualised SRs for each simulated portfolio. The mean and the standard deviation from those 1,000 SRs are reported in

Table 8.5. By summarising the information from those 1,000 simulations, we can conclude that our FPT-TSI strategy can significantly enhance investment performances.

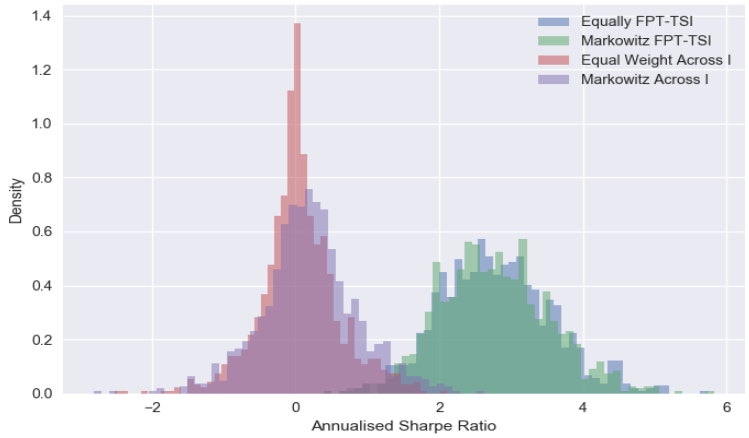

Figure 8.5: Sharpe ratio histograms for one-year backtests of 1,000 simulated portfolios

	Equally Weighted FPT-TSI	Equally Weighted Global Portfolio	Markowitz FPT-TSI	Markowitz Global Portfolio
Mean	2.8018	0.0530	2.7675	0.1993
StdDev	0.7784	0.7740	0.5502	0.6745

Table 8.5: Sharpe ratio statistics for one-year backtests of 1,000 simulated portfolios

8.3.4 Risk Management and Capital Allocation

In the last part of this section, we calculate the regulatory risk requirement and its capital allocation. We will not provide full details of 1,000 simulations; instead, our calculations are again based on portfolio #542. Also, in order to avoid repeated presentations, we only consider the Markowitz portfolios of the FPT-TSI and the global set.

Before calculating the FRTB IMCC, we need first assign proper liquidity horizons for each of the assets. In the following exercise, we assume those assets with larger volatilities will then have longer LHs. And different LHs in (7.1) are equally distributed to risk factors within the same RF bucket; for example, in the EQ class, 20 assets have 10-day LH, 20 then have 20-day LH, etc. In addition, for simplicity, we assume the stress scaling (cf. Section 7.2.2) under the FRTB IMA is 1.

Figure 8.6: Portfolio value and different risk metrics of portfolio #542 between year 1 and year 2. The left panel presents the FPT-TSI portfolio and the right panel shows the global portfolio. Both portfolios are of Markowitz types. And in both graphs, blue curve indicates the normalised portfolio values, green curve plots the FRTB IMCCs; red and purple curves represent the VaR and the ES metrics, respectively

Figure 8.6 above demonstrates the investment and the risk performances of the FPT-TSI and the global portfolios. From these graphs, we find that the FRTB IMCC introduces higher standards in risk capital requirements. This coincides with our discussions from Chapter 7. Secondly, by a fast glance, we may find that the FPT-TSI portfolio is riskier than the diversified one (global portfolio). However, note that the risk capital is calculated based on the total investment. As the portfolio value under the FPT-TSI increases much faster than the benchmark, therefore, the numbers in Figure 8.6 do not really refer to that the FPT-TSI portfolio has more risk.

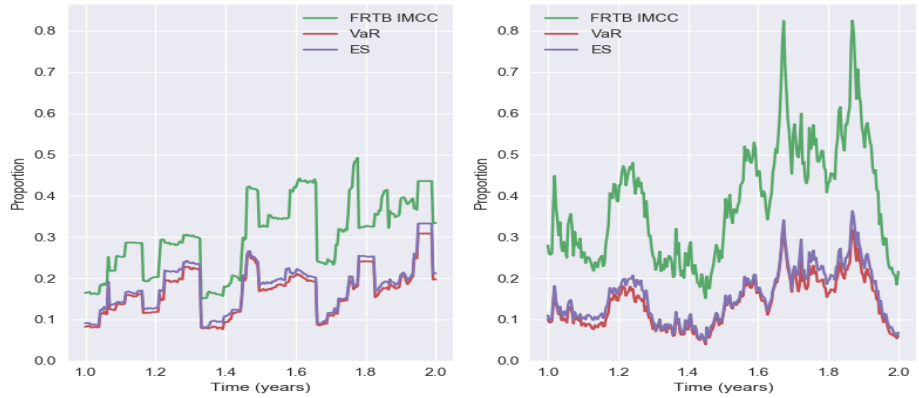

Figure 8.7: Risk metric proportions to the total portfolio value. Left panel: FPT-TSI portfolio; right panel: global portfolio

In fact, instead of using the absolute risk numbers, in Figure 8.7, we plot the risk pro-

portion to the total portfolio value; and by which we find that, based on traditional metrics (VaR/ES), the FPT-TSI strategy does not generate evidently extra risk. In addition, by comparing two green curves, we see that under the FRTB IMCC, a more diversified portfolio (right panel) even has bigger proportions of risk. If one recalls in Chapter 7 that the FRTB IMA restricts cross-hedging, then the observation here is no more surprising. This exercise indicates us that, facing the new regulation, choosing the 'correct' underlying assets becomes crucial to banks. In view of this, though our FPT-TSI strategy may not be applicable to banks, we do hope that the idea and the framework in this chapter would be helpful.

Now we conclude this part by showing the allocated capitals in each portfolio. Since we have 260 trading days, it is not realistic to present all the allocations of every day. As a brief summary, we calculate the averaged allocations of each RF-LH bucket through the 260 days and the results of which are demonstrated in Figure 8.8 below.

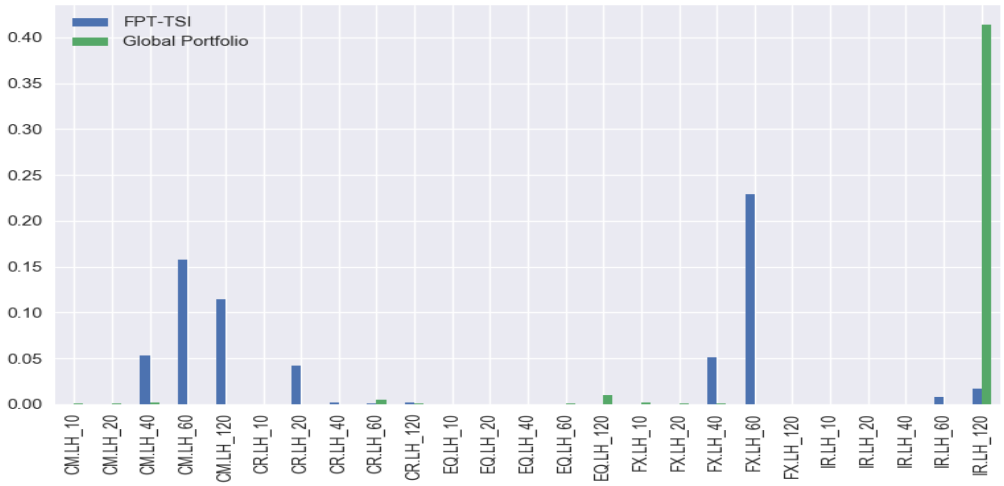

Figure 8.8: Annually averaged risk contributions of each RF-LH bucket for the FPT-TSI and the global portfolios

The allocations are implemented by the Euler method with a kernel smoothing. And the numbers reported are in an absolute sense. From Figure 8.8, we immediately see that the 120-day IR makes the highest contribution in the global portfolio. Therefore, for the purpose of capital optimisation, one should consider removing some risk factors in such a bucket. On the other hand, risk in the FPT-TSI portfolio is mainly from assets with longer LHs. Recall that, by our construction, those assets with longer LHs also have larger volatilities. So the allocations in Figure 8.8 also tell us that, the selected assets by the FPT-TSI usually have more significant volatilities.

8.4 Conclusion

In this chapter, we provide a general mathematical framework for defining the TSI problem. And given the definition, by combing our previous studies, we propose the FPT-TSI strategy. The numerical section of this chapter verifies the effectiveness of using the model-dependent approach to implement the FPT-TSI. However, in the real data test (cf. Appendix 8.A), though to some extent the investment performance is acceptable, the success rate, especially in comparison with simulated results from Table 8.3, cannot achieve the desired level.

In practice, the limitation of the model-dependent approach is mainly from the low-accuracy of SDE identifications. Also, the instability and the regime-switchings of price dynamics affect the strategy's performance. But these two are the issues commonly observed from most trading strategies. In the future, the potential research would be focusing on increasing the accuracy of model identifications; or, recall the end of Section 8.2, apart from the model-dependent approach, we may also consider applying the hybrid scheme.

Appendix 8.A China Stock Market Exercise

In this appendix, we provide an analysis on the China stock market. Figures below summarise the historical information of stocks which posses 20% increase within a 2 months trading cycle. Observations from which inspire us to set corresponding simulation parameters in Section 8.3 and choose 20% and 2-month as crucial parameters in the FPT-TSI strategy.

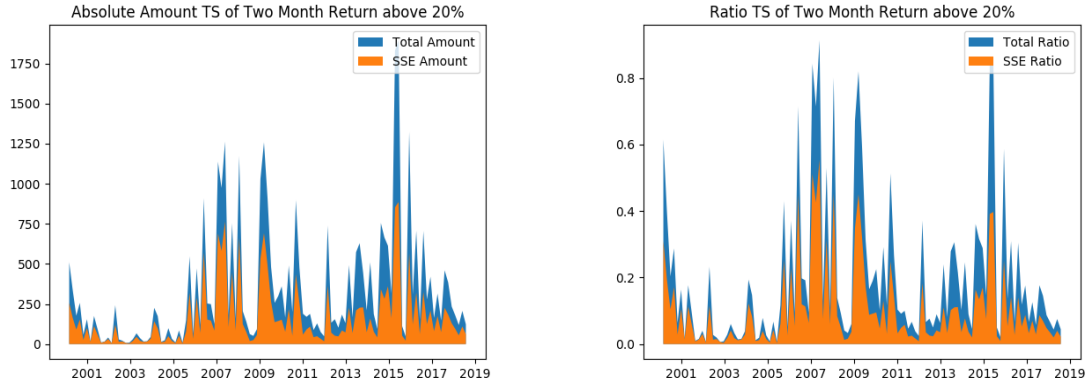

Figure 8.9: China stock market statistics (historical time-series) for stocks which have more than 20% increase within 2 months time. Left panel: in terms of absolute stock numbers; right panel: in terms of ratios in the total stock amounts. Yellow region: accounting for the Shanghai market only; blue region: total numbers of Shanghai and Shenzhen markets

We further examine the FPT-TSI in the real market. Candidate model pools and the FPTD functions are listed in Table 8.2. An extra statistical module is included in the real data backtest and details of which can be provided upon request. The backtest period is chosen between 2007-01-01 and 2018-07-31, accounting for more than 11 years time. We use the daily adjusted closing price to conduct our analysis and the data source is extracted from the *Wind* database. In total, there are 2,765 single name stocks being considered and the benchmark is chosen as the Shanghai Stock Exchange Composite Index (000001.SS).

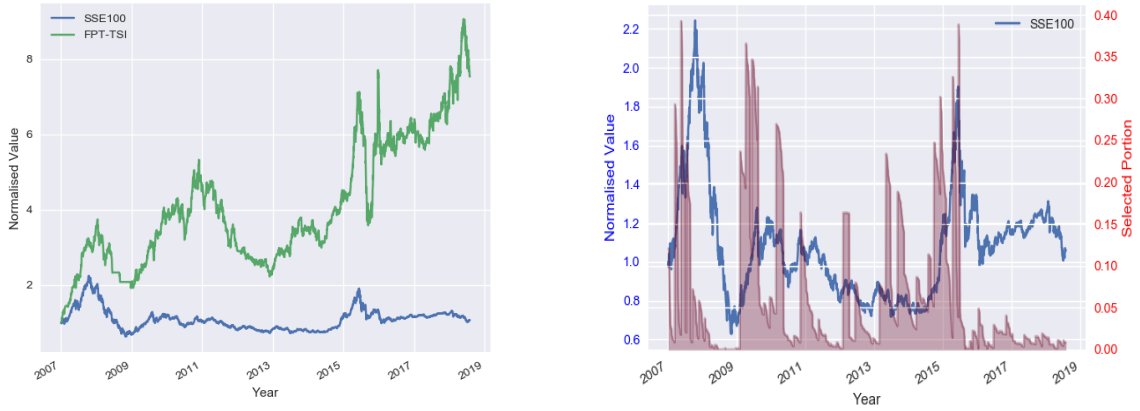

Figure 8.10: Backtest of China stock market between 2007-2018. Left panel: normalised values of the FPT-TSI (green) and the benchmark (blue); right panel: normalised benchmark values and the densities of TSI signals (red shadow region)

Figure 8.10 above shows the backtest result and its further details. In the left panel, we plot the normalised values of the FPT-TSI and the market index (00001.SS); from which we find the FPT-TSI generates 7.53 times growth during the 127 months. This roughly corresponds to 21% and 71% annual returns under accumulative and average senses. However, for the market index, the 127 months accumulated value is about 1.06. On the other hand, the right panel plots the additional information from the FPT-TSI. The red shadow region shows the proportion of the number of selected stocks over the total amount of single stocks in the market. Since we are applying a long-only strategy, a higher proportion should in principle indicate a better market environment. This is indeed observed in 2007, 2010, and 2015, which are three major bull market periods.

In the end, using a fixed 1-year and monthly rolling window, we calculate the annual relative returns of the FPT-TSI and the market index. Major statistics are reported in Table

8.6 (note: we assume 0% interest rate in the Sharpe ratio) and the histogram of returns is provided in Figure 8.11.

	Mean	StdDev	Skewness	Kurtoris	SR	IR	α	β
SSE100	0.0262	0.3405	1.1719	5.3372	0.0771	NA	NA	NA
FPT-TSI	0.1859	0.4177	1.7676	9.7805	0.4450	0.5527	0.1625	0.8926

Table 8.6: Annual return statistics for the FPT-TSI and the market index

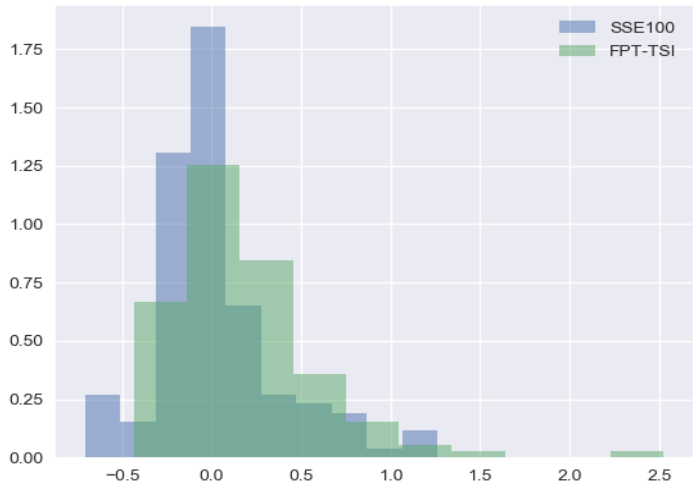

Figure 8.11: Annual return histogram

Appendix 8.B Further Illustration on the Simulation Exercise and the FPT-TSI

This appendix provides further explanations to the previous simulation exercise and the FPT-TSI. Figure 8.12 below first demonstrates asset parameter choices used in Section 8.3. By taking the portfolio #542 as an example, we plot its 2-month FPT probabilities at the initial state. The left panel shows the upward probabilities and from which we find about 20% assets in each asset class have a significant upward trend (probabilities $>$ 75%). Similarly, the right panel shows the downward probabilities and 20% of assets are set in a downward regime. The rest 60% assets are set in neutral regime. This explains settings in Table 8.1.

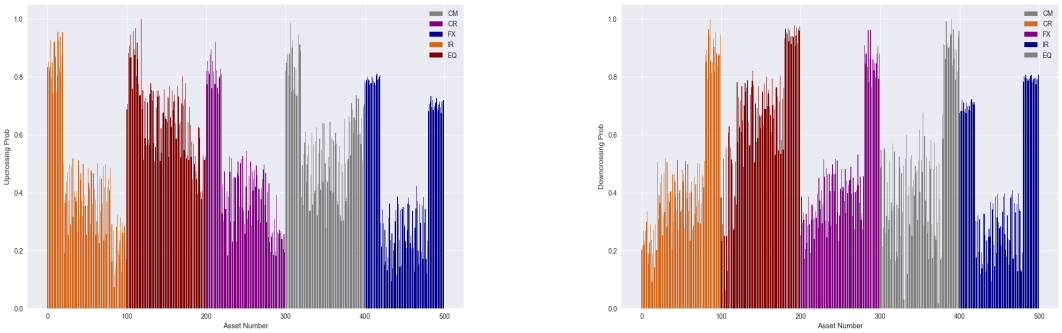

Figure 8.12: Initial state probabilities for portfolio #542 of upward- and downward-hittings in 2 months time (between $t_0 = 0$ and $t_1 = 2/12$). Left panel: upward hitting; right panel: downward hitting. The underlying processes for each asset class are specified as: commodity - OU, credit - Bubble; foreign exchange - OU; interest rate - CIR; equity - DBM. The y-axis refers to the hitting probability and the x-axis represents the number of asset. There are 100 assets under each class and in total 500 assets

Again, use the portfolio #542 as an illustration, Figure 8.13 plots the actual signal generated by Equation (8.5). Note that, the signals in Figure 8.13 are actually used in the backtests for both the simulation exercise and the real data test. The plot in Figure 8.2 is only for the convenience of presentation.

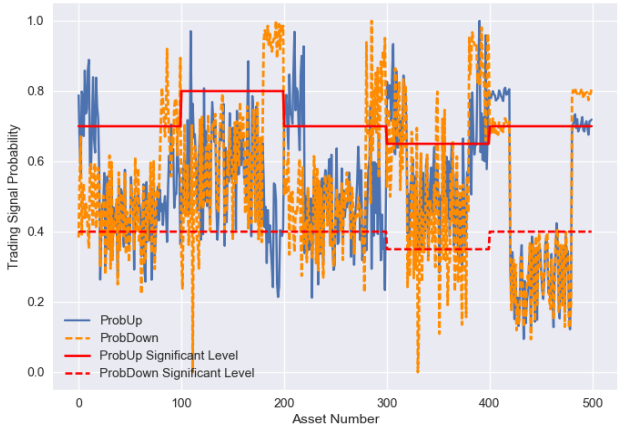

Figure 8.13: First stage signal illustration (Equation (8.5)) of portfolio #542. Blue and orange curves refer to the upcrossing- and the downcrossing-probabilities ($\underline{m}^u$ and $\underline{m}^l$, respectively). Red solid line indicates α^u and red dashed line plots α^l

The last graph below corresponds to the statistics in Table 8.3. It shows the success or failure of attaining the bi-monthly 20% increase in each of those 1,000 simulated portfolios.

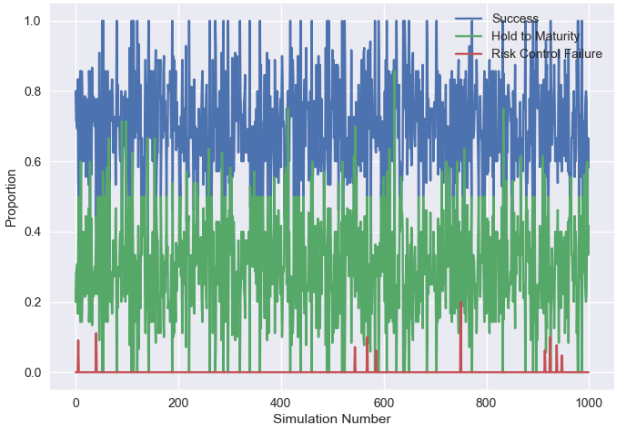

Figure 8.14: Blue curve: success rate of attaining 20% increase target; green curve: proportions of assets which are held until the end of 2 months; red curve: failure rate of touching the 2-month 99% VaR threshold

Chapter 9

Conclusion

The core theme of this thesis is using the perturbation technique to solve closed-form asymptotics of FPTDs; given the success of which, we also investigated the FPT applications in various aspects of finance. In this chapter, we provide a comprehensive summary of the thesis. Separate conclusions of each topic have been documented on pp. 80, 124, 154, and 184, respectively.

This chapter has two parts, where suggestions about future works are listed in the second. In the first part, instead of repeating the conclusions of each topic, we highlight our major findings and contributions of this research from three different angles, which are as follows.

Mathematically, we have tackled the issues of finding closed-form FPTD asymptotics and providing their error estimates (Chapter 3). As we mentioned at the beginning of this thesis, most FPTDs of diffusion processes seem like not possessing closed-form solutions. Therefore, by providing closed-form asymptotics, we are at least able to understand the FPT distributions in a more analytically tractable way. On the other hand, the mathematical derivations and proofs in this thesis, themselves are of great interest for studying. As one example, in Chapter 4, we found a triple-indexed recursion series which is deduced originally from the Hermite series. The recursion structure of the new series has been established, but whether there exists a general solution formula is still waiting to be answered. Another example is given by the proofs of the perturbation convergence analysis. Lemma 4.2.1 creatively proves the L^1-boundedness by splitting the domain of the OU process according to its functional turning point. And the lemma itself, together with its proof idea, are used later in Propositions 4.2.2, 5.2.2, and 6.4.3, to show the convergence of the perturbations in the OU, the

Bessel, and the bubble models.

Computationally, our closed-form FPTDs (Chapters 4-6) and two capital allocation schemes (Chapter 7) would facilitate the model implementations in related areas. In Section 4.3.3, we have provided the number that our perturbed FPTD of the OU process is 1,371 times computationally faster than the Talbot numerical inverse. To understand this number in a more intuitive way, we consider the following example. Assuming that the Talbot inverse would spend 1.37 seconds to compute one level-crossing probability for a single stock, and assuming there are 3,000 stocks in a market. Then the total time for trading signal processing (Chapter 8) would be 68.5 minutes in this market, which is more than an hour. However, by applying our asymptotic results, the computation time reduces to less than 3 seconds. The efficiency enhancement demonstrated above has become another motivation for us to combine the FPT with systematic trading. Besides, in the capital allocation topic, we successfully retrieved simple allocation schemes from a sophisticated risk measure (FRTB IMCC). The computations for FRTB IMA allocations are guaranteed to be no more complex than that under the current VaR-based regulatory framework. Therefore, banks could use our methods to manage their risks and optimise their capital charges without paying extra computational costs.

Conceptually, many new arguments related to economic bubble, regulatory risk management, and systematic trading, have been discussed in this thesis. In the economic bubble topic (Chapter 6), we have demonstrated the feasibility of modelling financial bubbles using our new diffusion process. Especially, the connection between the positive feedback mechanism and the asymmetric feature of the model has been well-explained (cf. p. 93, Section 6.2). In the risk management topic (Chapter 7), one of our most prominent contributions would be establishing the correct mathematical formulation of the FRTB IMCC. This mathematical framework enables us to further conduct coherent analysis and derive capital allocation schemes. Following the framework, we have spotted capital arbitrage opportunities from either the break of the IMCC coherency or the freedom in choices of the reduced sets (cf. p. 152, Section 7.4.3). In the end, the systematic trading topic (Chapter 8) introduces the FPT-TSI. The trading idea from the new strategy is different to the diversification concept in traditional strategies, and we have documented its core features in detail in the context (cf. p. 170, Section 8.2.3). Moreover, it is shown on p. 171 that the trading cycle parameter Δt_j in the FPT-TSI can be used to control the liquidity risk, which is an important lesson

that we learned from the failure of the LTCM.

In below, we propose a few directions of future works which are associated with the current research. Roughly speaking, the future works can be classified into three categories, the *extensions* of the FPT framework, the *applications* of current results, and the studies of *mathematical puzzles* remained in this thesis.

- [**Extension**] The current FPT framework only considers time-homogeneous diffusion processes with constant volatilities. One future direction would be taking the stochastic volatility into account. Alternatively, people may also check the perturbation technique in Lévy processes, or stochastic crossing barriers, etc.

- [**Extension**] From the dimension aspect, the current work only involves one-dimension ODEs. This restricts the applications in financial products with higher dimensions, e.g. barrier options or contingent claims. The future work from this point would be applying the perturbation in PDEs.

- [**Application**] As we mentioned in Chapter 8, one application of the current perturbation framework is to deduce the closed-form FPTDs for processes with drifts of $\sin(\cdot)$ and $\cos(\cdot)$ functions. If one can gain a success from which, then combine the functional regression, people may consider the hybrid scheme in the FPT-TSI (cf. p. 172).

- [**Application**] In Chapter 6, we have provided a calibration scheme for the bubble model. But such a scheme still relies on subjective inputs. One potential work on this topic is to enhance the calibration scheme, where MLE or LSE type would be a good candidate. Besides, bubble indicators, short rate modelling, etc., would also constitute future works.

- [**Application**] There are many potential works arise from the capital allocation topic (Chapter 8). The first one would be examining the performances of FRTB allocations in real-life trading books. And the studies of capital optimisation would be another direction to go with. Additionally, bank's behaviours under the FRTB, the prevention of systematic risk, etc., are also interesting areas for studying.

- [**Mathematical Puzzle**] One remaining math problem is to find the general solution of the triple-indexed recursion series (cf. Lemma 4.1.2, Corollaries 4.B.1 and 4.B.2),

if such a solution exists. By knowing the general solution, we could further simplify the perturbed density in the OU process, and may even find sharp bounds for the truncation errors. But this problem is out of the range of this thesis. It would require further knowledge on number theory, abstract algebra, etc.

- [**Mathematical Puzzle**] Another remaining math problem is related to the exact simulation of the bubble process. More specifically, this is related to the $\theta(r, s)$-function (cf. Equation (6.14)) in the Hartman-Watson distribution. In fact, we have conducted period-cancellation analysis to try to reduce the function's oscillation; after which the numerical performance was indeed more stable, but not desirable enough.

Bibliography

[1] Joseph Abate and Ward Whitt. A unified framework for numerically inverting Laplace transforms. *INFORMS Journal on Computing*, 18(4):408–421, 2006.

[2] Milton Abramowitz and Irene A Stegun. *Handbook of mathematical functions: with formulas, graphs, and mathematical tables*, volume 55. Courier Corporation, 1964.

[3] Larbi Alili, P Patie, and Jesper Lund Pedersen. Representations of the first hitting time density of an Ornstein-Uhlenbeck process. *Stochastic Models*, 21(4):967–980, 2005.

[4] Michael A Arbib. Hitting and martingale characterizations of one-dimensional diffusions. *Zeitschrift für Wahrscheinlichkeitstheorie und Verwandte Gebiete*, 4(3):232–247, 1965.

[5] Robert J Aumann and Lloyd S Shapley. *Values of non-atomic games*. Princeton University Press, 1974.

[6] Louis Bachelier. *Théorie de la spéculation*. Gauthier-Villars, 1900.

[7] Paolo Baldi, Lucia Caramellino, and Maria Gabriella Iovino. Pricing general barrier options: a numerical approach using sharp large deviations. *Mathematical Finance*, 9(4):293–321, 1999.

[8] Pauline Barrieu, A Rouault, and M Yor. A study of the Hartman–Watson distribution motivated by numerical problems related to the pricing of Asian options. *Journal of Applied Probability*, 41(4):1049–1058, 2004.

[9] Harry Bateman. *Tables of integral transforms [volumes I & II]*, volume 1. McGraw-Hill Book Company, 1954.

[10] BCBS. *Revisions to the Basel II market risk framework*. Basel Committee on Banking Supervision, 2009.

[11] BCBS. *Fundamental review of the trading book - interim impact analysis*. Basel Committee on Banking Supervision, 2015.

[12] BCBS. *Minimum capital requirements for market risk*. Basel Committee on Banking Supervision, 2016.

[13] BCBS. *Revisions to the minimum capital requirements for market risk*. Basel Committee on Banking Supervision, 2016.

[14] Louis J Billera and David C Heath. Allocation of shared costs: a set of axioms yielding a unique procedure. *Mathematics of Operations Research*, 7(1):32–39, 1982.

[15] Fischer Black and John C Cox. Valuing corporate securities: Some effects of bond indenture provisions. *The Journal of Finance*, 31(2):351–367, 1976.

[16] Ian Blake and William Lindsey. Level-crossing problems for random processes. *IEEE transactions on information theory*, 19(3):295–315, 1973.

[17] Claudio Borio, Craig Furfine, Philip Lowe, et al. Procyclicality of the financial system and financial stability: issues and policy options. *BIS papers*, 1(March):1–57, 2001.

[18] Andrei N Borodin and Paavo Salminen. *Handbook of Brownian motion-facts and formulae*. Birkhäuser, 2012.

[19] Chris Brooks and Apostolos Katsaris. A three-regime model of speculative behaviour: modelling the evolution of the S&P 500 composite index. *The Economic Journal*, 115(505):767–797, 2005.

[20] Chris Brooks and Apostolos Katsaris. Trading rules from forecasting the collapse of speculative bubbles for the S&P 500 composite index. *The Journal of Business*, 78(5):2003–2036, 2005.

[21] Markus K Brunnermeier and Martin Oehmke. Bubbles, financial crises, and systemic risk. In *Handbook of the Economics of Finance*, volume 2, pages 1221–1288. Elsevier, 2013.

[22] Peter Carr and Vadim Linetsky. A jump to default extended CEV model: an application of Bessel processes. *Finance and Stochastics*, 10(3):303–330, 2006.

[23] John Cassidy. Dotcom: how America lost its mind and money in the internet era, 2003.

[24] Ren-Raw Chen and Louis Scott. Pricing interest rate options in a two-factor Cox–Ingersoll–Ross model of the term structure. *The review of financial studies*, 5(4):613–636, 1992.

[25] Marco Chiani, Davide Dardari, and Marvin K Simon. New exponential bounds and approximations for the computation of error probability in fading channels. *IEEE Transactions on Wireless Communications*, 2(4):840–845, 2003.

[26] Alexander MG Cox and David G Hobson. Local martingales, bubbles and option prices. *Finance and Stochastics*, 9(4):477–492, 2005.

[27] John C Cox, Jonathan E Ingersoll Jr, and Stephen A Ross. A theory of the term structure of interest rates. In *Theory of Valuation*, pages 129–164. World Scientific, 2005.

[28] AB Olde Daalhuis. Confluent hypergeometric functions. *NIST Handbook of Mathematical Functions, FWJ Olver, DW Lozier, RF Boisvert, and CW Clark, eds., Cambridge University, New York*, pages 321–349, 2010.

[29] Mike Dash. *Tulipomania: The story of the world's most coveted flower and the extraordinary passions it aroused.* Hachette UK, 2011.

[30] Angelos Dassios and Luting Li. An economic bubble model and its first passage time. *arXiv preprint arXiv:1803.08160*, 2018.

[31] Angelos Dassios and Luting Li. Explicit asymptotics on first passage times of diffusion processes. *arXiv preprint arXiv:1806.08161*, 2018.

[32] Angelos Dassios and Jia Wei Lim. Recursive formula for the double-barrier Parisian stopping time. *Journal of Applied Probability*, 55(1):282–301, 2018.

[33] Angelos Dassios and Jayalaxshmi Nagaradjasarma. The square-root process and Asian options. *Quantitative Finance*, 6(4):337–347, 2006.

[34] Angelos Dassios, Yan Qu, and Jia Wei Lim. Azéma martingales and Parisian excursions of Bessel and CIR processes. *Working paper*, 2018.

[35] Angelos Dassios and Shanle Wu. Perturbed Brownian motion and its application to Parisian option pricing. *Finance and Stochastics*, 14(3):473–494, 2010.

[36] Angelos Dassios and You You Zhang. The joint distribution of Parisian and hitting times of Brownian motion with application to Parisian option pricing. *Finance and Stochastics*, 20(3):773–804, 2016.

[37] Angelos Dassios and Hongbiao Zhao. A dynamic contagion process. *Advances in applied probability*, 43(3):814–846, 2011.

[38] Michel Denault. Coherent allocation of risk capital. *Journal of risk*, 4:1–34, 2001.

[39] Joseph L Doob. *Classical potential theory and its probabilistic counterpart: Advanced problems*, volume 262. Springer Science & Business Media, 2012.

[40] Kevin Dowd. Too big to fail? Long-term capital management and the Federal Reserve. Cato Briefing Paper 52, 1999.

[41] Eduardo Epperlein and Alan Smillie. Portfolio risk analysis cracking VAR with kernels. *Risk Magazine*, 19(8):70, 2006.

[42] Eugene F Fama and Kenneth R French. The cross-section of expected stock returns. *the Journal of Finance*, 47(2):427–465, 1992.

[43] Eugene F Fama and Kenneth R French. Common risk factors in the returns on stocks and bonds. *Journal of financial economics*, 33(1):3–56, 1993.

[44] Vladimir Filimonov, Guilherme Demos, and Didier Sornette. Modified profile likelihood inference and interval forecast of the burst of financial bubbles. *Quantitative finance*, 17(8):1167–1186, 2017.

[45] Jean-Pierre Fouque, George Papanicolaou, Ronnie Sircar, and Knut Sølna. *Multiscale stochastic volatility for equity, interest rate, and credit derivatives*. Cambridge University Press, 2011.

[46] Peter M Garber. *Famous first bubbles: The fundamentals of early manias*. MIT Press, 2001.

[47] Evan Gatev, William N Goetzmann, and K Geert Rouwenhorst. Pairs trading: Performance of a relative-value arbitrage rule. *The Review of Financial Studies*, 19(3):797–827, 2006.

[48] Murray Geller and Edward W Ng. A table of integrals of the exponential integral. *Journal of Research of the National Bureau of Standards*, 73(3):191–210, 1969.

[49] Anja Göing-Jaeschke and Marc Yor. A clarification note about hitting times densities for Ornstein-Uhlenbeck processes. *Finance and Stochastics*, 7(3):413–415, 2003.

[50] Anja Göing-Jaeschke, Marc Yor, et al. A survey and some generalizations of bessel processes. *Bernoulli*, 9(2):313–349, 2003.

[51] Vygintas Gontis, Shlomo Havlin, Aleksejus Kononovicius, Boris Podobnik, and H Eugene Stanley. Stochastic model of financial markets reproducing scaling and memory in volatility return intervals. *Physica A: Statistical Mechanics and its Applications*, 462:1091–1102, 2016.

[52] Vygintas Gontis, Aleksejus Kononovicius, and Stefan Reimann. The class of nonlinear stochastic models as a background for the bursty behavior in financial markets. *Advances in Complex Systems*, 15(supp01):1250071, 2012.

[53] Carol Anne Hargreaves and Chandrika Kadirvel Mani. The selection of winning stocks using principal component analysis. *American Journal of Marketing Research*, 1(3):183–188, 2015.

[54] Philip Hartman and Geoffrey S Watson. "Normal" distribution functions on spheres and the modified Bessel functions. *The Annals of Probability*, pages 593–607, 1974.

[55] Steven L Heston. A closed-form solution for options with stochastic volatility with applications to bond and currency options. *The review of financial studies*, 6(2):327–343, 1993.

[56] Steven L Heston, Mark Loewenstein, and Gregory A Willard. Options and bubbles. *The Review of Financial Studies*, 20(2):359–390, 2006.

[57] Mark H Holmes. *Introduction to perturbation methods*, volume 20. Springer Science & Business Media, 2012.

[58] Jeff Holt. A summary of the primary causes of the housing bubble and the resulting credit crisis: A non-technical paper. *The Journal of Business Inquiry*, 8(1):120–129, 2009.

[59] Tomoyuki Ichiba and Constantinos Kardaras. Efficient estimation of one-dimensional diffusion first passage time densities via Monte Carlo simulation. *Journal of Applied Probability*, 48(3):699–712, 2011.

[60] Nobuyuki Ikeda and Shinzo Watanabe. *Stochastic differential equations and diffusion processes*, volume 24. Elsevier, 2014.

[61] Kazuyuki Ishiyama. Methods for evaluating density functions of exponential functionals represented as integrals of geometric Brownian motion. *Methodology and Computing in Applied Probability*, 7(3):271–283, 2005.

[62] Kiyosi Itô, P Henry Jr, et al. *Diffusion processes and their sample paths*. Springer Science & Business Media, 2012.

[63] Robert A Jarrow and Philip Protter. Forward and futures prices with bubbles. *International Journal of Theoretical and Applied Finance*, 12(07):901–924, 2009.

[64] Robert A Jarrow, Philip Protter, and Kazuhiro Shimbo. Asset price bubbles in incomplete markets. *Mathematical Finance: An International Journal of Mathematics, Statistics and Financial Economics*, 20(2):145–185, 2010.

[65] Robert A Jarrow and Stuart M Turnbull. Pricing derivatives on financial securities subject to credit risk. *The journal of finance*, 50(1):53–85, 1995.

[66] Michael C Jensen, Fischer Black, and Myron S Scholes. The capital asset pricing model: Some empirical tests. 1972.

[67] Zhi-Qiang Jiang, Wei-Xing Zhou, Didier Sornette, Ryan Woodard, Ken Bastiaensen, and Peter Cauwels. Bubble diagnosis and prediction of the 2005–2007 and 2008–2009 Chinese stock market bubbles. *Journal of economic behavior & organization*, 74(3):149–162, 2010.

[68] Ioannis Karatzas and Steven Shreve. *Brownian motion and stochastic calculus*, volume 113. Springer Science & Business Media, 2012.

[69] John Kent. Some probabilistic properties of Bessel functions. *The Annals of Probability*, pages 760–770, 1978.

[70] John T Kent. Eigenvalue expansions for diffusion hitting times. *Probability Theory and Related Fields*, 52(3):309–319, 1980.

[71] John T Kent. The spectral decomposition of a diffusion hitting time. *The Annals of Probability*, pages 207–219, 1982.

[72] Charles P Kindleberger and Robert Aliber. *Manias, panics, and crashes*. Springer, 2003.

[73] Alexander Kiselev and Lenya Ryzhik. A simple model for asset price bubble formation and collapse. *arXiv preprint arXiv:1009.0299*, 2010.

[74] Petr Lánskỳ, Laura Sacerdote, and Francesca Tomassetti. On the comparison of Feller and Ornstein-Uhlenbeck models for neural activity. *Biological cybernetics*, 73(5):457–465, 1995.

[75] Luting Li and Hao Xing. Capital allocation under fundamental review of trading book. *arXiv preprint arXiv:1801.07358*, 2018.

[76] Yadong Li, Marco Naldi, Jeffrey Nisen, and Yixi Shi. Organising the allocation. *Risk Magazine*, 2016.

[77] Vadim Linetsky. Computing hitting time densities for CIR and OU diffusions: Applications to mean-reverting models. *Journal of Computational Finance*, 7:1–22, 2004.

[78] Robert Litterman. Hot spots and hedges. *The Journal of Portfolio Management*, 23(5):52–75, 1996.

[79] Rand Kwong Yew Low, Robert Faff, and Kjersti Aas. Enhancing mean–variance portfolio selection by modeling distributional asymmetries. *Journal of Economics and Business*, 85:49–72, 2016.

[80] Rand Kwong Yew Low and Enoch Tan. The role of analyst forecasts in the momentum effect. *International Review of Financial Analysis*, 48:67–84, 2016.

[81] Daniel W Lozier. NIST digital library of mathematical functions. *Annals of Mathematics and Artificial Intelligence*, 38(1-3):105–119, 2003.

[82] Fabio Maccheroni, Massimo Marinacci, Aldo Rustichini, and Marco Taboga. Portfolio selection with monotone mean-variance preferences. *Mathematical Finance: An International Journal of Mathematics, Statistics and Financial Economics*, 19(3):487–521, 2009.

[83] Harry Markowitz. Portfolio selection. *The journal of finance*, 7(1):77–91, 1952.

[84] Harry M Markowitz. Portfolio selection: Efficient diversification of investment. 344 p, 1959.

[85] Harry M Markowitz, G Peter Todd, and William F Sharpe. *Mean-variance analysis in portfolio choice and capital markets*, volume 66. John Wiley & Sons, 2000.

[86] Hiroyuki Matsumoto, Marc Yor, et al. Exponential functionals of Brownian motion, I: Probability laws at fixed time. *Probability surveys*, 2:312–347, 2005.

[87] HP Jr McKean et al. The Bessel motion and a singular integral equation. *Memoirs of the College of Science, University of Kyoto. Series A: Mathematics*, 33(2):317–322, 1960.

[88] Robert C Merton. On the pricing of corporate debt: The risk structure of interest rates. *The Journal of finance*, 29(2):449–470, 1974.

[89] Hyman P Minsky. *Financial instability revisited: The economics of disaster*. Board of Governors of the Federal Reserve System St. Louis, 1970.

[90] Leonard J Mirman and Yair Tauman. Demand compatible equitable cost sharing prices. *Mathematics of Operations Research*, 7(1):40–56, 1982.

[91] JP Morgan. *Riskmetrics-Technical Document, 4th edn.* JP Morgan, 1996.

[92] John J Murphy. *Technical analysis of the financial markets: A comprehensive guide to trading methods and applications*. Penguin, 1999.

[93] A Novikov, V Frishling, and N Kordzakhia. Time-dependent barrier options and boundary crossing probabilities. *Georgian Mathematical Journal*, 10(2):325–334, 2003.

[94] AA Novikov. A martingale approach to first passage problems and a new condition for Wald's identity. In *Stochastic Differential Systems*, pages 146–156. Springer, 1981.

[95] Fritz Oberhettinger and Larry Badii. *Tables of Laplace transforms*. Springer Science & Business Media, 2012.

[96] Frank WJ Olver. *NIST handbook of mathematical functions hardback and CD-ROM*. Cambridge university press, 2010.

[97] Basel Committee on Banking Supervision. *Amendment to the Capital Accord to Incorporate Market Risks*. BCBS, 1996.

[98] Soumik Pal and Philip Protter. Analysis of continuous strict local martingales via h-transforms. *Stochastic Processes and their Applications*, 120(8):1424–1443, 2010.

[99] Danilo Pelusi. A pattern recognition algorithm for optimal profits in currency trading. In *Mathematical and Statistical Methods for Actuarial Sciences and Finance*, pages 253–261. Springer, 2010.

[100] Goran Peskir. On the fundamental solution of the Kolmogorov–Shiryaev equation. In *From stochastic calculus to mathematical finance*, pages 535–546. Springer, 2006.

[101] Goran Peskir and Albert Shiryaev. *Optimal stopping and free-boundary problems*. Springer, 2006.

[102] Peter CB Phillips, Shuping Shi, and Jun Yu. Testing for multiple bubbles: Limit theory of real-time detectors. *International Economic Review*, 56(4):1079–1134, 2015.

[103] Sidney Redner. *A guide to first-passage processes*. Cambridge University Press, 2001.

[104] Carmen M Reinhart and Kenneth S Rogoff. Is the 2007 US sub-prime financial crisis so different? An international historical comparison. *American Economic Review*, 98(2):339–44, 2008.

[105] Daniel Revuz and Marc Yor. *Continuous martingales and Brownian motion*, volume 293. Springer Science & Business Media, 2013.

[106] LM Ricciardi, AD Crescenzo, V Giorno, and AG Nobile. An outline of theoretical and algorithmic approaches to first passage time problems with applications to biological modeling. *Mathematica Japonica*, 50:247–322, 1999.

[107] Michael Schatz and Didier Sornette. Inefficient bubbles and efficient drawdowns in financial markets. *Swiss Finance Institute Research Paper*, No. 18-49, 2018.

[108] Philipp J Schönbucher. *Credit derivatives pricing models: models, pricing and implementation*. John Wiley & Sons, 2003.

[109] E Schrödinger. Zur theorie der fall-und steigversuche an teilchen mit brownscher bewegung. *Physikalische Zeitschrift*, 16:289–295, 1915.

[110] Erwin Schrödinger. Quantisierung als eigenwertproblem. *Annalen der physik*, 385(13):437–490, 1926.

[111] Eduardo S Schwartz. The stochastic behavior of commodity prices: Implications for valuation and hedging. *The journal of finance*, 52(3):923–973, 1997.

[112] L. S. Shapley. A value for n-person games. In *Contributions to the theory of games, vol. 2*, Annals of Mathematics Studies, no. 28, pages 307–317. Princeton University Press, Princeton, N. J., 1953.

[113] Lloyd S Shapley. Cores of convex games. *International journal of game theory*, 1(1):11–26, 1971.

[114] Lloyd S Shapley. A value for n-person games. *The Shapley value*, pages 31–40, 1988.

[115] Robert C Shiller. Irrational exuberance. *Philosophy & Public Policy Quarterly*, 20(1):18–23, 2000.

[116] Albert N Shiryaev. Quickest detection problems in the technical analysis of the financial data. In *Mathematical Finance Bachelier Congress 2000*, pages 487–521. Springer, 2002.

[117] AN Shiryaev. The problem of the most rapid detection of a disturbance in a stationary process. In *Soviet Math. Dokl*, volume 2, 1961.

[118] Arnold JF Siegert. On the first passage time probability problem. *Physical Review*, 81(4):617, 1951.

[119] William Smith. On the simulation and estimation of the mean-reverting Ornstein-Uhlenbeck process. *Commodities Markets and Modelling*, 2010.

[120] Didier Sornette and Peter Cauwels. Financial bubbles: mechanisms and diagnostics. 2014.

[121] Denis Talay. Numerical solution of stochastic differential equations. 1994.

[122] Dirk Tasche. Risk contributions and performance measurement. *Report of the Lehrstuhl für mathematische Statistik, TU München*, 1999.

[123] Dirk Tasche. Capital allocation to business units and sub-portfolios: the Euler principle. *Pillar II in the New Basel Accord: The Challenge of Economic Capital*, pages 423–453, 2008.

[124] George E Uhlenbeck and Leonard S Ornstein. On the theory of the Brownian motion. *Physical review*, 36(5):823, 1930.

[125] Oldrich Vasicek. An equilibrium characterization of the term structure. *Journal of financial economics*, 5(2):177–188, 1977.

[126] Frederic YM Wan and Henry C Tuckwell. Neuronal firing and input variability. *J. theor. Neurobiol*, 1(2):197–218, 1982.

[127] Ming Chen Wang and George Eugene Uhlenbeck. On the theory of the Brownian motion II. *Reviews of modern physics*, 17(2-3):323, 1945.

[128] George Neville Watson. *A treatise on the theory of Bessel functions*. Cambridge university press, 1995.

[129] Christopher Wood. *The bubble economy: the Japanese economic collapse*. Sidgwick & Jackson, 1992.

[130] Yasuhiro Yamai, Toshinao Yoshiba, et al. Comparative analyses of expected shortfall and value-at-risk: their estimation error, decomposition, and optimization. *Monetary and economic studies*, 20(1):87–121, 2002.

[131] Marc Yor. On some exponential functionals of Brownian motion. *Advances in applied probability*, 24(3):509–531, 1992.